PREDICTED TRANSIENT PERFORMANCE OF A DERIVATIVE TWO-SPOOL TURBOFAN ENGINE WITH A 4-STAGE I.P COMPRESSOR

By

Lamine Mohamed Darbouche

This thesis is presented for the degree of Master of Science (M.Sc) to the faculty of Engineering

Department of Mechanical Engineering

Glasgow University

May, 1991.

ProQuest LLC.
789 East Eisenhower Parkway
P.O. Box 1346
Ann Arbor, MI 48106 – 1346

CONTENTS

ACKNOWLEDGEMENTS

It is my great pleasure to express gratitude to my supervisor Dr. N.R.L Maccallum for all the advice, help, enthusiasm and encouragement displayed by him throughout this work.

My thanks are extended to all staff of the Department of Mechanical Engineering for their help.

I am indebted to the Algerian Ministry of High Education and the Algerian Embassy as without their financial assistance my period of studies would not have been possible.

A very special and sincere thanks to my wife and daughter for their care, loyal support and understanding.

Finally I would like to thank my parents and family for the love and patience shown towards me at all times during my period of studies. It is to my parents, wife and family that this thesis is dedicated.

(VII)
UNITS

NOTE

In the present investigation the units used have all been in S.I units, with the exception of thrust which had been quoted in lbf instead of KN, and the reason for that is the common use of Imperial units in Aero-engine industries.

NOMENCLATURE

NOTATION

A	aspect ratio of aerofoil
a	distance of point of maximum camber from blade leading edge
(a/c)	maximum camber
c	blade chord
C_D	drag coefficient
C_{DA}	annulus drag coefficient
C_{DP}	profile drag coefficient
C_{DS}	secondary drag coefficient
C_L	lift coefficient
C_p	specific heat at constant pressure
C1 CN	coefficients-see Table 3.2
D1 DN	coefficients-see Table 3.2
ΔP_{st}	stage pressure rise
$\Delta T'$	isentropic temperature rise
f	fuel flow, ratio of heat transfer to the fluid to the work transfer from the fluid
FCSP	fraction of split defined in section 4.2
g	acceleratio due to gravity, blade staggered spacing
GEOM	fraction of the total frontal area defined in section 4.2
h	blade height, blade length
i	incidence = $\alpha 1 - \beta 1$
j	mechanical equivalent of heat
M	Mach number
m	polytropic index of non-adiabatic path, a variable in deviation rule
m	'm dot' mass flow rate of air or gas
N	shaft rotational speed,
N	'N dot' rate of change of shaft rotational speed
n	polytropic index of expansion or compression, number of blades
P	stagnation pressure
P_2/P_1	total pressure ratio over stage, pressure ratio
P_{26}/P_{24}	pressure ratio of the I.P compressor

Q	rate of heat transfer
R	compressor pressure ratio at surge, gas constant/ radius
s	space blading or pitch
(s/c)	pitch/chord ratio
T	stagnation temperature
T'	isentropic temperature
T_1	stagnation temperature at stage inlet
T_{24}	inlet stagnation temperature of the I.P compressor
T_{26}	stagnation temperature leaving the I.P compressor
t	time, blade maximum thickness
(t/c)	maximum thickness to chord ratio of blade
U	tangential velocity
u	blade speed
V	fluid velocity, velocity
v	volume
W	work transfer
X	thrust

GREEK SYMBOLS

α	air angle
$\alpha 1$	fluid inlet angle
$\alpha 2$	fluid outlet angle
α_m	fluid vector mean angle
β	blade angle, air/gas angle
$\beta 1$	blade inlet angle
$\beta 2$	blade outlet angle
γ	ratio of specific heat
δ	deviation = $\alpha 2 - \beta 2$, tip clearances
η	efficiency
ε	deflection = $\alpha 1 - \alpha 2$
ϕ	flow coefficient (V_a/u), slope of temperature-rise coefficient curve
λ	non-dimensional clearance (δ/h)
ω	mean total head pressure loss

Ω	work done factor
ξ	temperature coefficient, stagger angle of the blade
ρ	density
τ	time constant
ψ	blade loading ($2C_p \Delta T/u^2$), stage pressure rise coefficient= $\Delta P_s/(1/2)\rho u^2$
Δ	variation

SUBSCRIPTS

a	axial
act	actual
ad	adiabatic
air	air
AMB	ambient
b	blade
bp	by-pass
c	compressor
cg	core gas
chics	characteristics
ENG	engine
ht	with heat transfer
g	gas
H.P.	high pressure
i	inner/ inlet/ increment
ISEN	isentropic
I.P	intermediate pressure
L.P.	low pressure
nc	critical
nm	maximum
C.V.	calorific value
o	outer
p	polytropic
Ref	reference
s	static
st	stage
T	turbine

t	at time, turbine
th	thermal
f	final
*	nominal
670	refers to the New Engine
610	refers to the Reference Engine
4	refers to 4-stage I.P compressor
3	refers to 3-stage I.P compressor

For station Numbering, see next page.

STATION NUMBERING

1	entering the fan sections
13	by-pass duct
24	leaving the Inner fan and entering the I.P compressor
26	leaving the I.P compressor and entering the H.P compressor
3	leaving the H.P compressor and entering the combustion chamber
4	leaving the combustion chamber and entering the H.P turbine
5	leaving the H.P turbine and entering the L.P turbine
6	leaving L.P turbine
7	at the mixer
8	leaving the final nozzle

See fig 13.

SUMMARY

Given the need of a higher thrust, with a higher overall efficiency engine for civil aircraft, a method of designing a derivative engine from an existing engine is investigated in the present work.

The Rolls-Royce TAY MK670 civil aircraft engine is to be a higher thrust derivative of the TAY MK610. The increased thrust is to be achieved by increasing the flow and pressure ratio of the two-spool compression system. The major modifications in the derivative engine are a 4-stage Intermediate Pressure (I.P) compressor instead of a 3-stage, and increased fan tip diameter.

The first step in the simulation has been the prediction of the characteristics of the 4-stage I.P compressor, the characteristics of the 3-stage I.P compressor already being known.

The revised fan characteristics were then predicted. Finally, these components characteristics were used to predict the transient performance of the new engine. The development of the new fuel control schedules has been described.

The contents of this thesis are therefore as follows. There is first a brief review of the history and background of gas turbines. The main technical reporting in the Thesis then begins.

Chapter I gives an introduction to gas turbines and the prediction of transient performance. The prediction of the

characteristics of a multi-stage compressor is described in chapter II. The next chapter describes the scaling of the components for the TAY MK670 engine from the reference engine. This is followed by a chapter presenting the steady-running and transient performance of the MK670.

Discussion of results of the MK670 Engine and comparison between both of the Engines follows in Chapter V The principal findings are that, for the derivative engine when the transient fuel schedules are selected to give equivalent thrust responses to the reference engine, then it is predicted that acceleration and deceleration transients can be achieved without encoutering, or approaching too closely to surge in the compressors. Indeed in the most testing transient, which is the deceleration, the trajectory movement in the IP compressor is less severe in the derivative engine (MK 670) than in the original engine (MK 610).

Finally a conclusion and suggestions for further work are given in the last two chapters.

AERO-GAS TURBINES : HISTORY AND BACKGROUND

There have been several distinct avenues of Aero-Engine development but all have their origins in engineering ideas which pre-date successful manned flight. The piston engine reigned supreme until 1940's, when gas turbines began to take over. The gas turbine will be discussed more fully below. The quest for still higher speeds and altitudes brought an interest in the ramjet and rocket but, in the event, their application was limited to missiles and to vehicles designed to fly outside Earth's atmosphere. Nevertheless, the process of engine development is continuous, and smaller turbines are becoming acceptable, just as higher speeds and altitudes may make ramjets more attractive.

The reasons for the transition in the 1940's from the piston plus propeller engine to gas turbine are now discussed. Even with research and development, it was found that propellers would not be suitable for very high speed aircraft, and also that piston engines were getting more and more complicated. The answer was to look for basically a different type of propulsion system that was lighter and could run on less fuel consumption. Although ideas for jet engines had been successful in the 18^{th} century, practical proposals began to be taken seriously only in 1930's. Much of the practical inspiration came from two British Engineers, Dr.A.A.Griffiths of the Royal Aircraft Establishment and Frank Whittle a young R.A.F. officer. Griffith carried out both theoretical and practical work beginning in 1926. This led to the running of an axial compressor in 1936 and the involvement of the engineering company METROPOLITAN-VICKERS in 1937. The first METRO-VICK axial turbojet ran in 1940. Frank Whittle first suggested the use

of jet propulsion for aircraft in 1929, and the first engine designed by him was tested in 1937. ROLLS-ROYCE took up the Whittle design, which used a double-sided centrifugal compressor, and ran their first engine in 1942. The Germans also took an interest in jet propulsion, and it was a Heinkel design, the HE 178, which made the first flight of a true jet propelled aeroplane in August 1939. Heinkel had helped young Pabst Von Ohain to run his first centrifugal jet in 1937. At the same time JUNKERS had begun work on axial design.

The principle of the jet engine is very simple. Air is passed through a compressor and is pressurised. Fuel is then added and burnt in the combustion chamber, producing hot gas which flows out through a turbine. The turbine extracts just enough energy to power the compressor, to which it is attached by a shaft running through the centre of the engine, the rest of the energy is used to provide thrust by expanding the turbine exit gases at high velocity through an open nozzle.

From the early days there have been two types of jet engines. The first, favored by Whittle, uses a centrifugal compressor which takes the air from the engines intake and compresses it by spinning it outwards across both faces of a rapidly-rotating disc finned on both sides. The second type compresses the air as it moves along the length of the axial compressor (looking like a series of fans mounted one behind the other). The axial compressor is slimmer and can work at much higher pressure ratio, aiding fuel economy. Gradually the use of the axial flow compressor arrangement has become universal except in the smallest jet engines used in general aviation.

Initially it was difficult to make the gas turbine efficient enough to produce worthwhile power and thrust. It was also found difficult to develop materials capable of standing up to the high stress at high temperature. High temperature alloys and advanced cooling techniques are the key to the gas turbine performance, and they continue to be a major area of research.

Turboprop engines helped to overcome the high fuel consumption of the early jets, but they did little to relieve the inherent problems of the propeller. Whittle had taken out a number of patents covering an adaptation of the pure jet principle, and his company ran two engines driving fans at the end of the war. However, it was not until the ROLLS-ROYCE Conway engine was developed in late 1950's that the By-Pass principle was applied to a production engine. In this system, part of the air passing through the compressor is ducted around the outside of the core engine and either expelled through separate nozzles or re-introduced into the exhaust duct. Designers found the arrangement better if the compressor and turbine are each divided and connected to two different concentric shafts. With this arrangement, a two spool engines was created and the first few stages of low-pressure compressor is driven by the last stages of the turbine, and the high-pressure compressor is driven by a high pressure turbine. This arrangement enabled the cycle compression ratio to be raised from about 8/1 to 20/1 or higher, thus raising cycle efficiency. This by-pass type of engine is commonly called a turbofan.

By the early 1960's designers proposed to take the By-Pass technology further in the design of power plants. More efficient and quieter engines were needed and that led to change in

geometry and configuration of the gas turbines with a much higher by-pass ratio. Over several decades turbofan engine development to meet these requirement has continued.

During the last decade significant research has been carried out towards improving methods. The transient behaviour of aircraft gas turbine is of great practical importance to manufacturers and customers alike. Much more attention is given to the avoidance of the surge in the compressors, particularly when the engine is at the design stage. Simulation is widely used and plays an important role in this development, in predicting both steady-state performance of the engine and also its transient performance.

CHAPTER I

GENERAL INTRODUCTION TO GAS TURBINES

1.1 INTRODUCTION

This chapter starts with the general introduction to the Gas turbine, then it gives a discussion on the methods available in Gas turbine transient modelling. It includes, a brief description of how the prediction of transient performance has been developed. The effects of heat transfer are also described, as are the efforts that have been taken to incorporate these effects into computer models simulating the transient as well as the steady-running performance of Gas turbine.

The gas turbine provides a method of supplying mechanical power from a thermal source. Simple open-cycle Gas turbines are widely used in both industrial and naval applications. The major attractions are its lightness, low cost, and it requires no water.

In order to produce more power and efficiency, the design of gas turbines has become more complex. The first necessary step was the prediction of the performance in both steady-state and transient condition. Mathematical models are required for this.

Two types of Gas turbines cycles are in use : Aircraft Gas turbine cycles and Shaft power cycles. The second type includes all kind of Gas turbines except the first type, and could all be classified under the name of Industrial Gas turbines. The main

difference between the two is that in the former the useful power output is produced wholly or in part as a result of expansion in a propelling nozzle, wholly in turbojet and turbofan engines and partly in turboprop engines. In the latter type the useful power output is mechanical form, obtained by expansion in additional turbine stages. The simplest arrangements for both types are illustrated fig(1) and fig(2).

The Gas turbine cycles could further be divided into two type, Open and Closed cycles.

First, Aircraft gas turbine use air drawn from the atmosphere as the working gas, so the final constant pressure cooling occurs in the atmosphere. This is the open cycle.

While the second reuses the original gas, either air or some other gas, and it is recirculated through the machine. The cycle is referred to as a closed cycle. The alternative closed cycle is shown in fig(3).

1.2 PROPULSION FOR AIRCRAFT GAS TURBINES

Jet propulsion is based on creating an unbalanced force by exhausting gas at high velocity from the nozzle. This unbalanced force is called *thrust* and it is used for jet propulsion which is based on an open Brayton cycle. By contrast, in open Brayton cycle for stationary power plant, the turbine produces power in excess of the compressor requirements, the excess being available for driving the load. In jet propulsion system, the turbine produces just enough power to meet the needs of the compressor. The thrust is obtained by partially expanding the high temperature, high pressure

combustion gases in the turbine. The gases are finally expanded in a nozzle to produce high velocity gases. The velocity of the gases exiting from the nozzle can be determined if the nozzle inlet and outlet pressures and the inlet temperature are known. It is usually assumed that the expansion in the nozzle is isentropic. Then the thrust can be calculated by an application of the momentum equation. The aim of the gas turbine is to produce thrust. That is done by providing an increase in momentum to the air which is flowing past the aircraft.

Assuming an observer on the aircraft, the air enters the intake of the engine with a velocity V_1 which is equal and in the opposite direction to the speed of the aircraft, and leaves the engine with velocity V_2.

Assuming the mass flow, $\dot{m}$, is constant, then the thrust Xn is the rate of change of momentum:

$$Xn = \dot{m}V_2 - \dot{m}V_1$$

$$Xn = \dot{m}(V_2 - V_1) \qquad (1)$$

where:

$\dot{m}V_2$ is the Gross momentum thrust.

$\dot{m}V_1$ is the Intake momentum drag.

All current gas turbine cycles operate on an open approximation to the Brayton cycle fig(4). This cycle follows the constant pressure cycle. Ideally working gas is compressed from point 1' to point 2', heat is added to it at a constant pressure till it reaches point 3' and is then expanded to point 4'. Finally, the gas is cooled at constant pressure to initial temperature.

In aircraft gas turbines, when the aircraft is moving part of the compression is achieved in the intake to the engine by the ram compression. So the pressure and temperature at inlet to the engine, point 1A, are higher than the atmospheric values.

Due to the inefficiencies in the various components of the engine the actual cycle (1-2-3-5) departs somewhat from the Brayton cycle(1'-2'-3'-5') fig(4).

The fluid is compressed in the compressor of the engine from 1A to 2 or from 1 to 2 if the aircraft is stationary. The point 1 is of lower pressure due to losses at the intake. Then heat is added to the working fluid from 2 to 3, with a loss in pressure due to friction and losses associated with the combustion process. That results in lowering slightly the turbine inlet pressure from ideal point 3' compressor delivery pressure. Then gases are expanded to point 5. The expansion from 3 to C is the work needed to drive the compressor. This part of expansion occurs in the turbine(s). The expansion then continues from C to 5 in the nozzle, which produces the useful work output. In the ideal cycle the turbine and compressor works balance exactly. However in the real cycle the turbine work is larger to account for losses.

The useful work is in the form of an increase in Kinetic energy of the working gas or air:

$$\text{Increase in K.E. in unit time} = 1/2\dot{m}V_2^2 - 1/2\dot{m}V_1^2 \quad (2)$$

Thrust power is the product of the net thrust and the aircraft speed:

Thrust power = $\dot{m}V_1(V_2 - V_1)$

Now the propulsive efficiency is given by:

$$\text{Propulsive efficiency} = \frac{\text{Thrust power}}{\text{useful propulsive energy} + \text{unused K. E of the jet}}$$

$$\eta_P = \frac{\dot{m}V_1(V_2 - V_1)}{\dot{m}\left[V_1(V_2 - V_1) + (V_2 - V_1)^2 / 2\right]} = \frac{2}{1 + (V_2 / V_1)} \qquad (3)$$

From equation (1) and (3), it is clear that:

a) Xn is maximum when $V_1=0$, at static conditions, but η_p is then nul;

b) η_p is maximum when $V_2/V_1=1$ but then the thrust is nul.

For the gas turbine cycle itself:

$$\text{Thermal Efficiency} = \frac{\text{rate of useful work output}}{\text{rate of consumption of thermal Energy}}$$

$$\eta_T = \frac{(1/2)\dot{m}(V_2^2 - V_1^2)}{f(c.v)} \qquad (4)$$

The overall efficiency is the ratio of thrust power to the rate of consumption of the thermal energy.

$$\eta_o = \frac{mV_1(V_2 - V_1)}{f(c.v)} \qquad (5)$$

from equation {3}, {4} & {5} it is seen that:

$$\eta_o = \eta_T \times \eta_P \qquad (6)$$

It is clear from equation {6} that in order to produce a higher overall efficiency it is necessary to maximize both η_P and η_T.

η_T is maximized in the ideal cycle by increasing the pressure ratio and η_P is maximized by decreasing the jet speed. While in the actual cycle the thermal efficiency is maximised by increasing both the pressure ratio and the temperature of gases entering the turbine.

1.3 GAS TURBINE DEVELOPMENT

As stated earlier, the increase of pressure ratio will improve the thermal efficiency of the gas turbine fig(5). Therefore the development of a higher pressure ratio engines is apparent. Practical attempts have been made in designing a single-spool engine with a higher pressure ratio which lead to more complex problems. The front stages of the compressor were likely to stall at low speed, and likewise, at high speed stall occurred at the rear stages of the compressor. This problem was overcome by designing a two-spool engine which can achieve a higher pressure ratio of up to twenty or even more.

It is important to note that the by-pass engines increase the propulsive efficiency η_P. These design requirements gave birth to a three-spool engine which is more complex but more compact. These types of engines are illustrated fig(6).

1.4 POWER PLANTS

The choice of a power plant fig(7) depends on the specification

of the aircraft. It will depend not only on the required cruising speed but also on the desired range of the aircraft and maximum rate of climb, together with the altitude which is an important parameter as well, when the thrust and fuel consumption vary with height. Fig(8) indicates the flight regimes found to be suitable for the broad categories of power plant installed in the civil aircraft.

1.5 TRANSIENT BEHAVIOUR OF AIRCRAFT GAS TURBINE

Gas Turbines are widely used for the propulsion of aircraft. These engines have to accelerate from idling speed to maximum speed, and vice versa, in as short times as possible .It is very important to be able to predict engine response and performance during these transients to ensure that it is operating within the safety limits of the engine. In these two situations during transient movements a surge in a compressor or allowing gases at very high temperature to enter the turbine are to be avoided. Surge occurs when a compressor is forced to operate at too high pressure ratio for that value of non-dimensional rotational speed. Thus the possibility of encountering surge can be eased by matching all components of the engine (compressor(s), turbine(s) and final nozzle) such that the steady-running line lies further from the surge line. In order to design an engine, it is essential that the engine operates at high pressure ratio in order to achieve good efficiency and hence good fuel consumption. For optimum engine performance, transient behaviour has to be used at its highest understanding.

In the steady state, the fuel flow is fixed at given flight

conditions, and that will fix the rotational speed and all other parameters of the engine. This is due to the power balance condition between the components fig(9).

However, during acceleration or deceleration this power balance does not apply any longer. For acceleration, the turbine power must exceed the compressor power and the turbine entry temperature rises, and for this the fuel flow rises above the corresponding equilibrium value fig(10). It follows that for a given flight condition, the accelerating performance of the engine is a function of a non-dimensional rotational speed and non-dimensional fuel flow which are independent variables. This also applies for deceleration when the turbine power is now less than the compressor power.

1.6 PREDICTION OF TRANSIENT PERFORMANCE.

Since early in the history of the development of the Aircraft engines, research has been carried out on the transient prediction of the Gas turbines.

Today, a wide range of aircraft engines is in use, and each particular class or type is designed to meet the customers special requirements with regard to the size and purpose of the aircraft and its performance, operating system etc. In general, engines are very costly and this high development cost led to the need for accurate information on engine behaviour. Customers demand guarantees of engine performance and this requires an accurate prediction of performance, both steady-state and transient.

At the early design stage, simulation techniques using a mathematical approach are used to permit the investigation of the

transient performance.

During the years of research on transient modelling of the Gas turbine, two methods of gas turbine simulation have been developed based on component models. These are the Continuity of Mass Flow (CMF) method and the Inter Component Volumes (ICV) method.

1.6.1 CONTINUITY OF MASS FLOW (CMF) METHOD

In this method it is assumed that at any given time the mass flow leaving the engine matches the mass flow entering it, some allowances have been made such as for bleeds and fuel flow. The starting parameters of the flight conditions and rotational shaft speeds of the engine have to be known.

The calculation procedure is now outlined for a single-spool engine.

Based on the starting parameters, the compressor inlet pressure and temperature are calculated. A guess for the compressor outlet pressure is made. The compressor mass flow rate and exit temperature are obtained by gas dynamics calculation.

Energy balance equation is now carried out, using the known fuel flow rate from which the combustion chamber outlet temperature is obtained. The outlet pressure is calculated by applying a pressure loss factor to the inlet pressure. Now the conditions at the inlet turbine are determined (mass flow rate, inlet pressure, inlet temperature and shaft speed). The turbine exit temperature and pressure are found by using the turbine characteristic charts and some gas dynamics calculations. In the case where the turbine inlet mass flow rate is larger than the characteristics of the

turbine, a change of logic in the program is permissible in which the turbine pressure ratio is guessed first and a calculation of the turbine inlet non-dimensional mass flow rate is done. The compressor pressure ratio is then revised until the inlet turbine mass flow matches the one obtained previously. The value for the mass flow rate throughout the nozzle is now determined by the ratio of turbine exit pressure to ambient pressure, the turbine exit temperature and final nozzle area. If this value is different from the one at turbine exit obtained previously that means that the compressor outlet pressure initially guessed was incorrect. The value of this pressure is now revised and the above calculations are repeated and continued until the two mass flow rates obtained are compatible. The work produced or absorbed by each component is then calculated and the acceleration or deceleration rate is evaluated for the shaft. It is then assumed that this acceleration rate applies over the subsequent time interval (Newton's approximation). The process is repeated for the next time interval. This gives new shaft speeds which form the starting point for the next calculation procedure at the end of that time interval. The process is repeated until the transient has been completed.

For a complex engine a higher number of iterative loops is required. Further description of the CMF method is given in Ref(1). Difficulties were faced in achieving convergence Ref(2) when simulating more complex engine. However, this method has an advantage in the computing time which is significantly less than the other method, the "Inter-Component Volume" method. The weakness of the CMF method is that no allowance is made for the accumulation of air, or gas, mass during the transient within the

components and ducts of the engine.

1.6.2 INTERCOMPONENT VOLUMES (ICV) METHOD

In this method, allowance is made for the accumulation of mass within the components and ducts of the engine. Volumes are introduced between the various components of the engine, and all flow unbalances are assumed to occur within these volumes. The size of the intercomponent volume is the volume of the space between two components plus one half of the volume of each adjacent component. An initial pressure distribution has to be specified. This initial pressure distribution will give mass flows into and out of these intercomponent volumes. Generally, these mass flows will not match, therefore air/gas mass will accumulate, or diminish, in which cases the pressure will rise or fall during the subsequent time interval. This new pressure forms the starting point for the calculation of the next time step.

The flight conditions and shaft speeds are known, an initial guess of the pressure within these volumes is given, as accurately as possible. From the starting parameters, compressor inlet temperature and pressure are determined. Gas dynamics calculations, are used to find the compressor mass flow rate and exit temperature. The same calculation as that in the CMF method can be used for the combustion chamber. Turbine inlet temperature and pressure and shaft speed are known. These parameters can be used to determine the mass flow rate through the turbine and the exit temperature as well. Both exit parameters of the turbine and the ambient pressure are used to calculate the mass flow rate through the final nozzle.

This method has been used for previous simulations of typical turbofan engines Ref(1) and Ref(3). This method is used for much of the transient prediction work reported in this thesis. A more detailed description of the application of this method is given in chapter II.

For a particular volume:

$$M_0 = \frac{Pv}{RT} \qquad (1)$$

and

$$M_f = M_0 + \Delta M \times \Delta T \qquad (2)$$

where $$\Delta M = \dot{m}_{in} + \dot{m}_{out} \qquad (3)$$

so the new pressure :

$$P_n = \frac{M_f RT}{V} \qquad (4)$$

Then, as in the continuity of mass flow method, the energy balance equation is used to calculate the shaft acceleration. This new shaft speed is for the next pass through component calculations at the next time step. The new values of the pressure and shaft speed are substituted for the original values. This process is repeated until the two mismatches of the mass flow and work imbalance are negligible. The computing times are significantly longer than for the CMF method described previously. A period prior to the transient is given to overcome the problem of poor initial guesses of the pressure distribution in the engine.

1.7 COMPARISON OF PREDICTIONS OF CMF AND ICV METHODS

For single-spool engine it is reported Ref(1) that both methods yield very similar results except during the first fractions of a second of the transient. The difference is due to mass storage in the engine. This effect is high during the first instants of the transient but very small afterwards.

In the case of a two-spool turbofan engine with mixed exhausts Ref(4), the author found that in both accelerations and decelerations, the speed and thrust responses as predicted by CMF method are roughly 4 per cent faster than those predicted by the ICV method. Fans and Intermediate Pressure (IP) Compressor trajectories are identical. However, in the High Pressure (HP) Compressor, the trajectory predicted by the ICV method during the short period of rapid transient moves less from the working line than does that predicted by the CMF method.

To summarise, the predictions given by the ICV are more realistic than the CMF method because this procedure includes the effect of air/gas mass accumulation, which is ignored in the CMF method. However computing times are significantly longer by a factor of about 10.

1.8 THE EFFECT OF HEAT TRANSFER IN AERO-ENGINES

In the present work, these methods are initially assumed adiabatic flow through the components, in order to simplify the work.

In order to predict accurately the performance during transients,

it has been found in the last investigation Ref(17) that allowances for thermal effects must be included in the simulation model Ref(5). As an example of thermal effects, where a gas turbine is rapidly accelerated or decelerated, there is a bounded time that passes after completion of the speed transient before many components reach their equilibrium temperatures. During that limited time and during the speed transient, heat transfer takes place between all the components and the air passing through the engine resulting in a difference between the performance of the engine and that predicted from adiabatic assumptions.

1.8.1 HEAT TRANSFER EFFECTS

The thermal effects which are considered to be relevant in transients are:

a) Heat absorption in fans, compressors and turbines

b) Heat absorption in combustion chambers

c) Changes in characteristics of compressors due to heat transfer

d) Changes in efficiencies of compressors and turbines due to tip clearances effected by heat transfer

e) Changes in seals clearances which are different from the design stabilised values

f) Delay in the response of the combustion process.

All these effects alter the performance of the components, and hence of the engine as a whole. These changes lead to revised transient trajectories in the compressors and to important changes in predicted performance. The description of these effects given here is very brief and simply intended to give a general view of the investigation. These models have been studied by several investigators Ref(6,7,8).

1.8.1.1 HEAT ABSORPTION IN FANS, COMPRESSORS AND TURBINES

In adiabatic flow in a fan or compressor, elemental changes in temperature and pressure are related by the small-stage or polytropic efficiency, η_{pc}

$$C_p dT = \frac{1}{\eta_{pc}} v dP \qquad (1)$$

This leads to the relation between the index of compression, n, and the isentropic index, γ:

$$\frac{n-1}{n} = \frac{1}{\eta_{pc}} \frac{\gamma - 1}{\gamma} \qquad (2)$$

In the case of non-adiabatic flow, the above equations are modified to:

$$C_p dT = (1-f) \frac{1}{\eta_{pc}} v dT \qquad (3)$$

and

$$\frac{m-1}{m} = \frac{1-f}{\eta_{pc}} \frac{\gamma-1}{\gamma} \qquad (4)$$

Where f is the ratio of the heat transfer to the air in an element to the work transfer from the air in that element. Symbol m represents the index of this non-adiabatic, polytropic compression. It is assumed that the ratio f is constant along the compressor.

The final equivalent relation for non-adiabatic polytropic expansion in a turbine is:

$$\frac{m-1}{m} = (1-f)\,\eta_{pt} \frac{\gamma-1}{\gamma} \qquad (5)$$

The ratio, f, can be, numerically, as high as 0.2 in a compressor and 0.35 in a turbine for a single-spool engine.

1.8.1.2 HEAT ABSORPTION IN COMBUSTION CHAMBER

In a transient, heat transfer occurs between the combustion chamber flame tube and casing and the air/gas passing through the chamber, and these can represent a significant fraction of the changes in fuel flow especially in the early stage. A study for quantifying this effect is given in Ref(9).

1.8.1.3 CHANGES IN COMPRESSOR CHARACTERISTICS

The overall characteristics of a compressor are altered due to several effects.

For an accelerating engine, initially "cold", heat is transferred

from the air to the blades and casing. This increases the density of the air and lowers the axial component of the velocity at a particular stage of the compressor. This therefore changes the matching between stages. As a result, the working points of the stages are altered Ref(10) and Ref(6) and the overall pressure rise is changed.

In addition, the boundary layers of the flows over the aerofoils may be altered. As an example, heat transfer from the suction surface of the blade to the air which occurs during a deceleration or a hot reacceleration will cause changes in the growth of the boundary layer, and may lead to earlier separation Ref(11) and Ref(12).

Finally, a typical movement in the H.P compressor characteristics at an instant in an acceleration of an initial "cold" engine is shown in fig(11). It is shown that the constant speed characteristics is moved to a higher value and the surge pressure ratio (at a mass flow) is also increased.

Research carried out to quantify these effects Ref(13) has led to the following expression for change in effective speed :

$$\frac{\Delta N}{N} = C_1 \frac{T_b - T_{air}}{T_{air}} + C_2 \frac{\dot{Q}}{\dot{m} C_P T_m} \qquad (6)$$

and for the revised surge pressure ratio, the equation is :

$$\frac{R_{ht} - 1}{R_{ad} - 1} = 1 + C_3 f - C_4 \frac{\Delta(\delta)}{g} \qquad (7)$$

For a typical two spool turbofan H.P compressor the values of coefficients C_1, C_2, C_3 and C_4 have been predicted Ref(14) to be -0.1, -0.1, 0.36 and 1.1 respectively.

1.8.1.4 CHANGES AND EFFECT OF TIP CLEARANCES ON EFFICIENCY

A brief summary is given here on how tip clearances changes effect efficiency. More complete details are given in the original Paper Ref(15) and Ref(16).

Tip clearances depend on the growth of discs, blades and casing. The disc is represented by a massive hub, a thinner diaphragm and then an outer rim to which the blade is attached. Primarily, temperatures of both the hub and diaphragm are controlled by the air drawn from an appropriate stage of the compressor. The rim temperature follows the influence of the internal air as well as the external gas flow. Heat transfer equations are used to calculate disc outer rim expansions assuming that the interfaces were not allowed to move apart. After comparing this disc outer rim expansion with the one predicted by a finite element analysis of the complete disc, it was found that the movements predicted by the simplified model had to be scaled up by a factor of 1.3 to align them together. The blade expansions are more easily calculated. Finally casing expansions were found, the casing temperature being controlled by the temperature of the internal gas flow and by the external flows in the by-pass duct.

The predicted movements for the components of a characteristic stage in the H.P compressor of a two-spool engine turbofan are given in Ref(17).

The correlation of Lakshminarayana Ref(18) is used to establish the efficiency losses due to the blade tip clearances, and is given as :

$$\Delta\eta = \frac{0.7\lambda\psi}{\cos\beta_m}\left[1+10\left(\frac{\varphi\lambda A}{\psi\cos\beta_m}\right)^{0.5}\right] \qquad (8)$$

Thus changes in efficiency due to changes in tip clearance can be found.

Typical results are illustrated in fig(12), the tightening of the tip clearance of 0.1 mm is estimated to be worth an improvement of 0.6 per cent in compressor efficiency.

1.8.1.5 SEAL CLEARANCES CHANGES

For this model a two-spool engine is used as basis for illustrations. For this particular engine, the seals which are regarded as being important and investigated are an outer seal at the last stage of the H.P compressor and a seal on the H.P turbine disc.

The H.P compressor seal is designed just for a small amount of air escapes to the by-pass duct. The H.P turbine seal controls approximately a quarter of the cooling flow extracted from the compressor delivery. This flow is required for cooling the turbine blades. Both these seals have clearance opening that exceeds their design values at transients.

1.8.1.6 COMBUSTION DELAY

Saravanamuttoo Ref(22) has concluded that the delay is noticeable only in engines using vapourising burners. The two-spool turbofan used as illustration has pressure jet burners. This engine is therefore not affected by this type of delay.

CHAPTER II

PREDICTION OF CHARACTERISTICS OF A MULTI-STAGE AXIAL FLOW COMPRESSOR

2.1 INTRODUCTION

The Tay turbofan engine MK610 shown in fig(13) was designed around the core of the Spey RB-183-MK555. The wide chord fan and three stage I.P compressor are driven by a three stage L.P turbine which uses the latest technology. The cold by-pass air and hot exhaust are mixed in a forced mixer. The initial production versions are the Tay 610 and 620. The Tay 610 was qualified at a thrust level of 12,500 lb (sea level static) in June 1986.

The Tay MK650 gives a 9 per cent increase in maximum take off thrust and 15 per cent increase in maximum continuous, climb, and cruise thrusts achieved by a small increase in fan diameter and an advanced H.P turbine.

The proposed version of Tay MK670 version is to achieve a thrust of 17,500lb to re-engine aircraft in the 100-130 seat class, by an increase in fan diameter and extra stage in the I.P compressor with matching components.

This Chapter will indicate the two methods that have been employed to predict the overall characteristics of the proposed 4-stage I.P compressor. The first method is a very simple approach in which it is assumed that the work input in the additional stage equals the work input in each stage of the original 3-stage I.P

compressor, and that the small-stage, or polytropic, efficiency remains constant .

In the second method the flow through the compressor, row by row, has been predicted, using Howell's correlation and rules.

2.2 PREDICTION ON EQUAL WORK INPUT ASSUMPTION

First it is assumed that the work input in each stage of the original 3-stage compressor is equal at each individual condition within the overall operating area of the compressor.

It is then assumed that when the fourth stage is added, the work input in that stage equals the work input of each of the original stages. The final assumption is that the small-stage, or polytropic, efficiency of each stage is the same, at any one condition.

On the basis of these assumption, the overall characteristics of the 4-stage compressor can readily be predicted from the supplied characteristics of the 3-stage compressor- see Appendix A.

2.3.PREDICTION BY ROW-BY-ROW PROCEDURE

This is a much more detailed approach and takes account of the alteration of the stage matching at operating conditions, such as how the ratio of axial velocity to mean blade speed, varies. The method uses the correlation and rules developed by Howell Ref(19).

2.3.1 HOWELL'S RULES

In general, the complete design process for the compressor will

encompass the following steps. These steps are as follows:

1) Choice of rotational speed and annulus dimensions.

2) Determination of number of stages, using an assumed efficiency.

3) Calculation of the air angles for each stage at the mean radius.

4) Determination of the variation of the air angles from root to tip.

5) Investigation of compressibility effects.

6) Selection of compressor blading.

7) Check of efficiency previously assumed using the cascade data.

8) Estimation of off-design performance.

9) Rig testing.

Howell's rules are the results of a large number of cascade tests of the flow in various geometries of compressor blades.

This method involves stage by stage calculation using basic aerodynamic relationships as defined in appendix B and generalised design curves are shown in figs(14-26).

Maccallum and Grant Ref(12) have used a developed row by row method to investigate a multi-stage H.P compressor (12 stage). The development included allowance for compressible flow within the blade row passages. The results obtained showed a good agreement with test results.

This method requires the following data, the absolute air inlet angle approaching the first row or rotor blades, the blades inlet and outlet angles for all rows of rotor and stator blades. Other important geometric values of blade height, blade mean diameter, mean blade spacing, and mean chord are also needed.

By the use of velocity triangles the flow directions and velocities, and the work done are determined fig(14).

Refering to fig(15) the form of the blade is defined by its camber

angle, θ, position of maximum camber, (a/c), maximum thickness, (t/c). Upon the above references the blade form is decided. The ratio of pitch/chord (s/c) and the angle at which the blade is set must be known to determine the actual cascade.

By equating the momentum and pressure forces acting perpendicular to and along the cascade to the corresponding components of the lift and drag forces, this can prove that the fluid angles α_1 and α_2 and the mean total head pressure loss ω are related to the lift and drag coefficient by the following equation:

$$C_L = 2(s / c)(\tan\alpha_1 - \tan\alpha_2)\cos\alpha_m - C_D \tan\alpha_m$$

$$C_D = (s / c)(\varpi / (\tfrac{1}{2})\rho V_1^2)\cos^3\alpha_m / \cos^2\alpha_1$$

where α_m is obtained from

$$\tan\alpha_m = (1/2)(\tan\alpha_1 + \tan\alpha_2).$$

2.3.1.1 ESTIMATION OF BLADE ANGLES AND HEIGHTS IN 4-STAGE COMPRESSOR

In this prediction a knowledge of the geometry of each row of blades is necessary. The geometry of the 3-stage compressor was known, and is given as mean blade diameters, blade heights and blade angles, in Table 2.1. However the new geometry of the 4-stage compressor had not been provided to the writer, except the mean blade diameters. Thus estimates must be made of the geometry of the 4-stage compressor. First assumption was that the first three stages

of the new compressor would be the same as the original 3-stage compressor. The height of the new 4^{th} stage would be reduced according to an extrapolation. After which it was assumed that the blade angles of the original 3^{rd} stage would be used in the new 4^{th} stage, essentially to achieve axial flow at exit from the compressor. Finally it was assumed that the blade angles of the new 3^{rd} stage would be improved by extrapolation from the angles of the first two stages. Some rounding of values was done to avoid possible discontinuities. The resulting values are shown in Table 2.1.

2.3.1.2 DEFINITION OF THE NOMINAL DESIGN POINT

Typical low-speed cascade results are plotted in fig(16). The incidence *i* is defined as the difference between the fluid inlet angle α_1 and the blade inlet angle β_1, and the deflection ε is defined by the difference between the inlet angle of the fluid α_1 and the outlet angle of the fluid α_2, but for design purpose we operate on the so called "nominal" deflection $\varepsilon*$ which is equal to 0.8 of the stalling deflection ε, and the corresponding fluid outlet angle α_2*.

In design, it is desirable to use the nominal values, as they are the key for the axial compressor design and performance. It has been found that the nominal deflection $\varepsilon*$ was dependent on three variables, the fluid outlet angle, the pitch/chord ratio, and the blade camber in most compressor cascades.

A typical variation of these variables is shown in fig(17). The corresponding values of the outlet fluid angle α_2 for various values of (s/c) are given in fig(18). A study of fig(19) and fig(20) shows that the figures contain enough information to enable one to calculate the theoretical corresponding values of lift coefficient C_L and pressure

recovery $(\Delta P / \frac{1}{2}\rho V_1^2)$.

2.3.1.3.OFF DESIGN CONDITION

For performance at other than nominal incidence i^*, fig(21) can be used where the deflection and incidence are plotted as ratios of their own nominal values and the corresponding drag coefficient has also been incorporated.

The outlet angle of the fluid α_2 could vary from 0 to 60 deg, thus, it is important for a designer to fix this angle accurately. A simple empirical rule has been derived from theoretical and experimental results which led to the deviation at a nominal condition, and given by:

$$\delta^* = m\theta\sqrt{(s/c)}$$

where $$m = 0.23\left(\frac{2a}{c}\right)^2 + 0.1\left(\frac{\alpha_2^*}{50}\right)$$

and where (a/c) is the position of the maximum camber.

2.3.1.4. CRITICAL MACH NUMBER AND MAXIMUM MACH NUMBER

One other important factor is the critical Mach number M_{nc}. For a high speed cascade the characteristics are very similar to those for low speed until the M_{nc} is reached after which the losses are greater with an increase in Mach number until, when the maximum Mach number M_{nm} is reached, there is no pressure rise due to large losses. Fig(22) shows the relation between M_{nc} and M_{nm} for a typical cascade

plotted versus incidence. Fig(23) shows that the maximum Mach number M_{nm} is highly dependent on the throat width/inlet width ratio for any cascade.

2.3.1.5 DEFINITION OF SURGE LINE

In design performance, the knowledge of the position of the surge line is essential. One possible approach is to draw the surge line through the maximum pressure ratio points of the performance map Ref(20).

2.4 COMPARISON OF THE TWO METHODS

In the present investigation both the equal stage work input and row-by-row methods have been applied to the 4-stage compressor.

In the row-by-row method, arbitrary factors such as the "work done" factor fig(24) have to be introduced to make an adjustment between the prediction and experiment. With these factors, the predictions of the shapes of the constant speed lines and the position of the surge line represent a reasonable agreement with the experimental results.

Comparing the predictions of the two methods, reasonably good agreement was obtained Fig(25 and 26).

For this present analysis, the equal stage work input method was chosen for the prediction of the 4-stage compressor, because it is easier, quicker and does not require lengthy calculations. This analysis, and the results, are described in the next Chapter III.

CHAPTER III

SCALING OF THE COMPONENTS FOR THE TAY MK670 ENGINE FROM TAY MK610 COMPONENTS

3.1 INTRODUCTION

The definition of the design point for the Tay MK670 engine had been prepared by Rolls-Royce. The condition was for maximum Take-Off at sea level, with Mach Number effectively zero. The conditions on an I.S.A day, are given in Table 3.1.

As indicated earlier, in order to achieve this thrust at these shaft speeds, Rolls-Royce proposed to use a 4-stage I.P compressor instead of the 3-stage compressor of the MK610 engine and to use a Fan of 0.6223 m Outer Diameter instead of the original Fan of Diameter 0.5629 m.

In this chapter, descriptions are given of how the characteristics of the new Fan and new I.P compressor can be predicted.

3.2 SCALING FACTORS

The engine performance prediction program to be used incorporates scaling factors which allow general adjustments. The definitions of these scaling factors are given in Table 3.2. Both Tables 3.3 and 3.4 display the values of these factors.

Although the relationship between compressor delivery pressure P_2 and intake pressure P_1, and intake temperature T_1 and the shaft speed N is very complex, a simple relationship is found to emerge for all externally applied conditions.

The non-dimensional pressure ratio term P_2/P_1 is related to corrected speed $\frac{N}{\sqrt{T_1}}$ and normalized mass flow $\frac{\dot{m}\sqrt{T_1}}{P_1}$. This relationship can be demonstrated by dimensional analysis Ref(Maccallum lecture notes).

3.3 FAN

For the MK670 engine the fan tip diameter is increased from 0.5629 m to 0.6223 m i.e an increase of 10 per cent.

The fan hub diameter is scaled accordingly. Thus the flow area is increased and also the mean blade diameter has increased. Considering the effect of the latter, use must be made of the true non-dimensional speed group $\frac{ND}{\sqrt{RT_{in}}}$.

Consequently for equivalent performance points:

$$\left(\frac{ND}{\sqrt{RT_{in}}}\right)_{ENG} = \left(\frac{ND}{\sqrt{RT_{in}}}\right)_{CHICS}$$

or

$$\left(\frac{N}{\sqrt{T_{in}}}\right)_{ENG} = \left(\frac{N}{\sqrt{T_{in}}}\right)_{CHICS} \times \frac{D_{610}}{D_{670}} \qquad (1)$$

ie

$$\left(\frac{N}{\sqrt{T_{in}}}\right)_{ENG\,(670)} = \left(\frac{N}{\sqrt{T_{in}}}\right)_{CHICS\,(610)} \times 0.905$$

The characteristics for the fan of medium and high by-pass ratio Turbofan engines differ markedly from blade hub to blade tip. One method of making allowance for this is to have separate characteristics for the inner and outer sections of the fan, where the inner fan compresses the core flow air and the outer fan compresses the by-pass air.

This procedure had been adopted for the original Tay engine MK610 and it has been continued in the present work for the MK670 engine.

Thus the multiplying factor of 0.905 should be applied to both sets of $(N/\sqrt{T})$ characteristics values for the MK610 engine to give the corresponding $(N/\sqrt{T})$ values for the MK670 engine. So C23=0.905 and C44=0.905 for the Inner and Outer Fans respectively (see Table 3.3).

3.3.1 INNER FAN

At take-off, from Table 1, the non-dimensional speed $\left(\frac{N}{\sqrt{T_{in}}}\right)_{ENG}$ at

the design point=408.4 and from the relationship above:

$$\left(\frac{N}{\sqrt{T_{in}}}\right)_{CHICS} = \frac{\left(\frac{N}{\sqrt{T_{in}}}\right)_{ENG}}{C23}$$

Thus the non-dimensional speed of the characteristics is found to be 451.3.

The corresponding value of the pressure ratio at $\frac{N}{\sqrt{T_{in}}} = 451.3$ is read from the characteristics block of the reference engine and found to be:

$$\left(\frac{P_{24}}{P_1}\right)_{CHICS} = 1.5535$$

$$\text{but } \left(\frac{P_{24}}{P_1}\right)_{ENG} = 1.66$$

from which the value of C21 is found :

$$\left[\left(\frac{P_{24}}{P_1} - 1.0\right)\right]_{ENG} = \left[\left(\frac{P_{24}}{P_1} - 1.0\right)\right]_{CHICS} \times C21 \qquad (2)$$

ie C21=1.1924.

(Note: the coefficient is applied to the pressure rise component ie(pressure ratio-1.0)).

By interpolating, the Alpha value(distance between two non-dimensional speed lines) is calculated and found to be 6.55 ie the equivalent design point value is located between the sixth and the seventh speed line at 0.55 from the sixth speed line.

Similarly, the non-dimensional mass flow of the engine is

given to be 148.0 and the equivalent non-dimensional mass flow of the characteristics is equal to 122.6, the ratio of these two values gives the value of factor needed C18 which is evaluated to be 1.207 from the equation below:

$$\left(\frac{\dot{m}\sqrt{T_{in}}}{P_{in}}\right)_{ENG} = \left(\frac{\dot{m}\sqrt{T_{in}}}{P_{in}}\right)_{CHICS} \times C18 \qquad (3)$$

At the last stage the values of efficiency in both cases are to be determined. The efficiency of the engine is provided in table 1 and equal to 0.936. The corresponding efficiency of the characteristics is found to 0.891, thus the difference of the two gives the factor D9.of 0.04492 from the equation below:

$$\eta_{ENG} = \eta_{CHICS} + D9 \qquad (4)$$

3.3.2 OUTER FAN

From above the factor C44 on the non-dimensional speed is found to be 0.905. The same procedure as above is taken to obtain the other factors.

At take off at the design point, the non-dimensional speed $\left(\frac{N}{\sqrt{T_{in}}}\right)_{ENG}$ is 408.4 and from Equation (1) the non-dimensional speed $\left(\frac{N}{\sqrt{T_{in}}}\right)_{CHICS}$ is 451.3. The pressure ratio of the engine from table available from Rolls-Royce 1.78 and the equivalent value of this in the characteristics is 1.68. Thus from Equation (2) the

factor C43 was found to be 1.147.

By interpolating the Alpha values, the distance between the non-dimensional speed lines was 0.538 from the sixth line.

The equivalent value of the capacity of the characteristics is calculated to be 356.71, and the capacity provided at the design point is to be 429.6 and again, the ratio of these two values

$$\left(\frac{\dot{m}\sqrt{T_{in}}}{P_{in}}\right)_{ENG} \div \left(\frac{\dot{m}\sqrt{T_{in}}}{P_{in}}\right)_{CHICS}$$

gives the value of the factor needed C41 and equal to 1.204. This value is within 1.5 per cent of the value of the square of the ratio of the fan tip diameters which is regarded as satisfactory agreement.

The efficiency at the design point is equal to 0.856 and the corresponding efficiency at characteristics at Alpha equal to 6.538 is found to be 0.8551and from Equation (4) the factor D42 is calculated to be 0.0009.

3.4 IP COMPRESSOR

In this component, for the Tay MK670 the mean diameter of the blades is needed to calculate the factor C34. From the overall engine schematic the mean diameter of the blades was increased from 0.5654 m to 0.6154 m ie an increase of 8 per cent. The factor C34 is obtained by using Equation (1) and found to be equal to 0.9189 (Table 3.4).

At maximum Take-Off condition the non-dimensional speed is provided in Table 3.1 and is 378 and its corresponding value in

the characteristics is 411.36. Now the equivalent value for the pressure ratio is read from the characteristics of the three-stage compressor of the reference engine and found to be equal to 1.445 after which we can easily find the Alpha value of this point and is to be 6.9763.

After locating the position of the design point in the 3-stage characteristics, the 4-stage characteristics are now used to determine the corresponding value of the factor C31 which is obtained from the Equation (3) and found to be 1.2459 where:

$$\left(\frac{\dot{m}\sqrt{T_{in}}}{P_{in}}\right)_{ENG} = 96.1 \quad \text{and} \quad \left(\frac{\dot{m}\sqrt{T_{in}}}{P_{in}}\right)_{CHICS} = 77.129$$

Now the pressure ratio of the 4-stage compressor which corresponds to the design point is found to be 1.6203 and the pressure ratio available from Table 3.1 is given and equal to 1.77 and by applying Equation (2) the factor C33 is determined to be 1.2413.

Finally, the efficiency block is used with the same procedure to evaluate the characteristics efficiency and then the deduction of the engine efficiency from the characteristics efficiency gives the value of factor D32 and equated to be 0.00409 which was obtained from Equation (4).

3.5 HP COMPRESSOR

This component, which is basically unaltered, is to be matched with the new Fan and the 4-stage I.P compressor. So, in order to match the higher $\left(\frac{\dot{m}_{24}\sqrt{T_{24}}}{P_{24}}\right)$

into the I.P compressor with the fixed capacity $\left(\frac{\dot{m}_{26}\sqrt{T_{26}}}{P_{26}}\right)$ into the H.P compressor, P_{26} is forced up. Experience of the H.P compressor in service also indicates that the efficiency is higher than the values given in the characteristics data for the MK610 engine.

At the maximum take-off, the non-dimensional speed of the engine is given to be 611.9, and the non-dimensional mass flow is 59.3, and the pressure ratio is 6.83. The use of the Equation (4) in Table 3.2, with the original factor for the non-dimensional speed, gives the capacity of the characteristics as being equal to 56.2, the pressure ratio being the MK610 working line value of 6.70. The ratio of these two capacity of 59.3 and 56.2 values gives the factor C7 equal to 1.0551.

From Equation (3) in Table 3.2 and pressure ratios of 6.83 for the MK670 and 6.70 for the MK610, the factor C22 is found to be 1.0225.

Hence the efficiency factor D1 is calculated from Equation (2) in Table 3.2, where the efficiency of the characteristics is 0.847 and the engine efficiency is 0.871 giving the factor D1 equal to 0.0315.

3.6 HP TURBINE

The altered compressor components did not affect the downstream components behaviour. Thus, use of the same H.P turbine was desirable.

3.7 LP TURBINE

For matching this component with the reference component an increase of 2 per cent was necessary in the capacity factor C11.

3.8 COLD AND HOT CHUTE AREA

Rolls-Royce suggested the use of the larger areas for the engine to give a reasonable steady-working lines for the components. An increase of 19 per cent for both cold and hot chute areas is used in this investigation.

3.9 FINAL NOZZLE AREA

The final nozzle area is adjusted to match all other components of the engine, so a 16 per cent increase is adopted in this New Engine to give a matching steady-working line for the components.

3.10 SHAFT INERTIAS

The polar moments of inertia used for the Reference Engine were 10.96 and 3.58 kg m^2 for the LP and HP shafts respectively.

For the New Engine the values used are 15.0 and 3.58 kg m^2 for these two shafts. These values give the appropriate ratio increase in LP shaft inertia increase, assuming the HP shaft is unchanged. [In practice the HP shaft inertia was increased some 20 per cent due to heavier materials being used in the HP turbine and the LP shaft inertia in practice was also 20 per cent higher than the figure of 15.0 kg m^2. However the simpler procedure of scaling up only the LP shaft inertia has been adopted to simplify the subsequent comparisons which are to investigate the effect of changes in the LP compression system only].

The effect of using higher values of LP shaft inertia of 20 and 25 kg m^2 are illustrated and discussed in Chapter 6.

3.11 SUMMARY OF FACTORS

All these factors are displayed in Tables 3.2, 3.3 and 3.4.

The results of using these factors to predict the performance of the New Engine are discussed in the next chapter.

CHAPTER IV

PREDICTED STEADY RUNNING AND TRANSIENT PERFORMANCE OF ENGINE TAY MK670

4.1 INTRODUCTION

When designing gas turbines, the first requirement is to predict the performance of the various components - compressors and turbines. Once these components characteristics have been established, the steady-state performance of the whole engine can be evaluated. As the design and development of the engine and its components progresses, the predicted characteristics of the components can be substituted by experimental characteristics, for example taken from rig tests.

4.2 SIMULATION OF THE TAY MK670 USING THE INTERCOMPONENT VOLUME METHOD

The resulting engine develops a maximum thrust at sea level, Mach 0.2, of about 15,600 lbf.

The computational procedure for this two-spool engine which is shown diagrammatically in Diagram 4.1 is described briefly below. The details of the procedure and the equation are given in Appendix C.

The simulation program is written in FORTRAN 77. This was first run on a digital computer mainframe system ICL2988 available at Glasgow University Computer Center (G.U.C.C) and now is available on the IBM 3080 on CMS. It was the latter facility which was used in the present work at Glasgow University Department of Mechanical Engineering.

The computational procedure used in this investigation is based upon the characteristics of each of the engine components. For the compressors - Inner Fan, Outer Fan, I.P and H.P - these are stored as a table of a number of non-dimensional speed lines with a number of points on each line. For each point, the pressure ratio, non-dimensional mass flow rate and isentropic efficiency values are listed.

First, provision for interchange of flow between the two sections of the fan was introduced. The characteristics initially provided were made basically on frontal area split in the ratio 1 to 3 between the Inner and Outer sections of the fan. This was quantified by parameter called GEOM which is defined as the fraction of the total frontal area allocated to the Inner section in the initial characteristics. Thus GEOM was assumed to be 0.25. Then, the next step is to allow for interchange of flow between these two components. It was assumed that the axial component of velocity of the air into the Fan is constant, at any instant, over the whole annular area, and that the fraction of this area which is the Inner fan is not necessarily equal to GEOM, but is some fraction of it. This fraction of split is called Fraction of Split (FCSP) which is calculated in the program at each time interval.

The requirement for starting this digital simulation of two-spool gas turbine engine is the selection of the initial shaft speeds together with the externally applied conditions of the fuel flow, ambient temperature, pressure and flight Mach number. Guessed pressure values, corresponding to the six volumes are also specified.

The engine stagnation entry conditions are calculated from the flight Mach Number and ambient static pressure and temperature. A pressure recovery factor of 0.995 is used in the intake calculations to account for non-dimensional diffusion losses (see Appendix C).

4.2.1 FAN

The fan is treated as two separate components as stated earlier, the Inner and Outer fans (see sections 3.3 and 4.2). The logic of this split, which is assumed not to be fixed at all time intervals, has been employed previously in the Tay Continuity of Mass Flow simulator and proved to be successful and has produced satisfactory results.

4.2.1.1 OUTER FAN

The inlet temperature and pressure ratio and non-dimensional speed of the Outer fan are the known parameters at the start of the calculation. The parameters GEOM and FSCP are then used to correct for the actual value of the non-dimensional mass flow rate. From the known parameters, the mass flow rate through the Outer fan can be calculated. Then the isentropic exit temperature

is calculated together with the isentropic efficiency from which the actual exit temperature can be found (see Appendix C).

4.2.1.2 INNER FAN

Due to to the horizontal nature of the pressure ratio of the characteristics of this component, another logic has been used to determine the exit parameters. The known inlet values are, pressure, temperature and non-dimensional speed. The mass flow through the Outer Fan is also known. By the use of both GEOM and FSCP, and assuming uniform inlet velocity, the mass flow rate through the Inner fan can be calculated. The known inlet temperature and pressure allow the calculation of the non-dimensional mass flow rate. Entering with non-dimensional mass flow rate allows the determination, with interpolation if necessary, of the pressure ratio and isentropic efficiency. By knowing the inlet pressure, the outlet pressure could be obtained. The outlet temperature is found in the same manner as that in the Outer Fan (see Appendix C).

4.2.2 I.P COMPRESSOR

The calculation proceeds in a similar way to that for the Outer Fan. Inlet pressure and temperature, non-dimensional speed and pressure ratio are the known parameters at the beginning of the calculation. The use of interpolation gives non-dimensional mass flow rate and isentropic efficiency. The inlet pressure and temperature are known. Therefore the physical

mass flow rate can be calculated. The same procedure to that for the Outer Fan is applied to obtain the I.P compressor outlet temperature (see Appendix C).

4.2.3 H.P COMPRESSOR

This component is handled in exactly the same way as the I.P compressor. The inlet parameters are known, from which the mass flow rate and exit temperature are then calculated (see Appendix C).

4.2.4 H.P TURBINE

The H.P compressor mass flow rate and the value of Cp from the combustion chamber are used as starting values. An initial guess for the efficiency is also made. The H.P turbine characteristics are tabulated as follows:

There are a total of 22 constant non-dimensional speed lines with 15 points on each line, for each point, there is a work factor and non-dimensional mass flow rate and isentropic efficiency. The γ value which is used to calculate an isentropic temperature change is obtained from C_p. The guessed efficiency is used to find an outlet temperature which allows a value of work factor to be calculated. By interpolation between work factor and non-dimensional speed a better value for efficiency is calculated and the outlet temperature is used to calculate a new value for C_p. Then a new value for C_p is adopted. Now the above loop is repeated five times. On the last loop, linear interpolation

is used on the work factor and non-dimensional speed to calculate a non-dimensional mass flow rate. As the inlet pressure and temperature are known, a physical mass flow rate is defined. The mass flow rate obtained is then used to revise the initially guessed mass flow rate. The above iterative procedure is repeated until the calculated and guessed mass flow rates match each other. Finally, the values for the exit temperature and mass flow rate are found (see Appendix C).

4.2.5 L.P TURBINE

The L.P turbine characteristics are stored in similar manner to those of the H.P Turbine.

The L.P turbine calculations are identical to those for the H.P turbine. The starting values for C_p and mass flow rate are taken as being for the gases leaving the H.P turbine.

4.3 PERFORMANCE OF THE ENGINES

The predicted performance of the complete engine is calculated by integrating the performance characteristics of the individual components.

In the present investigation, the Tay MK610 has been taken as the "Reference Engine". The characteristics of the components of this engine have been obtained mainly by experiment, or by matching with engine data. The performance of the engine and of its components is illustrated in figs (27-36). The information provided for the new design MK670 engine has been used to give the new set of component characteristics and the resulting

engine is referred to as the "New Engine".

The resulting predicted steady-state and transient performances of the New Engine and the Reference Engine are given in this Chapter. Because of lack of information on materials proposed for the New Engine, the transient performance predictions for both engines have been based on adiabatic assumptions.

4.3.1 THE REFERENCE ENGINE TAY MK610

Two flight conditions are important and have been selected as being the conditions at which comparison between the New and the Reference Engine should be made. These conditions are sea level, Mach 0.2, and altitude of 32,000 ft (10 km), Mach 0.8.

4.3.1.1 STEADY-STATE PERFORMANCE

Before the transient investigation, the steady-running prediction is necessary in order to find out the position of the working line on the characteristics of the various components. At sea level, Mach 0.2, the fuel flow of the Reference Engine operates between a maximum of 0.84 kg/s and a minimum of 0.095 kg/s. For the altitude case of 32,000 ft, Mach 0.8, maximum fuel flow of 0.25 kg/s and minimum fuel flow of 0.048 kg/s have been used as the defining end conditions.

At altitude of 32,000 ft, Mach 0.8, the predicted position of the steady working-lines for the Inner and Outer sections of the fan are slightly lowered. The explanation of this is that at the

high Mach Number, the final nozzle is choked, which gives the nozzle a high capacity. This makes it easier for the Fan to deliver air through the by-pass duct to the final nozzle, thus the working line in both fans is lowered figs(30 and 35).

Considering the predictions for the I.P compressor shown in the figs(31 and 36), the adiabatic operating line of the I.P compressor at Mach 0.8 at altitude is slightly raised from the one at sea level, Mach 0.2. The explanation for this is also related to the final nozzle becoming choked at Mach 0.8, and having a higher capacity. This easing of the restriction on the by-pass flow allows the fan and the L.P shaft to rotate slightly more rapidly, relative to the H.P shaft. Thus the I.P compressor, which provides the air to the H.P compressor is rotating more rapidly. But the non-dimensional flow into the H.P compressor will not have risen, so the I.P compressor has to operate against a higher outlet pressure, so its pressure ratio, and hence working line, is raised.

The H.P compressor results show that the working lines are almost the same for both cases.

4.3.1.2 TRANSIENT ACCELERATION

The adiabatic behaviour of all components of this engine are illustrated in figs(27 to 36). These simulations are applied for sea level, Mach 0.2, and altitude of 32,000 ft, and Mach 0.8.

The first transient illustrated is an acceleration which is carried out at the conditions mentioned above.

The idling speeds for this acceleration were 2185 r.p.m for

the LP shaft and 7376 r.p.m for the HP shaft at sea level, Mach 0.2, fig(26). At altitude of 32,000 ft, Mach 0.8, fig(31) the initial LP shaft and HP shaft speeds were 4190 r.p.m and 9339 r.p.m respectively. The maximum and minimum fuel flow limits adopted in this simulation were 0.84 kg/s and 0.25 kg/s and 0.099 kg/s and 0.058 kg/s at sea level, Mach 0.2, and at 32,000ft, above sea level, with Mach 0.8, in this order. The transient fuel flow was factored at 0.9 of the value provided by the Rolls-Royce "Spey" Schedule. This factor was fixed the same for both acceleration and deceleration transients, and for the two conditions sea level and altitude mentioned earlier. For reference see figs(27 and 32).

The thrust response at sea level, Mach 0.2, illustrated in fig(29) shows that the thrust starts at 3.25 per cent of its maximum and reaches 50 per cent in 5.0 seconds. It is seen that the thrust rises fairly slowly in the first 4 seconds of the acceleration and then rises rapidly for about 1.5 seconds until the maximum fuel flow of 0.84 kg/s is reached. In the remaining part of the transient the engine is stabilising towards the speed corresponding to this maximum fuel flow. The change from the slow rate of thrust increase to the rapid rate, which occurs at 4 seconds is due to the HP compressor reaching the speed where the $(N/(T)^{1/2})_{inlet}$ has the value 549 (rev/min $(K)^{1/2}$) when the 7^{th} stage bleed starts to close. This makes the engine cycle become more efficient and thus the acceleration becomes more rapid - hence the more rapid thrust rise. It is to be noted that while the LP-HP shaft speed relationships in accelerations and decelerations differ from the steady-running relationship, - fig(27) - the thrust response follows closely the response of the

LP shaft speed. This is to be expected because the net thrust is approximately proportional to the total air flow through the engine and this total air flow is primarily influenced by the LP shaft speed (the thrust is of course also proportional to the difference in relative velocities of gases at exit and inlet).

At altitude of 32,000 ft, Mach 0.8, fig(32) the thrust starts at 10 per cent of the maximum and 50 per cent thrust is reached in 1.5 seconds.

The LP-HP speed relationships at sea level, Mach 0.2, are plotted in fig(27).

The behaviour in the Inner and Outer sections of the fan can be seen from figure(30). At sea level, Mach 0.2, these trajectories predicted were found to be very similar to and move alongside the steady-working lines. At altitude of 32,000 ft, Mach 0.8, figure(35), there is a small departure from the steady-running line.

The predicted I.P compressor trajectories at sea level, Mach 0.2, fig(31) show that the transient acceleration trajectory starts along the steady-working line but then becomes significantly lower than the steady-working line. At altitude 32,000ft, Mach 0.8, fig(36), the transient acceleration trajectory is similarly lower. The explanation of this is given in section 5.4.2.

The predicted H.P compressor trajectory in the accelerations figs(31 and 36) rises above the steady-running line. This is because, when the fuel flow is increased to accelerate the engine, this raises the turbine inlet temperature. However the H.P turbine capacity group ($m\ (T_i)^{0.5}/P_i$) has to remain almost

constant, so to a first approximation the pressure at inlet to the H.P turbine has to rise, thus the H.P compressor delivery pressure and hence the H.P compressor pressure ratio have to increase. At sea level, Mach 0.2, fig(31), the trajectory is still significantly below the surge line.

However, at altitude of 32,000 ft, Mach 0.8, fig(36), the transient acceleration is close to the surge. In research experiments, it was found that as altitude increases the trajectories move closer to, and then cross the surge Ref(23) line. This is at least in part due to the effect of the lower Reynolds Number in the H.P compressor when at altitude. This causes thicker boundary layers and a resulting deterioration in the efficiency of the H.P compressor which raises the working line.

4.3.1.3 TRANSIENT DECELERATION

The adiabatic transient deceleration is then carried out at both sea level, Mach 0.2, and altitude of 32,000 ft, Mach 0.8. The starting speeds were the maximum speeds of the acceleration transient and at sea level, Mach 0.2, these were 8540 r.p.m and 12114 r.p.m for LP shaft and HP shaft respectively. In the case of altitude of 32,000 ft and Mach 0.8, the starting speeds were 7410 r.p.m and 10948 r.p.m. Maximum and minimum fuel flow limits of 0.0990 kg/s and 0.058 kg/s and 0.84 kg/s and 0.25 kg/s were used as the terminating conditions with the provided fuel schedule flow factor of 0.90 for both cases, sea level, Mach 0.2, and at 32,000 ft, Mach 0.8.

At sea level, Mach 0.2, the thrust reduced to 50 per cent in about 0.9 second, whereas at altitude of 32,000ft Mach 0.8 it is reduced to 50 per cent in 1.0 second.

Considering the transient trajectories, the predicted results obtained for this deceleration for the inner and outer fan fig(30), we can see that the deceleration trajectories can be seen to be moving closely and alongside with the steady-operating lines at sea level, Mach 0.2, but there is a small departure from the steady-working lines at altitude of 32,000 ft, Mach 0.8, fig(33).

For the I.P compressor predicted results fig(31), the adiabatic trajectories can be seen to move significantly above the steady-running line at sea level, Mach 0.2. The trajectory moves even closer to the revised surge line at altitude 32,000 ft, Mach 0.8, fig(36).

The predicted transient results for the H.P compressor, fig(31), show that at sea level, Mach 0.2, condition the transient was predicted to be moving below but close to the the steady-running line. At altitude 32,000 ft, Mach 0.8, fig(36), it was found to be moving closely below the steady-running line as well but not as close as in the case at sea level.

4.3.2 THE NEW ENGINE - TAY MK670

For a better comparison, the same conditions as the Reference Engine are used.

4.3.2.1 STEADY-STATE PERFORMANCE

The predicted performance of the engine and its components is

illustrated in figures(37 to 48). These simulations are applied for sea level, Mach 0.2, and altitude of 32,000 ft, and Mach 0.8, the same as for the Reference Engine, in order to give a good comparison between the two engines. The results are reported in this chapter and discussed in Chapter 5.

At sea level, Mach 0.2, the fuel flow operated between a minimum of 0.1 kg/s and maximum of 1.0 kg/s. This increase in fuel, relative to the Reference Engine, was due to the increase in the mass flow of the air entering the engine. The minimum and maximum shaft speeds were 1910 r.p.m and 8067 r.p.m and 7204 r.p.m and 12426 r.p.m for the LP and HP shafts, fig(38). At altitude of 32,000 ft, Mach 0.8, the minimum fuel flow was 0.065 kg/s and the maximum was 0.3 kg/s, the idling speeds for the LP and HP shafts were 3698 r.p.m and 9592 r.p.m and the maximum were 6654 r.p.m and 11392 r.p.m fig(44).

The steady-running fuel flow line, expressed non-dimensionally as ($f / N_H P_{26}$) was found to be lower than for the Reference Engine. This is primarily due to the efficiency of the H.P compressor of the MK670 engine being 3.9 per cent higher than the efficiency of the corresponding component in the MK610 engine (see Factor D1 in Table 3.2). Thus the fuel flow factor needed to be adjusted to give the same thrust response as the Reference Engine.

The behaviour of the Inner and Outer sections of the fans, fig(41 and 47) show that the steady-working line for the case of altitude 32,000 ft, Mach 0.8, has shifted slightly down from the sea level, Mach 0.2, case. The explanation of this has been given in paragraph 4.3.1.1.

The operating line for the I.P compressor figs(42 and 48) show that the altitude steady-line is raised from the one at sea level in the same manner as had happened for the Reference Engine.

The H.P compressor results fig(42 and 48) did not show any major difference between the two flight conditions.

In summary, it is noted that, with the revised component characteristics and the revised control areas of final nozzle area 16 per cent increase, section 3.9 and mixer shute areas, both 19 per cent increases, section 3.8, reasonable steady-running lines are obtained in all components.

4.3.2.2 TRANSIENT ACCELERATION

The illustration of the adiabatic transient is carried out at sea level, Mach 0.2, and altitude of 32,000 ft, Mach 0.8. First at sea level, Mach 0.2, the idling speeds were chosen with comparison to the reference engine to give a starting thrust of 3.25 per cent of its maximum. The evaluated idling speeds were found to be 2080 r.p.m and 8500 r.p.m for the LP and HP shafts respectively. Minimum fuel flow used was 0.106 kg/s and maximum of 1.0 kg/s. An adjusted fuel schedule factor of 0.73 was used to give a thrust response from 3.25 per cent of maximum thrust, consistent with the Reference Engine. The same factor was also used for the acceleration at 32,000 ft, Mach 0.8. The fuel flow factor is lower for this engine than for the Reference Engine. The first reason for that is because the steady-running line of the fuel flow in this engine is lower, as discussed in section 4.3.2.1. Secondly, with the new 4-stage I.P

compressor, this delivers a higher pressure ratio making P_{26} higher which puts the function of the fuel lower, fig(37). The thrust response starts at 3.25 per cent and reaches 50 per cent in just over 5.0 seconds fig(40). This is identical with the response of the Reference Engine. The relationships between the LP-HP speeds is plotted in fig(37).

At altitude of 32,000 ft, Mach 0.8, the operating limit for the fuel flow was 0.065 kg/s to give a starting thrust of 10 per cent, and reaches 50 per cent in 2 seconds fig(45). This is a slightly slower response than for the Reference Engine which took 1.5 seconds. The values of the idling speeds were 3698 r.p.m and 9592 r.p.m fig(44).

The predicted transients for the Inner and Outer section of the fan can be seen in figure(41) for sea level, Mach 0.2, and figure(47) for altitude Mach 0.8, these trajectories were very similar to and move alongside with the steady-running line. There is a small departure from the steady-operating line in the altitude case.

The 4-stage I.P compressor results at sea level, Mach 0.2, fig(42), show that the predicted transient acceleration trajectory is significantly lower than the steady-running line, as occurred also for the Reference Engine. At altitude 32,000 ft, Mach 0.8, fig(48), the transient acceleration is also lower than the steady-working line.

The H.P compressor transient acceleration at sea level, Mach 0.2, fig(42), shows that the transient acceleration is significantly lower than the surge. At altitude 32,000 ft, Mach 0.8, the transient is slightly closer to the surge line.

4.3.2.3 TRANSIENT DECELERATION

The adiabatic transient deceleration was predicted at both sea level, Mach 0.2, and altitude 32,000 ft, Mach 0.8, conditions. Firstly, at the sea level, Mach 0.2, the maximum fuel flow was 1.0 kg/s with starting speeds of 7805 r.p.m and 12468 r.p.m for LP and HP shafts. The adjusted fuel flow factor used in this operation was 0.80 for both cases, sea level, Mach 0.2, and altitude 32,000 ft, Mach 0.8. Finally, at the altitude mentioned above, the starting speeds were 6654 r.p.m and 11392 r.p.m for both shafts respectively. The fuel factor was adjusted to the value of 0.80 to give the same response as for the thrust reduction of the Reference Engine. It is noticeable that the factor of the fuel for the New Engine is lower that for the Reference Engine although it gives the same response of both engines. The explanation for that has been given above in section 4.3.2.2. The thrust response at sea level, Mach 0.2, fig(40), was reduced to 50 per cent in roughly 0.8 seconds. In the case of altitude fig(45) it was reduced to 50 per cent in 1 second.

The predicted transients for the two sections of the fan at sea level, Mach 0.2, fig(41), were found to move closely and alongside with the steady-running line. At the altitude case there was a small departure from the steady-running line.

From the predicted 4-stage I.P compressor transient at sea level, Mach 0.2, fig(42), can be seen that the movement of the transient does not approach closely the revised surge line. At the altitude of 32,000 ft, Mach 0.8, the transient trajectory again does not approach the revised surge line too closely, fig(48).

Additional techniques for assigning the movements of the trajectories in the I.P compressor are introduced in Chapter 5.

The H.P compressor trajectories, figs(42 and 48), for both cases are found to move closely below the steady-operating line.

A detailed discussion of these results is given in the following Chapter.

CHAPTER V

DISCUSSION OF RESULTS FOR THE NEW ENGINE MK670 COMPARED WITH THE REFERENCE ENGINE MK610

5.1 INTRODUCTION

This chapter gives a discussion of the predicted results obtained from the present work for the New Engine MK670 and these results are to be compared with those from the Reference Engine MK610. The condition to be considered are still the same - at sea level, Mach 0.2, and altitude of 32,000 ft, Mach 0.8.

5.2 SHAFT SPEED RELATIONSHIP

The shaft speed relationship for the New Engine MK670 fig(37) shows a few changes, and makes a very interesting comparison with Reference Engine MK610 fig(27) in that it demonstrates quite clearly the movement of the steady-working line which is slightly higher but takes a similar shape of curve to that of the Reference Engine.

The LP shaft speed limits for the MK610 seems to be slightly larger than for the New Engine MK670 and the reason for this is due to the larger diameter of the fan of the New Engine MK670 together with a higher mean diameter of the 4-stage I.P compressor. This has the result that, for instance, the equivalent non-dimensional speed line of 86 for the I.P compressor for the Reference Engine becomes 79.5 for the New Engine MK670. Thus,

after scaling, the MK670 is expected to run at a lower LP shaft speed than the MK610 to give the equivalent mass flow rate for the Reference Engine. In this way, the penalty of the centrifugal loading is eased. It is seen from comparing figs(37 and 27) that for a given HP shaft speed, the LP shaft speed of the New Engine does indeed run slower than in the case for the Reference Engine.

5.3 SHAPES OF THRUST RESPONSES

At sea level, Mach 0.2, it had been arranged that, for both engines, the accelerations should start from engine speeds which gave 3.2 per cent of the respective maximum thrusts.

The coefficient on the fuel shedule of the New Engine is set to a value of 0.73 to give a 50 per cent thrust in 5.0 seconds as had been the case for the Reference Engine (see section 4.3.2.2). However, the rate of thrust rise in the rapidly rising part of the transient in the New Engine is less than in the Reference Engine, so 90 per cent of thrust is reached in 6.3 seconds for the New Engine whereas 90 per cent thrust is reached in 5.8 seconds in the case of the Reference Engine. The explanation of slower thrust increase in the New Engine MK670 is due to many factors. Principally it is due to the higher starting value of shaft speed N_H of 8500 r.p.m for the New Engine compared with a starting value of shaft speed N_H of 7376 r.p.m for the Reference Engine. The rapid thrust rise starts when N_H reaches roughly 10,000 r.p.m for both engines (it is at this condition that the H.P compressor 7^{th} stage bleed starts to close, so the engine accelerates more rapidly (see section 4.3.1.2)). So, there is no need for such rapid

acceleration for the New Engine to get N_H from 8500 r.p.m to N_H 10,000 r.p.m in 4 seconds compared with the Reference Engine starting at N_H of 7376 r.p.m to N_H 10,000 r.p.m in 4 seconds.

This eased acceleration schedule can be seen in fig(37 and 27) for New Engine and Reference Engine respectively. Typicaly the acceleration schedule line at pressure ratio of 4.0 is 16.5 per cent higher than steady-running line for the New Engine but in the Reference Engine the acceleration schedule line at pressure ratio equals to 4.0 is higher by 43.0 per cent from the steady-running line.

This eased acceleration schedule also means less rapid speed increase in the rapid acceleration period in the New Engine with comparison to the Reference Engine. So the rapid thrust increase in the New Engine is less rapid than the rapid increase with the Reference Engine.

For the transient deceleration at sea level, Mach 0.2, the thrust responses of both engines have shown very similar deceleration transient paths.

In the altitude case, for accelerations, both engines are set to start at 10 per cent of the maximum thrust fig(32 and 47). The Reference Engine MK610 reaches its 90 per cent thrust in 2 seconds and the New Engine MK670 reaches that value in 2.3 seconds. This difference is not very significant.

At sea level, Mach 0.2, the New Engine is capable of reaching a thrust of 15,600 lbf whereas the Reference Engine could only reach a thrust of 12,200 lbf. For the altitude case, a maximum thrust of 3,600 lbf and 2,700 lbf is reached for the two engines, MK670 and MK610 respectively.

The maximum thrust at the altitude case for both engines is

lower than the one at sea level case and the reason for that is the low air density and low pressure at that condition.

5.4 TRAJECTORIES IN COMPONENTS

The transient trajectories which are involved in this paragraph are those in the fans and the two compressors at the two conditions, sea level, Mach 0.2, and altitude 32,000 ft, Mach 0.8.

The results are discussed below.

5.4.1 INNER AND OUTER FAN

As stated earlier in section 3.3, this component during this investigation was treated as two different components - Inner fan which takes the mass flow of air to the core and Outer fan which takes the air which goes to the by-pass duct.

In both components at sea level, Mach 0.2, the transient trajectories for the two engines are very close to the steady-running lines in very similar manner.

At altitude, as was expected the steady-running lines and trajectories have shifted down for both fans due to high flight Mach Number which chokes the final nozzle (see section 4.3.1.1).

5.4.2 I.P COMPRESSOR

It has been noted in (sections 4.3.1.2, 4.3.1.3, 4.3.2.2 and 4.3.2.3) that the transient trajectories in the I.P compressor in both the acceleration and deceleration move significantly away

from the steady-running line - figs(31, 36, 42 and 48). In the acceleration, the trajectory starts very close along the steady-running line and then suddenly drops below it. This sudden displacement away from the steady-running line came at the same time as the change from the slow rate of increase of thrust to the rapid rate of increase. That change was associated with the 7^{th} stage bleed in the H.P compressor closing and the I.G.V's at the inlet of the H.P compressor beginning to open, which brought about rapid rate of shaft speed increase (section 4.3.1.2). When the I.G.V's at inlet to the H.P compressor are opening, the air demand $(m(T)^{0.5}/P)$ into that compressor rises rapidly. In order meet this requirement the pressure at delivery of the I.P compressor is forced to drop, relative to steady-running. So the trajectory in the I.P compressor drops below the steady-running line. The reverse process occurs in the deceleration and trajectories rise. This rise could cross the surge line. None of the present examples illustrated has met this condition, which is obviously a real danger.

It would be of interest to have some techniques of assessing quantitatively how the trajectories in the I.P compressor have moved, especially in deceleration, in order to compare between events in the I.P compressors of the two engines - Reference and New. It is suggested that one such method would be on compressor characteristics fig(31), to consider the ratio of the area encircled between the deceleration trajectory and steady-running line to the area between the steady-running line and the horizontal line at the pressure ratio equal to unity. The vertical lines would be such that the initial time interval is covered. This

suggestion is illustrated in fig(80). Taking the time limits as being, in the deceleration, from 0.0 second to 1.0 second this gives values for this ratio of 0.34 for the Reference Engine fig(31) and 0.29 for the New Engine fig(42) in the sea level, Mach 0.2, transients. The equivalent ratio in the altitude 32,000 ft, Mach 0.8, transient decelerations are 0.22 and 0.20 for the Reference Engine and the New Engine respectively.

Explanation is required for why the New Engine, with its 4-stage I.P compressor, experiences less severe I.P compressor deceleration trajectory movements than the Reference Engine, with its 3-stage I.P compressor. One suggestion to explain that is that the speed matching and speed ranges of the LP and HP shafts in the two engines are quite different, where the LP shaft speeds in New Engine are lower. The starting point at sea level, Mach 0.2, used in both engines, is a thrust of 3.2 per cent of the maximum thrust. These speed ranges are shown in Table 5.1. The possible effects of these altered speed ranges on the engine response, and in the I.P compressor in particular, are now considered.

5.4.2.1 EFFECTS IN I.P COMPRESSOR IN DECELERATION

The changes mentioned above in the speed ranges from the Reference to the New Engine, and specially the lowered LP speeds, have considerable effect on the kinetic energies stored in the shafts before the deceleration begins. Consequently, for the deceleration at sea level, the LP shaft in the New Engine has to loose some 4.66 MJ during deceleration, as compared with the 4.10 MJ for the Reference Engine. This is an increase of 14 per cent, even though the LP shaft inertia has gone up by 37 per cent.

For the New Engine, the HP shaft rotational Kinetic Energy to be lost is only 1.63 MJ, as compared with 1.81 MJ for the Reference Engine. These energy values, and differences are also displayed in Table 5.1. In addition, the powers absorbed in the compression systems on the two shafts immediately before the deceleration begins, have been calculated, these are also given in Table 5.1. It is noticeable that the power absorptions, which are a measure of braking effects on the shafts, are roughly 36 per cent and 19 per cent higher in the LP and HP shafts respectively in the New Engine as compared to the Reference Engine. For a first approximation to the relative difficulty of the decelerations, the two shafts can be summed, so, for the New Engine as compared with the Reference Engine, the rotational Kinetic Energy to be absorbed has gone up by 6 per cent, while the "braking" effect of the compressors has gone up by 26 per cent. As a result, the deceleration which is forced by fuel reduction should be "less severe" for the New Engine and the movement of the transient trajectory from the steady-running line should be less marked. This estimation in advance is in line with the slightly less severe deceleration schedule that was required - fig(37) compared with fig(27) - and the measurement of the trajectory displacements where the ratios were 0.29 compared with 0.34 described earlier in this section.

The summing of the two shafts of the engines, used above, was only a first approximation. More detailed analysis should comprise comparisons of the rotational kinetic energies and power absorption of the individual shafts. In the present example a suggestion would be that the LP shaft speed should have a

further delay from the HP shaft speed, and make the trajectory in the I.P compressor worse. Nevertheless it is thought that these are less significant effects, and the main effect is the small increase of the kinetic energy to be absorbed of the summed shaft system as compared with the larger increase in the aerodynamic "braking" ability.

5.4.3 HP COMPRESSOR

From idling to maximum speed the transient acceleration working line for the H.P compressor is raised from the steady state towards surge. It is very noticeable from figs(31 and 42) that there is a considerable overshoot in the non-dimensional speed before the engine stabilizes. This is due to an overshoot in the HP shaft speed, and a lagging of the LP shaft which causes the increase of the temperature at delivery from the I.P compressor to lag.

The transient trajectory in the acceleration in the New Engine does not rise quite as much above the steady-running line as had happened in the Reference Engine. This again can be quantified by measuring the areas between the trajectory and the steady-running line for the same non-dimensional speed range. This has been done between $(N/(T_{26})^{0.5})$ values of 560 and 650 for the sea level, Mach 0.2, acceleration. The area enclosed for the New Engine is only 0.75 of the area enclosed for the Reference Engine. For the 32,000 ft, Mach 0.8 case, the limits of non-dimensional speed $(N/(T_{26})^{0.5})$ used are 567.0 and 614.0, and a similar reduction, to a factor of 0.66 was measured. These reductions are

associated with the less severe acceleration schedules that were needed for the New Engine, as discussed in section 5.3.

For the decelerations, the movements of the trajectories are downwards from the steady-running line which are slightly less marked for the New Engine as compared with the Reference Engine. This is due to a less rapid deceleration schedule required by the New Engine, as discussed in section 5.4.2.1.

CHAPTER VI

EFFECT OF GEOMETRIC CHANGES

6.1 INTRODUCTION

This chapter discusses a number different geometric changes and their effects on various components of the engine. Each geometric change and its effect on the component are treated separately and the corresponding graphs are shown in figs(49-79). All these changes were applied to the New Engine (ie with 4-stage I.P compressor etc). The original version of this New Engine is used as datum in the comparisons which follow.

6.2 INERTIA ESTIMATION

The estimated moments of inertia used in the present work for the New Engine are 15.0 kg m^2 and 3.58 kg m^2 for the LP and HP shafts respectively, as compared with 10.96 kg m^2 and 3.58 kg m^2 for the Reference Engine. For further detail, see section 3.10.

It would be worth studying the effect of varying the L.P system inertia of the New Engine over a range of values. Additional inertia values for the L.P system of 20 and 25 kg m^2 have therefore been selected. The results obtained are shown in figs(49 - 58).

6.2.1 EFFECT OF L.P INERTIA ON THRUST RESPONSE

When increasing the inertia of the disc it was found necessary to revise the coefficient schedules to achieve the thrust responses in same times. These new coefficients were increased accordingly in acceleration and decreased in deceleration. For acceleration, the coefficients were increased to 0.735 and 0.74 from 0.73, and at deceleration the coefficients were decreased to 0.71 and 0.62 from 0.80 for inertia of 20 kg m^2 and 25 kg m^2 respectively see figs(50 and 55). Thrust response similar to those of the New Engine with LP inertia of 15.0 kg m^2 were then obtained.

6.2.2 EFFECT OF L.P INERTIA ON SHAFT SPEED RELATIONSHIPS

From figs(49 and 54) it is clearly noticeable that the transient working lines have moved further away from the steady-running lines and that was due to the higher inertia. The higher is the inertia, the higher the shift is, whether upwards or downwards depending on the transients. The steady-running lines were not affected at all.

6.2.3 EFFECT OF L.P INERTIA ON FAN SYSTEM

The trajectories in the Inner and Outer fans were not affected by the change of inertia, Figs(52 and 57), in either acceleration or deceleration transient. This is to be expected since the transient trajectories in these components virtually coincide with the steady-running lines.

6.2.4 EFFECT OF L.P INERTIA ON I.P AND H.P COMPRESSORS

With the originally selected LP inertia of 15.0 kg m^2 reasonable trajectories were predicted in the I.P and H.P compressor while achieving satisfactory thrust responses in the acceleration and deceleration. When the LP inertia is raised to 20 kg m^2 the trajectory in the H.P compressor during the acceleration is moved closer to surge fig(53) due to the higher fuel schedule coefficient that has to be used. With the LP inertia of 25 kg m^2 the further raised fuel schedule causes a further movement of the trajectory in the H.P compressor towards surge fig(58) and also the overshoot in $(N/(T_{26})^{0.5})$ is such that it moves beyond the highest of the tabulated values. In the I.P compressor, it is only during the deceleration that there is a danger of surge. It is seen that as the LP inertia is increased to 20 and then 25 kg m^2, the trajectory in the deceleration moves closer to surge and then actually surges. This deterioration is largely due to the move severe deceleration fuel schedules that have to be used in order to achieve the thrust reduction response.

In summary, raising the LP system inertia increases the departures of the trajectories in the I.P and H.P compressors if fuel schedules are revised in order to maintain the thrust responses.

6.3 EFFECT OF CONTROL AREA CHANGES

A few changes were made to investigate the effect of the change of areas on the transient trajectories of the engine. The

areas taken into consideration are the final nozzle area, air area at mixer, gas area at mixer and lastly the combination of the two.

6.3.1 FINAL NOZZLE AREA

An increase of 10 per cent was allowed in this investigation and the results obtained are discussed below. In this case the fuel flow factors in the transient fuel schedules have not been altered and so the thrust responses will differ from the datum.

6.3.1.1 EFFECT OF FINAL NOZZLE AREA ON SHAFT SPEEP RELATIONSHIPS

At the lower shaft speeds the relationship fig(59) showed a good agreement with datum engine. At the higher shaft speeds the HP shaft speed is reduced for a given LP shaft speed.

The explanation of this is that by increasing the final nozzle area the Outer fan the pressure ratio across LP turbine is increased, so the work output per unit mass flow rises and also the Outer fan has an easier duty (see section 6.3.1.3) and the LP shaft can speed up, for a given HP speed (ie for a given LP speed, the HP speed drops).

6.3.1.2 EFFECT OF FINAL NOZZLE AREA ON THRUST RESPONSE

The increase of final nozzle area has caused the thrust response at acceleration to reduce by 16 per cent compared to the datum engine. Further more it made the thrust responding half a second faster and steeper than the MK670 with the datum final

nozzle area.

Now at the deceleration case the response showed very little difference except as mentioned above the deceleration starts at a lower value of thrust than the designed engine MK670 with original provided value of the final nozzle area.

6.3.1.3 EFFECT OF FINAL NOZZLE AREA ON FAN SYSTEM

The change of final nozzle area has clearly affected the steady-running line of the outer fan. The steady-running line has shifted down as has obviously the trajectory in both transients. The same applied to the Inner fan where the shift downwards of steady-running line was less noticeable. The transient acceleration and deceleration trajectories were also lowered.The results are shown in fig(62).

6.3.1.4 EFFECT OF FINAL NOZZLE AREA ON THE LP &HP SYSTEM

The results plotted in fig(63) give a very clear idea on how the I.P compressor was considerably effected. The steady-running line has shifted above, especially at high non-dimensional speeds. The reason for this is that, as has been noted in sections 6.3.1.3 and 6.3.1.1, the pressure ratio working lines in the fan have been lowered and the LP shaft speed has increased, at an HP speed. The I.P compressor is therefore, to a first approximation, running at a higher $(N/(T_{24})^{0.5})$ but delivery to an H.P compressor which will accept only the same $(m(T_{26})^{0.5}/P_{26})$. Hence the pressure at I.P compressor exit, P_{26}, must rise. Pressure at inlet to I.P compressor, P24, has fallen, so pressure ratio across I.P

compressor rises, ie steady-running line rises. In the transient deceleration, the trajectory is very close to the surge line, and that is to be avoided. It is important to note that increasing the nozzle area in the two-spool turbofan moves the I.P steady-running line towards surge, which is the opposite effect to that obtained in a single-spool engine.

In the other hand, the H.P compressor does not seem to be effected at all, which was expected when the L.P turbine is choked.

It is noted that there is an increase in L.P turbine power resulting from the redistribution of pressure ratio between the L.P turbine and the nozzle. The major advantage of the use of the variable nozzle is that it permits selection of air flow and thrust independently. Ref(23) gives more detail about this and Ref(22) gives an excellent picture of the problems involved in matching the engine and intake for a supersonic transport.

6.3.2 AIR AREA AT MIXER

In the present work an increase of 5 per cent was allowed for the air area at the mixer to investigate its effect on the components of the engine. All the results obtained for this case are plotted in figs(64 - 68).

This condition did not affect the components of the engine except the acceleration transient response of the thrust. This thrust response seem to be 0.4 second faster than the datum engine. For the rest of the components no movements have been found.

6.3.3 GAS AREA AT MIXER

An allowance of 5 per cent decrease is made for this component to see how would this effect the engine, and the graphs are shown in figs(69 - 73). As above, the only thing effected was the thrust response in the acceleration, in which it is 0.45 second faster than the predicted MK670 engine.

6.3.4 AIR AREA PLUS GAS AREA AT MIXER

This condition gives the combination of the two previous conditions where an increase of 5 per cent was allowed for the air area at mixer and 5 per cent reduction in gas area at mixer which is expected to give a faster response by 0.85 seconds for the thrust in the acceleration and the predicted results are shown in figures(74 - 78).

The results show that the thrust response was faster by 0.6 seconds instead of 0.85 seconds. This small disagreement, which is probably partly due to non-linear behaviour of the engine and also inaccuracies in the modelling program, is not highly significant.

6.4 COMPONENT EFFICIENCY

In the current investigation a change in the efficiency of the H.P compressor was tested by reducing the factor D1 by 3 per cent. Fig(79) shows the graphs of the two components I.P and H.P

compressors. This condition has shown a significant results, where the H.P compressor steady-running line has shifted significantly upwards towards the surge line which leads the transient acceleration working line close to the surge. One interesting result which has come out is the movement of the steady-running line of the I.P compressor which on its turn has shifted upwards as well. This is because, with its less efficient H.P compressor, the HP shaft speed has been reduced, for a particular LP shaft speed. Thus, at that LP speed, the $(m(T_{26})^{0.5}/P_{26})$ capacity of the H.P compressor is reduced, so the I.P compressor delivery pressure, P_{26}, has to rise. Hence the steady-running line in the I.P compressor has to rise.

The trajectories in the I.P and H.P compressor have been shown, but their movements, relative to the steady-running lines, are the same as for the datum MK670 engine.

CHAPTER VII

CONCLUSIONS AND SUGGESTIONS FOR FURTHER WORK

7.1 GENERAL CONCLUSION

The modelling procedure for the prediction of the performance of a two-spool turbofan aircraft engine during steady-state and acceleration and deceleration transients existed already. That simulating program which was written by MACCALLUM Ref(24) was modified, slightly improved. It was then used to predict the performance of a Reference Turbofan Engine which had an I.P compressor having 3-stages.

The Engineer's manufacturer, Rolls-Royce, had proposed that a higher thrust engine be built, based on much of the Reference Engine, but with a larger fan and a 4-stage I.P compressor. The main purpose of the project was to predict the transient performance of this New Engine, and forecast if any potential dangers, particularly compressor surges, might occur. The first requirement in this project therefore was to predict the performance characteristics of the components being changed - the fan and the I.P compressor. The new characteristics of the fan were readily predicted using non-dimensional methods. For the I.P compressor, with its additional stage, two procedures were examined. The first method assumed equal work input per stage and uniform

polytropic index (ie constant polytropic efficiency). The second method was a row-by-row method using Howell's rules. The predictions by the two methods were found to be similar. The first method (equal work input) was therefore used as it was much simpler to apply.

The program uses the Inter-Component Volume (ICV) method which permitted accumulation, or release of flow, in the volumes between adjacent components.

The performance of the New Engine, both steady-state and transient, was then predicted from the engine program, using the newly predicted characteristics of the components (fan and I.P compressor) which had been modified. The New Engine at maximum speed developed 30 per cent more thrust at sea level than the Reference Engine. The accelerations at sea level started from 3.2 per cent of maximum thrust and the fuel schedules were adjusted to give similar times to 50 per cent thrust. In the same way the deceleration fuel schedules were adjusted to give similar thrust reduction responses.

Comparing the transient trajectories in the various components of the two engines, there were no dangerous excursions in the fans. In the I.P compressor the trajectories in the deceleration are easier in the New Engine than for the Reference Engine. This was quantified by the ratio of the area enclosed between the deceleration trajectory and steady-running line and the horizontal line at the pressure ratio equal 1.0 (see section 5.4.2). The two vertical lines represent the initial time interval used for comparison fig(80). These values for this ratio of 0.34 for the Reference

Engine and 0.29 for the New Engine, at sea level, Mach 0.2, the New Engine area is 85 per cent of the Reference Engine area. In the case of altitude of 32,000 ft, Mach 0.8, the equivalent ratios are 0.22 and 0.20 for MK610 and MK670 engines respectively. The area on New Engine is 90 per cent of the Reference Engine area. The explanation of this is the relatively small increase (6 percent) in rotational kinetic energy (summed) to be lost in the deceleration, compared with the increase of 26 per cent in the "braking" abilities of the compressors(summed). Thus a less severe deceleration fuel schedule is required.

In the H.P compressor, the areas are measured between the trajectory and the steady-running lines for the same non-dimensional speed range (section 5.4.3). The enclosed area for the New Engine is only a 75 per cent of the area for the Reference Engine, at sea level, Mach 0.2. At the altitude case, the area measured for the New Engine was 66 per cent of the area for the Reference Engine.

In the present work, an increase in final nozzle area was applied to see its effect on the performance of the New Engine, this increase has caused the thrust response at acceleration to reduce by 16 per cent compared to the datum engine (section 6.3.1.2), together with a reduction in HP shaft speed for a given LP shaft speed (section 6.3.1.1).

A change in the efficiency is also tested by reducing the factor D1 by 3 per cent. This showed a significant results, where the H.P compressor steady-running line has shifted highly towards the surge line which leads the transient acceleration working line to be close to the surge line. The

steady-running line of the I.P compressor has shifted on its turn upwards close to the surge line as well. The reason for that is explained in detail in section 6.4.

Neither bleeds nor change in variable inlet guide vane(IGV) were necessary in this investigation due to the easy transients responses in the I.P compressor.

7.2 SUGGESTIONS FOR FURTHER WORK

Due to the lack of incorporation of models describing heat transfer effects in gas turbine engine, where heat exchange occurs between the working fluid and the components of the engine. Therefore, the prediction of this New Engine performance including the heat transfer effects would be required.

A very important investigation is the fuel schedule adjustment when adding some stages to a compressor. It is also desirable to investigate the shaft speed decrease in the extra stage compressor.

It has been seen that the thrust increase could be achieved by adding another stage to the I.P compressor in a two-spool engine. An investigation of a great importance would be the case of adding another stage in the H.P compressor with probably more bleeds or change in inlet guide vane and compare the two engines.

REFERENCES

1) FAWKE, A.J. and SARAVANAMUTTOO, H.I.H.
"Digital computer methods for prediction of gas turbine dynamic response."
SAE Paper 710550, 1971.

2) FAWKE, A.J.
"Digital computer simulation of gas turbine dynamic behaviour."
PhD Thesis, 1970, University of Bristol.

3) STODDART, R.
"Prediction of the transient performance of the Rolls-Royce TAY engine using the method of Inter-Component Volumes."
Final Year Project for B.Eng Glasgow University, May 1987.

4) MACCALLUM, N.R.L
"Comparison of CMF and ICV methods for predicting gas turbine transient response."
Department of Mechanical Engineering Report, Glasgow University, August 1989.

5) PILIDIS, P. and MACCALLUM, N.R.L.
"The effect of heat transfer on gas turbine transients."
A.S.M.E. Paper 86-GT-275, 1986.

6) MACCALLUM, N.R.L.
"Axial compressor characteristics during transients."
AGARD Conf Proc No 324, Paper 22, 1982.

7) LARJOLA, J.
"Simulation of surge margin changes due to heat transfer effects in gas turbine transients."
A.S.M.E. Paper 84-GT-129, 1984.

8) PILIDIS, P. and MACCALLUM, N.R.L.
"A study of the prediction of tip and seal clearances and their effects on gas turbine transients."
A.S.M.E. Paper 84-GT-245, 1984.

9) MACCALLUM, N.R.L. and CHIA, B.H
"Thermal modeling of an aero-gas turbine combustor."
Department of Mechanical Engineering Report.
University of Glasgow, August 1989.

10) MACCALLUM, N.R.L.
"Effect of "bulk" heat transfer in aircraft gas turbines on compressor surge margins."
Heat and fluid flow in steam and Gas turbine plant,
I.Mech.Engrs., London, 1974, 94-100.

11) GRANT, A.D.
"The effect of heat transfer on boundary layer stability in axial flow compressors."
ibid, 252-258.

12) MACCALLUM, N.R.L. and GRANT, A.D.
"The effect of boundary layer changes due to transient heat transfer on the performance of an axial-flow air compressor."
S.A.E. Trans, March 4, 1977, 86, 770284.

13) MACCALLUM, N.R.L.
"Thermal influences in gas turbine transients - effects of changes in compressor characteristics."
A.S.M.E. Paper 79-GT-143, 1979.

14) MACCALLUM, N.R.L. and PILIDIS, P.
"The prediction of surge margins during gas turbine transients."
A.S.M.E. Paper 85-GT-208, 1985.

15) PILIDIS, P. and MACCALLUM, N.R.L.
"A study of the prediction of tip and seal clearances and their effect in gas turbine transients."
A.S.M.E. Paper, 84-GT-245, 1984.

16) PILIDIS, P.
"Digital simulation of gas turbine performance."
PhD Thesis, 1983, University of Glasgow.

17) MACCALLUM, N.R.L. and QI, O.F.
"The transient behaviour of aircraft gas turbines."
University of Glasgow, 15 Sep 1989.

18) LAKSHMINARAYANA, B.
"Methods of predicting the tip clearance effect in axial flow turbomachines."
J. basic Engng, 1970, 92, 467-480.

19) HOWELL, A.R.
"The present basis of axial flow compressor design."
Part 1. Cascade theory and performance, Aeronaut. Res. Counc. Rep. Memo. 2095, 1942.

20) AUBREY STONE.
"Effect of stage characteristics and matching on axial flow compressor performance."
Trans. ASME, Vol.80, p.1273-93, SAN-DIEGO, CALIF, August 1958.

21) SARAVANAMUTTOO, H.I.H., COHEN, H. and ROGERS, G.F.C.
"Gas turbine theory."
2nd edition (Longman), London 1972.

22) SARAVANAMUTTOO, H.I.H., FAWKE, A.J. and HOLMES, M.
"Experimental verification of a digital computer simulation method for predicting gas turbine dynamic behaviour."
I.Mech.Engrs. Proceedings 1972, Vol.186 27/72.

23) LARBI MERAHI.
"Gas turbine models for compensation of transient fuel flow schedules"
M.Sc thesis, Department of Mechanical Engineering, Glasgow University, 1988.

24) MACCALLUM, N.R.L.
"ICV prediction program for two-spool turbofan engine with common exhaust nozzle."
Program, Department of Mechanical Engineering, Glasgow University, May 1989.5

APPENDIX A

4-STAGE COMPRESSOR PERFORMANCE PREDICTION BY EQUAL STAGE WORK AND CONSTANT POLYTROPIC INDEX

The characteristics of the compressor of the Reference Engine is used in this calculations. Based on the values of the pressure ratios, the isentropic temperature T'_{26} can be calculated from the equation below :

$$\frac{T'_{26}}{T_{24}} = \left(\frac{P_{26}}{P_{24}}\right)^{\frac{\gamma-1}{\gamma}}$$

where γ is assumed to be 1.4.

Then, from the next equation below, a value of the stagnation temperature T_{26} is calculated :

$$(T_{26})_3 - T_{24} = \frac{1}{\eta_{ISEN}}\left(T'_{26} - T_{24}\right)$$

Now, the use of the equation below gives the value of the polytropic index group (n-1)/n :

$$\frac{(T_{26})_3}{T_{24}} = \left(\frac{P_{26}}{P_{24}}\right)^{\frac{n-1}{n}}$$

By obtaining this index group a further calculation is applied to get the value of the stagnation temperature$(T_{26})_4$ for the 4-stage

compressor :

$$\left[(T_{26})_4 - T_{24}\right] = \frac{4}{3}\left[(T_{26})_3 - T_{24}\right]$$

where $(T_{26})_4$ is defined to be the stagnation temperature for the 4-stage compressor.

The following equation gives the pressure ratio $(P_{26}/P_{24})_4$ of the 4-stage compressor:

$$\left(\frac{P_{26}}{P_{24}}\right)_4 = \left(\frac{(T_{26})_4}{T_{24}}\right)^{\frac{n}{n-1}}$$

The use of the equation below gives the isentropic temperature of the 4-stage compressor T'_{26}:

$$\frac{T'_{26}}{T_{24}} = \left(\frac{P_{26}}{P_{24}}\right)^{\frac{\gamma-1}{\gamma}}$$

Finally, the isentropic efficiency of the 4-stage compressor is determined from the equation below:

$$\eta_{ISEN} = \frac{T'_{26} - T_{24}}{T_{26} - T_{24}}$$

APPENDIX B

HOWELL'S RULES

After obtaining the nominal fluid angles α_1^* and α_2^*, the pitch/chord ratio (s/c) at the mean diameter can be found from fig(18), from which the aspect ration A=(h/c) for rotor could be assumed. Hence, the chord would be calculated knowing the height of the blade which defines the number of blades from the equation below:

$$n = \frac{2\pi \times \text{mean radius}}{s}$$

Similar procedure would be adopted to the stator where the 50 degree of reaction would be assumed to give the same design point values of flow coefficient (Va/u) and temperature rise coefficient ($C_p\Delta T_S/0.5^*u^2$) and an equivalent nominal deflection ε^*. The mean work done factor Ω is needed and can be calculated from fig(24).

The expressions of Howell's necessary to obtain the performance of 50 per cent reaction blading are given by:

$$\frac{V_a}{u} = \frac{1}{(\tan\alpha_1 + \tan\alpha_2)}$$

The nominal deflection ε^* which is equal to 0.80 of the stalling deflection ε of both rotor and stator are now determined. Then α_3^* and α_4^* are found. The nominal values of ($\tan\alpha_1$-$\tan\alpha_2$) and ($\tan\alpha_3$-$\tan\alpha_4$) which are different are computed, and the nominal point is chosen for both. The mean value of $\tan\alpha_2^*$ and $\tan\alpha_4^*$is found.

One other important item of information is necessary before the design of the blade. The blade inlet angle β_1 will be known from the

air inlet angle, but the outlet blade angle β_2 cannot be determined from the air outlet angle α_2 until deviation angle $\delta = \alpha_2 - \beta_2$ has been determined. An analysis of the relation between the air and blade outlet angles from cascade tests, shows that their difference is dependent mainly on blade camber and the pitch/chord ratio. It is also dependent on the shape of the camber-line of the blade section and on the air outlet angle itself. The following imperical equation gives the derived relationship:

$$\delta = m\theta\sqrt{(s/c)}$$

where

$$m = 0.23\left(\frac{2a}{c}\right)^2 + 0.1\left(\frac{\alpha_2}{50}\right)$$

a is the distance of the point of maximum camber from leading edge of the blade.

The position of the blade chord can be fixed relative to the axial direction by the stagger angle ζ given below:

$$\xi = \beta_2 - \frac{\theta}{2}$$

The following equations are used with the help of the figures to determine the stage performance.

$$\frac{C_P}{\frac{1}{2}u^2} = 2\Omega\frac{V_a}{u}(\tan\alpha_1 - \tan\alpha_2)$$

$$\eta_S = 1 - \frac{2}{\sin 2\alpha_m}\left(\frac{C_D}{C_L}\right)$$

$$\frac{\Delta P_S}{\frac{1}{2}\rho u^2} = \eta_S \times (C_P \Delta T_S / \tfrac{1}{2}u^2)$$

$$C_L = 2(s/c)(\tan\alpha_1 - \tan\alpha_2)\cos\alpha_m$$

$$C_L = 2(s/c)(\tan\alpha_1 - \tan\alpha_2)\cos\alpha_m$$

$$C_D = C_{DP} + C_{Da} + C_{Ds}$$

The value of C_{DP} is taken from graph fig(21), where C_{Da} and C_{DS} are given below:

$C_{Da} = 0.02 (s / h)$

and

$C_{DS} = 0.018\ C_L^2$

The value of C_{DP}, α_1 and α_2 for other points on the characteristics are found from fig(21) knowing that $(i-i^*)/\varepsilon^*$ is equivalent to

$(\alpha_1-\alpha_1^*)/\varepsilon^*$. The rest of the calculation is purely arithmetical.

APPENDIX C

THE ENGINE CALCULATION

(Note: Symbols P and T represent stagnation pressure and stagnation temperature respectively, unless carrying subscript, s, for static values).

1-INTAKE CALCULATIONS

Having the initial condition parameters (Flight Mach number, Ambient temperature and pressure), the entry stagnation Temperature and Pressure can be calculated by using the equation as follows:

$$T = T_{AMB} \times (1 + 0.2M^2)$$

$$P = \text{RECOVERY} \times P_{AMB} \times \left(\frac{T_1}{T_{AMB}}\right)^{3.5}$$

Where RECOVERY is the pressure recovery factor of 0.995 used to account for non-isentropic diffusion losses.

2.0 OUTER FAN

Known parameters	P_i, T_i, N, FCSP, GEOM=0.25
Guessed parameters	P_o

Required parameters m and T_o

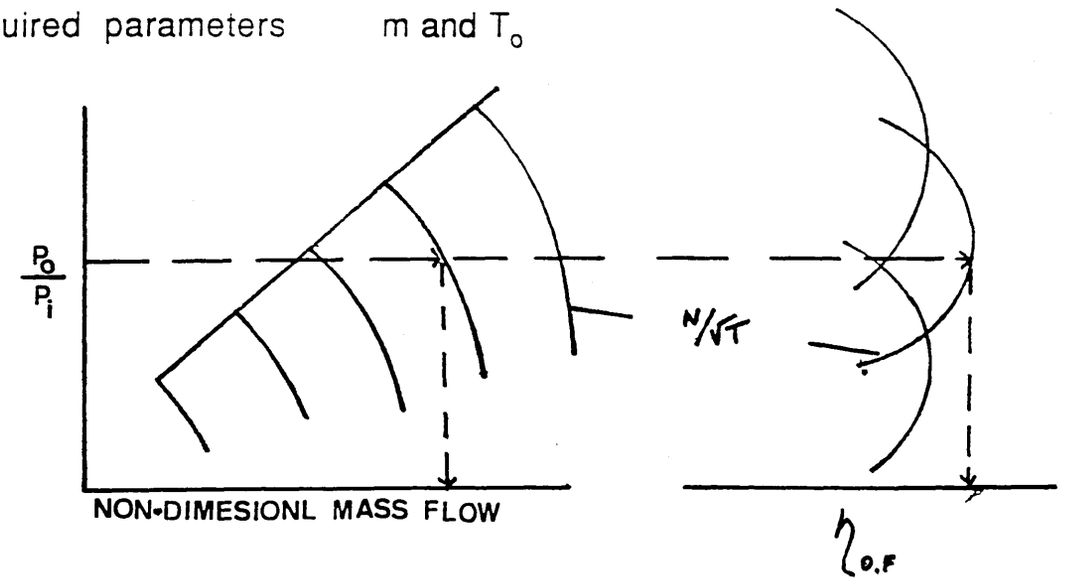

Capacity

1) Calculate Pressure Ratio and Non-dimensional Speed

2) Linear interpolation on characteristics defines the value of the Capacity.

3) The use of the equation below defines the actual Capacity:

$$\left(\frac{\dot{m}\sqrt{T_i}}{P_i}\right)_{ACT} = \left(\frac{1-GEOM \times FCSP}{1-GEOM}\right) \times \left(\frac{\dot{m}\sqrt{T_i}}{P_i}\right)_{CHICS}$$

4) Hence $\dot{m}$

Outlet Temperature

1) Initially $C_p = 1$

2) Calculate γ from $\gamma = \frac{C_p}{C_p - R}$

3) Calculate isentropic outlet temperature, T'_o from:

$$T'_o - T_i = T_i\left[\left(\frac{P_o}{Pi}\right)^{\frac{\gamma-1}{\gamma}} - 1\right]$$

4) Linear interpolation on characteristics defines the oveall efficiency

5) Calculate value for T_o from $\eta_{ov} = \frac{T'_o - T_i}{T_o - T_i}$

6) Calculate more accurate value for C_p from equation below

$$C_p = 0.944 + 0.00019\left(\frac{T'_o - T_i}{T_o - T_i}\right)$$

7) Repeat process to find actual value of T_o.

3.0 INNER FAN

Known parameters P_i, T_i, N, FCSP, GEOM

Required parameters $\dot{m}$, T_o, P_o

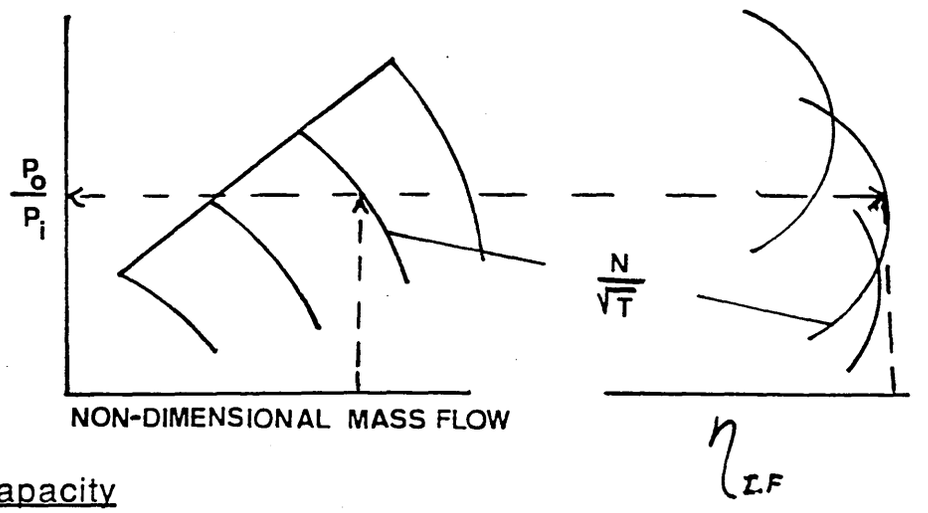

Capacity

1) Use outer fan mass flow rate, m_{OF} FCSP and GEOM to calculate the inner fan mass flow rate, m_{IF} fro equation below:

$$\dot{m}_{IF} = \dot{m}_{OF} \times \left(\frac{FCSP \times GEOM}{1 - FCSP \times GEOM}\right)$$

2) Calculate actual capacity

3) Use FCSP to calculate equivalent characteristics capacity:

$$\left(\frac{\dot{m}\sqrt{T_i}}{P_i}\right)_{CHCS} = \frac{1}{FCSP}\left(\frac{\dot{m}\sqrt{T_i}}{P_i}\right)_{ACT}$$

4) Linear interpolation on characteristics defines thr pressure ratio.

5) Hence P_o.

Outlet Temperature

1) Calculations are identical to the one above.

4.0 FRACTION OF SPLIT (FCSP)

For the steady state condition, FCSP is initially assumed to be unity. It is then re-calculated at each time interval. For the transient calculation, the Factor of Split should initially be guessed. An accurate value of the FCSP can be obtained by conducting the steady state calculation at the fuel flow rate from which the transient begin. The stabilised value of FCSP is then used as the guessed starting value for the transient.The equation used to calculate FCSP is given as :

$$FCSP_{NEW} = FCSP\left[1 + 0.1\left(\frac{\dot{m}\ out\ of\ vol24 - \dot{m}\ into\ vol24}{\dot{m}\ through\ inner\ fan}\right)\right]$$

5.0 THE COMPRESSOR CALCULATION (IP AND HP)

Known parameters	P_i, T_i, N
Guessed parameters	P_o
Required parameters	$\dot{m}$, T_o

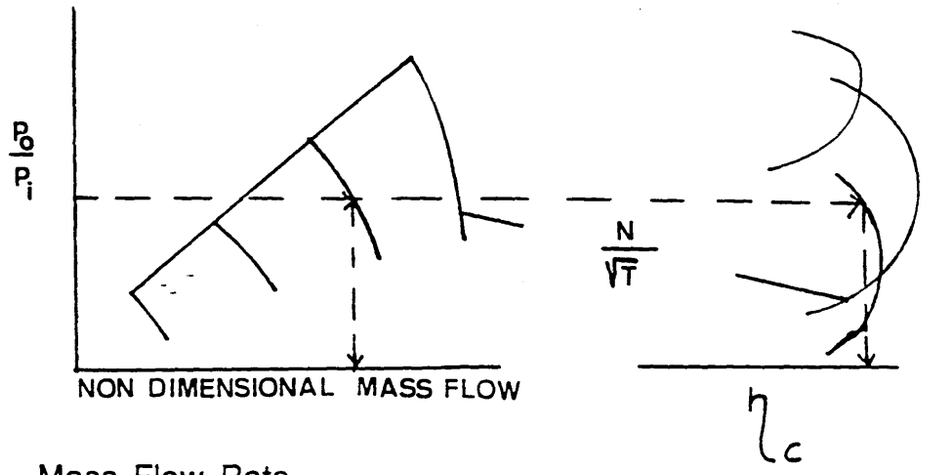

Mass Flow Rate

1) Calculate pressure ratio and non-dimensional speed

2) Linear interpolation on characteristics defines the capacity

3) Hence $\dot{m}$

Outlet Temperature

1) Initially $C_p = 1$

2) Calculate Gamma from $\gamma = \dfrac{C_p}{C_p - R}$

3) Calculate isentropic outlet temperature, T'_o, from

$$T'_o - T_i = \eta_c T_i \left[\left(\frac{P_o}{P_i} \right)^{\frac{\gamma - 1}{\gamma}} - 1 \right]$$

4) Linear interpolation on characteristics defines η_C

5) Calculate value for T_o from

$$\eta_C = \frac{T'_o - T_i}{T_o - T_i}$$

6) Calculate a better value for C_p from

$$C_p = 0.944 + 0.00019\left(\frac{T_o + T_i}{2}\right)$$

7) Repeat process to find the actual value of T_o.

6.0 TURBINE CALCULATION

Known parameters	P_i, T_i, N
Guessed parameters	P_o, η_T
REquired parameters	$\dot{m}$, T_o

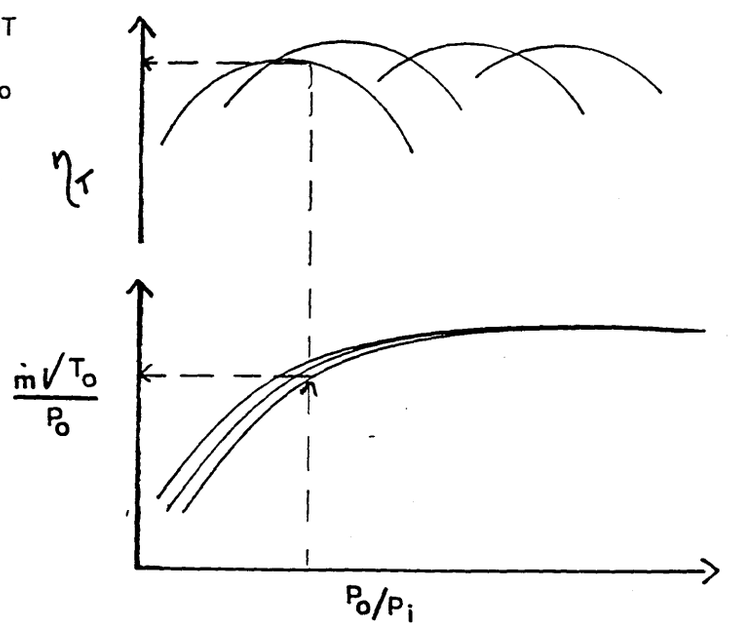

1) Initially let $\dot{m}$ be the outlet mass flow of the previous component, and C_p the value for previous component.

2) Calculate γ as above

3) Calculate isentropic outlet temperature, T'_o, from

$$T_i - T'_o = T_i\left[1 - \left(\frac{P_o}{P_i}\right)^{\frac{\gamma-1}{\gamma}}\right]$$

4) Calculate value for T_o from

$$T_i - T_o = \eta_T\left(T_i - T'_o\right)$$

5) Calculate work factor, $\left(\frac{C_p \Delta T_{i\to o}}{T_i}\right)$

6) Linear interpolation on characteristics defines better η_T

7) Calculate better value for C_p from

$$C_P = 0.944 + 0.00019\left(\frac{T_i + T_o}{2}\right)$$

modified for fuel/air ratio of products

8) Repeat above process five times

9) On the fifth process, linear interpolation on characteristics defines a value of m

10) Compare calculated m and originally estimated m

11) Revise estimated m

12) Repeat above iterative loop until the two values of m fall within the required tolerance, given m.

13) The last calculated value of T_o is assumed to be the actual value of T_o.

7.0 BY-PASS DUCT AND MIXER CALCULATION

Both by-pass duct and gas nozzle are intercomponent volumes:Vol BP and Vol 6 respectively. Therefore, the mismatch

of mass flow rate entering and leaving these volumes has to be determined.

The mass flow rate entering one of these volumes is equal to the mass flow rate leaving the previous component, meaning for Vol BP, the outer fan and for Vol 6 the L.P turbine. The mass flow rate at exit from one of these volumes is found by use of the following equation which is derived from basic gas dynamic theory:

$$\dot{m} = \frac{PA}{\sqrt{T}}\left[\frac{2\gamma}{(\gamma-1)R}\left(\frac{P_s}{P}\right)^{\frac{2}{\gamma}}\left\{1-\left(\frac{P_s}{P}\right)^{\frac{\gamma-1}{\gamma}}\right\}\right]$$

The areas used above are the core gas and by-pass air flow areas at the mixer chutes.

In the case of the by-pass duct, the exit temperature and mass flow rate are corrected for the addition of bleed flows from the core of the engine.

The flow in the core gas duct is assumed to be isentropic. However, the by-pass duct model has a pressure loss factor included in the calculation.

8.0 FINAL NOZZLE CALCULATION

The core gas and by-pass air are assumed not to mix. Each flow is treated separately but in an identical manner to the other. Both flows are assumed to be isentropic.

Firstly, it is determined whether or not the flow is choked. By

the use of the basic gas dynamics theory:

$$\frac{P}{P_s} = \left(1 + \frac{\gamma - 1}{2} M^2\right)^{\frac{\gamma}{\gamma - 1}}$$

If choked M=1 $\quad \therefore \quad \frac{P}{P_s} = \left(\frac{1+\gamma}{2}\right)^{\frac{\gamma}{\gamma - 1}}$

Thus, if

$$\frac{P}{P_{AMB}} \geq \left(\frac{1+\gamma}{2}\right)^{\frac{\gamma}{\gamma - 1}}$$ the flow is choked.

The volume Vol 78 is the intercomponent volume from the mixer to the throat of the final nozzle. The mass flow rates entering this volume are equal to the core gas and by-pass air mass flow rates leaving the mixer. The exit areas required by each of the these mass flow rates can be calculated from the following equation which is derived from basic gas dynamic theory:

$$\frac{\dot{m}\sqrt{T}}{PA} = M\sqrt{\frac{\gamma}{R}}\left(1 + \frac{\gamma - 1}{\gamma} M^2\right)^{\frac{\gamma + 1}{2(1-\gamma)}}$$

For choked flow, M=1, the equation reduces to :

$$\frac{\dot{m}\sqrt{T}}{PA} = \sqrt{\frac{\gamma}{R}}\left(\frac{1+\gamma}{2}\right)^{\frac{\gamma + 1}{2(1-\gamma)}}$$

The mass flow rates used in the above equation are those entering the final nozzle.

The required exit area is equal to the sum of the two calculated areas. A coefficient of discharge is then used to modify the required exit area. Until steady state running is achieved, this required area will doffer from the actual nozzle exit area. The ratio of required exit area to actual exit area, and the mass flow rates entering the final nozzle, are used to perform a simple proportional calculation to determine the actual mass flow rates at exit from the final nozzle.

				TAY MK610					
DMEANR	**DMEANS**	**HGHTR**	**HGHTS**	**CHORD R**	**CHORD S**	**B 1**	**B 2**	**B 3**	**B 4**
564	578	48.9754	46.3977	33.37	33.998	33	24	26.5	17
558	570	43.8201	42.2735	28.857	31.666	31	22	30	11.5
570	568	40.7269	39.7277	26.486	37.077	39.5	35	26.5	- 7
				TAY MK670					
DMEANR	**DMEANS**	**HGHTR**	**HGHTS**	**CHORDR**	**CHORDS**	**B 1**	**B 2**	**B 3**	**B 4**
564	578	48.9754	46.3977	33.37	33.998	33	24	32	17
558	570	43.8201	42.2735	28.857	31.666	31	22	30	11.5
552	562	40.7	39.7	26.4	29.334	31	22	27	7
564	560	37.7	37.2	24.4	34.675	37.5	33	25	- 7

Table 2.1 DIMENSIONS OF I.P COMPRESSORS

TABLE 3.1

SPECIFICATION OF THE COMPONENTS		UNITS	MAX TAKE-OFF
Altitude		m	0
Mach No			0
Deviation from ISA		C	15
Ambient Pressure		KN/m2	101.3
Ambient Temperature		K	303.15
Totat Inlet Pressure		KN/m2	101.3
Total Inlet Temperature		K	303.15
Thrust		KN	80.064
Specific Fuel Consumption		Kg/sec.KN	0.02922
Fuel Flow		Kg/hr	3820.67
Total Inlet Flow		Kg/sec	221.175
Bypass Ratio			2.9
Overall Pressure Ratio			20.1
Turbine Entry Temperature		K	20.1
LP Speed		rpm	7110
HP Speed		rpm	12666
Outer Fan	Pressure Ratio		1.78
	Efficiency		85.60%
	Inlet Flow		429.6
	Speed N/ T		408.4
Inner Fan	Pressure Ratio		1.66
	Efficiency		93.60%
	Inlet Flow		148
	Speed N/ T		408.4
IP Compressor	Pressure Ratio		1.77
	Efficiency		82.90%
	Inlet Flow		96.1
	Speed N/ T		378
HP Compressor	Pressure Ratio		6.83
	Efficiency		87.10%
	Inlet Flow		59.3
	Speed N/ T		611.9
	Delivery Pressure		295
	Delivery Temperature		769.2
HP Turbine	Efficiency		87.70%
	Inlet Flow		15.64
	Speed N/ T		330.6
LP Turbine	Efficiency		89.60%
	Inlet Flow		48.5
	Speed N/ T		211.4
Hot Chute		m2	0.43316
Cold Chute		m2	0.65045
Final Nozzle		m2	0.7582
Mixing Pressure Ratio			1.06

DESIGN POINT FOR THE NEW ENGINE MK670

Table 3.2

Performance Parameters	RELATIONSHIP	FACTORS			
		INNER FAN	OUTER FAN	IP COMP	HP COMP
Capacity	$\left(\frac{\dot{m}\sqrt{T}}{P}\right)_{ENG} = \left(\frac{\dot{m}\sqrt{T}}{P}\right)_{CHS} \times FACTOR$	C18	C41	C31	C7
Efficiency	$\eta_{ENG} = \eta_{CHICS} + FACTOR$	D9	D42	D32	D1
Pressure Ratio	$(PR - 1.0)_{ENG} = (PR - 1.0)_{CHS} \times FACTOR$	C21	C43	C33	C22
Non-dim Speed	$\left(\frac{N}{\sqrt{T}}\right)_{ENG} = \left(\frac{N}{\sqrt{T}}\right)_{CHICS} \times FACTOR$	C23	C44	C34	C24

DEFINITION OF SCALING FACTORS

TABLE 3.3

			SCALING FACTORS	
			INNER FAN	
PERFORMANCE PARAMETERS	**FACTORS**	**TAY MK610**		**TAY MK670**
CAPACITY	C18	1.0094		1.207
N-DIM SPEED	C23	1		0.905
PRESSURE RATIO	C21	1.0008		1.192412
	D21	0		0
EFFICIENCY	C9	1		1
	D9	-0.0153		0.04492
			OUTER FAN	
CAPACITY	C41	0.99713		1.204
N-DIM SPEED	C44	1		0.905
PRESSURE RATIO	C43	0.99903		1.147
	D43	0		0
EFFICIENCY	C42	1		1
	D42	-0.0205		0.0009

VALUES OF SCALING FACTORS FOR INNER AND OUTER FAN

TABLE 3.4

			IP COMPRESSOR	
PERFORMANCE PARAMETERS	**FACTORS**	**TAY MK610**		**TAY MK670**
CAPACITY	C31	1.0156		1.2459
N-DIM SPEED	C34	1		0.9189
PRESSURE RATIO	C33	1.0081		1.2413
	D33	0		0
EFFICIENCY	C32	1		1
	D32	0.0023		-0.00409
			HP COMPRESSOR	
CAPACITY	C7	1.0136		1.0551
N-DIM SPEED	C24	1.00034		1.00034
PRESSURE RATIO	C22	1.006		1.0225
	D22	0.0115		0.0115
EFFICIENCY	C1	1		1
	D1	-0.0077		0.0315
			HP TURBINE	
CAPACITY	C3	1.0236		1.0236
EFFICIENCY	C2	1		1
	D2	-0.0141		-0.0141
			LP TURBINE	
CAPACITY	C11	0.47428		0.484
	C10	1		1
	D10	-0.0057		-0.0057

VALUES OF SCALING FACTORS FOR I.P AND H.P COMPRESSORS AND H.P AND L.P TURBINES

	Reference Engine MK610		New Engine MK670	
THRUST %	3.2 %	100.0 %	3.2 %	100.0 %
L P SPEED (r.p.m)	2185	8540	2080	7806
H P SPEED (r.p.m)	7376	12115	8500	12468
KE in LP shaft (MJ)	0.287	4.383	0.356	5.011
L P shaft KE to be lost in Deceleration (MJ)	4.096		4.655	
KE in H P shaft (MJ)	1.068	2.881	1.418	3.052
H P shaft KE to be lost in Deceleration (MJ)	1.813		1.634	
Power absorption in LP compressors MW		14.32		19.52
Power absorption in HP compressor MW		17.50		20.78

Table 5.1 Speeds and Rotational Kinetic Energies of the Engines Sea level, Mach 0.2.

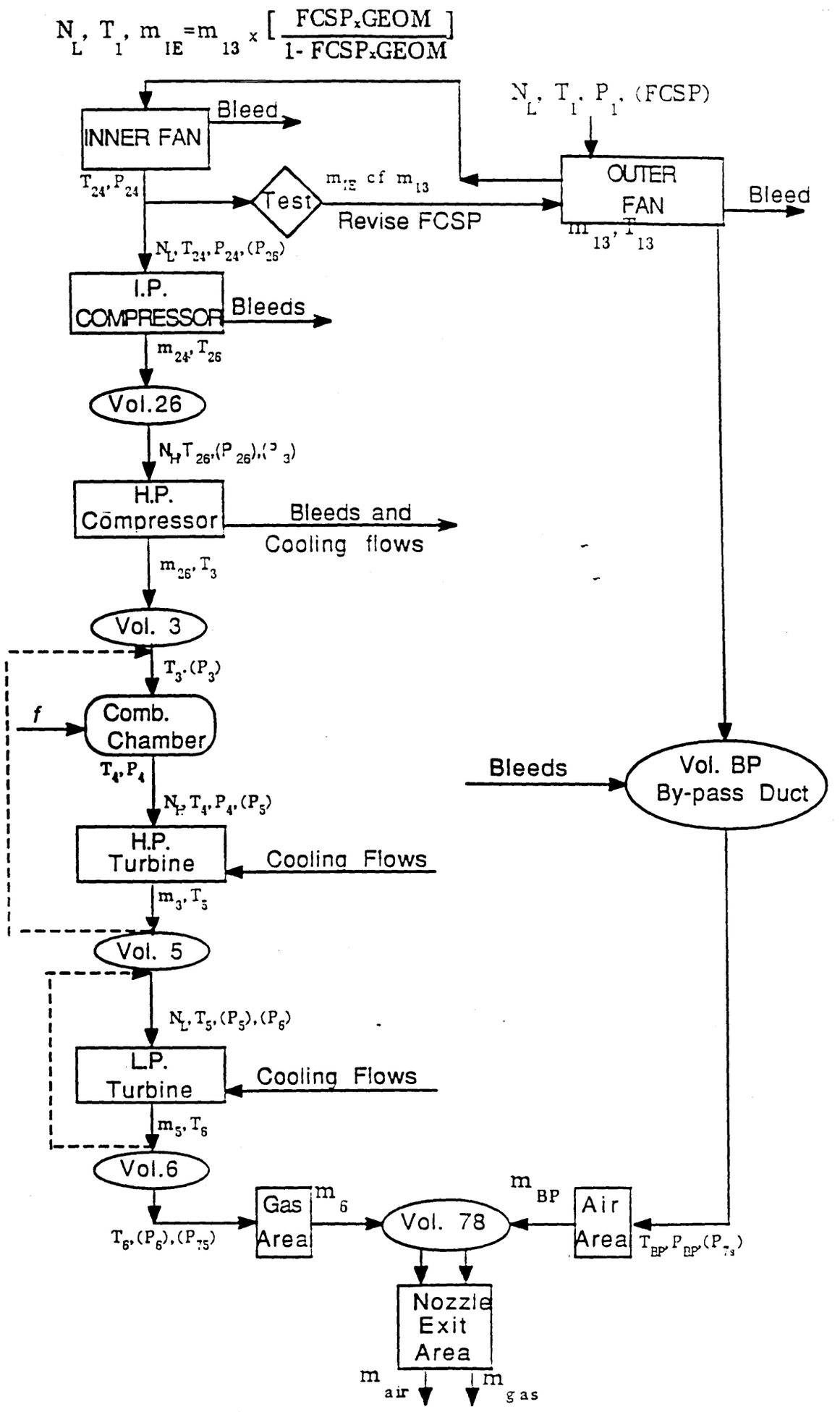

Calculate new pressures and Accelerations

DIAGRAM 4.1

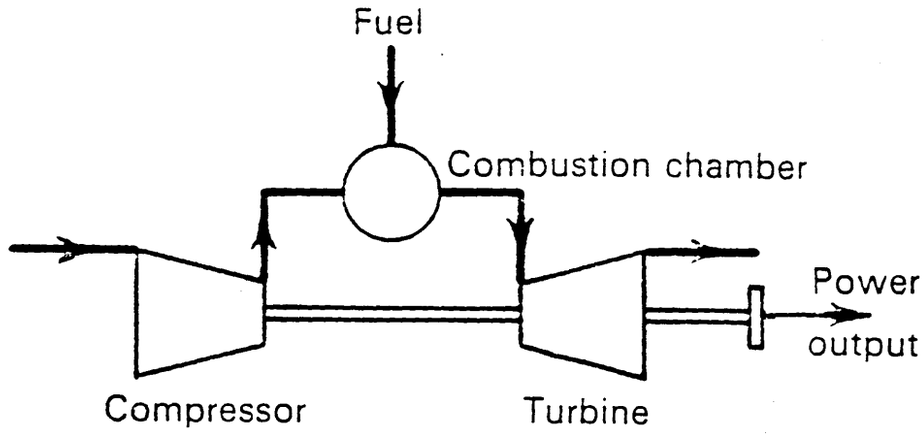

Fig 1 Simple gas turbine system.

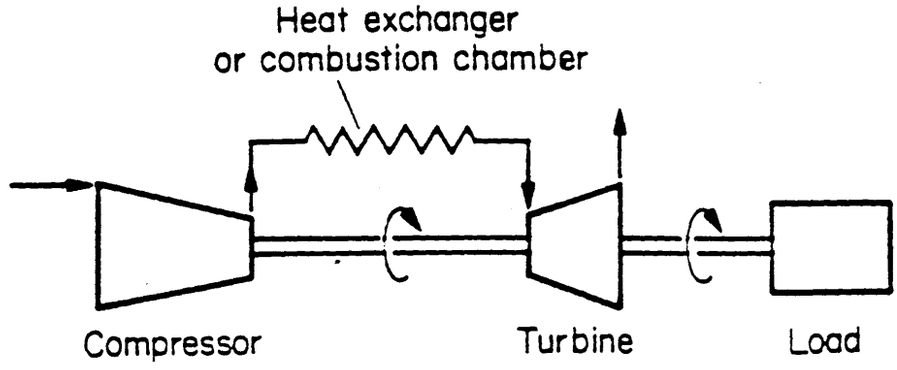

Fig 2 Single-shaft arrangement.

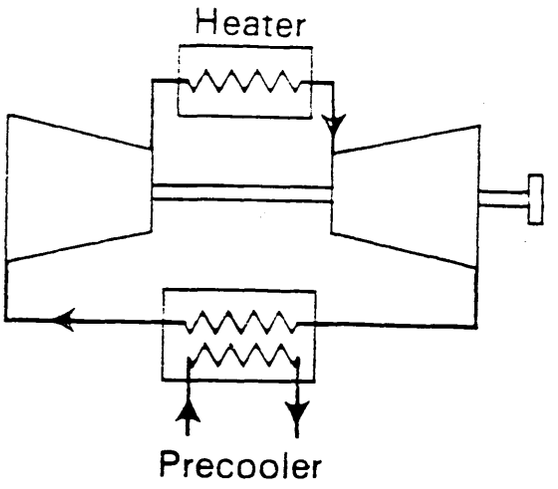

Fig 3 Simple closed cycle.

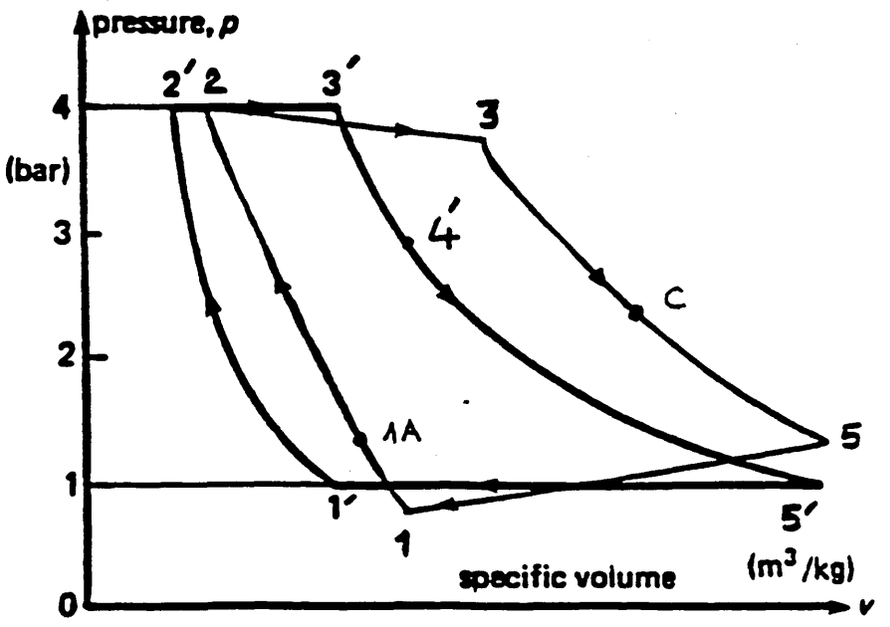

Fig 4 Brayton cycle.

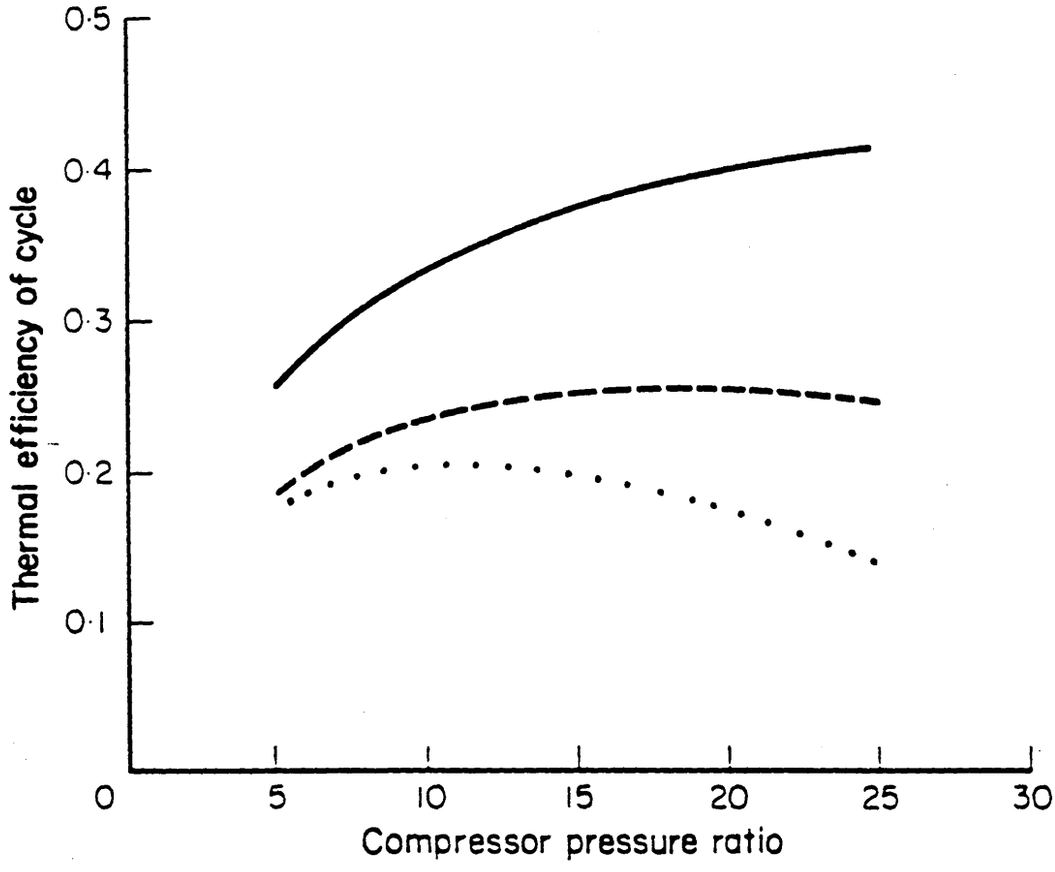

Cycle thermal efficiency as a function of other factors: ——, $\eta = 0.9$, $T_i = 1400$ K; – – –, $\eta = 0.8$, $T_i = 1400$ K; . . ., $\eta = 0.8$, $T_i = 1200$ K (η is compressor and turbine efficiency, T_i is turbine inlet temperature)

Fig 5

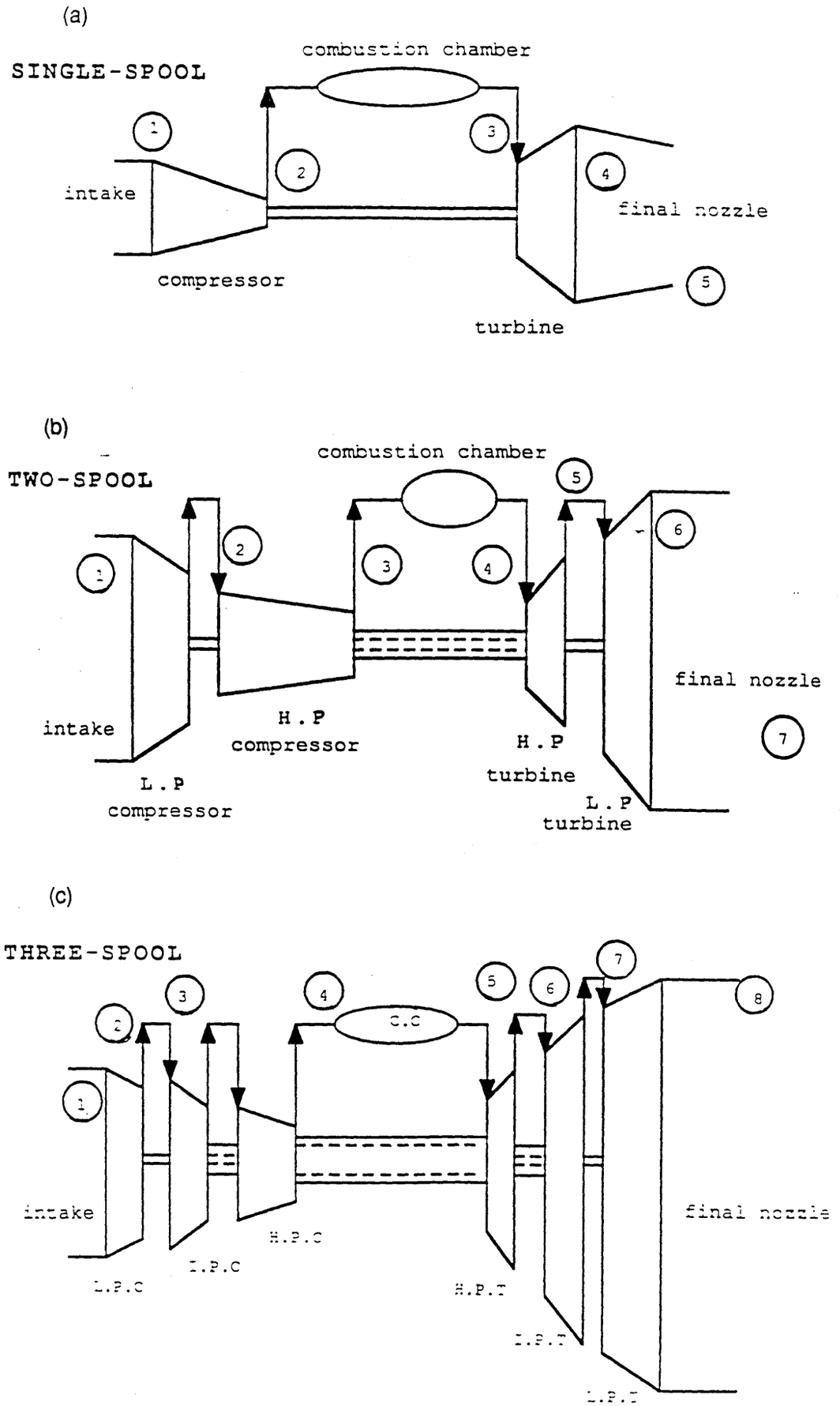

Fig 6 Different configurations of aircraft gas turbine engines.

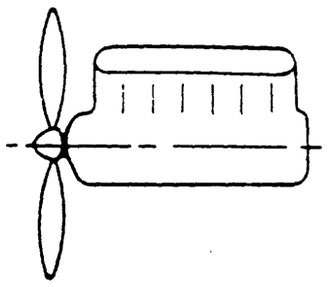

(a) Piston engine

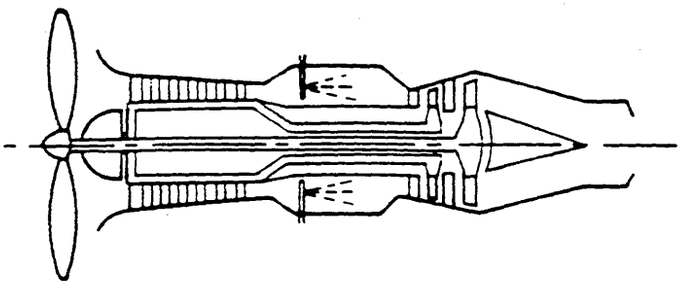

(b) Turboprop engine

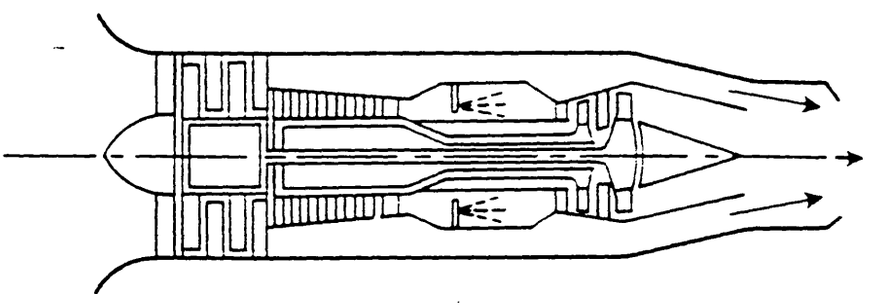

(c) Turbofan engine

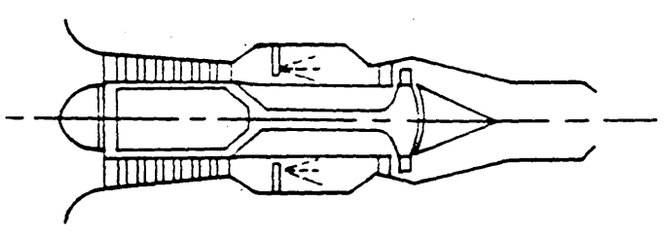

(d) Turbojet engine

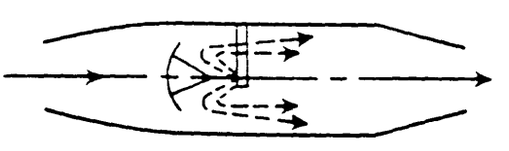

(e) Ramjet engine

Fig 7 propulsion engines.

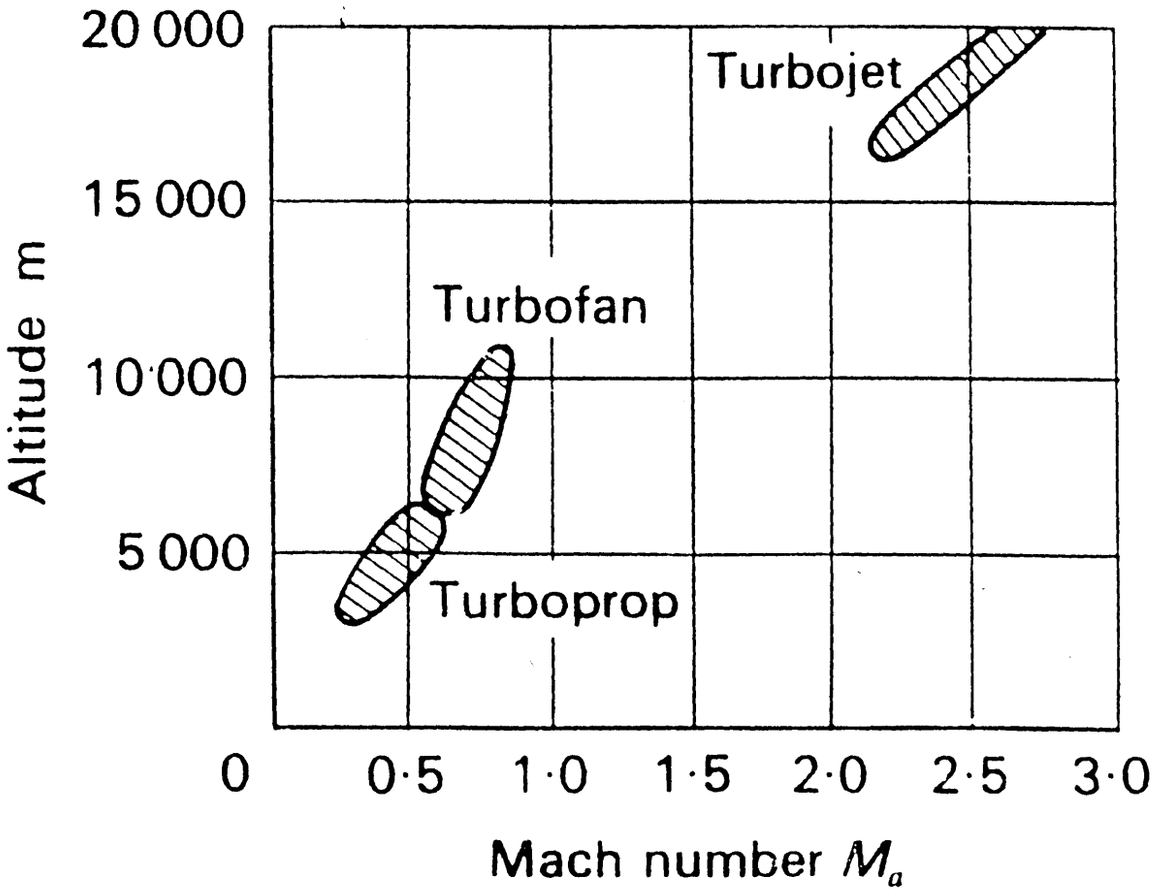

Fig 8 Flight regimes.

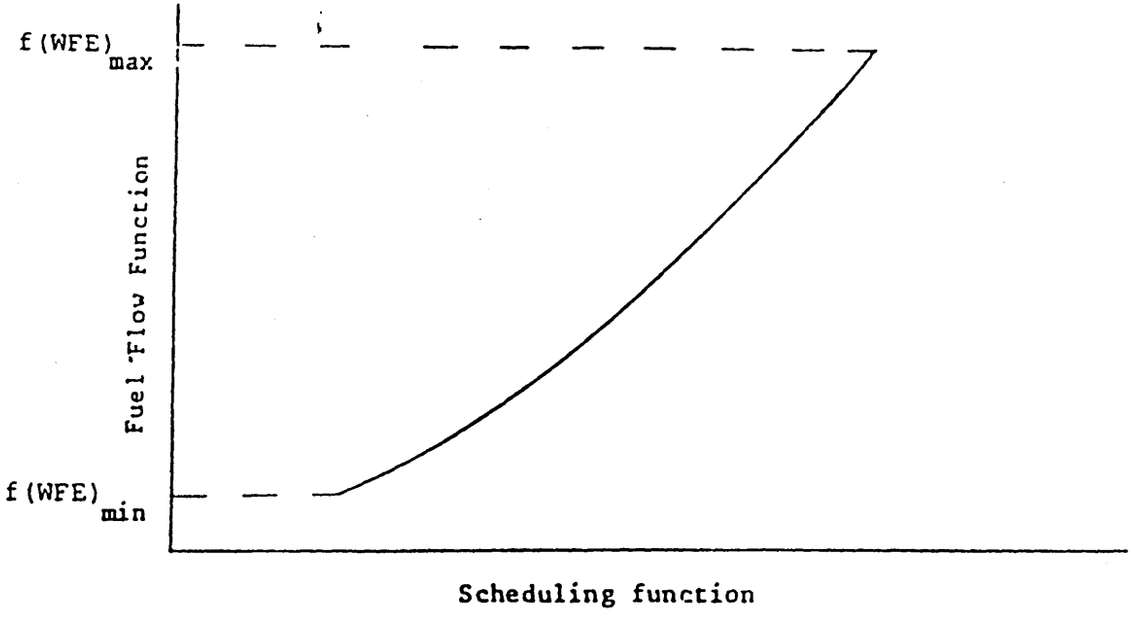

Fig 9 Fuel schedule.

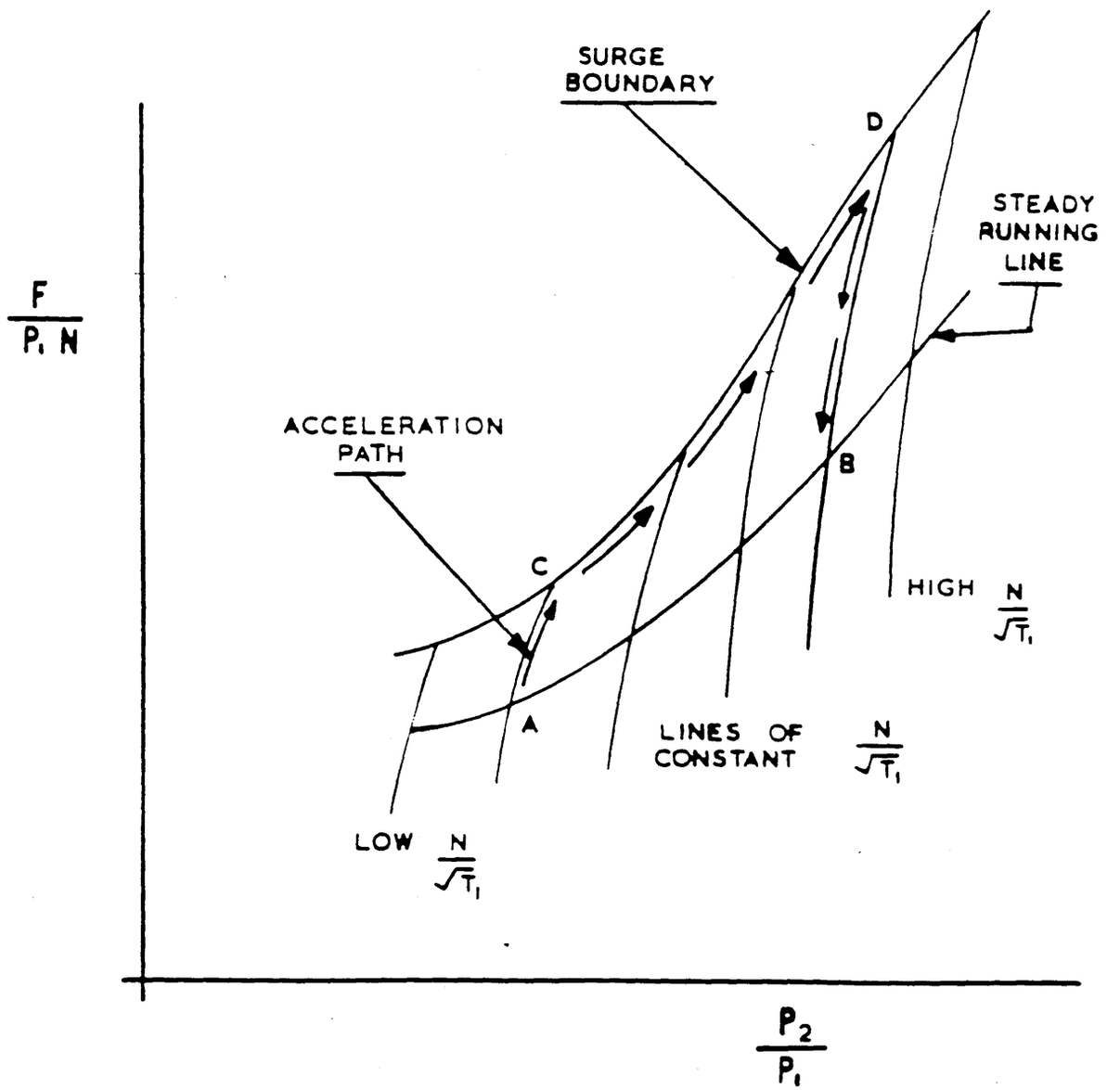

Fig 10 Typical fuel flow characteristics.

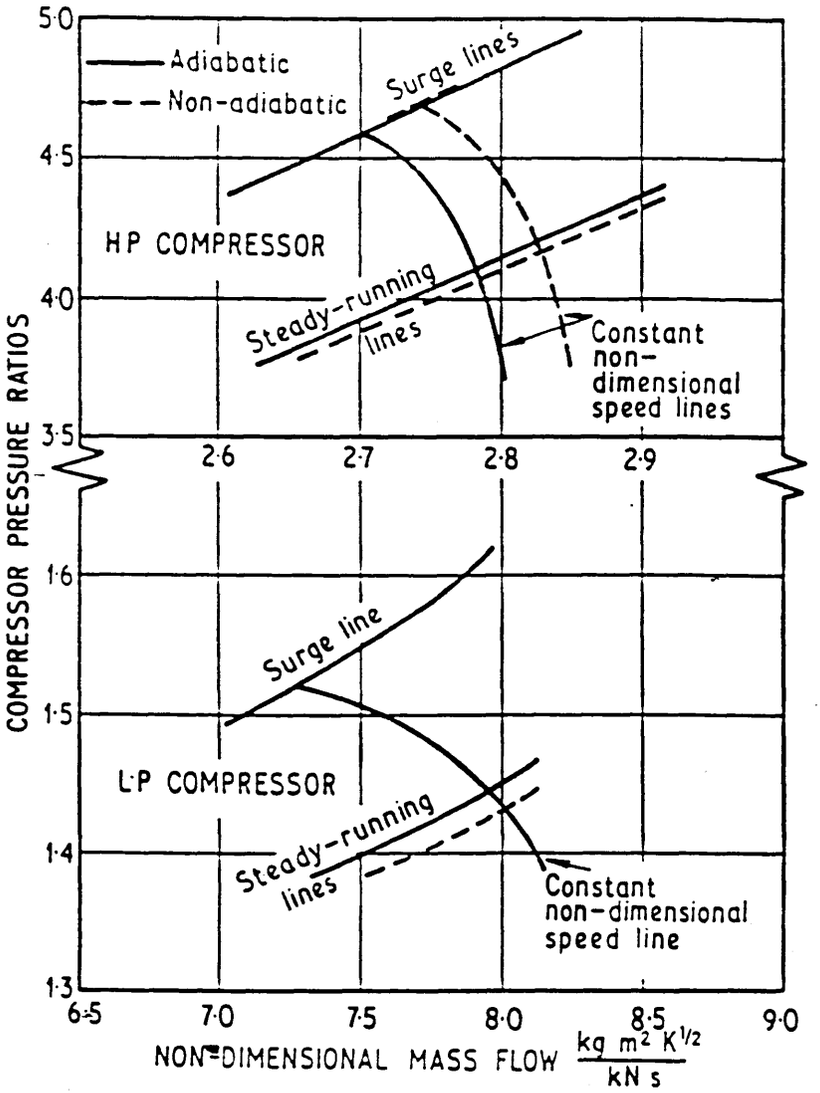

Effects of heat transfer on surge and steady-running lines at 3·6 s in sea level acceleration (1)

Fig 11

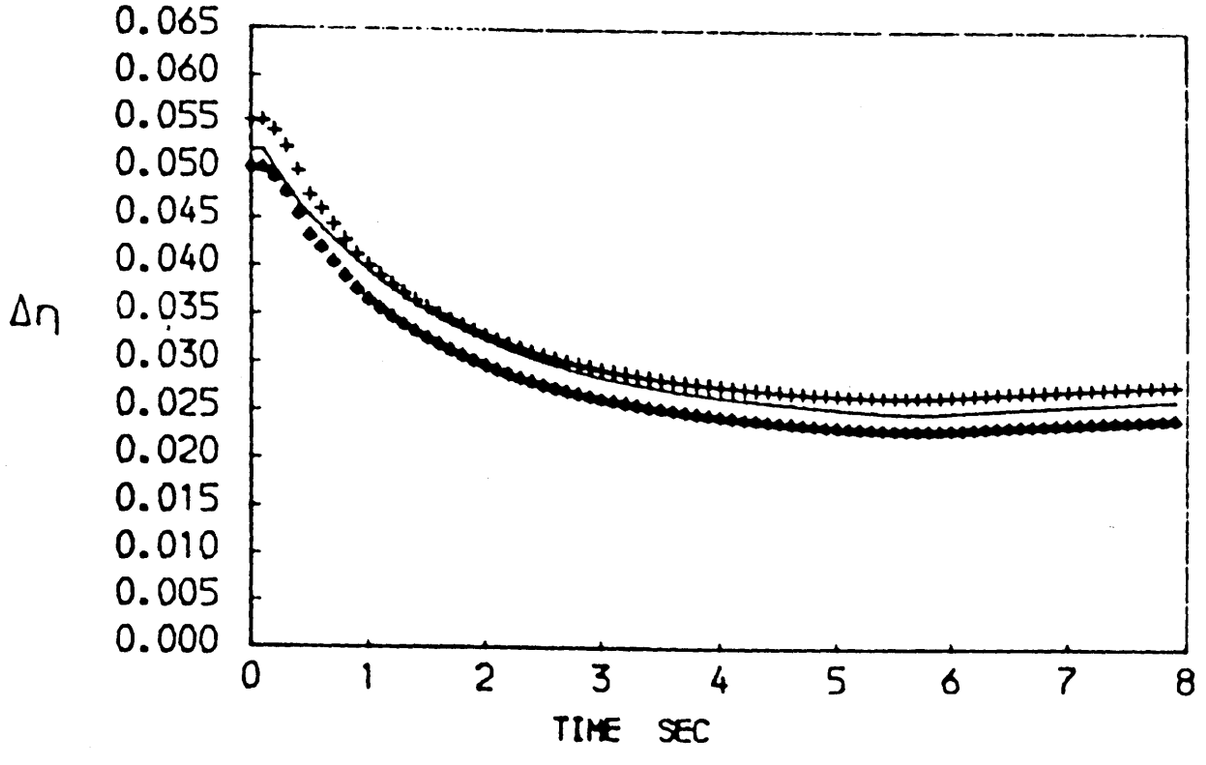

EFFECTS OF CLEARANCE MOVEMENTS ON H.P. COMPRESSOR EFFICIENCY
EFFICIENCY LOSS COMPARED TO ZERO CLEARANCE
MODELS. ENGINE + ONE STAGE • SIMPLIFIED—

Fig 12

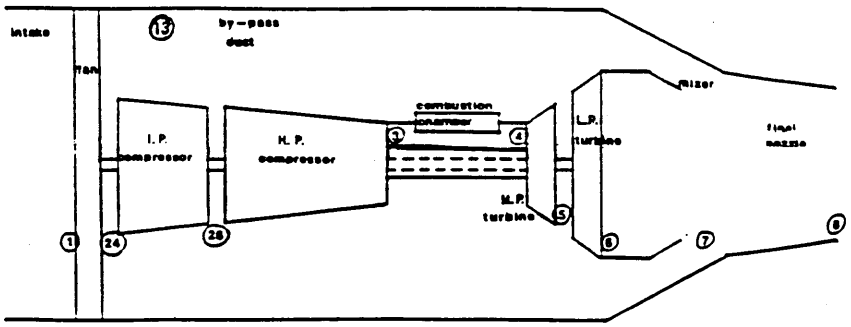

Tay turbofan engine station arrangements

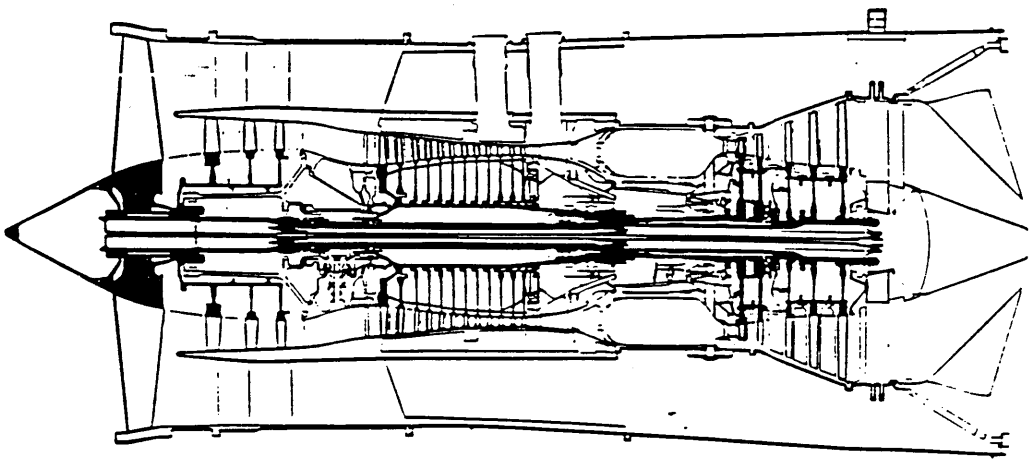

Cross-section of Rolls-Royce Tay turbofan

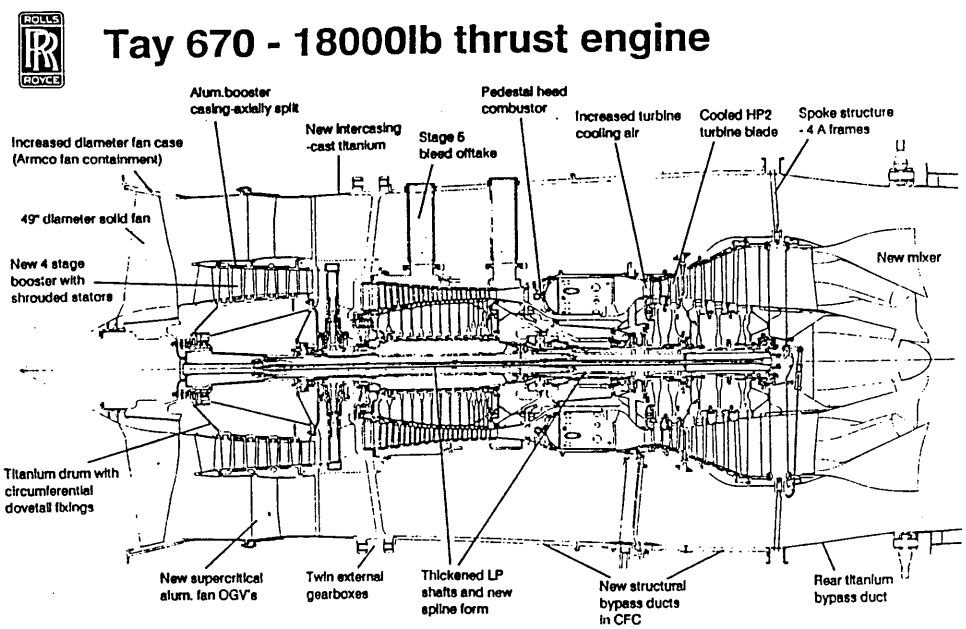

FIG 13 TAY TURBOFAN ENGINE

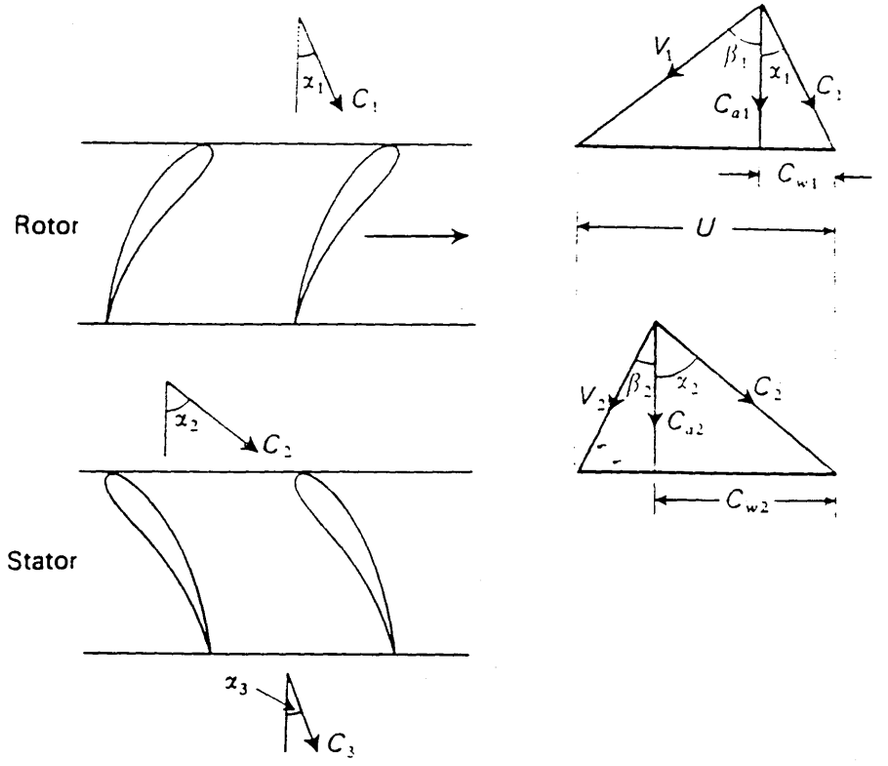

FIG 14 VELOCITY TRIANGLES FOR ONE STAGE

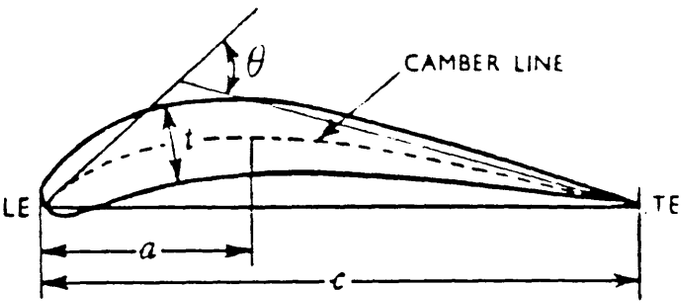

a Distance of point of maximum camber from LE.
c Chord.
θ Camber angle $= \beta_1 - \beta_2$.
t Maximum thickness.

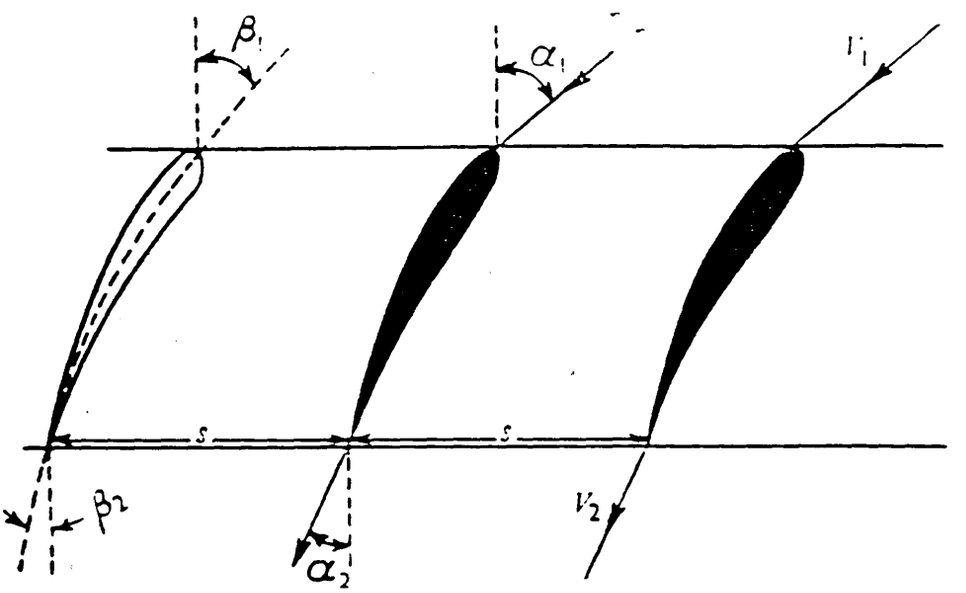

α_1 Air or fluid inlet angle.
α_2 Air or fluid outlet angle.
β_1 Blade inlet angle.
β_2 Blade outlet angle.
V_1 Inlet velocity.
V_2 Outlet velocity.
i Incidence $= \alpha_1 - \beta_1$.
δ Deviation $= \alpha_2 - \beta_2$.
ϵ Deflexion $= \alpha_1 - \alpha_2$.
s Pitch.

FIG 15 COMPRESSOR CASCADE NOTATION

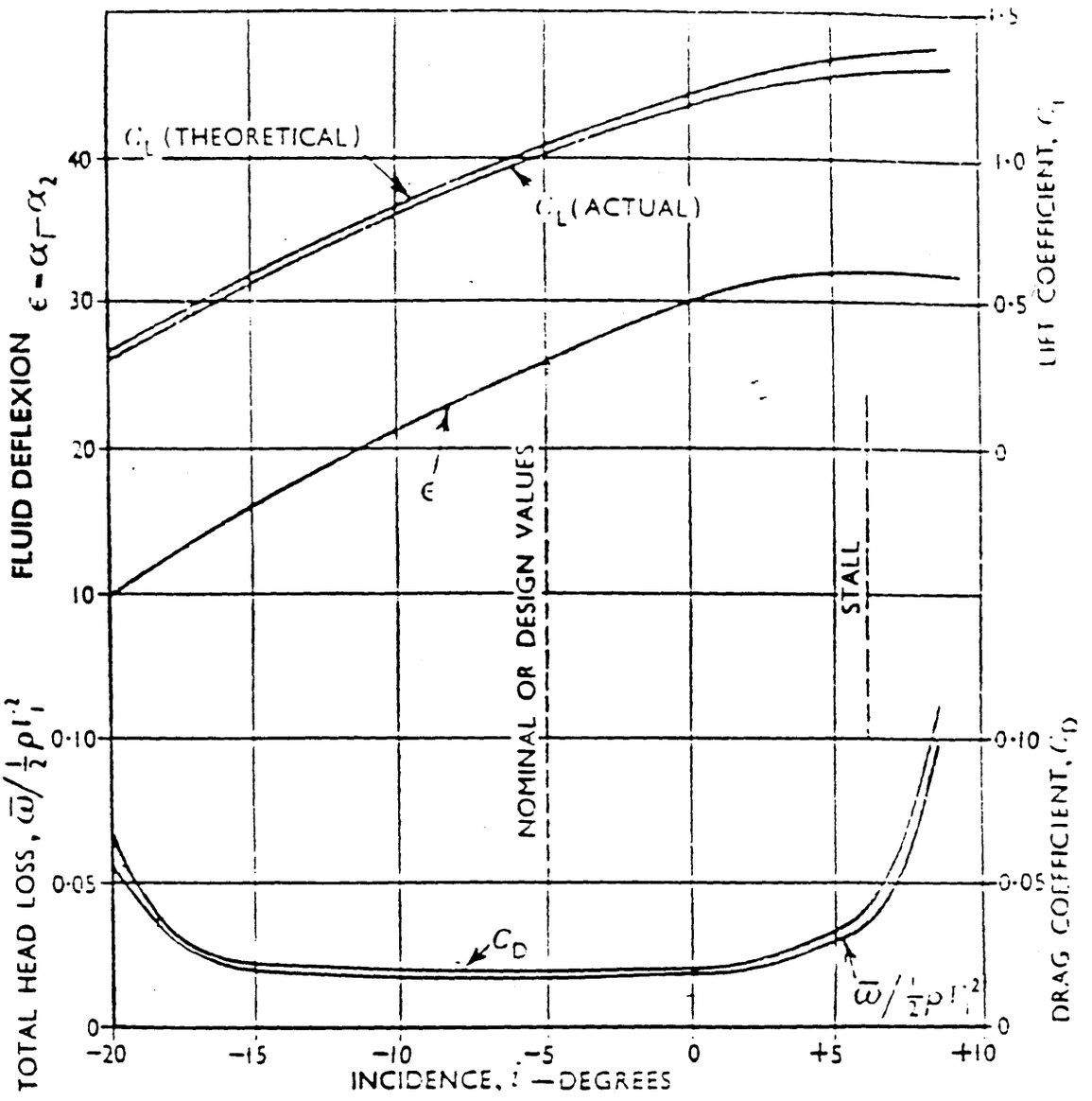

FIG 16 TYPICAL LOW-SPEED CASCADE TEST RESULTS
FROM REF(19)

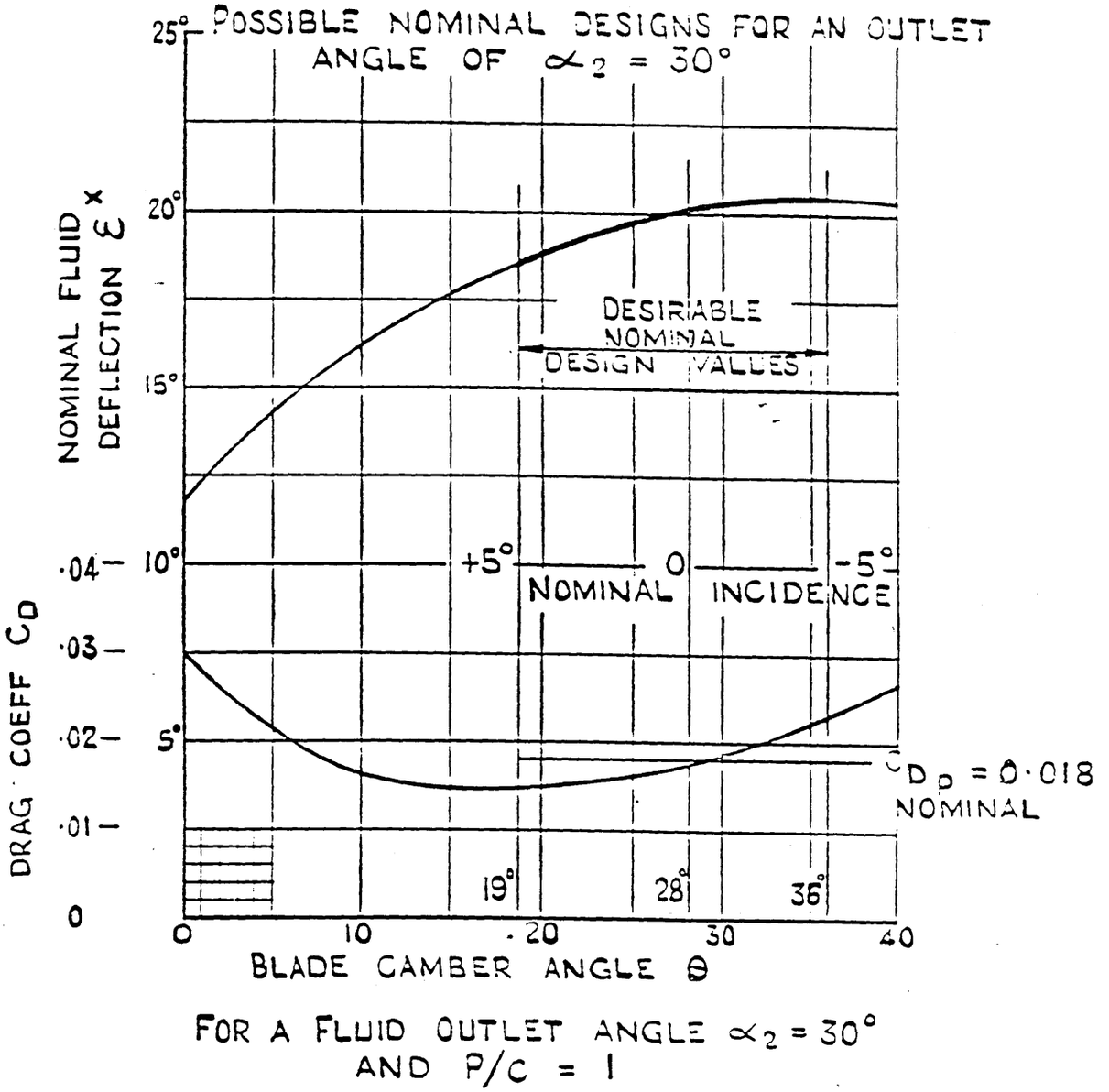

Fig17 Drag Coefficients and Design Deflection from Ref(19).

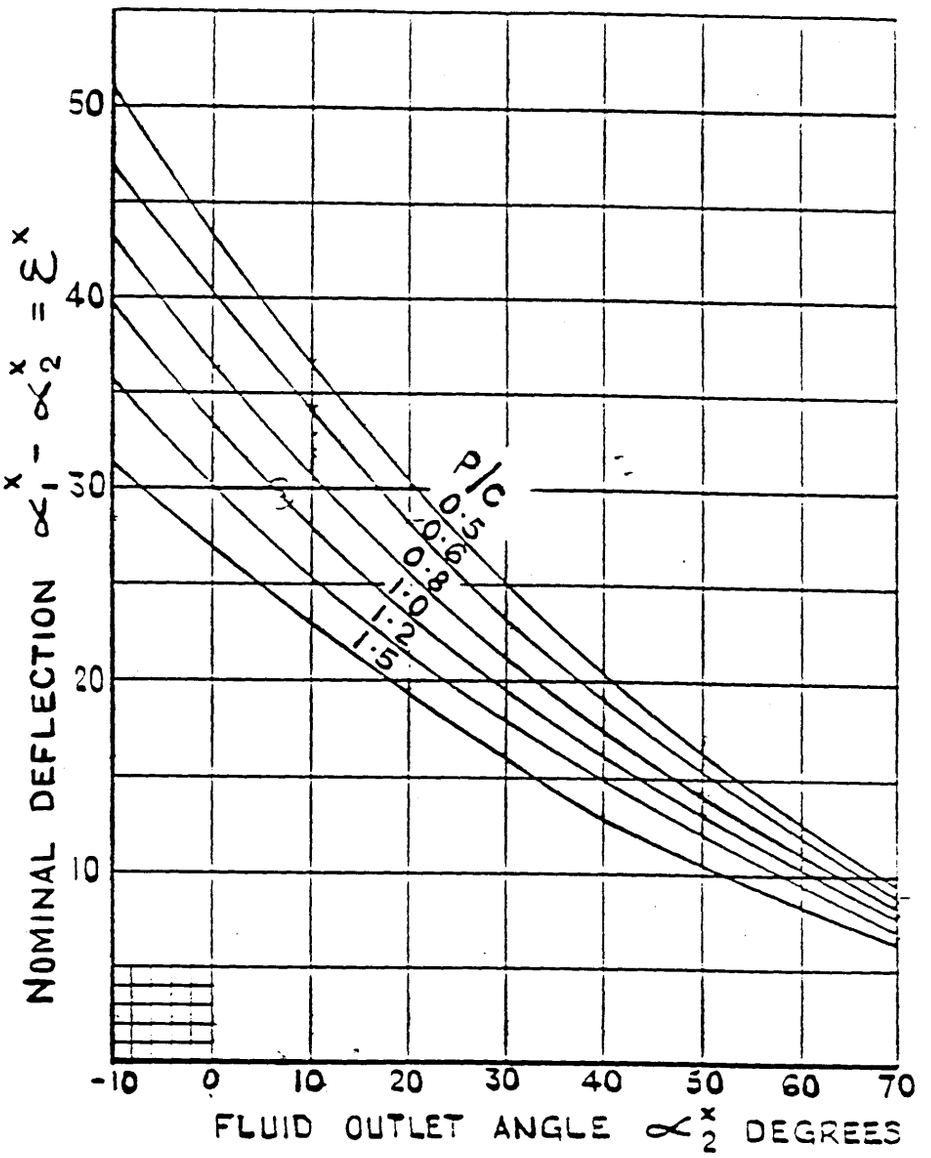

Fig18 Design deflection from Ref(19).

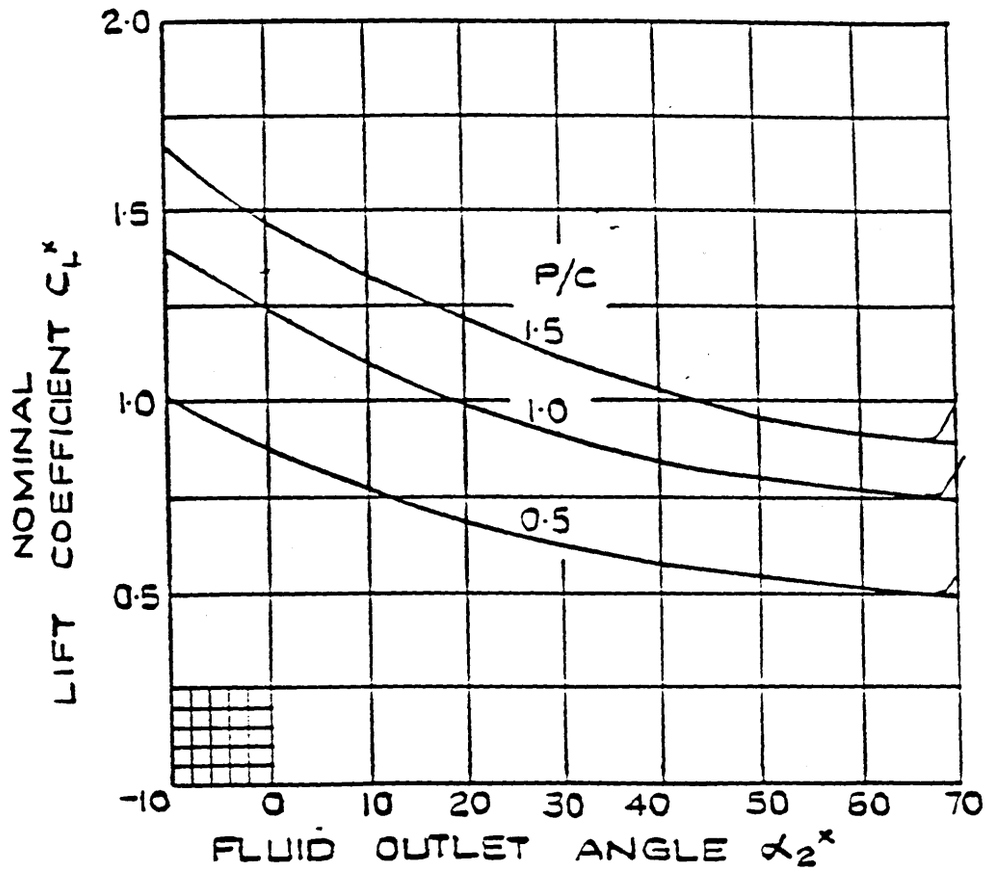

Fig19 Nominal Lift Coefficients from Ref(19)

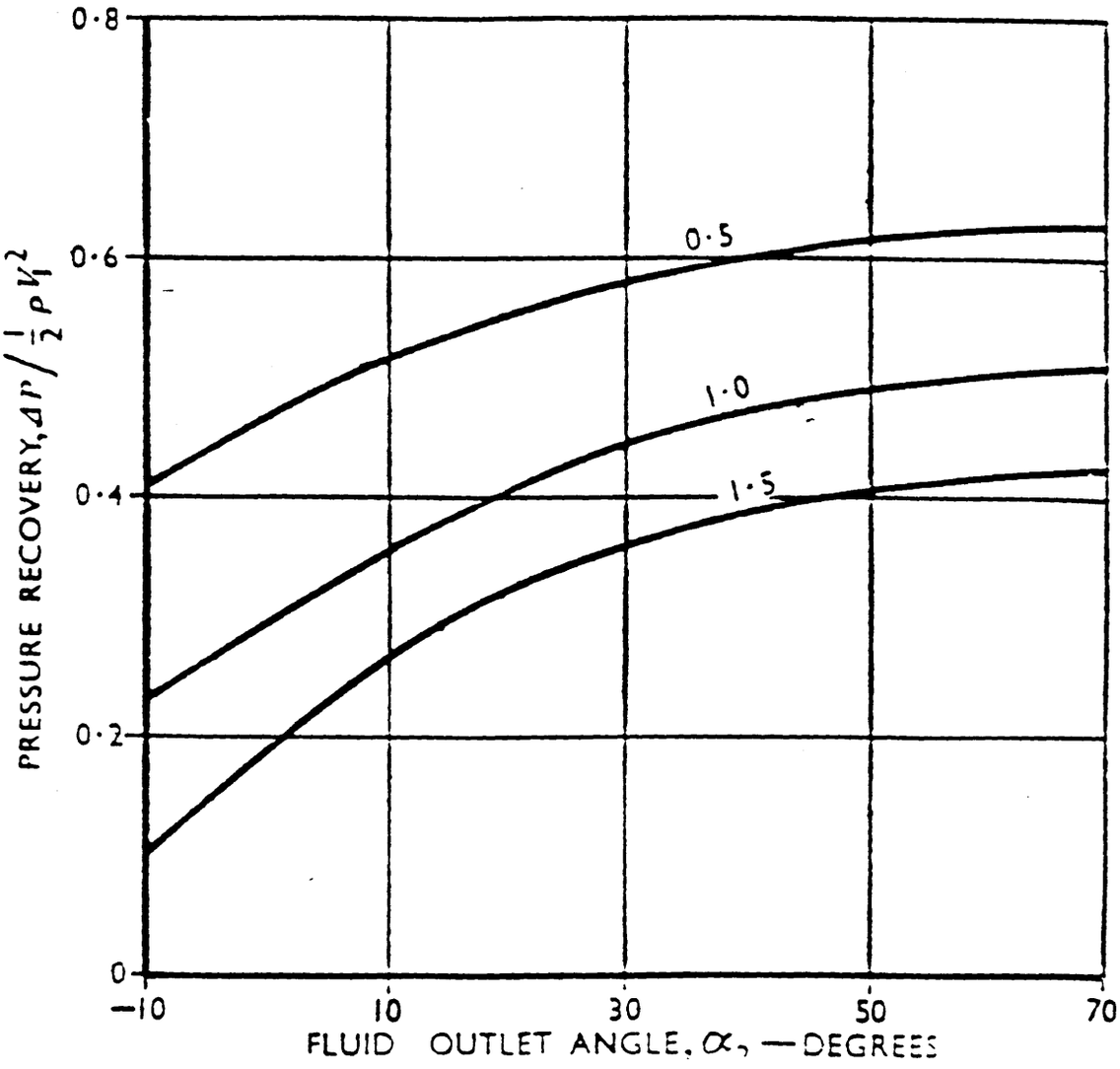

FIG 20 NOMINAL VALUE OF PRESSURE RECOVERY

FROM REF(19)

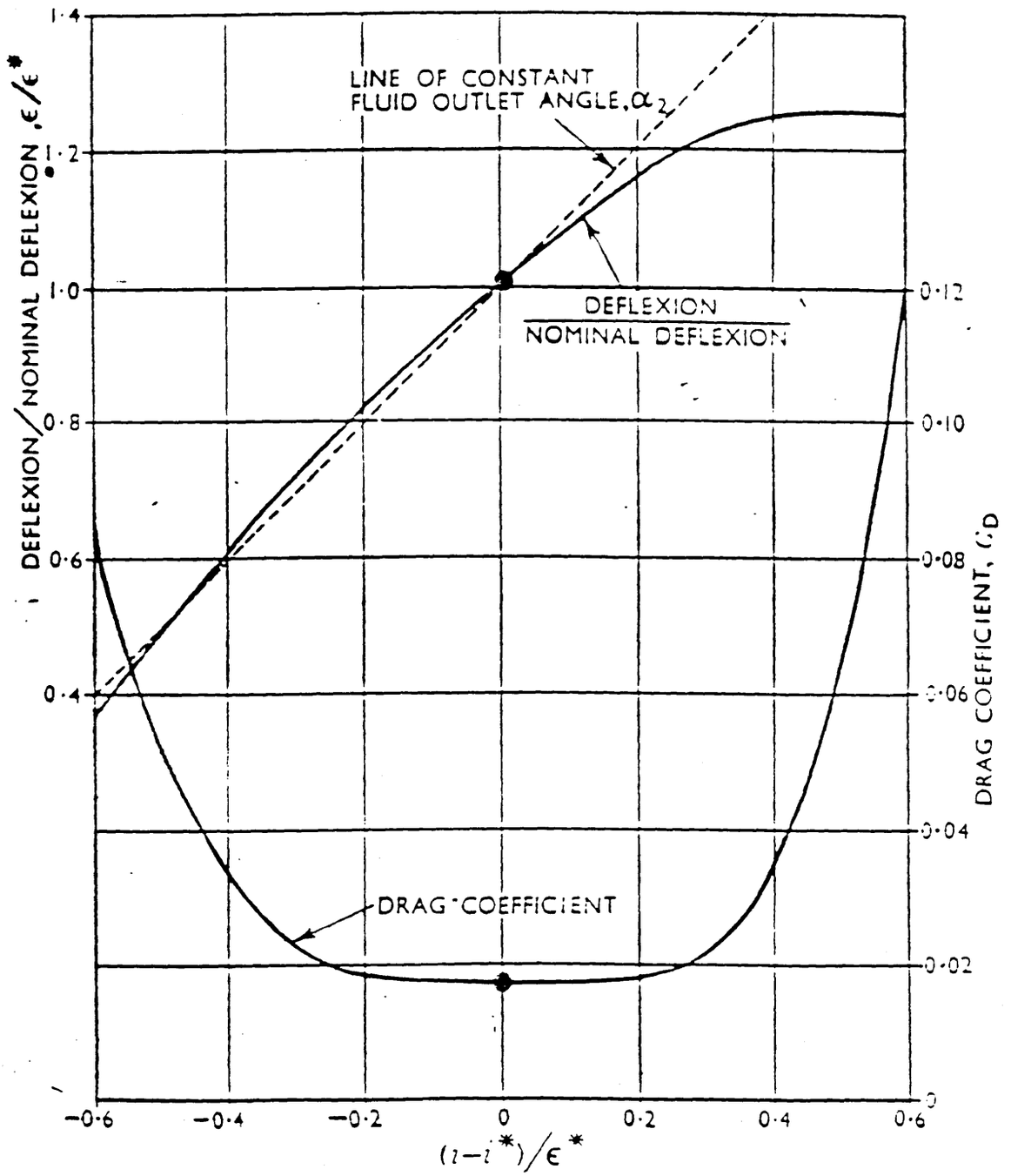

FIG 21 DEFLECTIONS AND DRAG COEFFICIENTS AT OTHER THAN NOMINAL INCIDENCES

FROM REF(19)

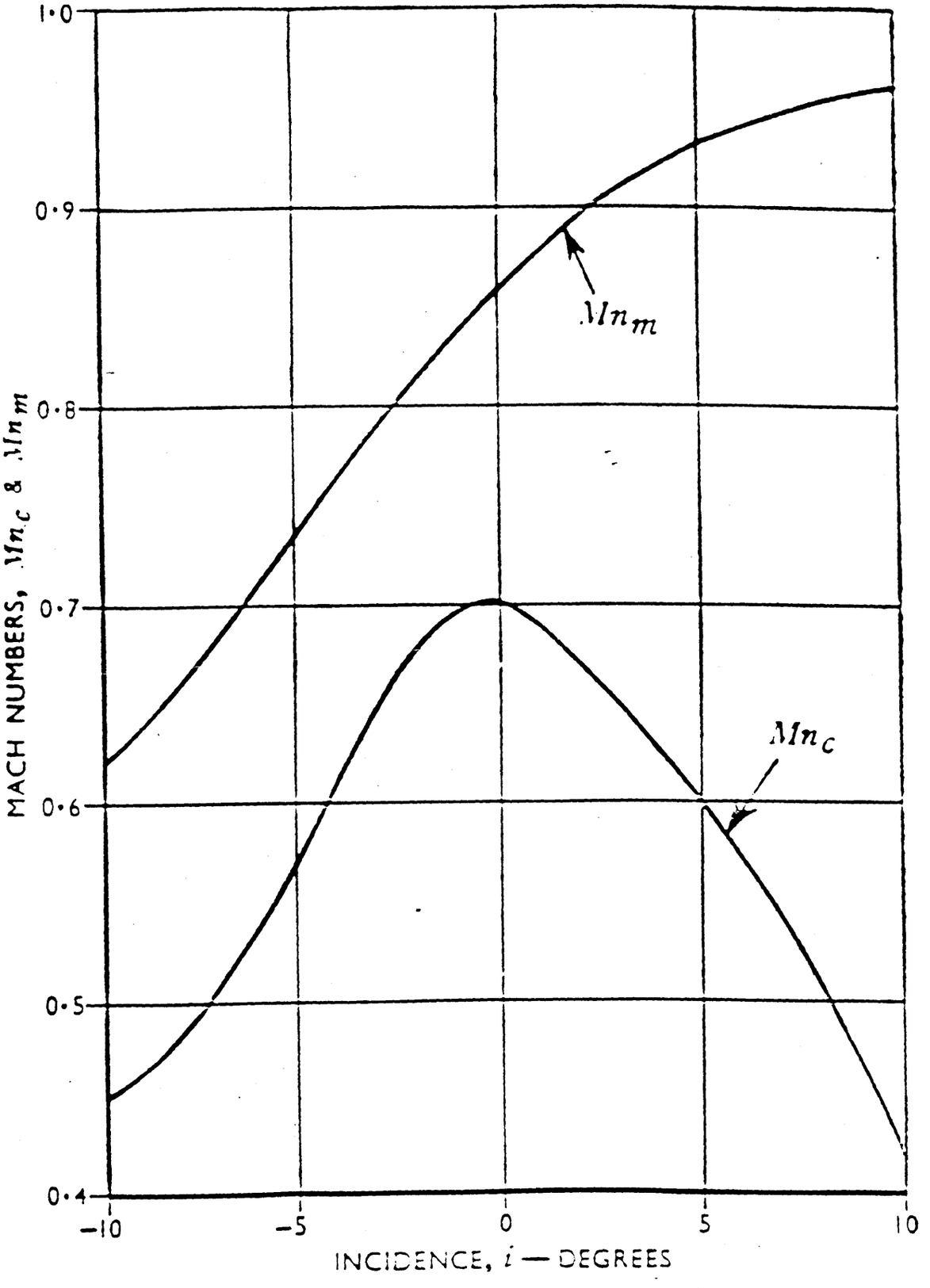

FIG 22 CRITICAL AND MAXIMUM MACH NUMBERS

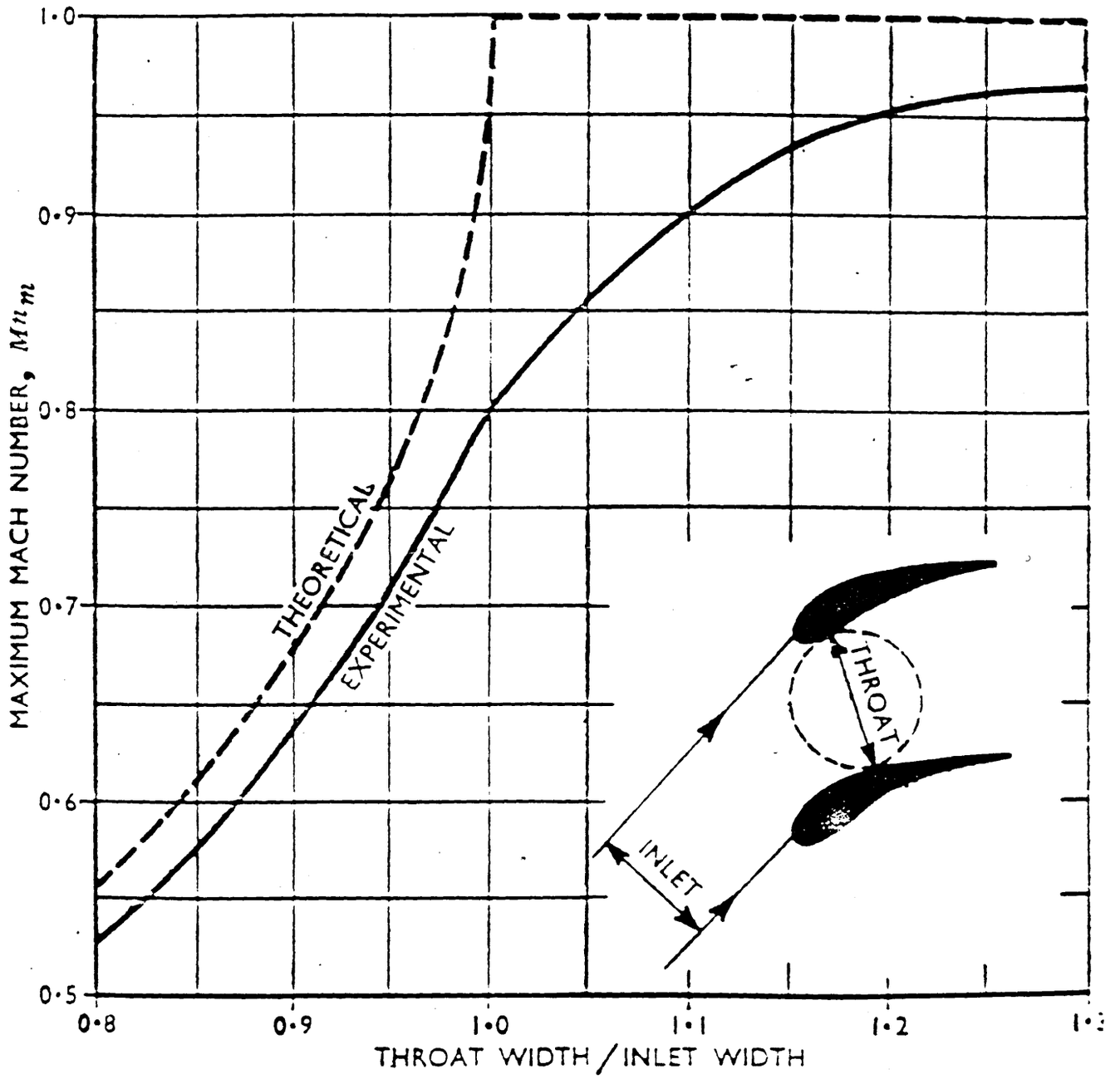

FIG 23 MAXIMUM MACH NUMBER AND THROAT WIDTH

FROM REF(19)

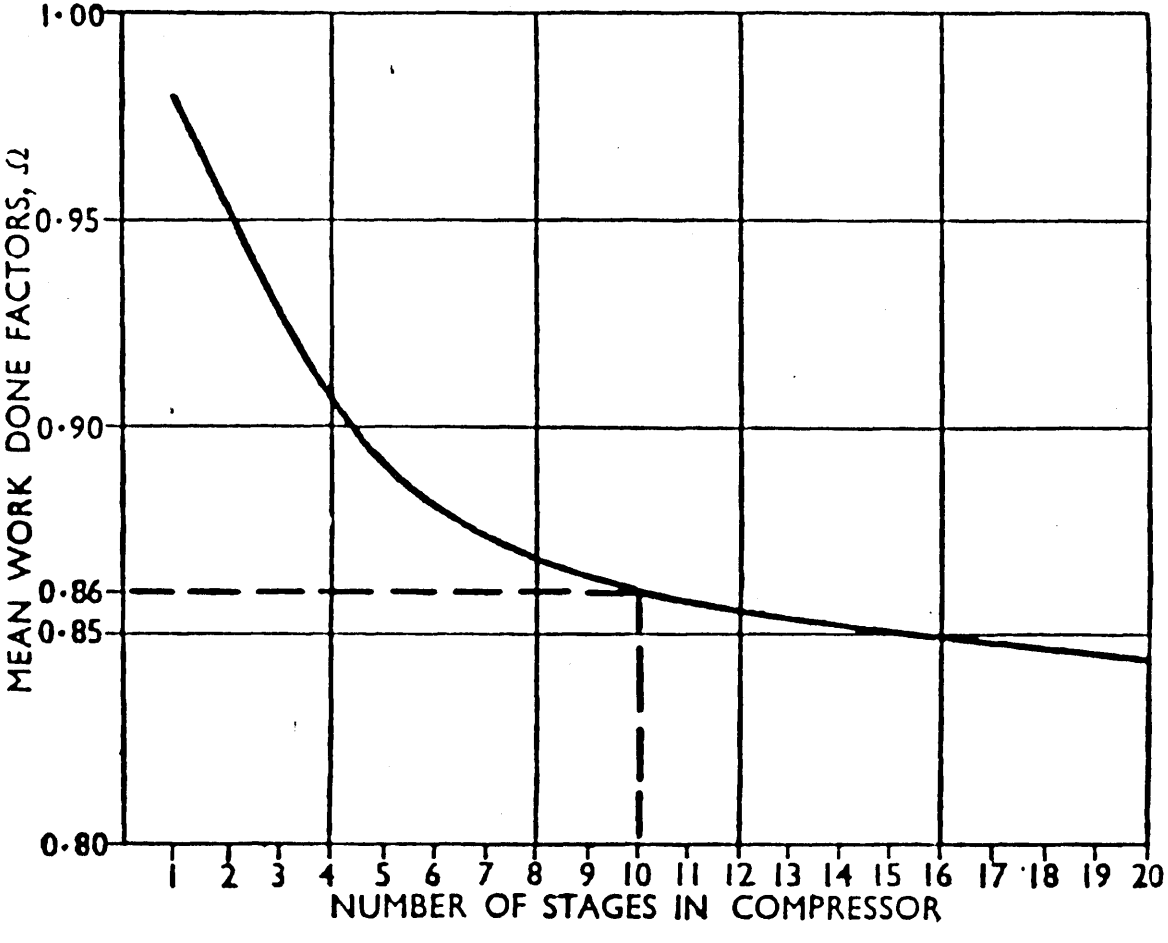

FIG 24 APPROXIMATE MEAN VALUES OF WORK-DONE FACTORS FOR DIFFERNT NUMBERS OF STAGES FROM REF(19)

FIG 25 IP MK670 COMPRESSOR CHARACTERISTICS USING HOWELL'S RULES

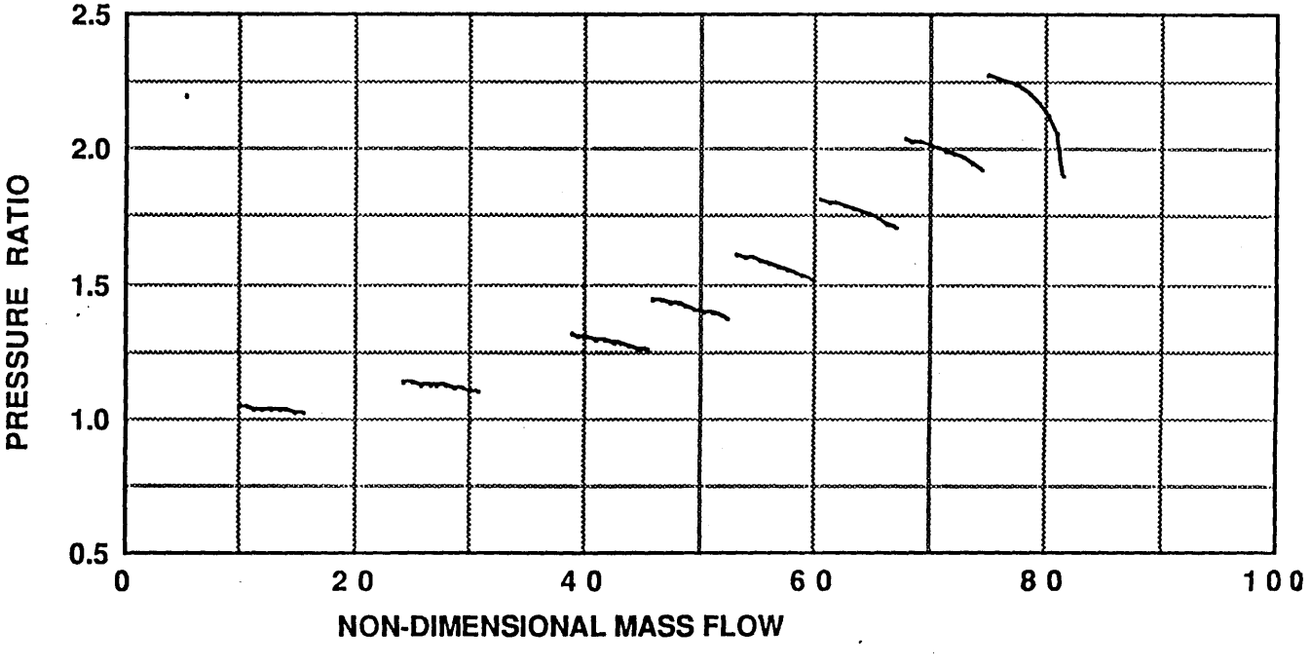

FIG 26 IP MK670 CHARACTERISTICS USING SIMPLIFIED METHOD COMPARED WITH HOWELL'S METHOD FIG 25

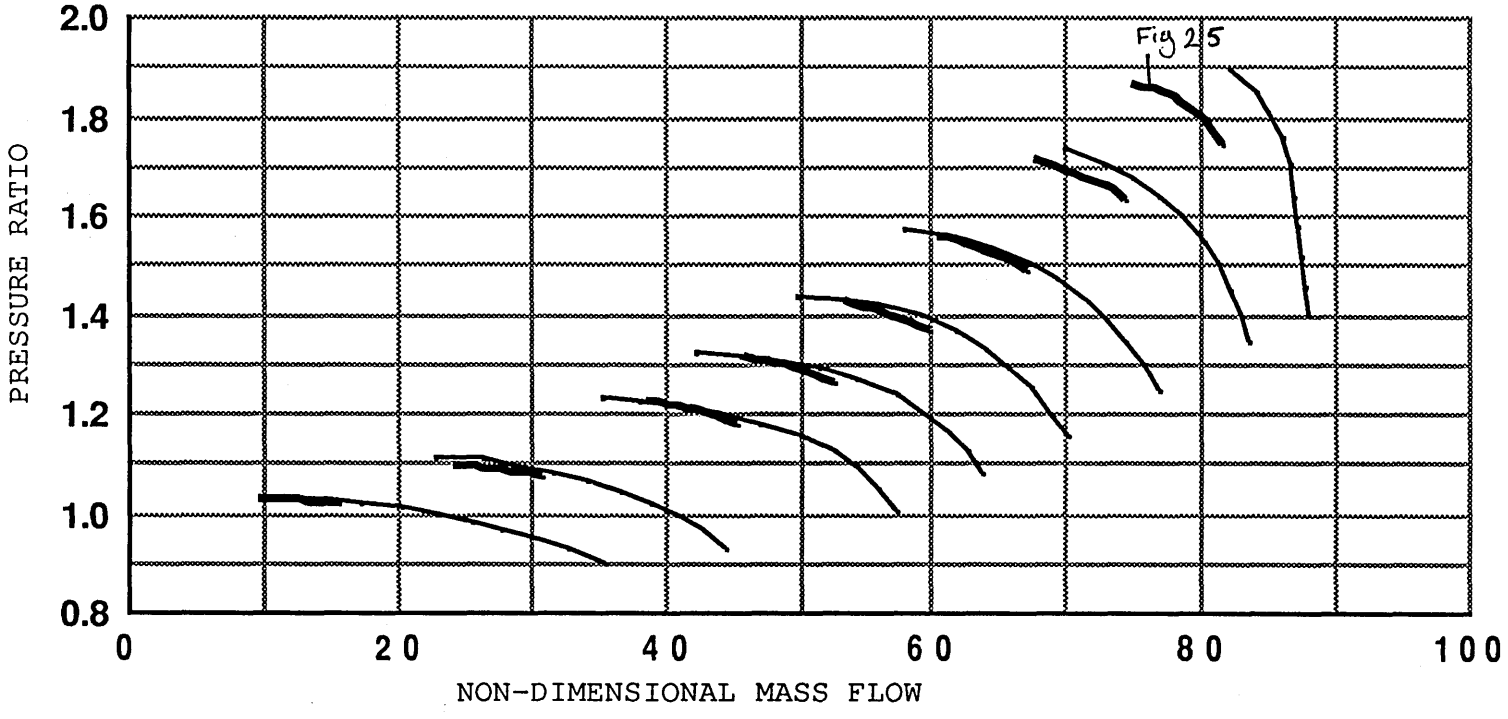

FIG 27 TAY MK610 PREDICTED FUEL SCHEDULE TRAJECTORIES & LP-HP SHAFT SPEED RELATIONSHIPS

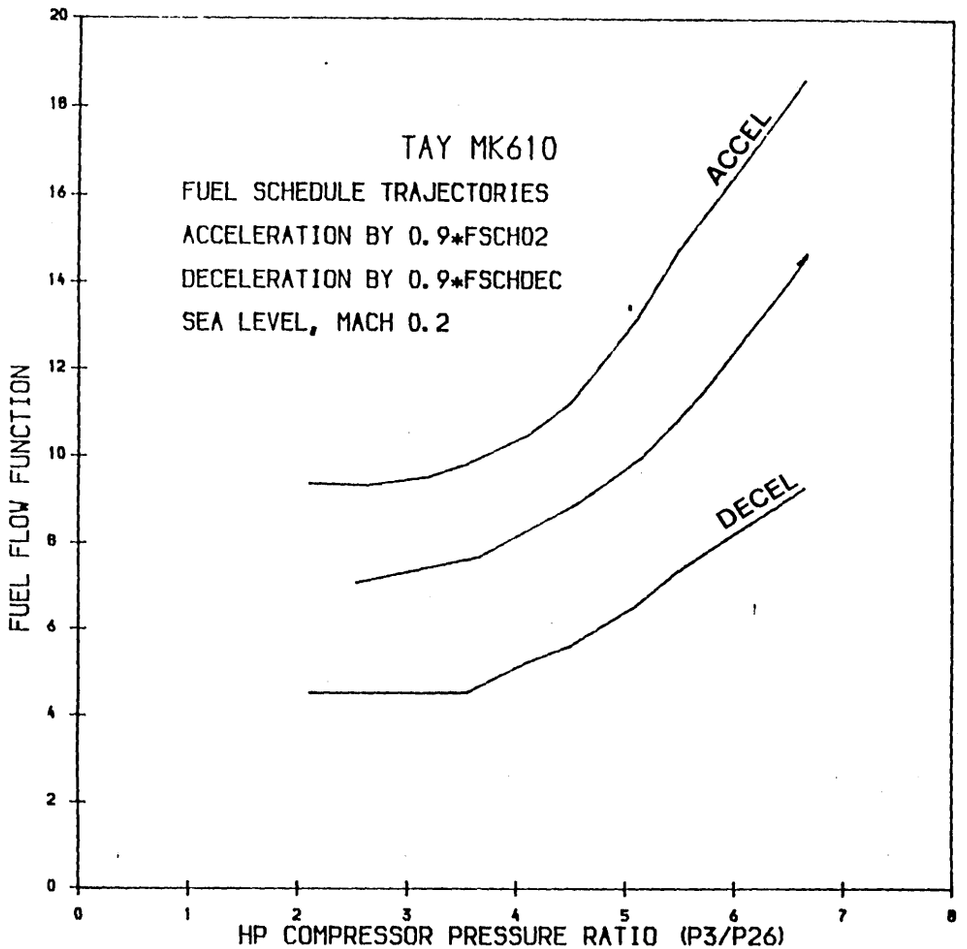

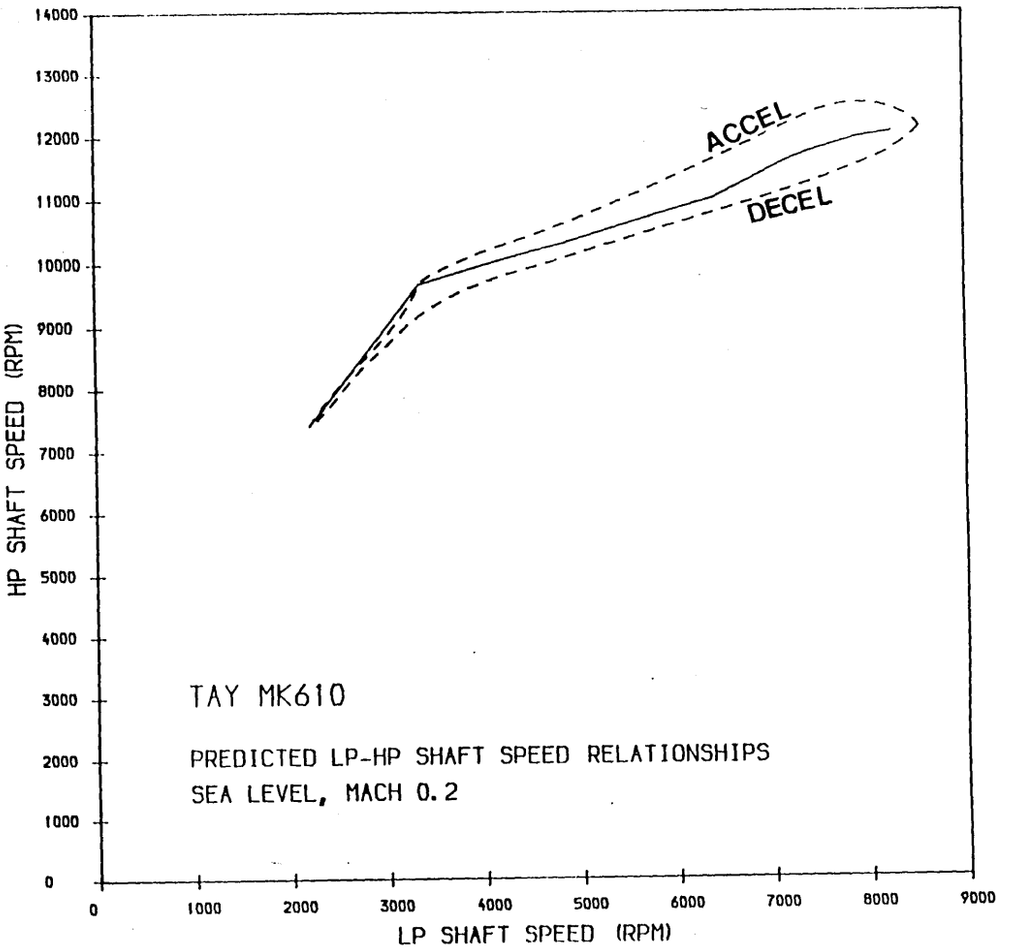

FIG 28 TAY MK610 PREDICTED ADIABATIC TRANSIENTS AT SEA LEVEL MACH NUM=0.2

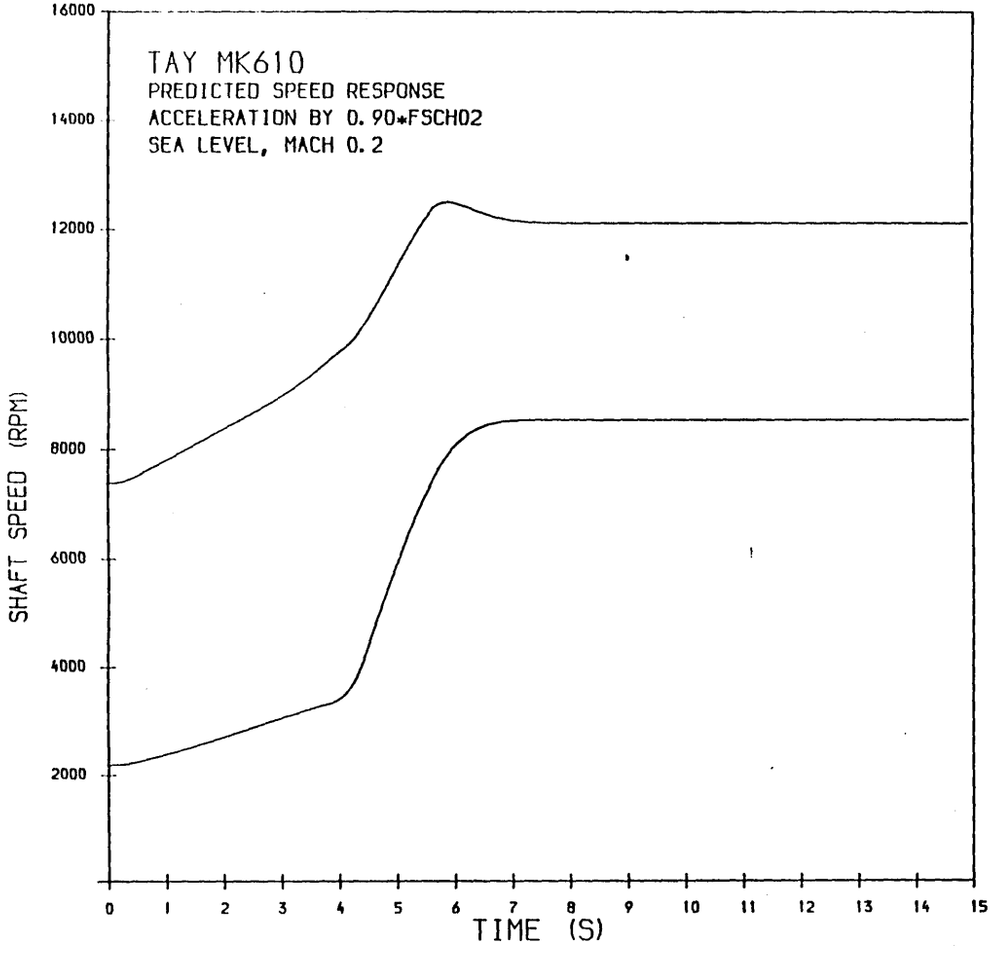

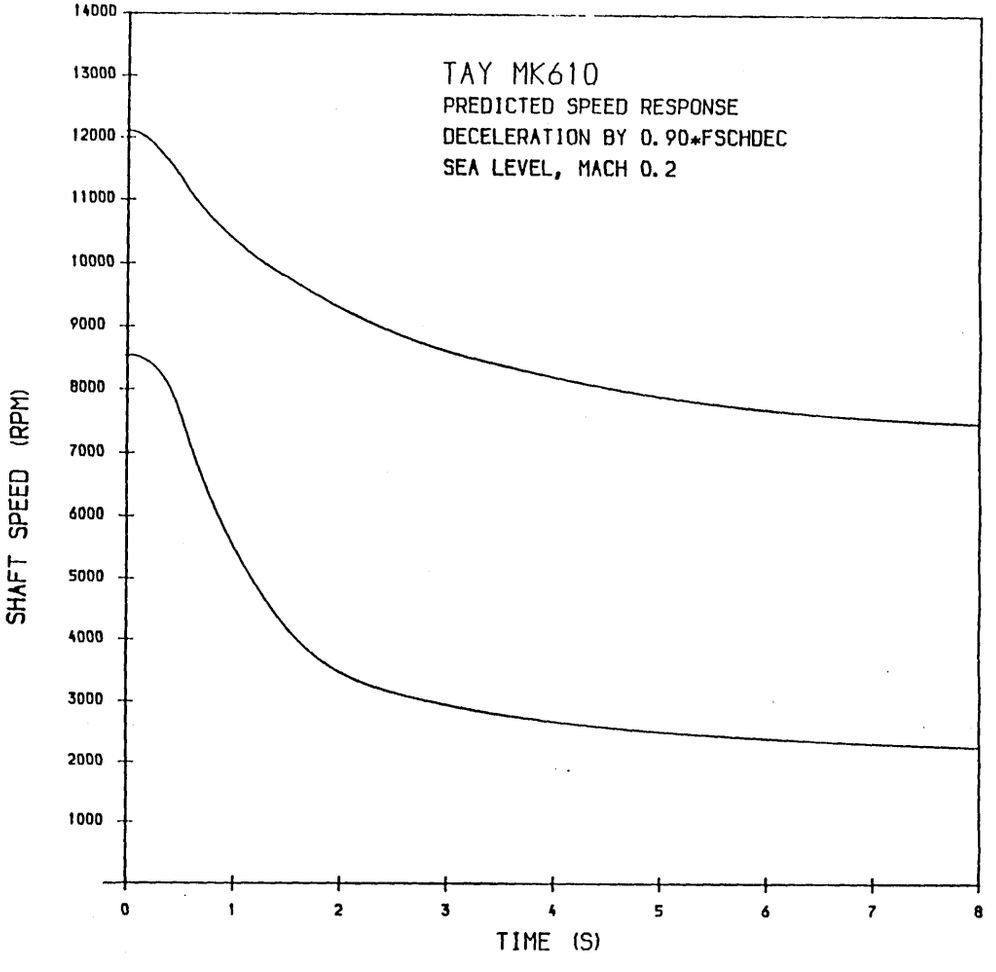

FIG 29 TAY MK610 PREDICTED ADIABATIC TRANSIENTS AT SEA LEVEL MACH NUM=0.2

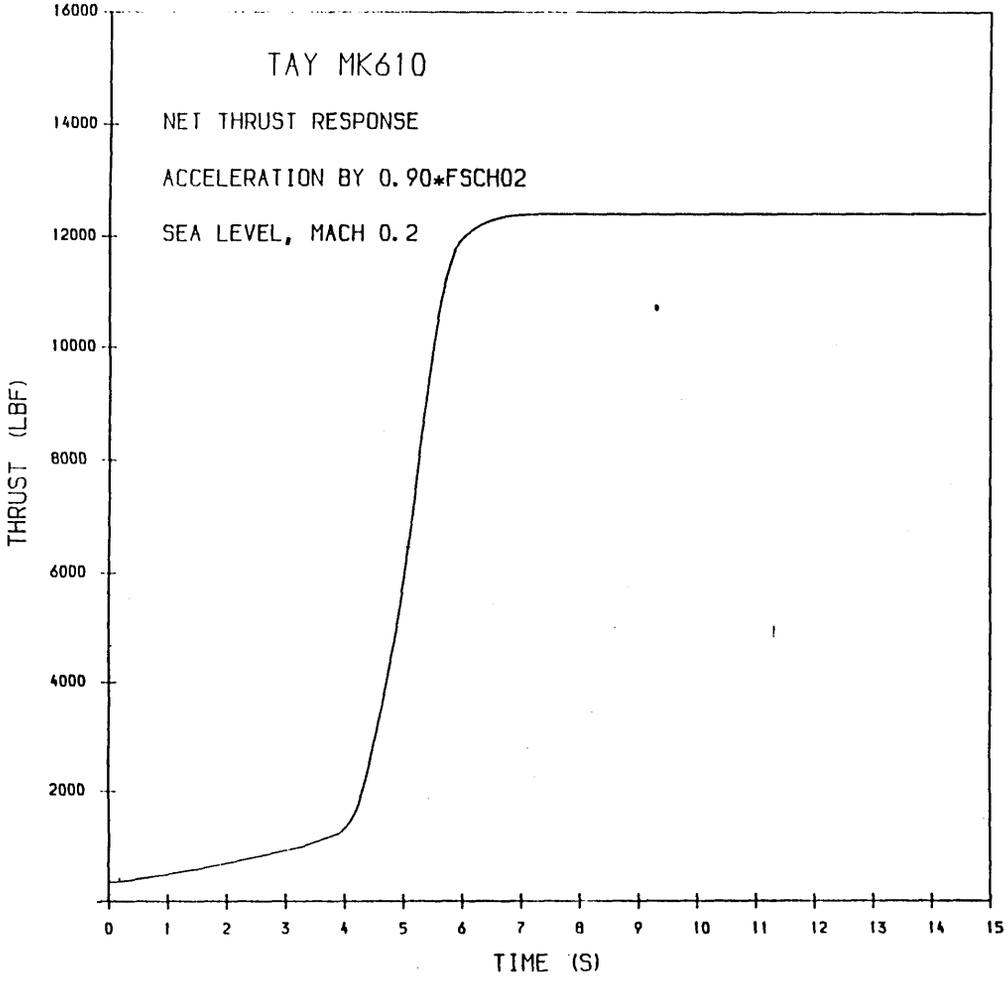

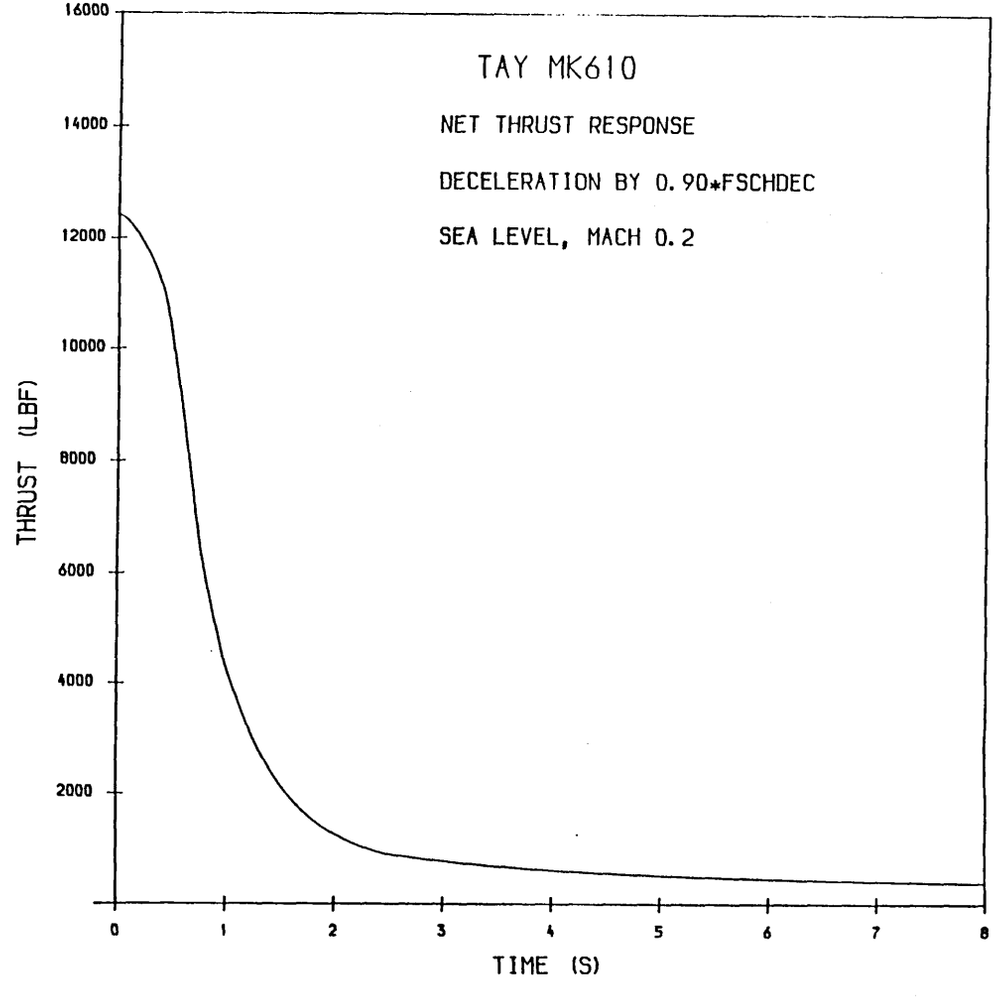

FIG 30 TAY MK610 PREDICTED PATHS OF THE FAN SECTIONS DURING TRANSIENT ACCEL & DECEL AT SEA LEVEL MACH NUM=0.2

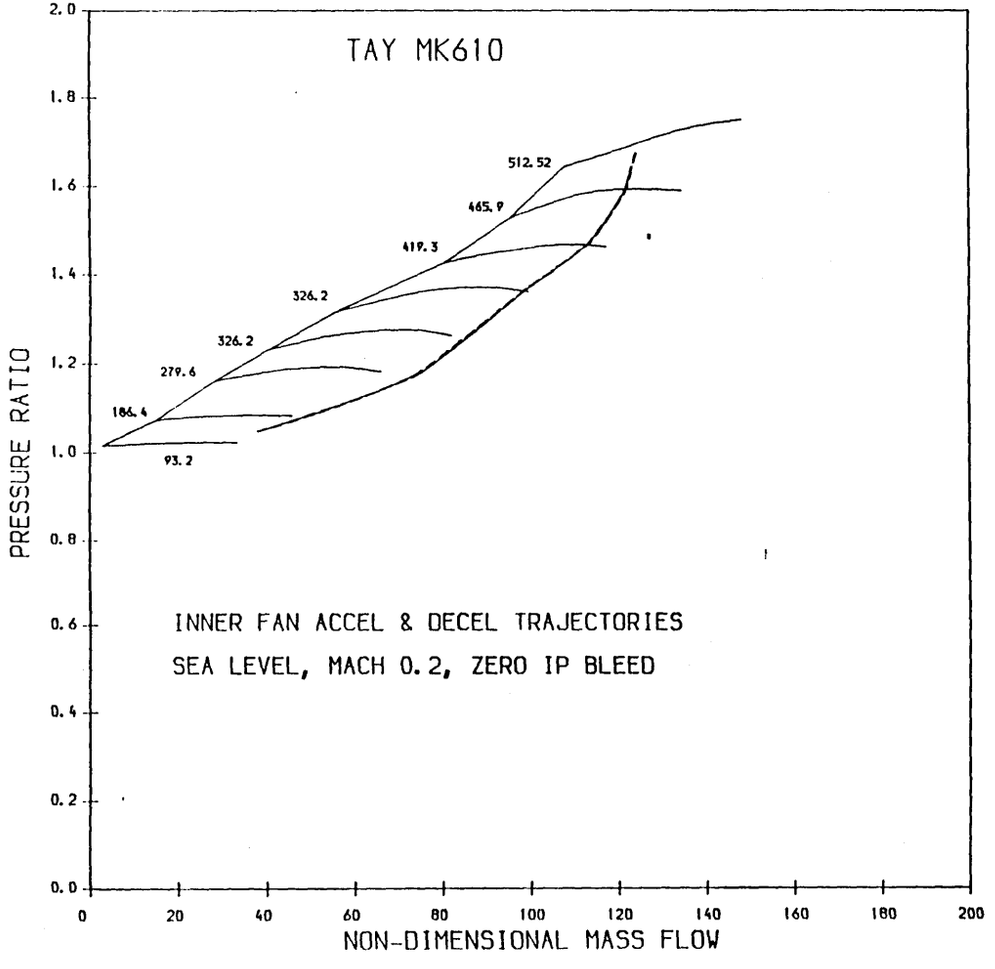

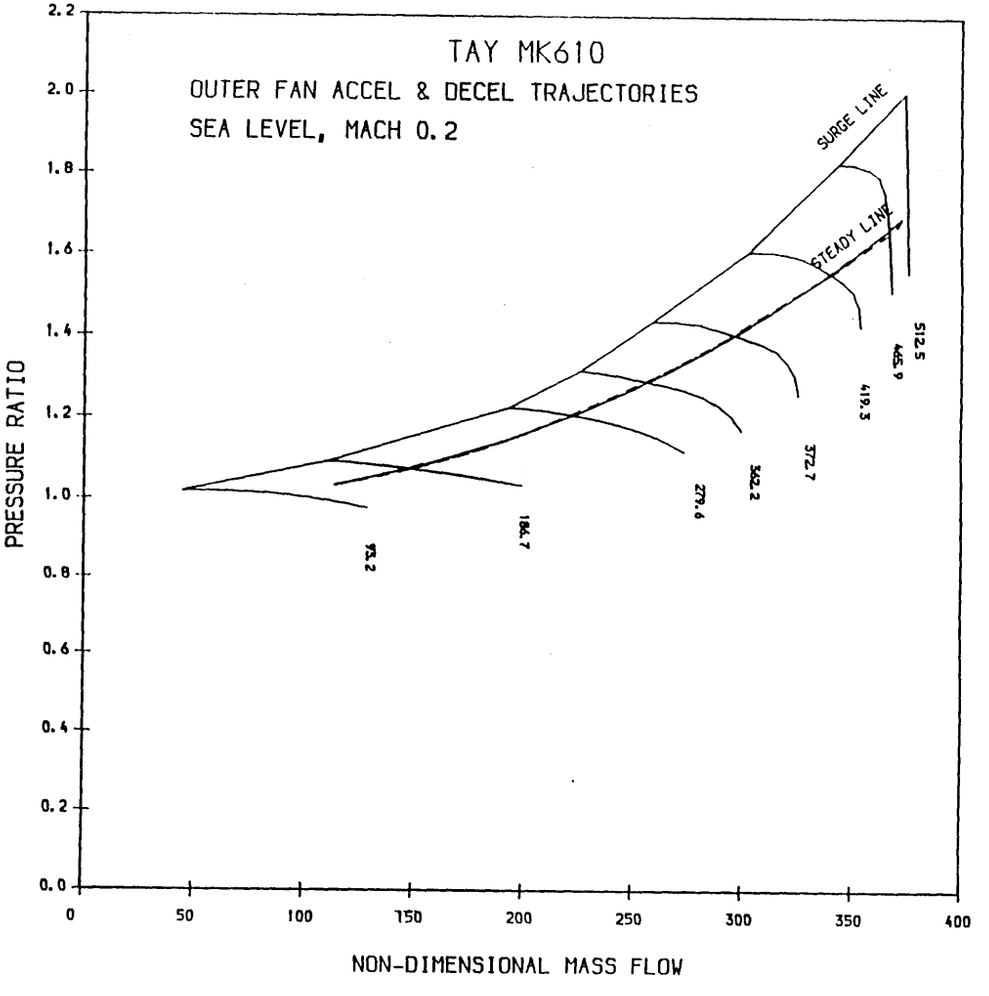

FIG 31 TAY MK610 PREDICTED ACCELERATION AN DECELERATION OF THE IP AND HP COMPRESSOR AT SEA LEVEL MACH NUM=0.2

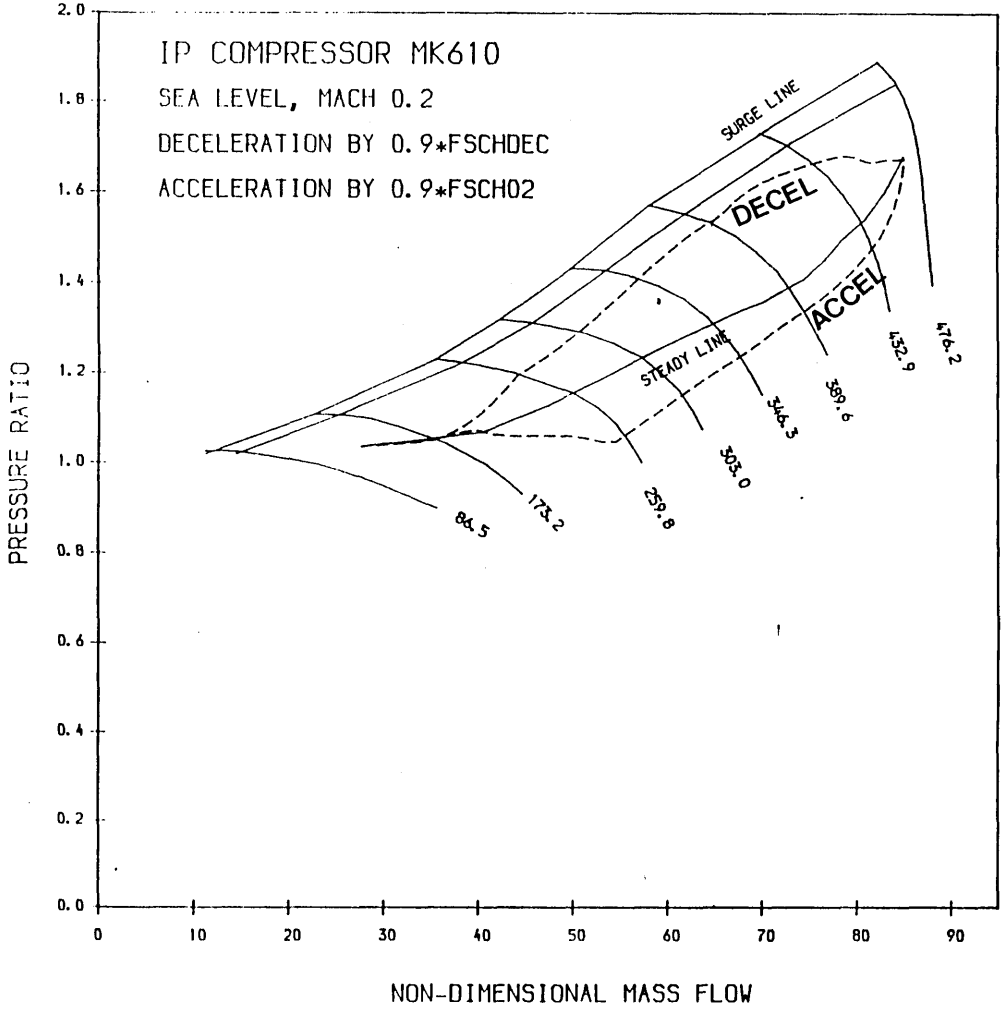

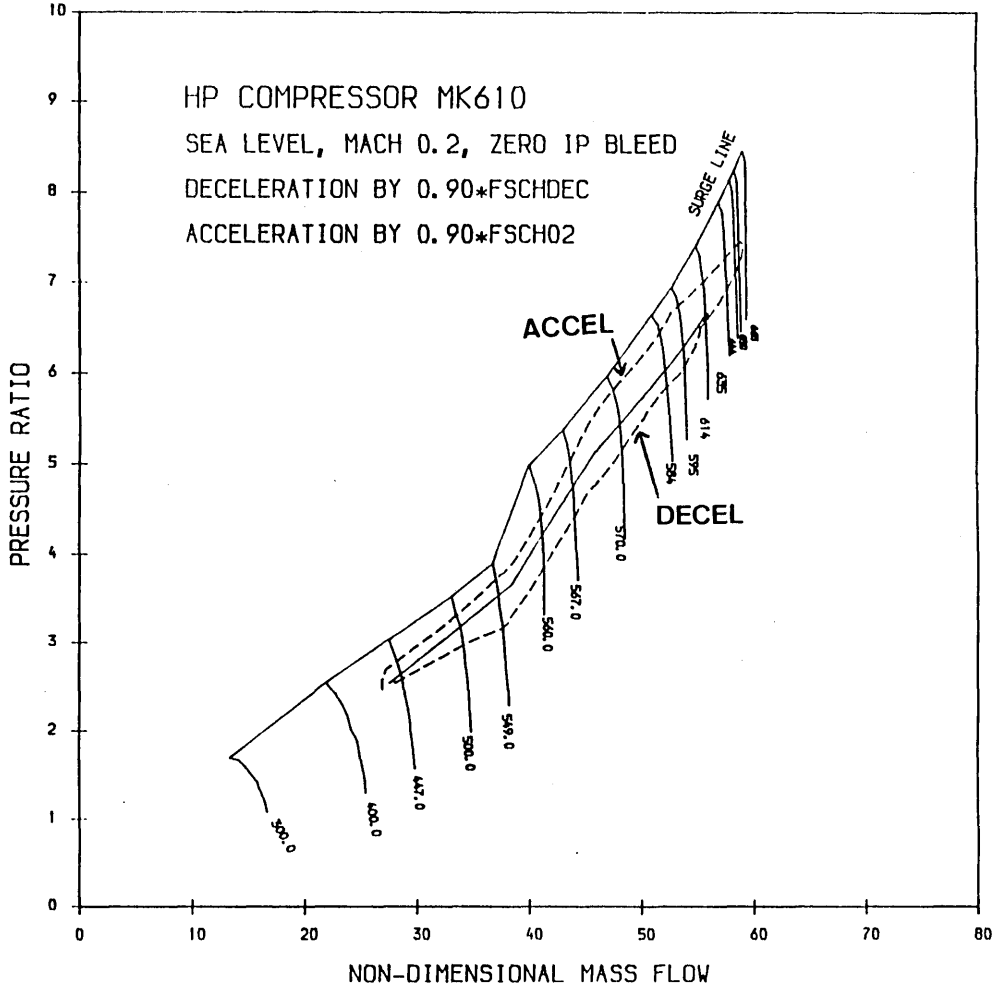

FIG 32 TAY MK610 PREDICTED ADIABATIC THRUST RESPONSE & FUEL SCHEDULE TRAJECTORIES AT 32,000 FT MACH NUM=0.8

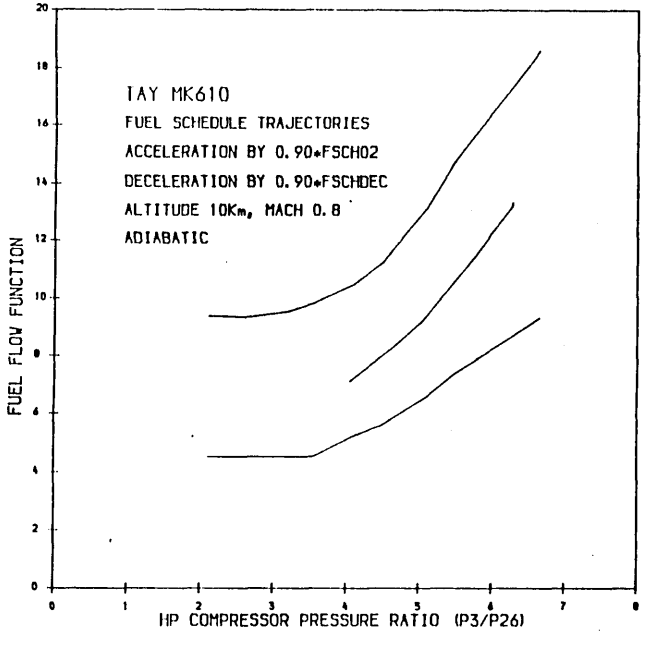

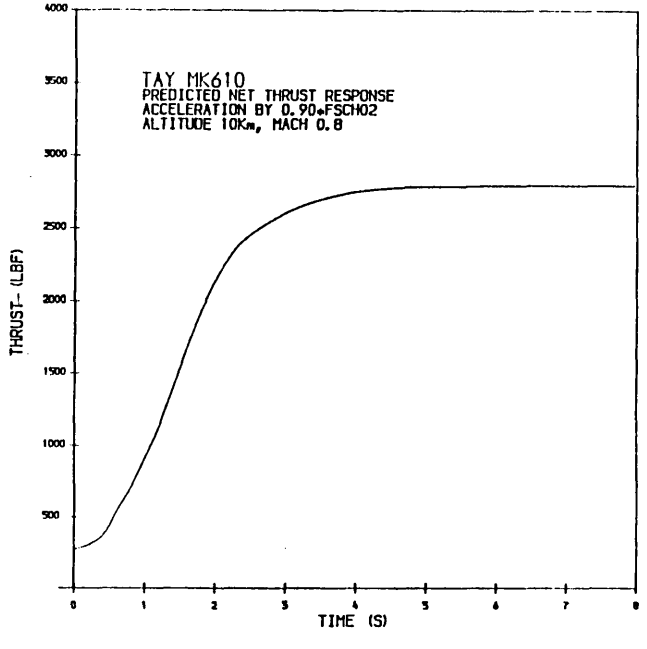

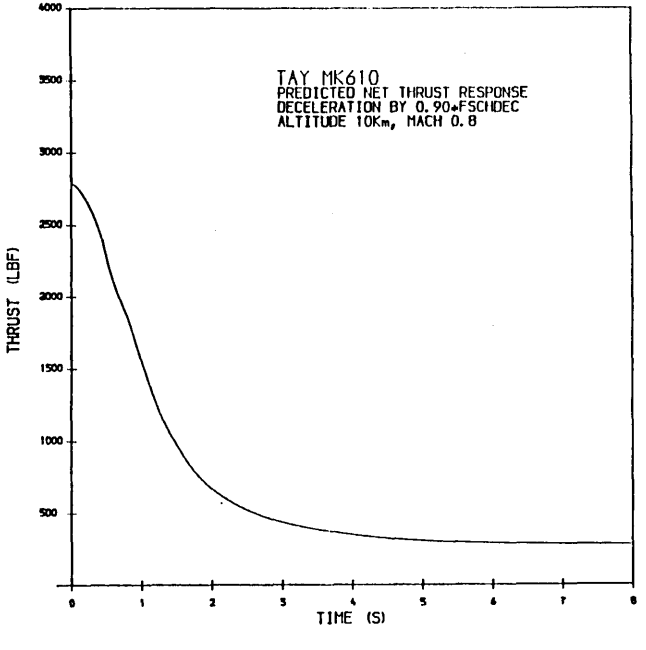

FIG 33 TAY MK610' PREDICTED ADIABATIC TRANSIENTS AT 32,000 FT
MACH NUM=0.8

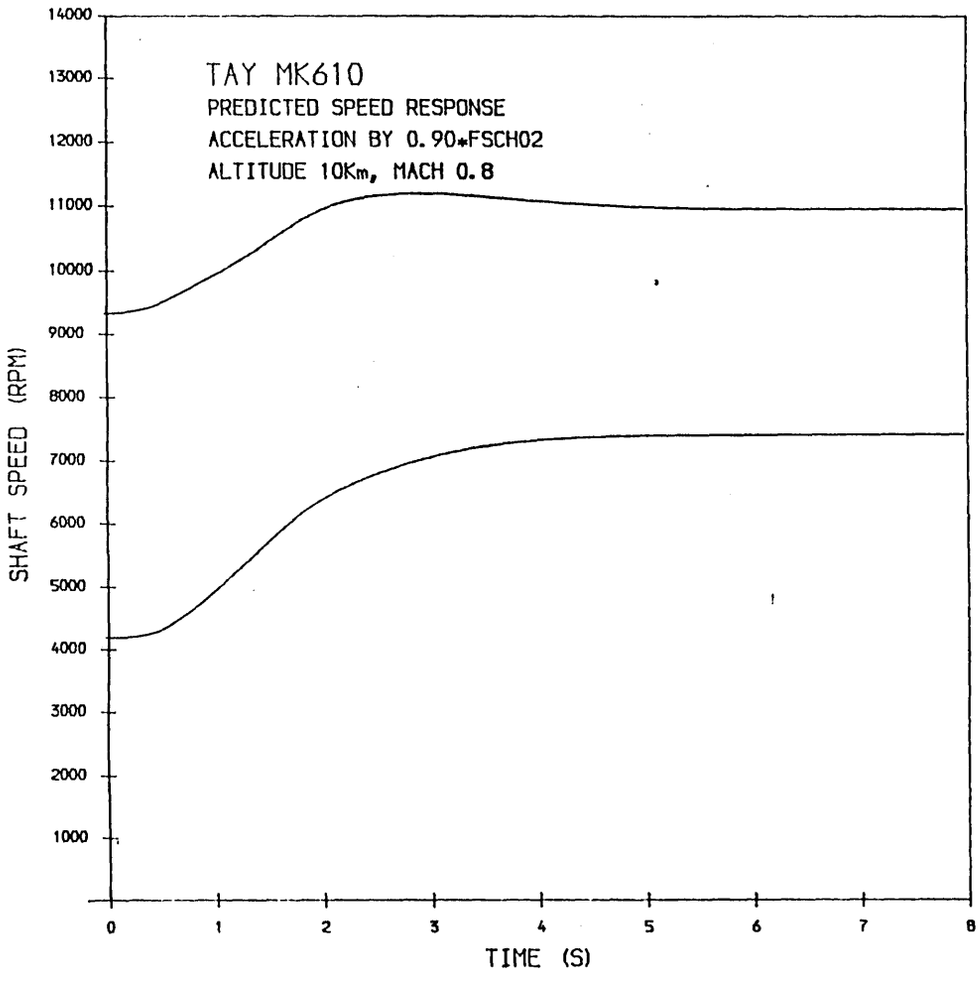

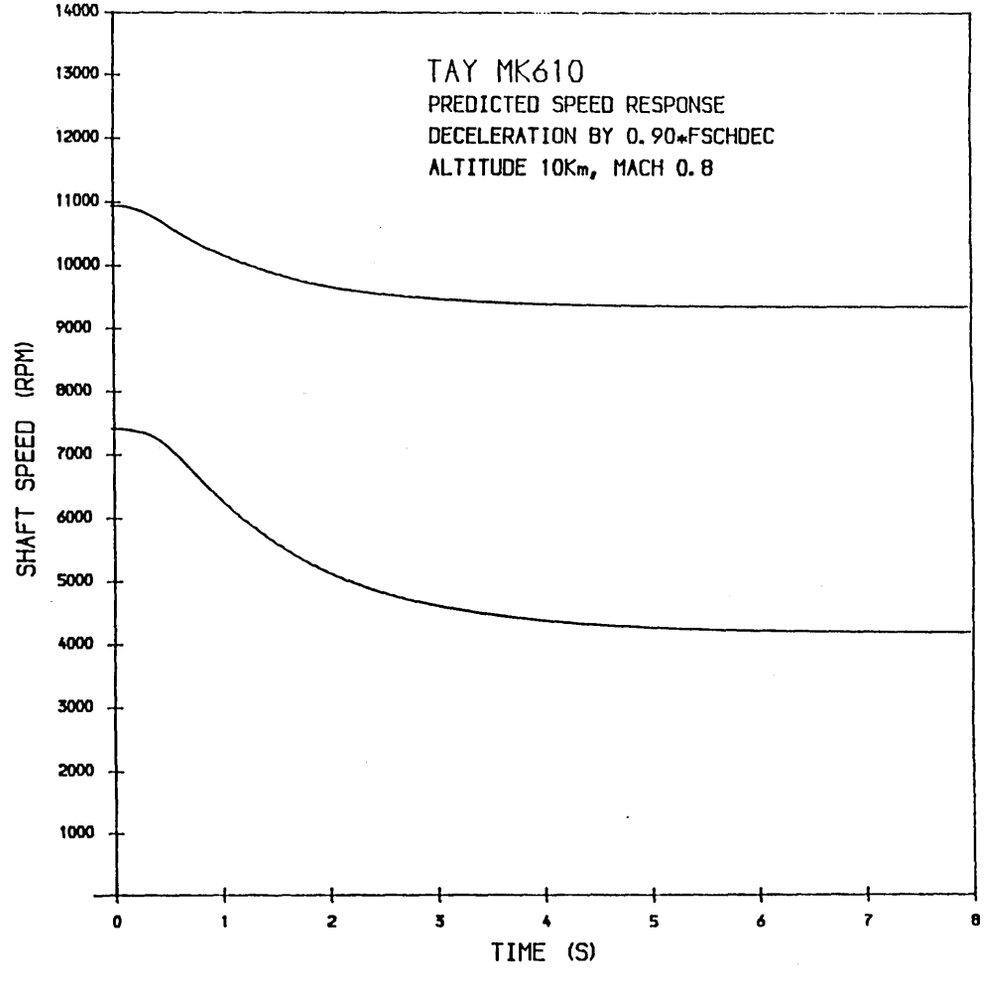

FIG 34 TAY MK610 PREDICTED ADIABATIC TRANSIENTS AT 32,000 FT MACH NUM=0.8

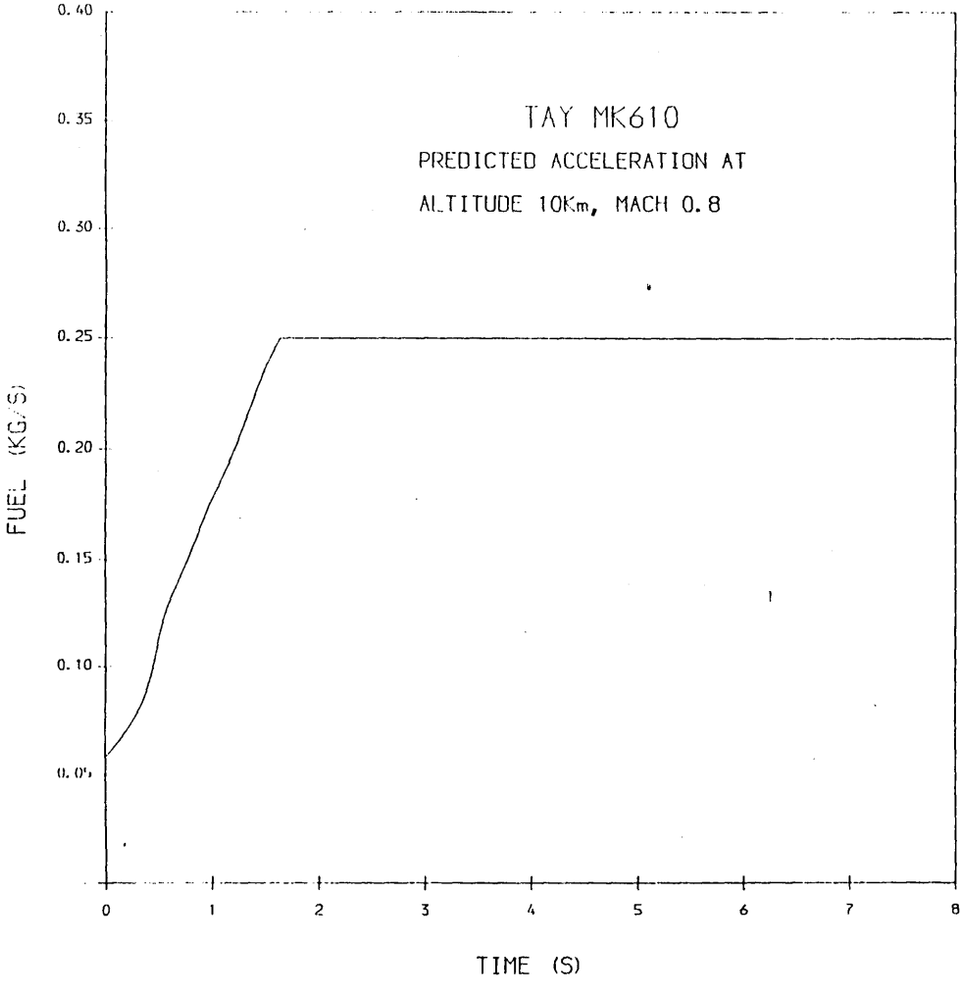

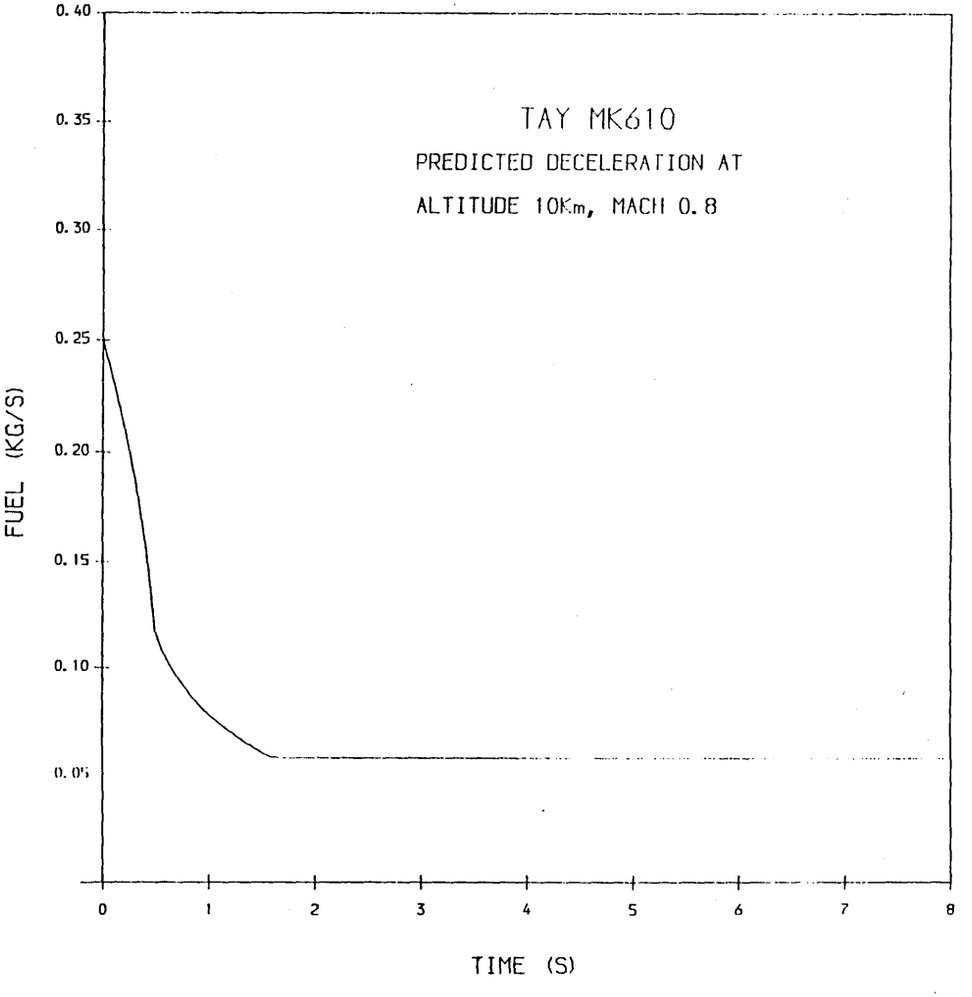

FIG 35 TAY MK61Q PREDICTED PATHS OF THE FAN SECTIONS DURING TRANSIENT ACCEL & DECEL AT 32,000 FT MACH NUM=0.8

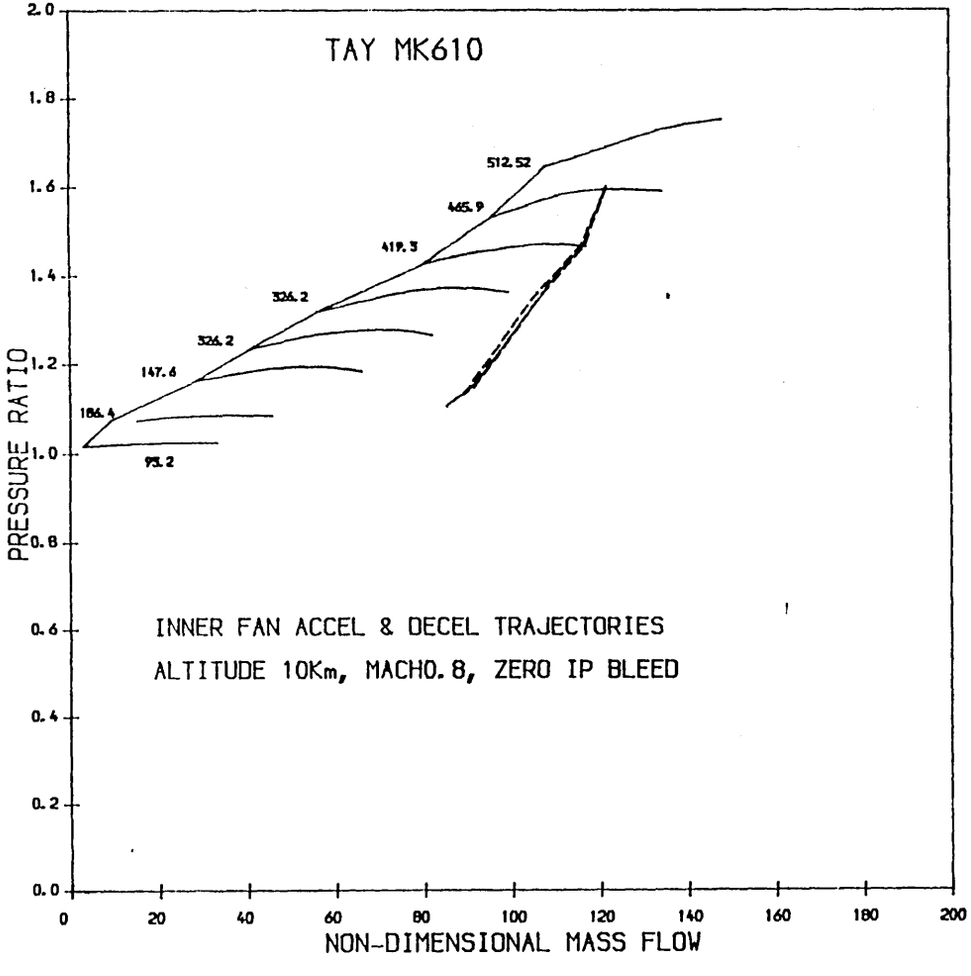

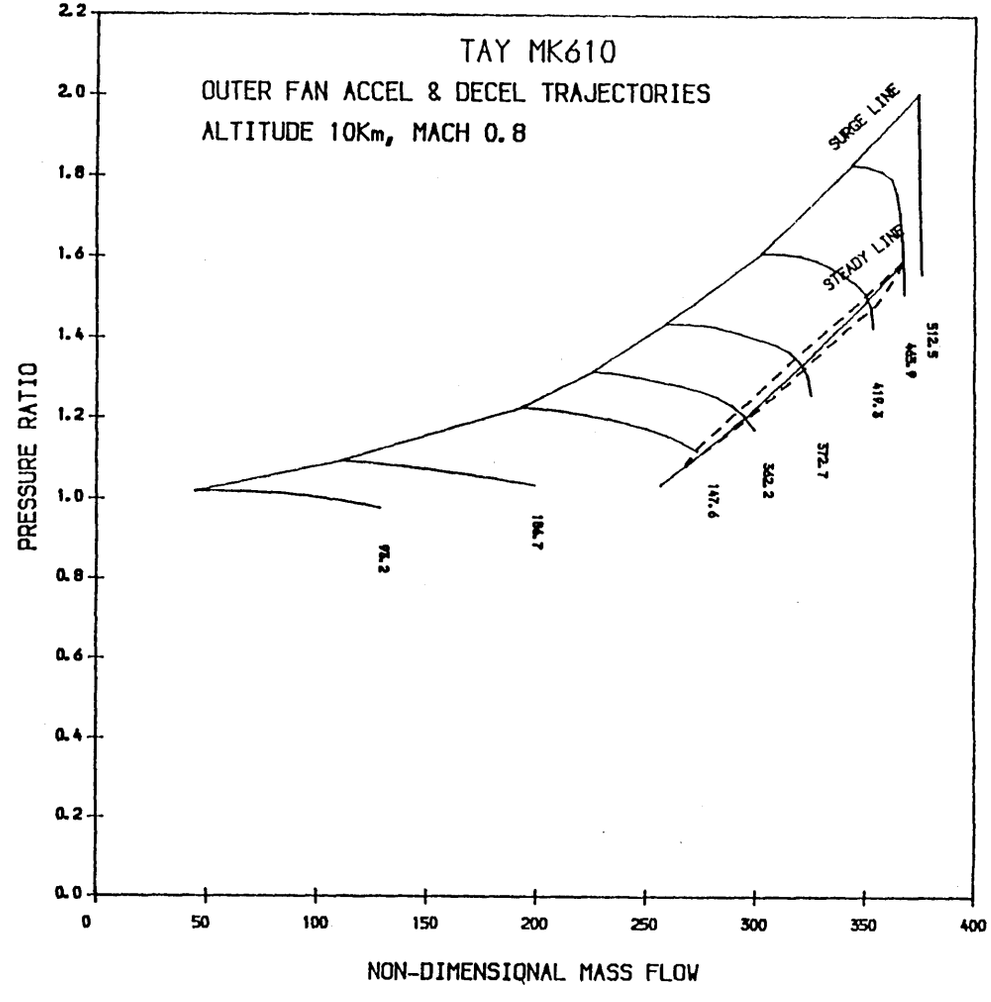

FIG 36 TAY MK610 PREDICTED ACCELERATION AN DECELERATION OF THE IP AND HP COMPRESSOR AT 32,000 FT MACH NUM=0.8

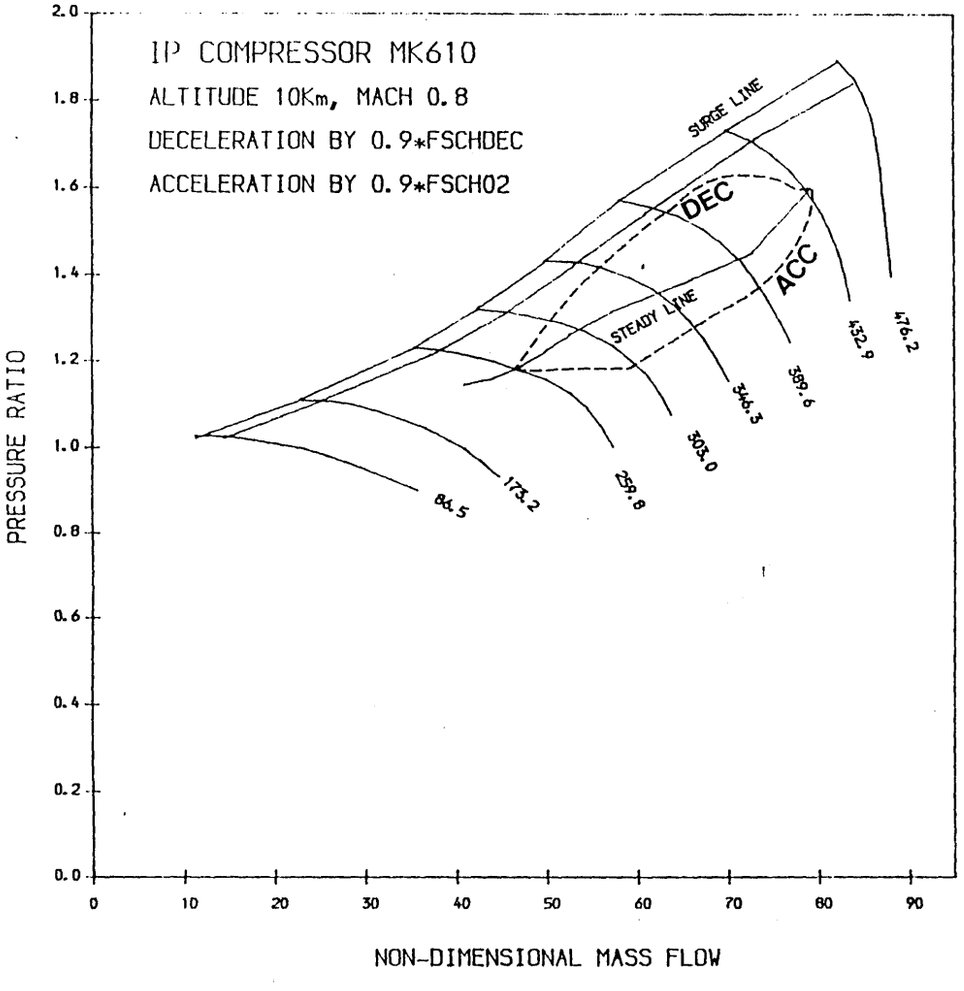

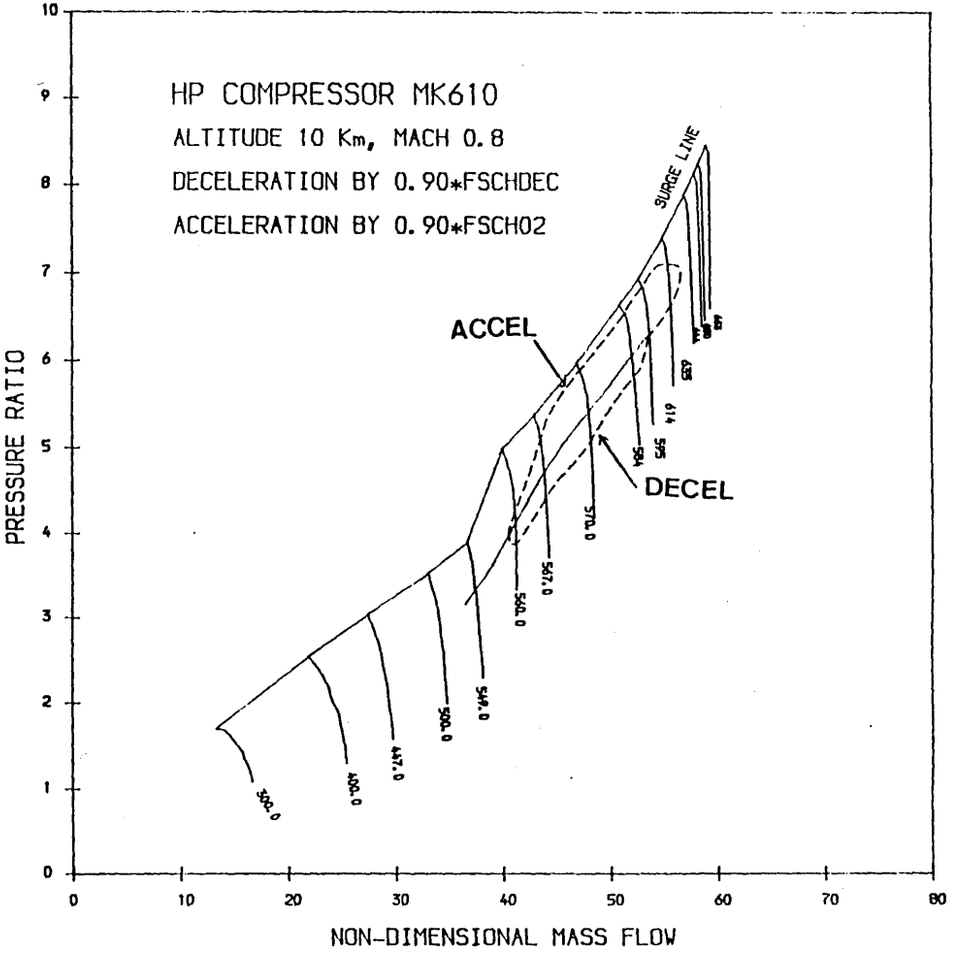

FIG 37 TAY MK670 PREDICTED FUEL SCHEDULE TRAJECTORIES & LP-HP SHAFT SPEED RELATIONSHIPS

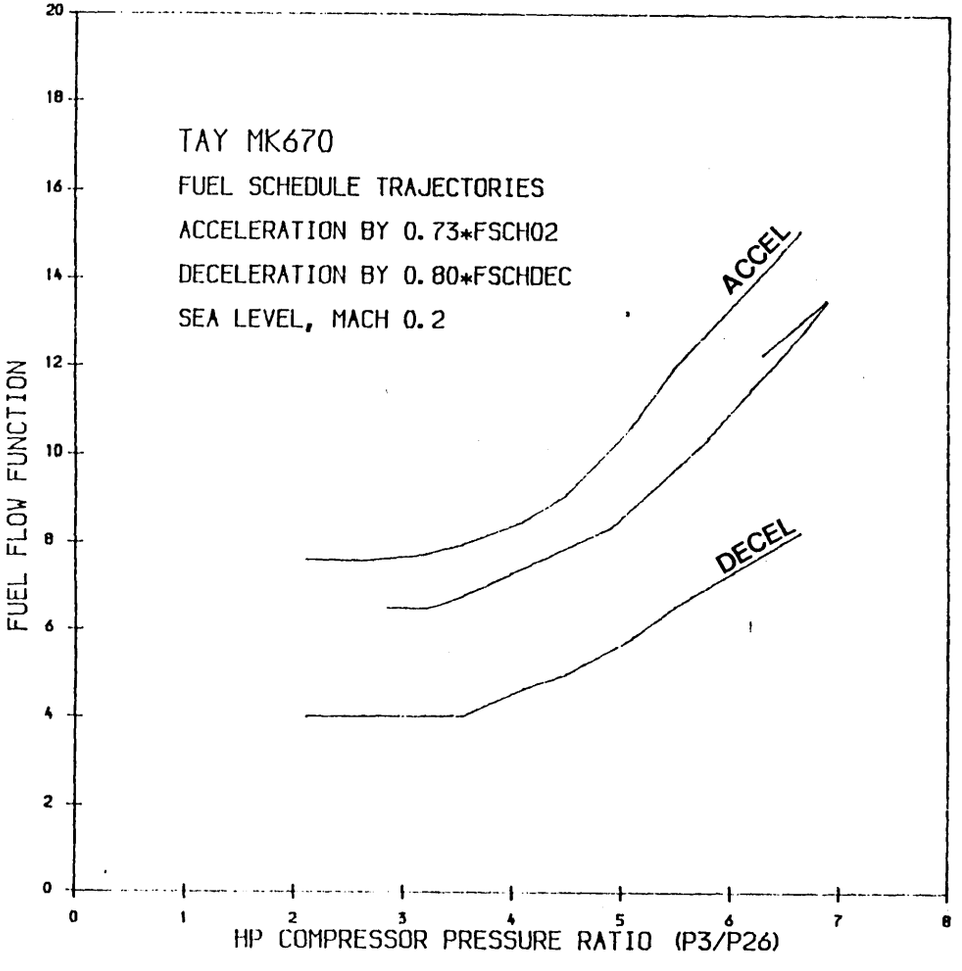

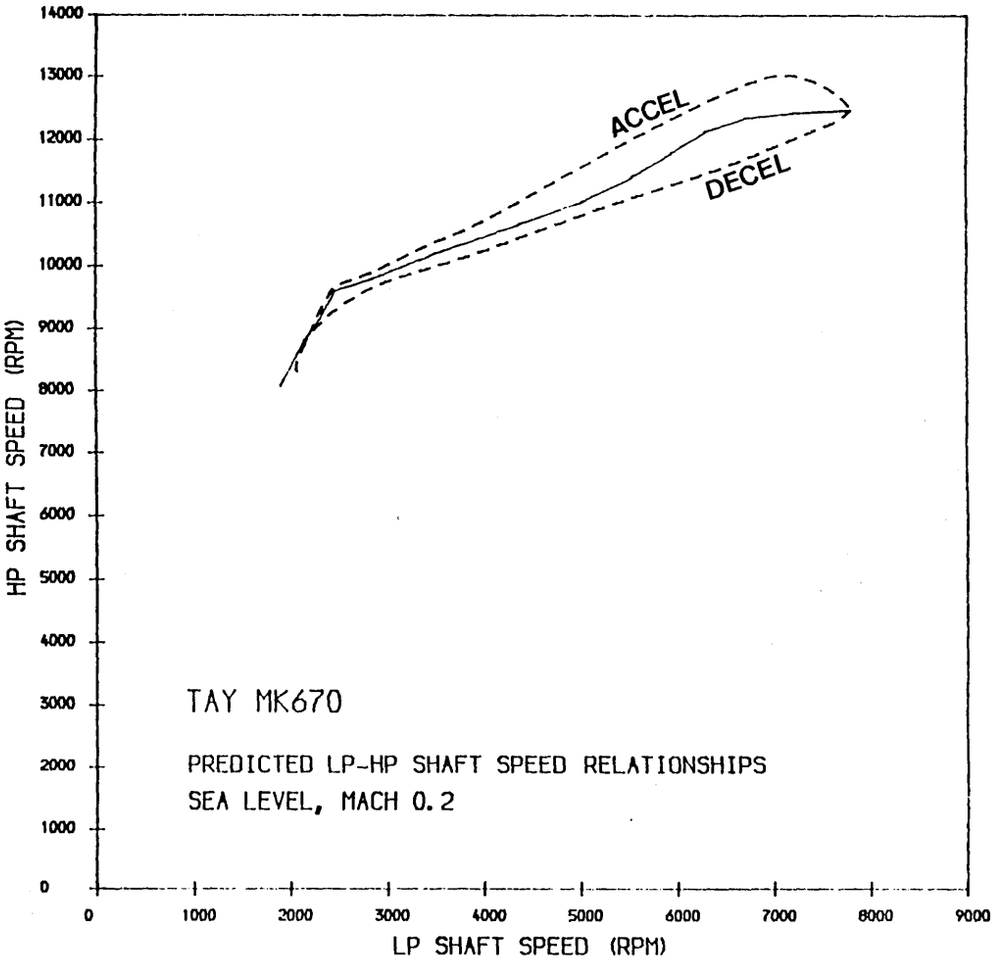

FIG 38 TAY MK670 PREDICTED ADIABATIC TRANSIENTS AT SEA LEVEL MACH NUM=0.2

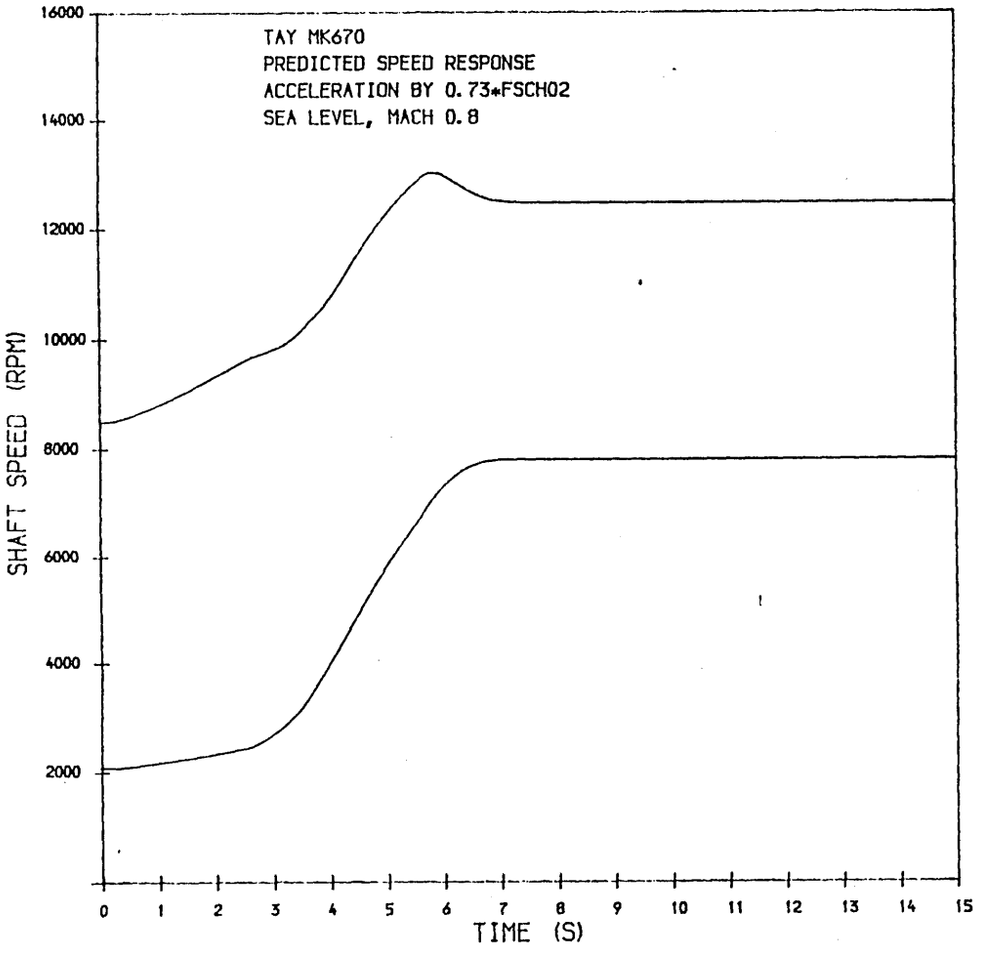

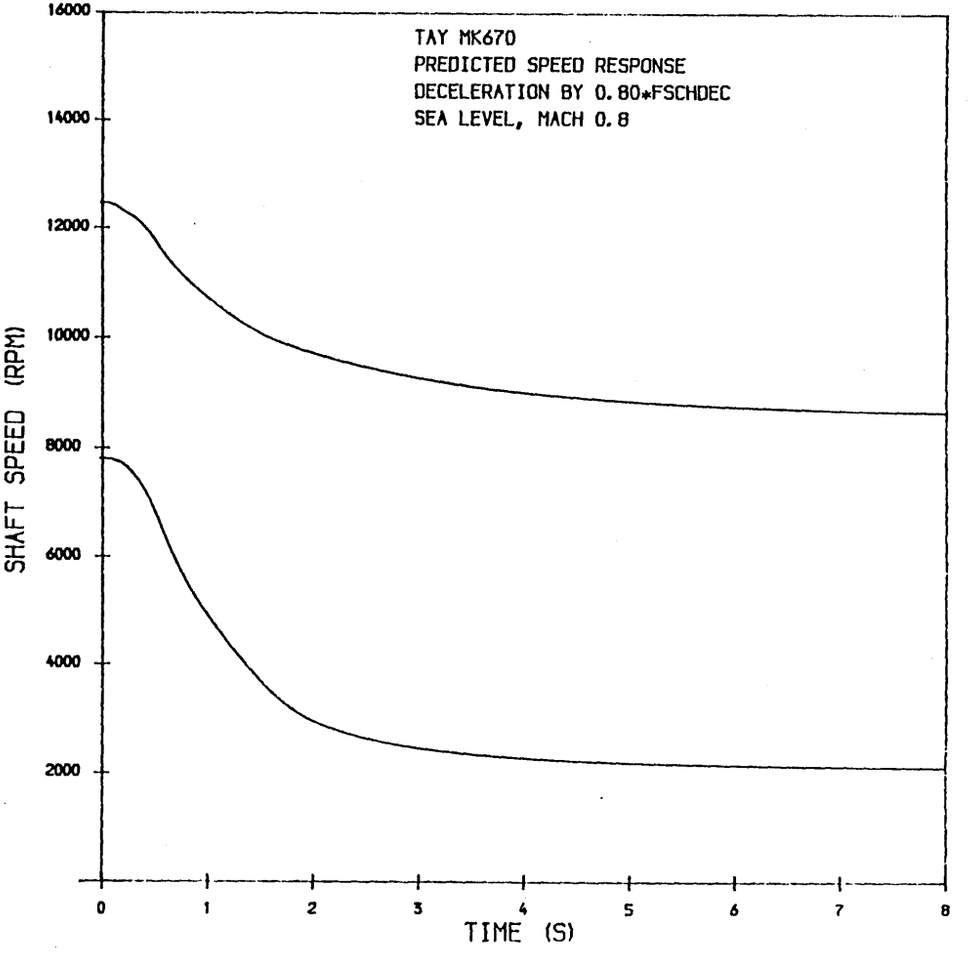

FIG 39 TAY MK670 PREDICTED ADIABATIC TRANSIENTS AT SEA LEVEL MACH NUM=0.2

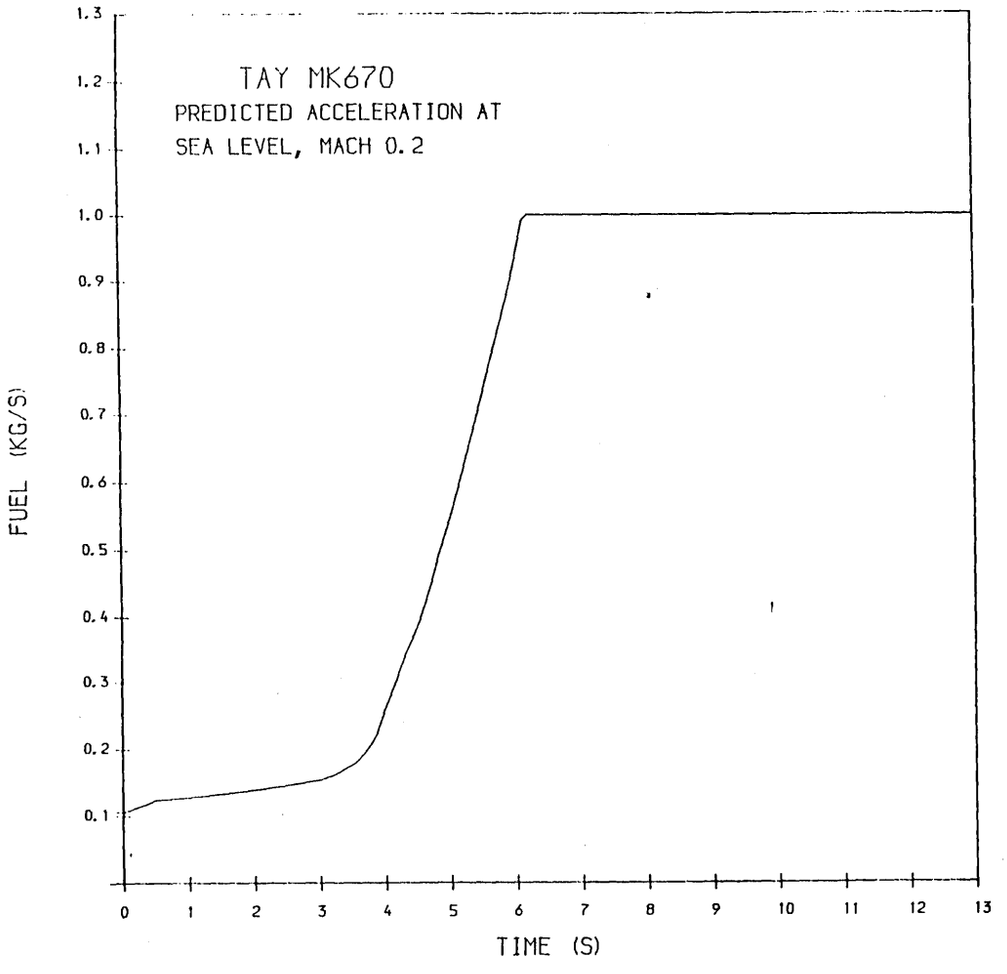

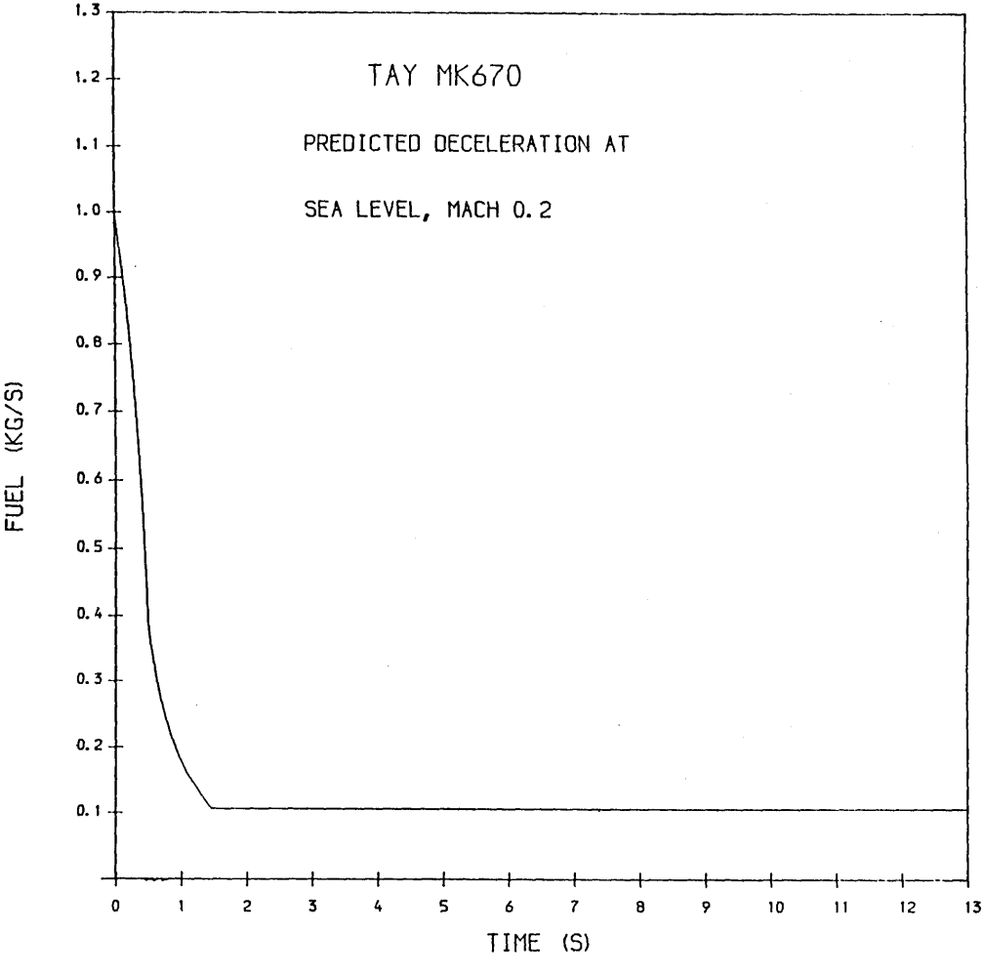

FIG 40 TAY MK670 PREDICTED ADIABATIC TRANSIENTS AT SEA LEVEL MACH NUM=0.2

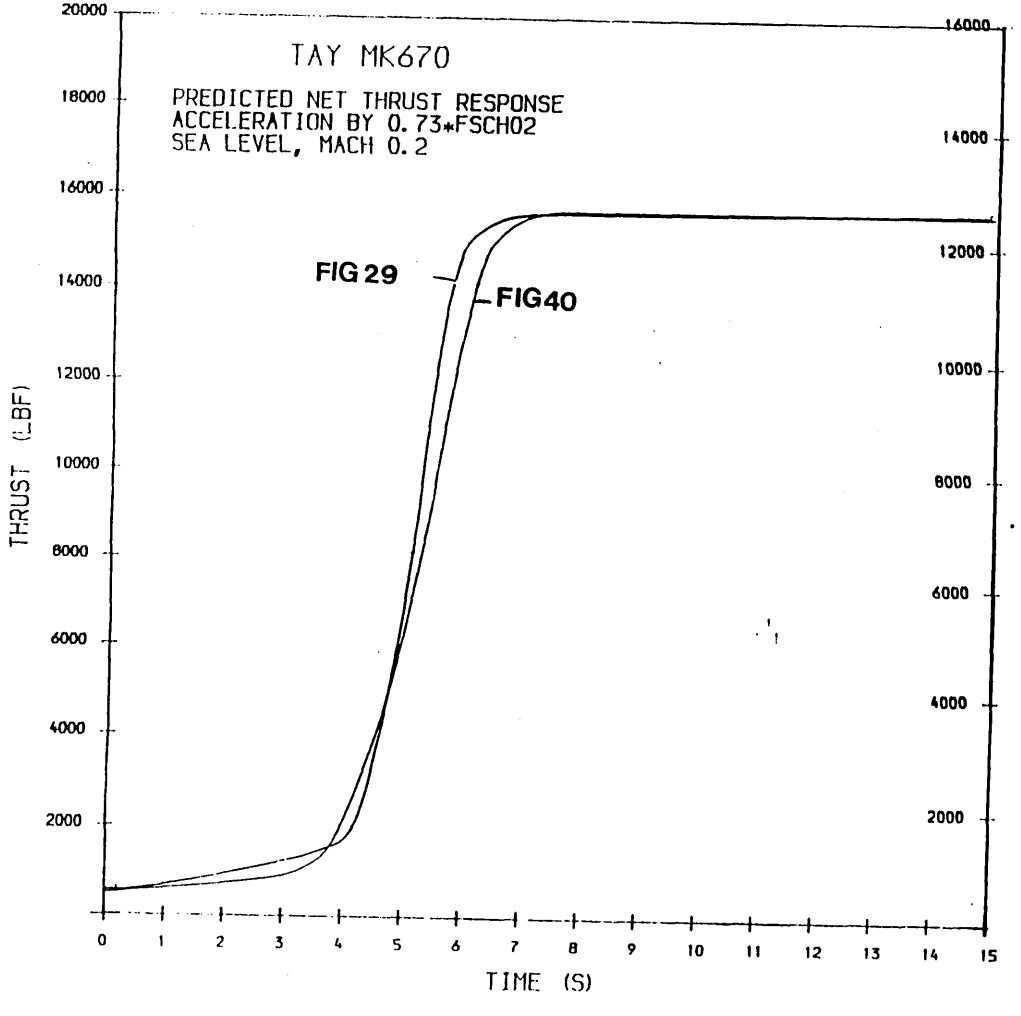

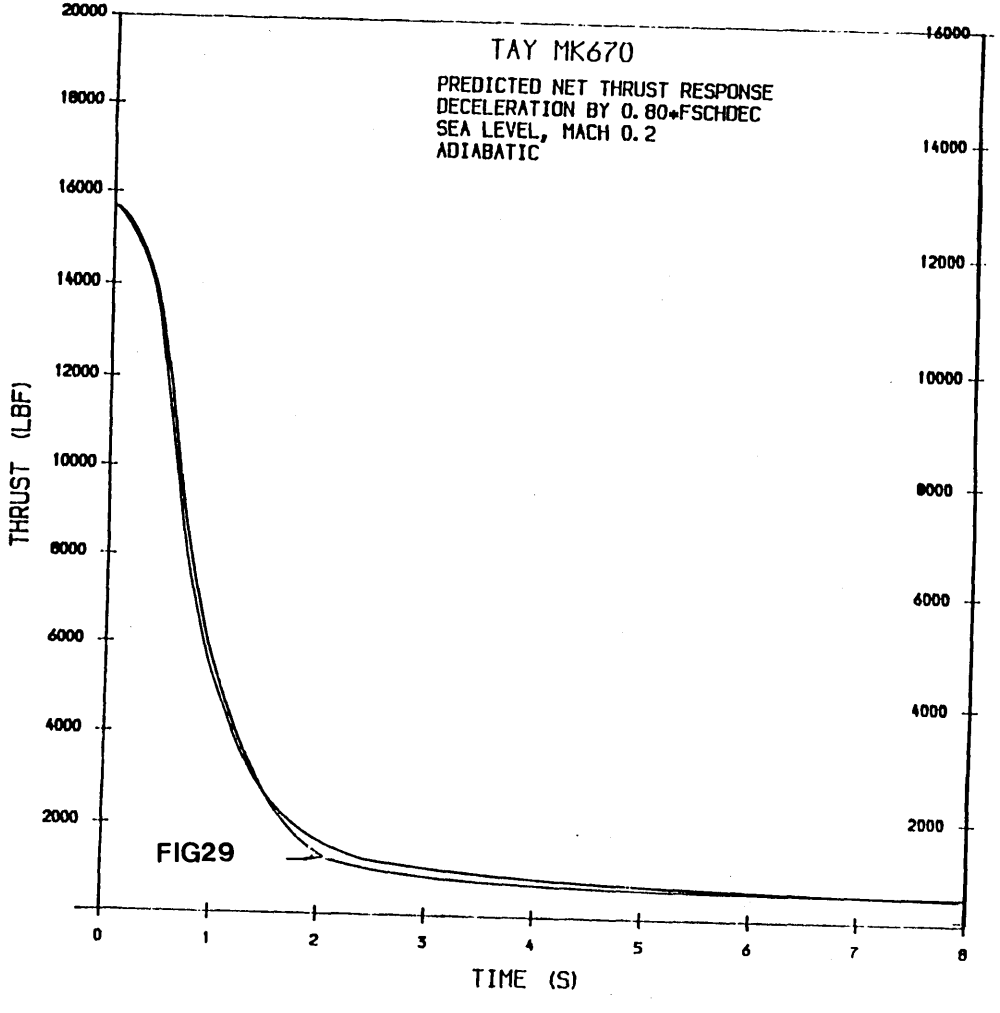

FIG 41 TAY MK670 PREDICTED PATHS OF THE FAN SECTIONS DURING TRANSIENT ACCEL & DECEL AT SEA LEVEL MACH NUM=0.2

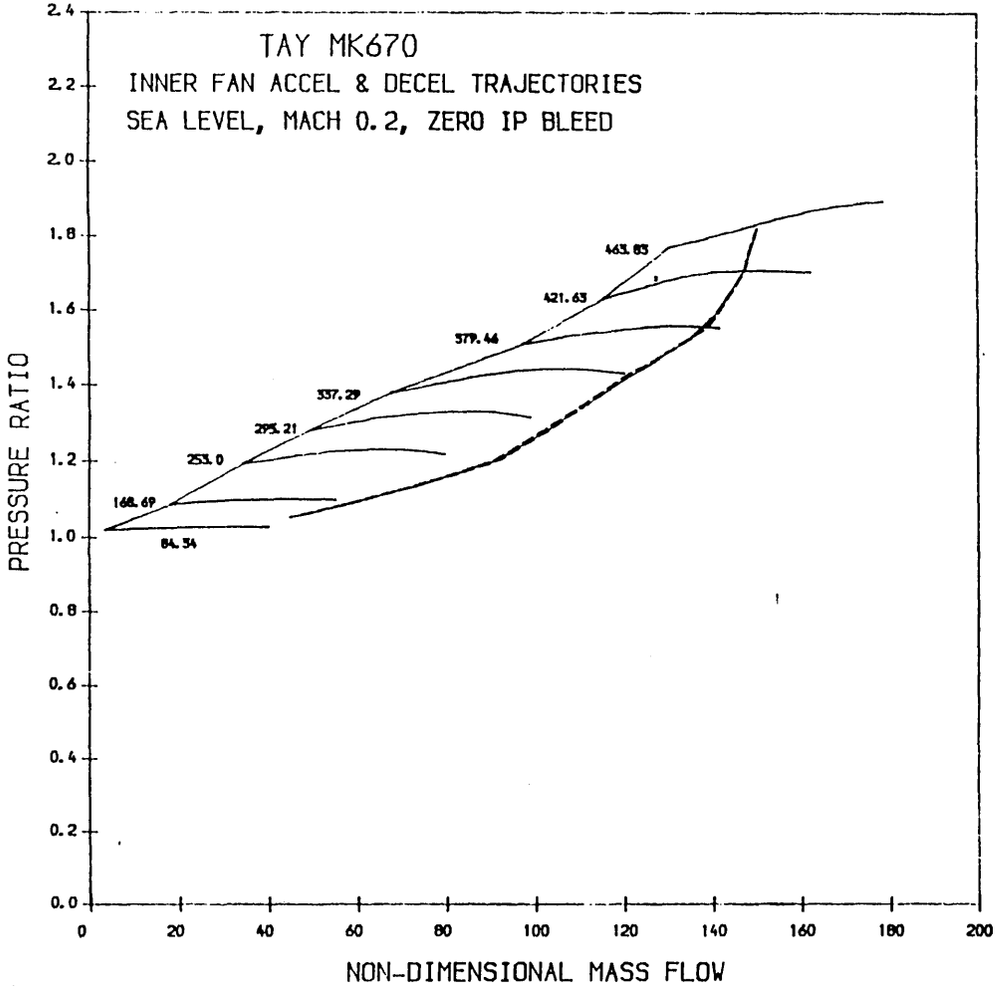

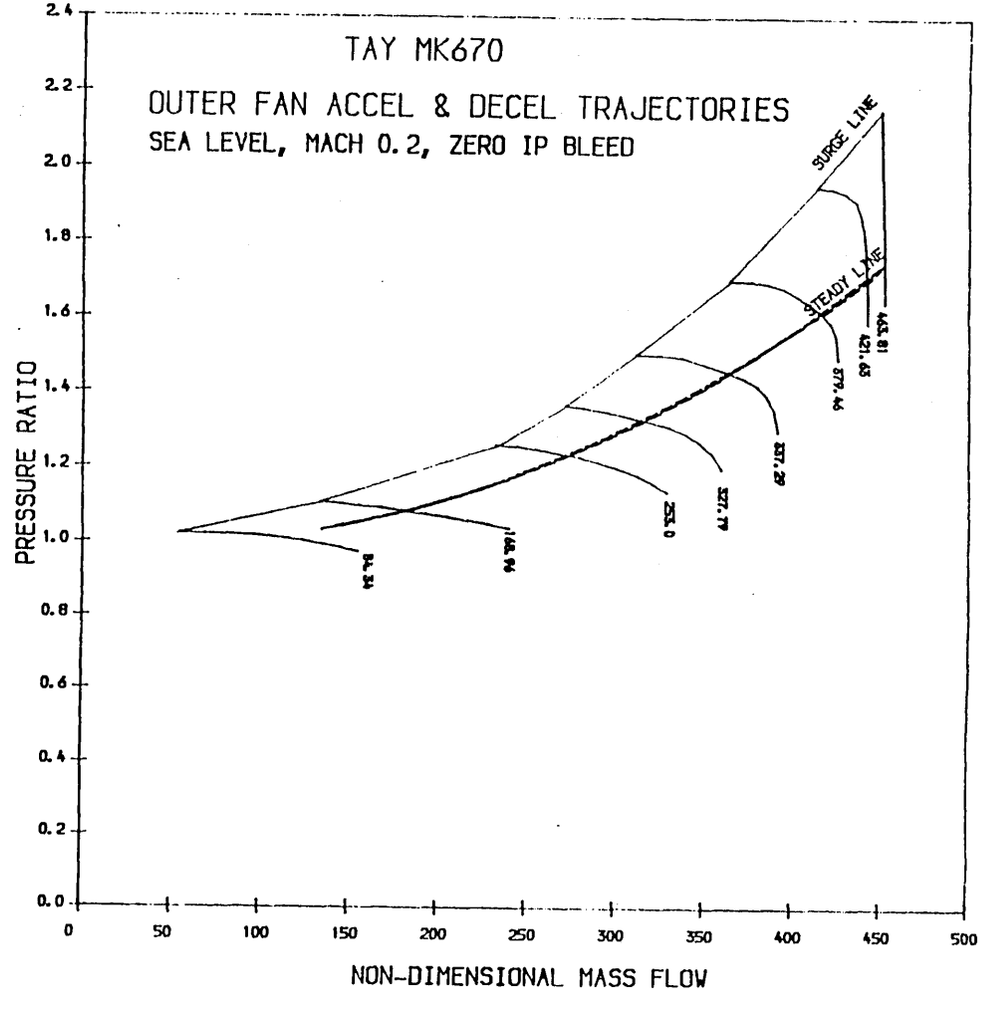

FIG 42 TAY MK670 PREDICTED ACCELERATION AN DECELERATION OF THE IP AND HP COMPRESSOR AT SEA LEVEL MACH NUM=0.2

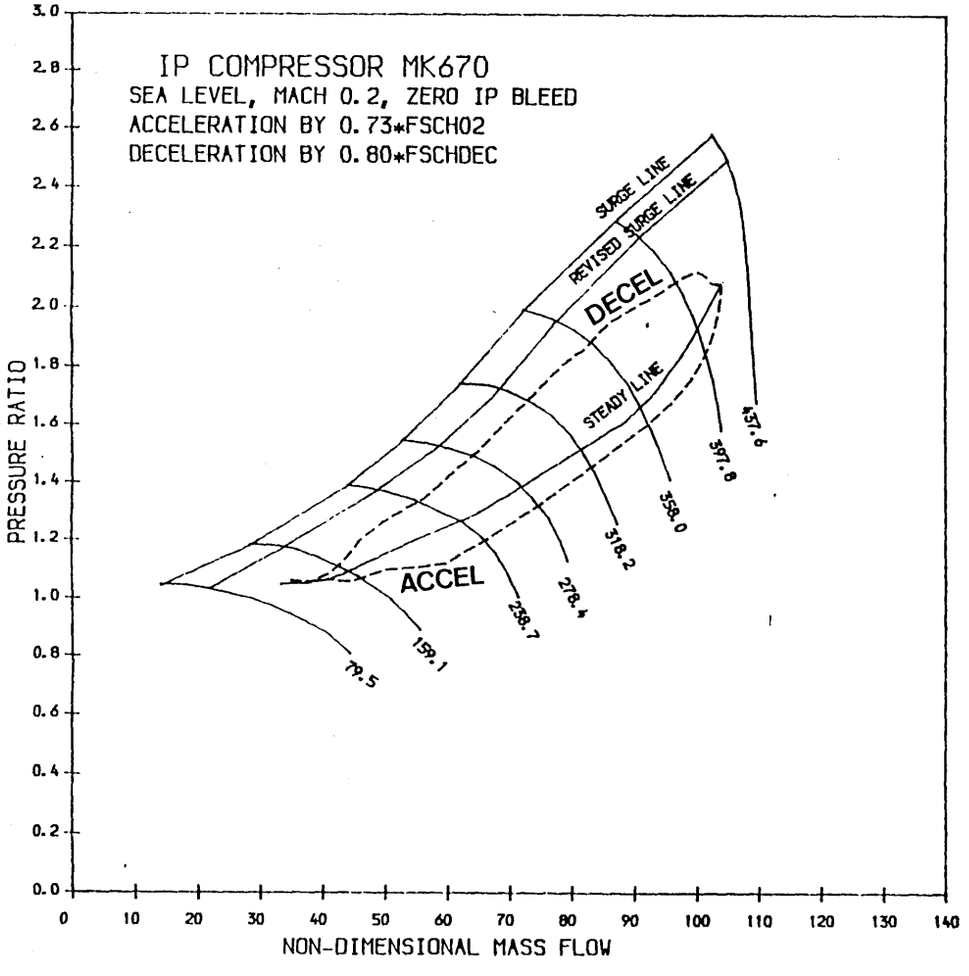

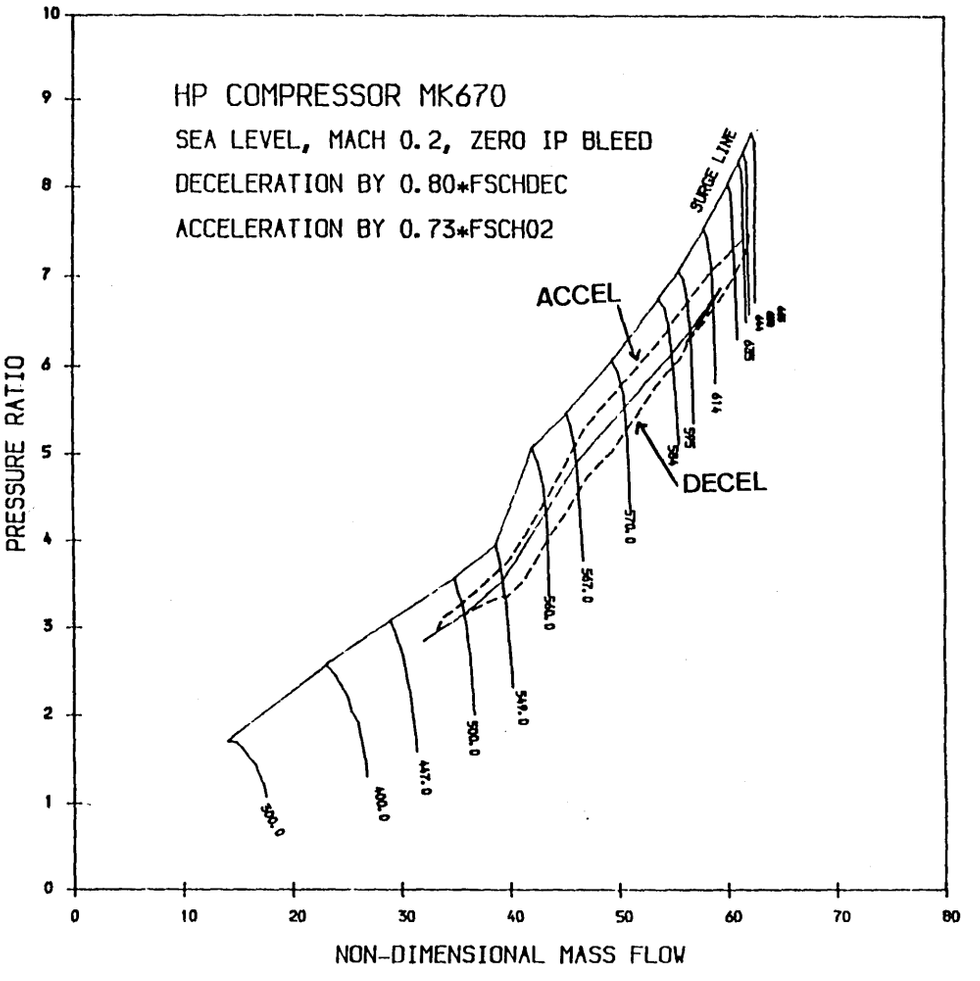

FIG 43 PREDICTED FUEL SCHEDULE TRAJECTORIES

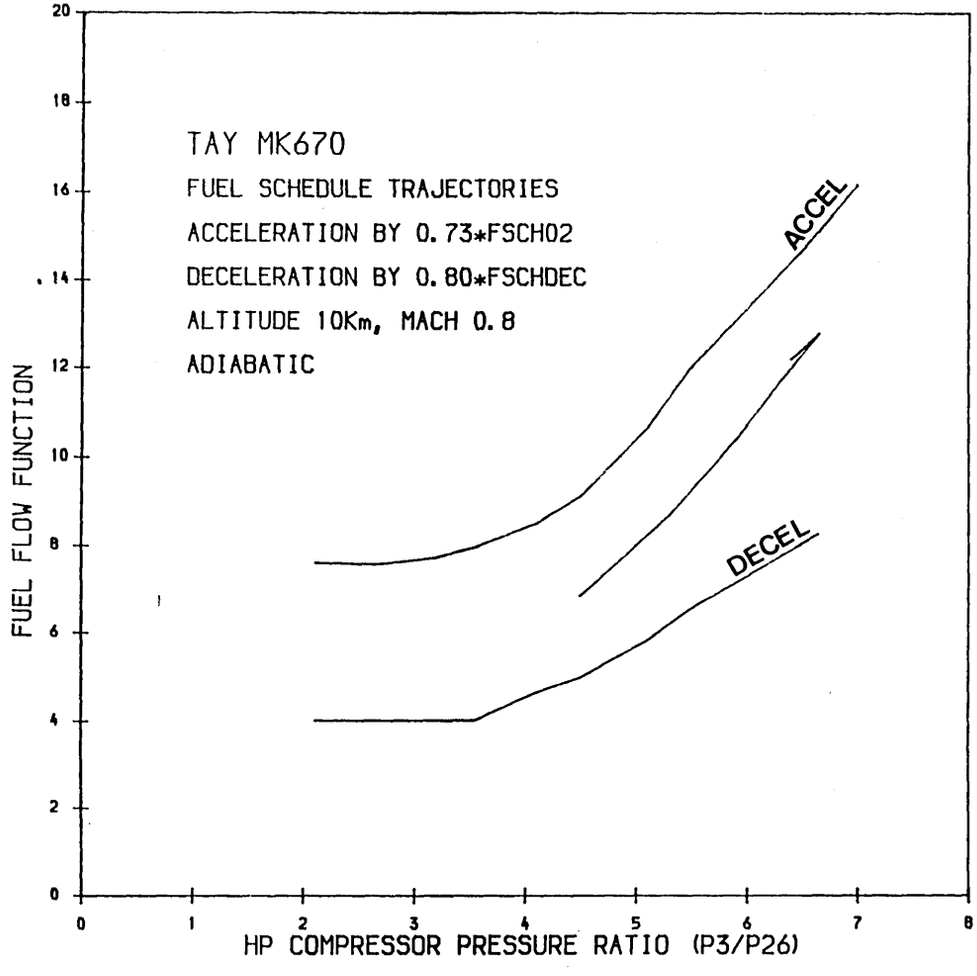

FIG 44 TAY MK670 PREDICTED ADIABATIC TRANSIENTS AT 32,000 FT

MACH NUM=0.8

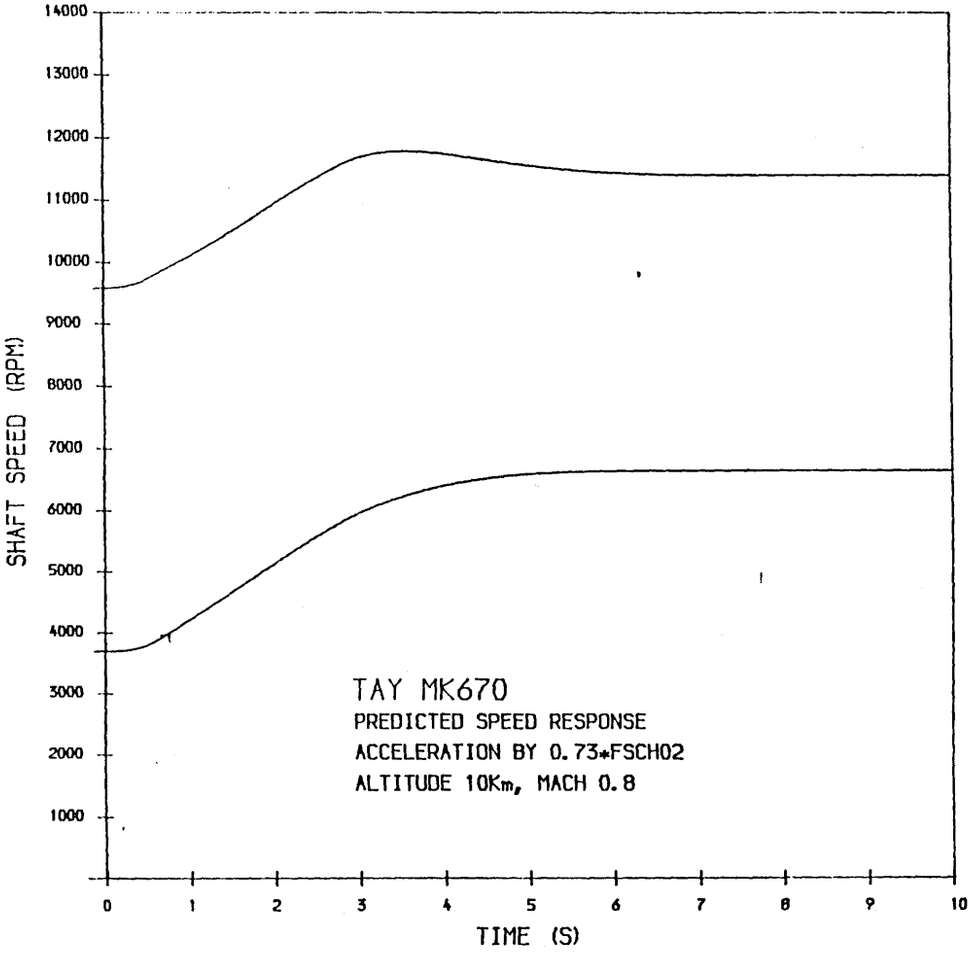

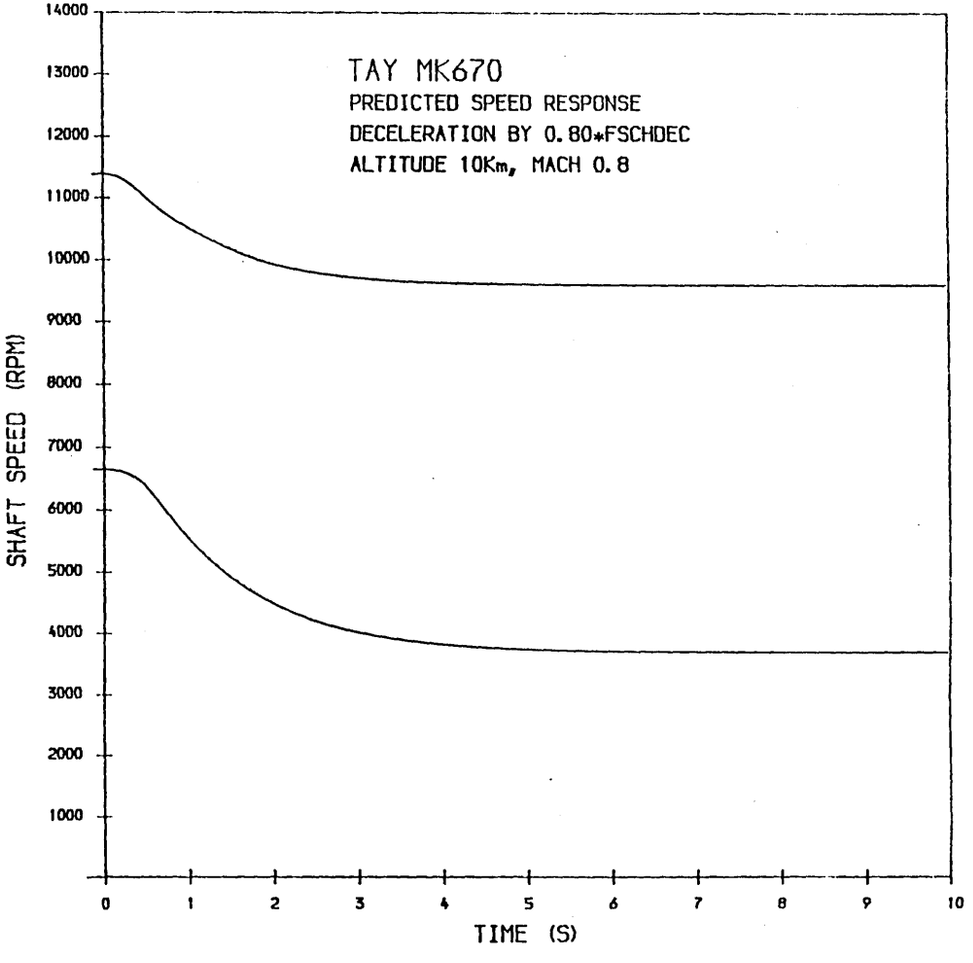

FIG 45 TAY MK670 PREDICTED ADIABATIC TRANSIENTS AT 32,000 FT
MACH NUM=0.8

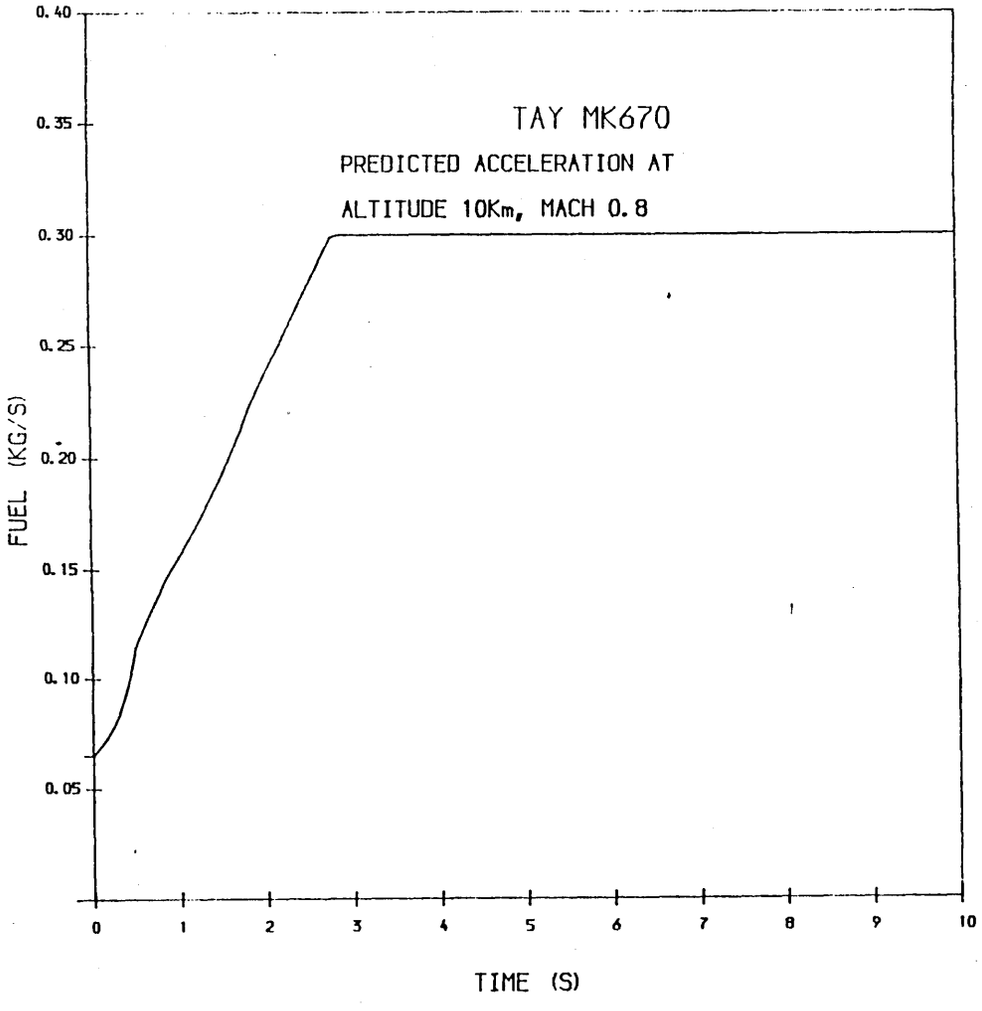

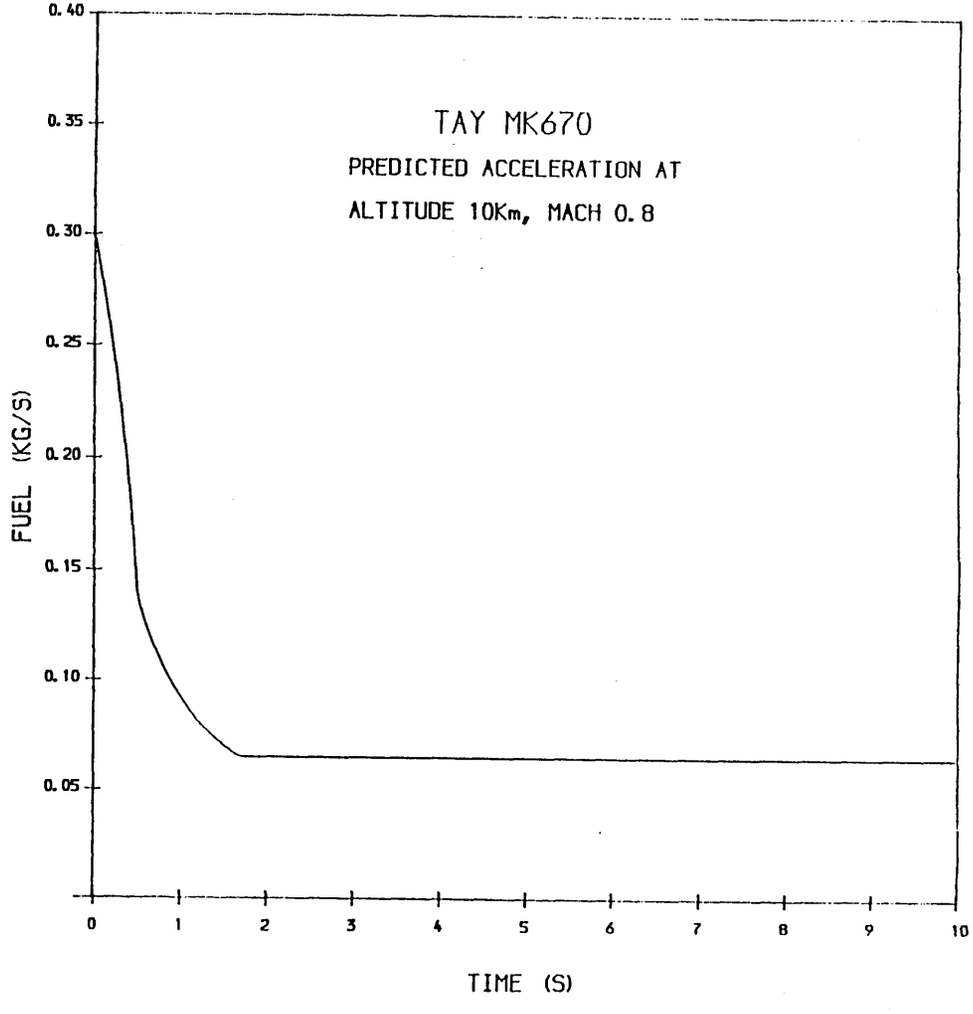

FIG 46 TAY MK670 PREDICTED PATHS OF THE FAN SECTIONS DURING TRANSIENT DECELERATION AT 32,000 FT MACH NUM=0.8

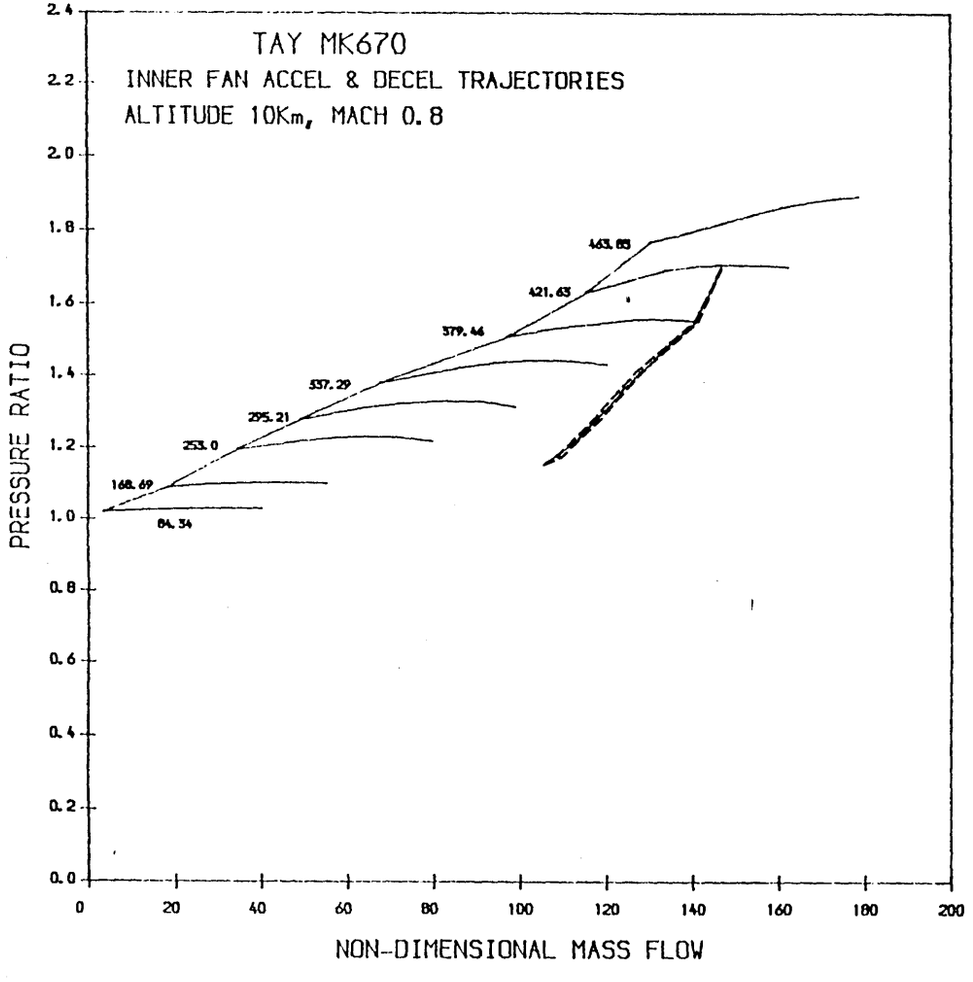

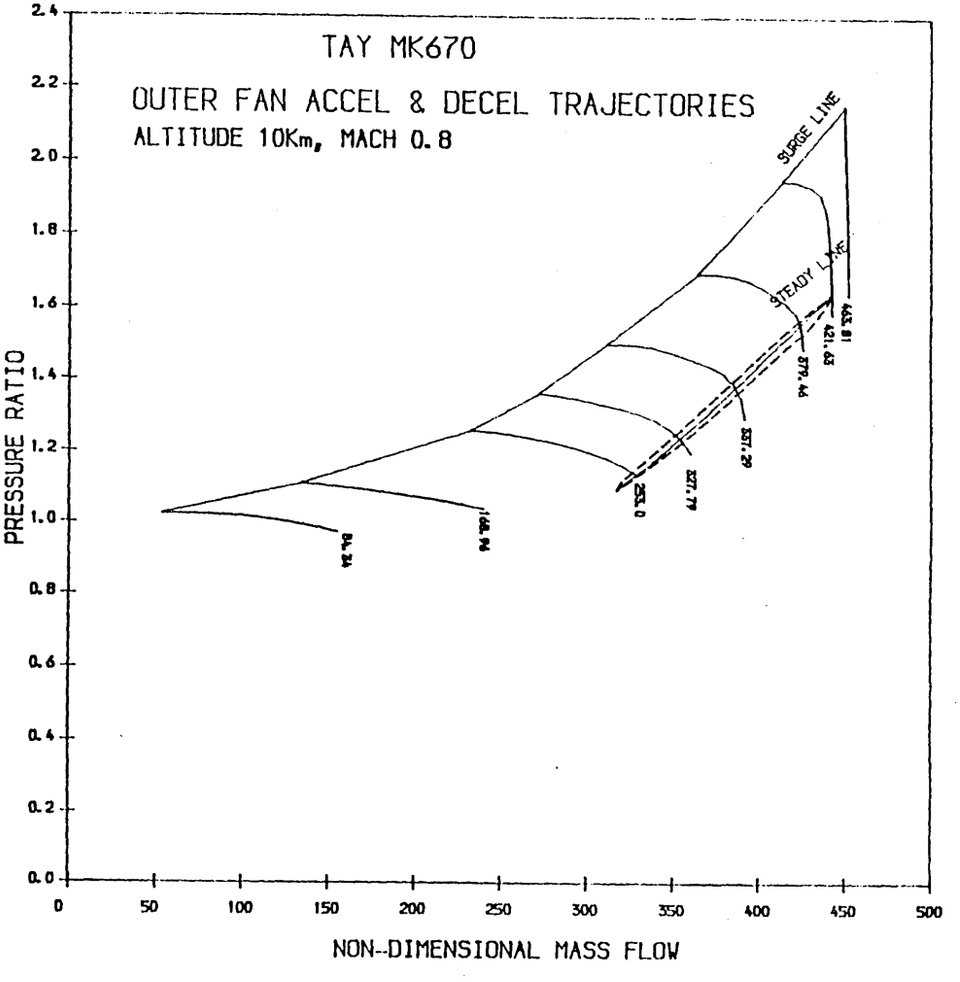

FIG 47 TAY MK670 PREDICTED ADIABATIC TRANSIENTS AT 32,000 FT
MACH NUM=0.8

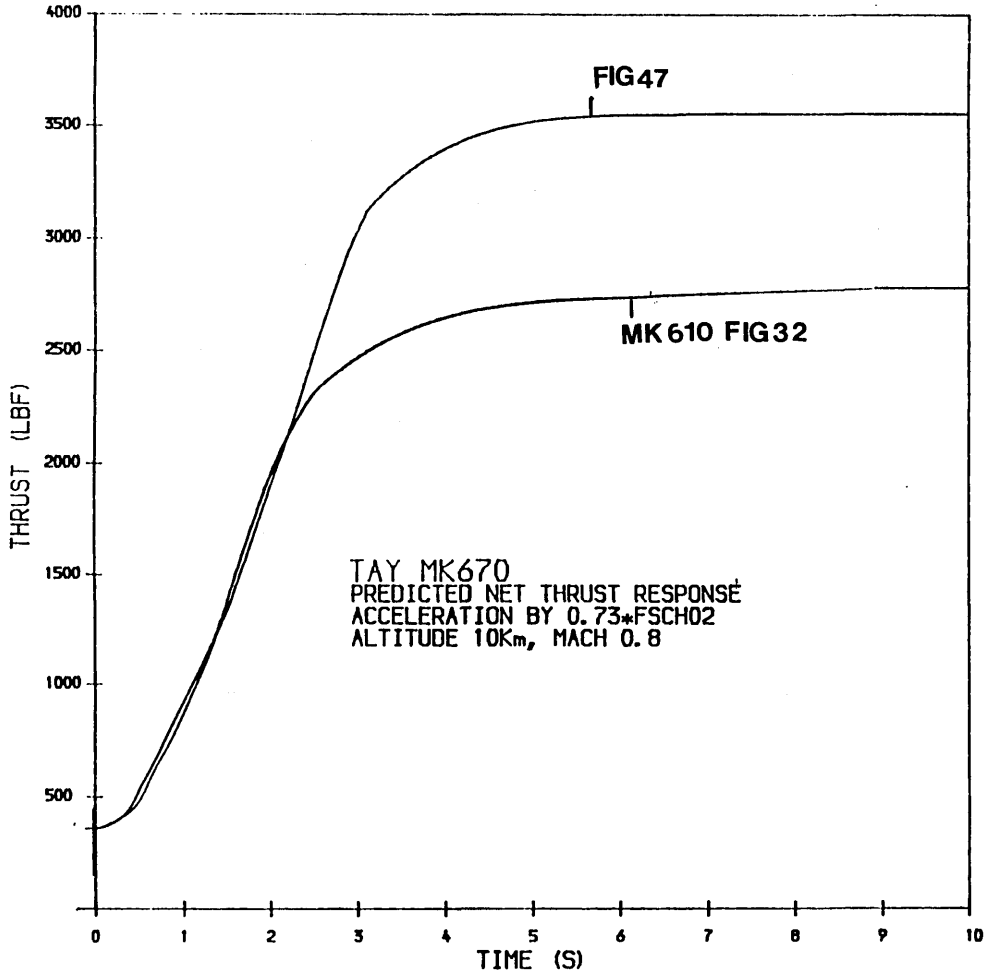

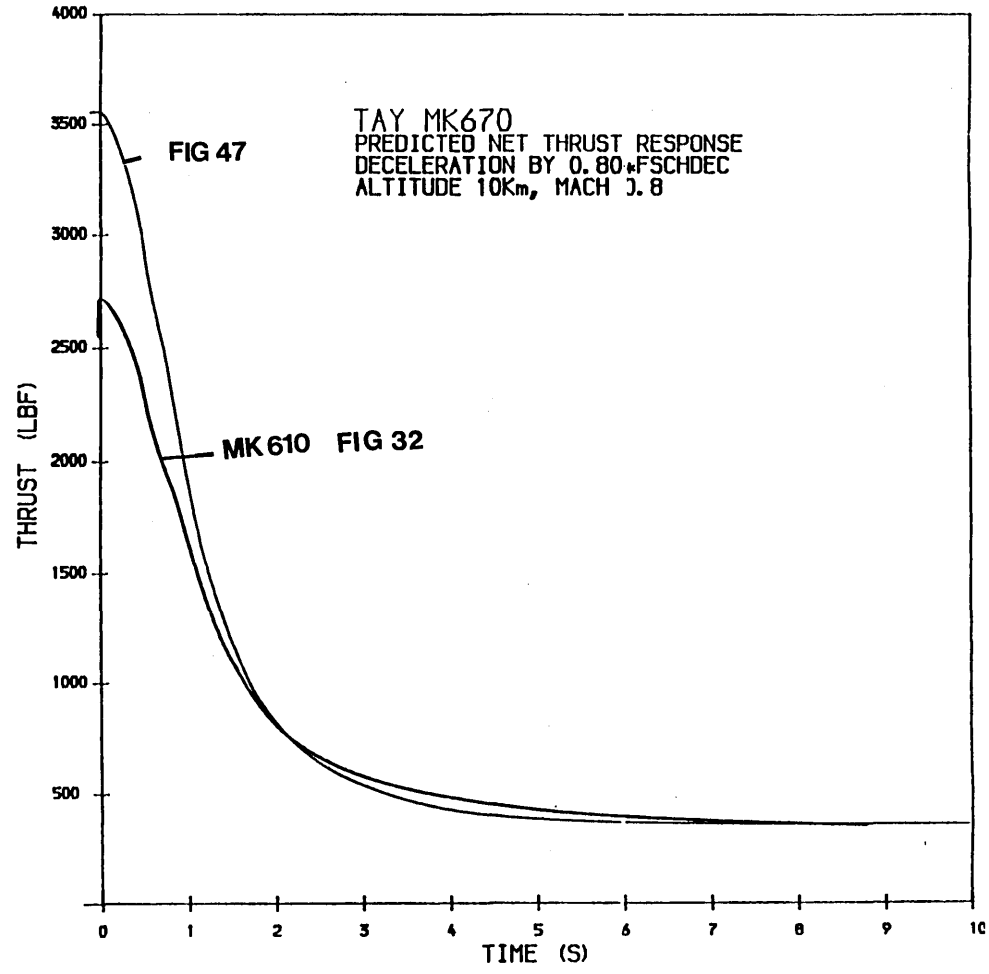

FIG 48 TAY MK670 PREDICTED ACCELERATION AN DECELERATION OF THE IP AND HP COMPRESSOR AT 32,000 FT MACH NUM=0.8

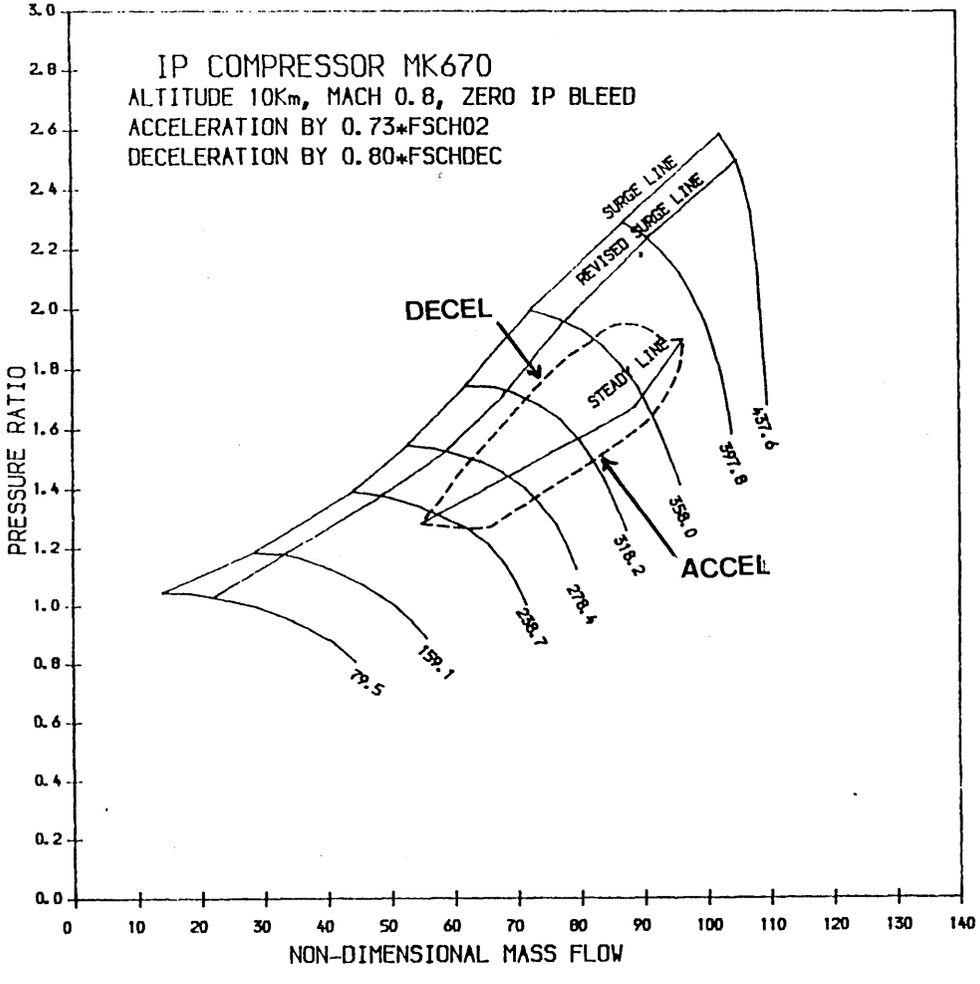

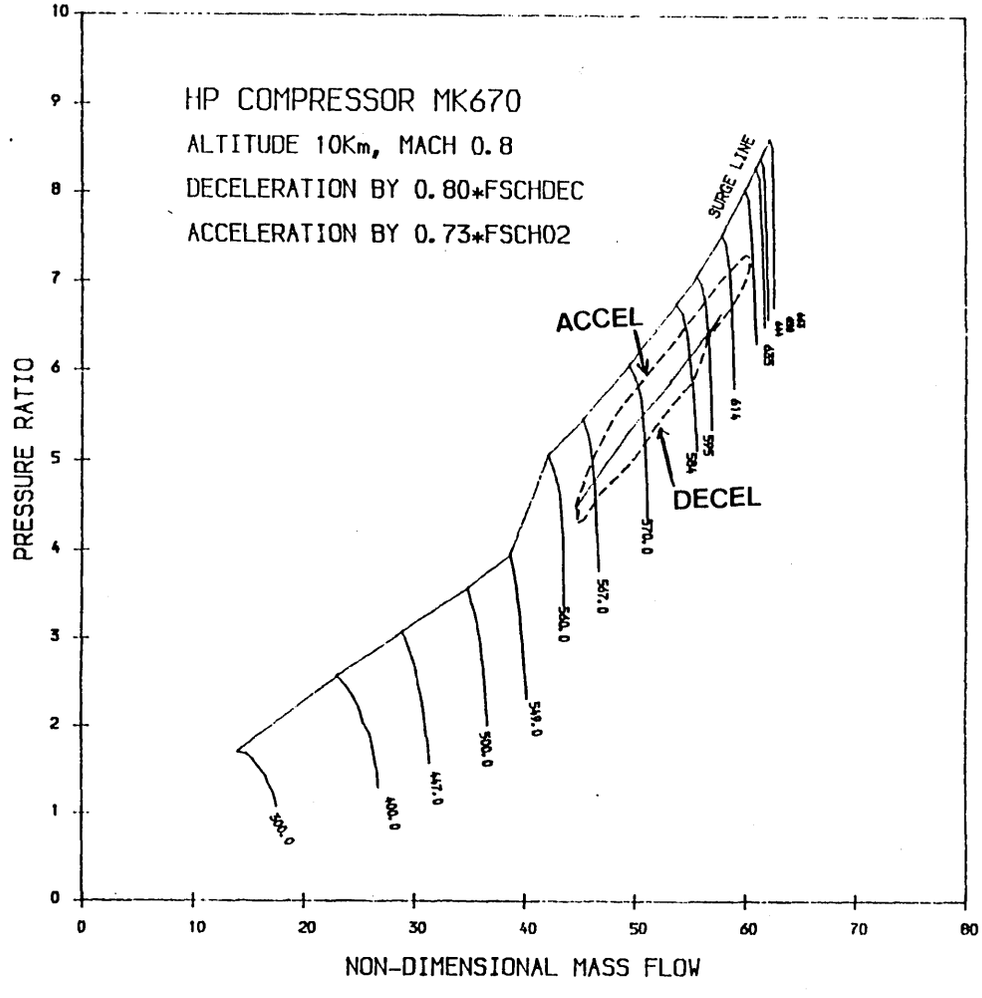

FIG 49 TAY MK670 PREDICTED LP & HP SHAFTSPEED RELATIONSHIPS

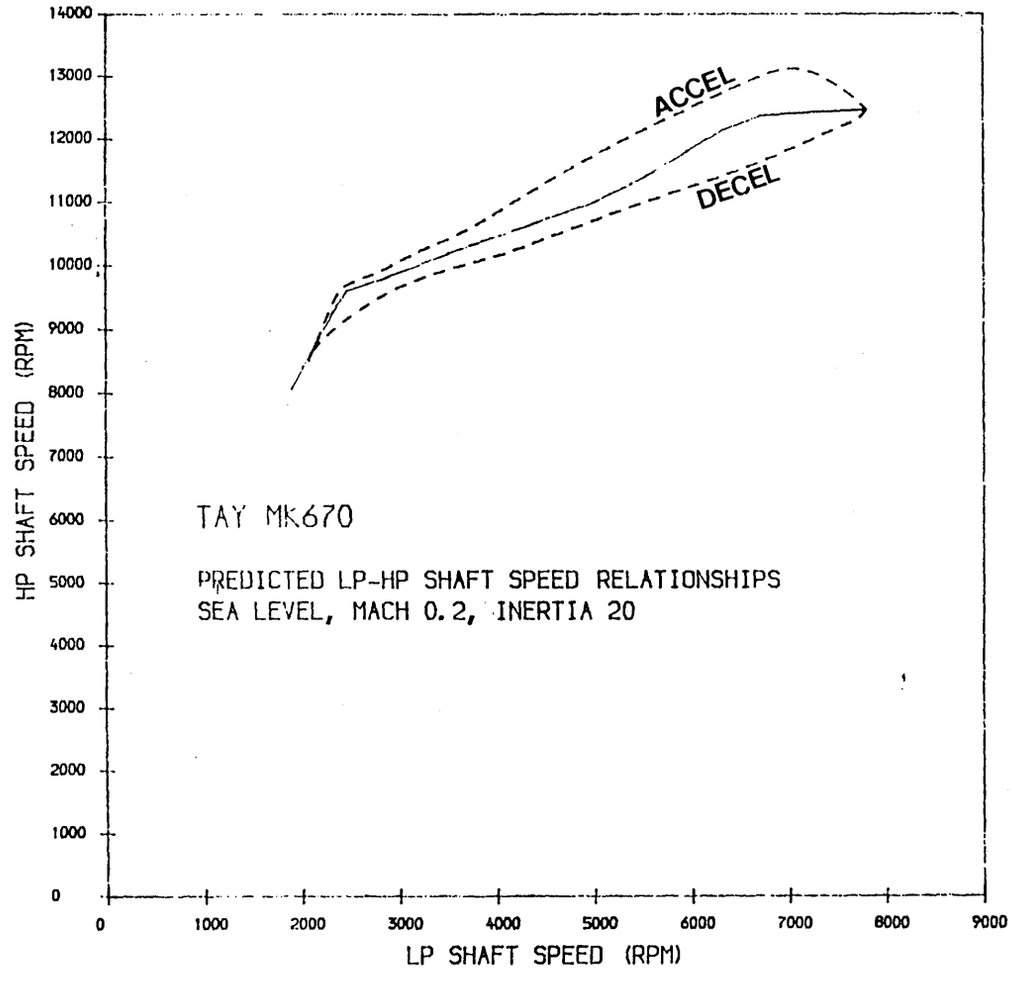

FIG 50 TAY MK670 PREDICTED ADIABATIC TRANSIENTS AT SEA LEVEL MACH 0.2

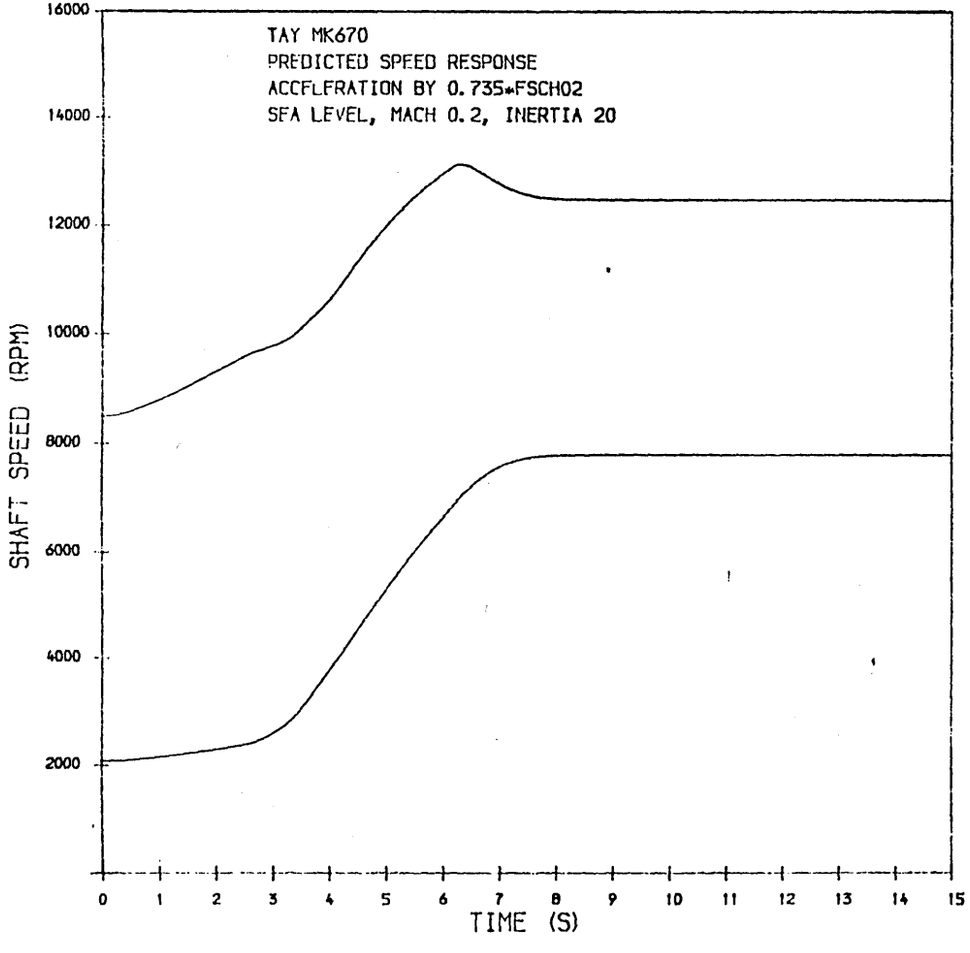

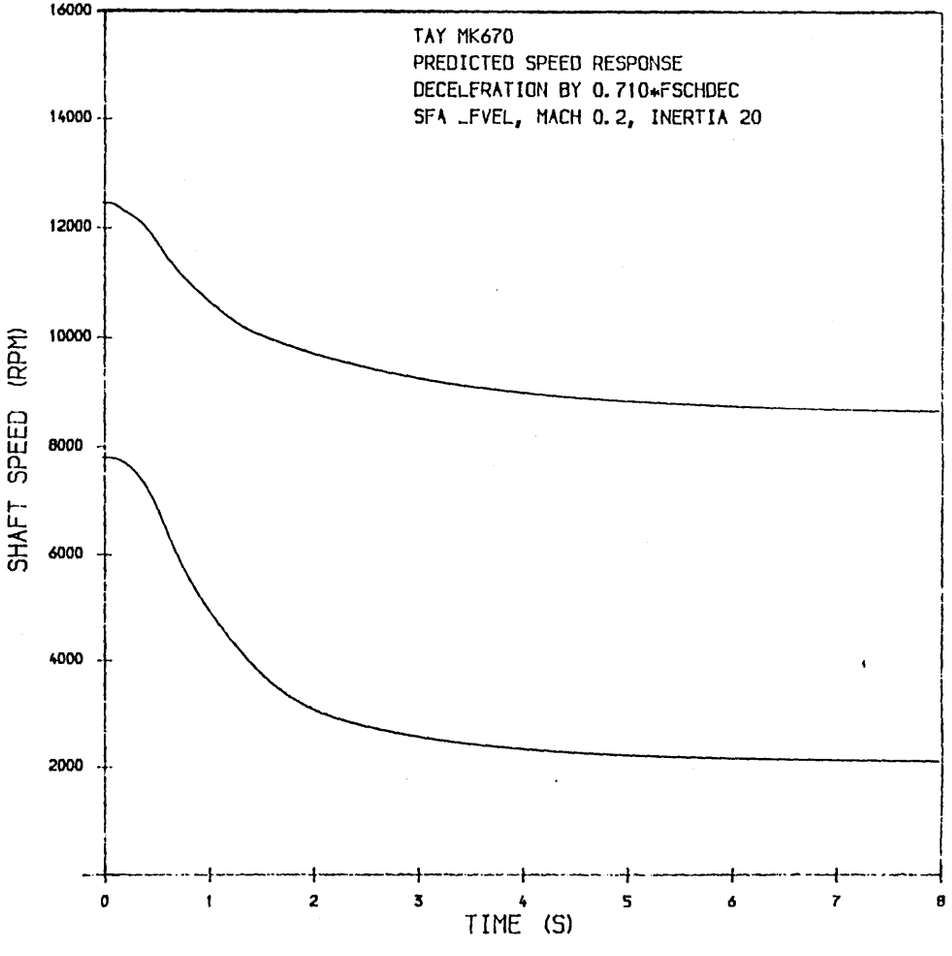

FIG 51 TAY MK670 PREDICTED ADIABATIC TRANSIENTS AT SEA LEVEL, MACH 0.2.

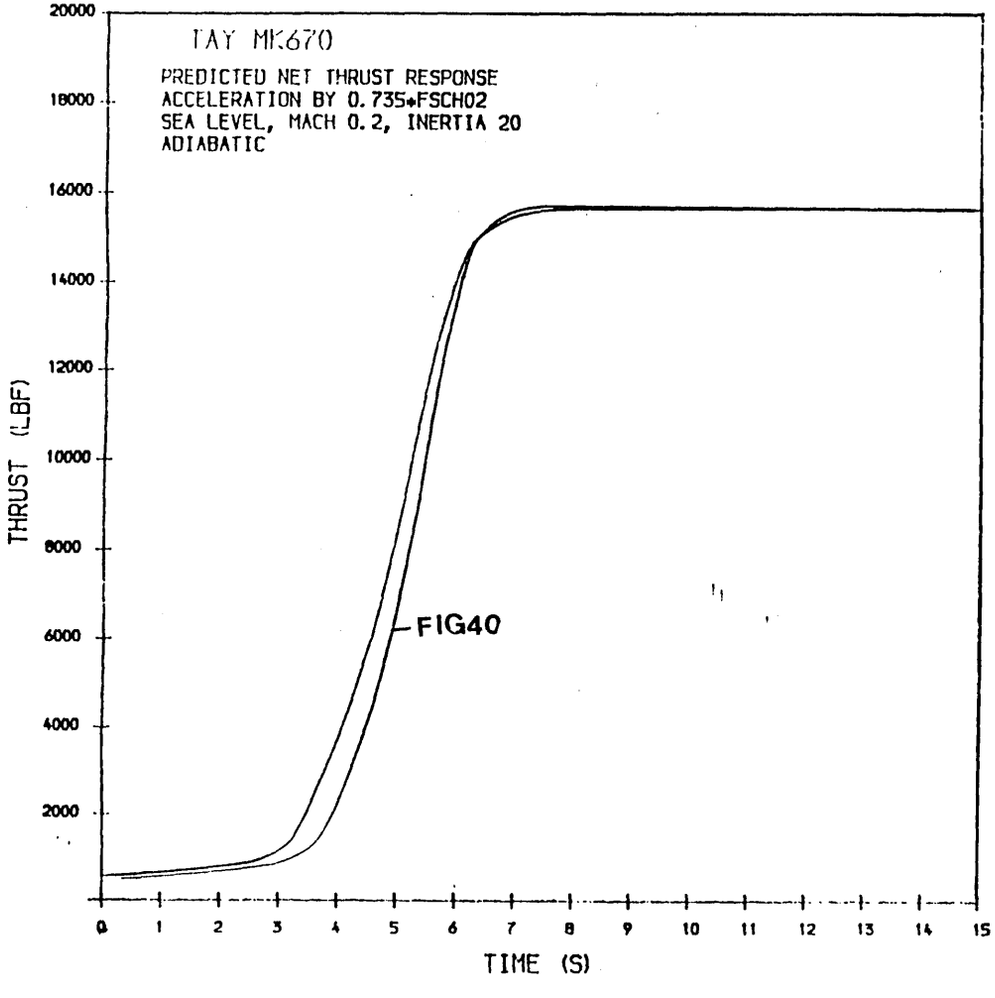

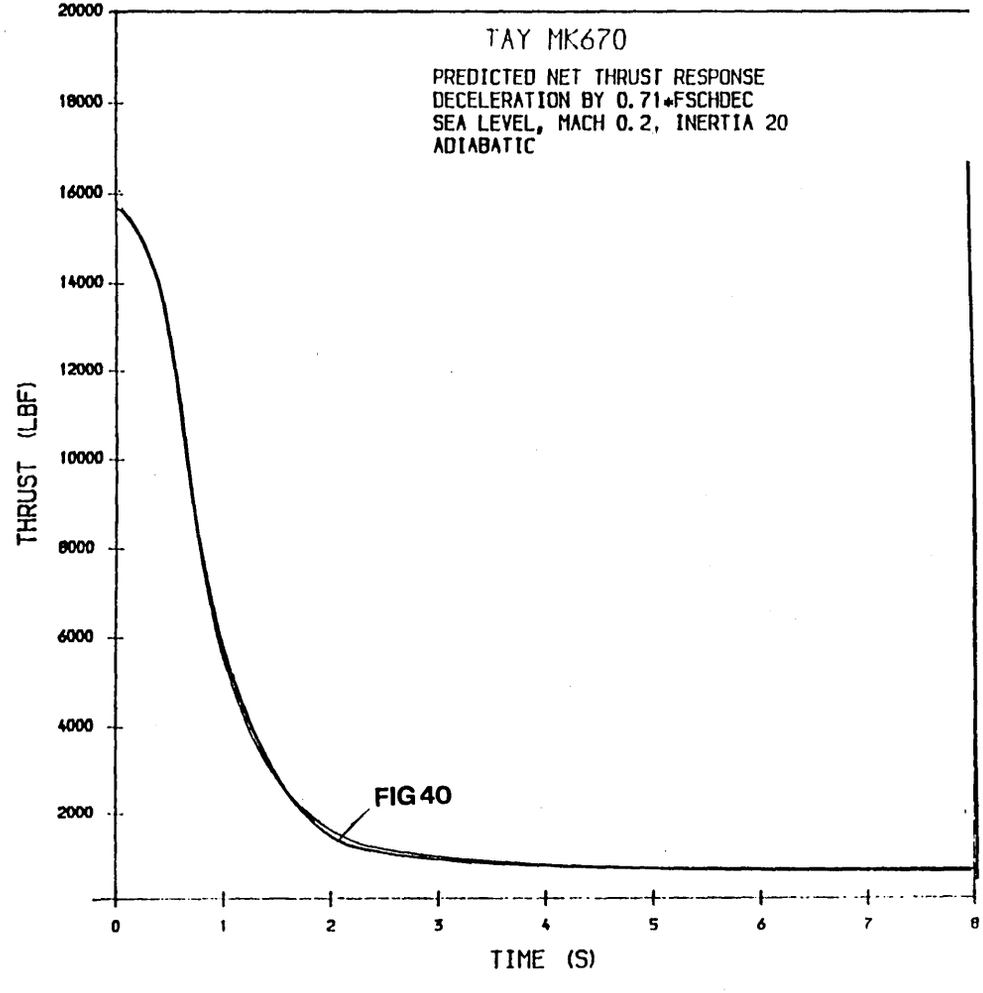

FIG 52 TAY MK670 PREDICTED PATHS OF FAN SECTION DURING TRANSIENT

ACCELERATION & DECELERATION AT SEA LEVEL MACH 0.2

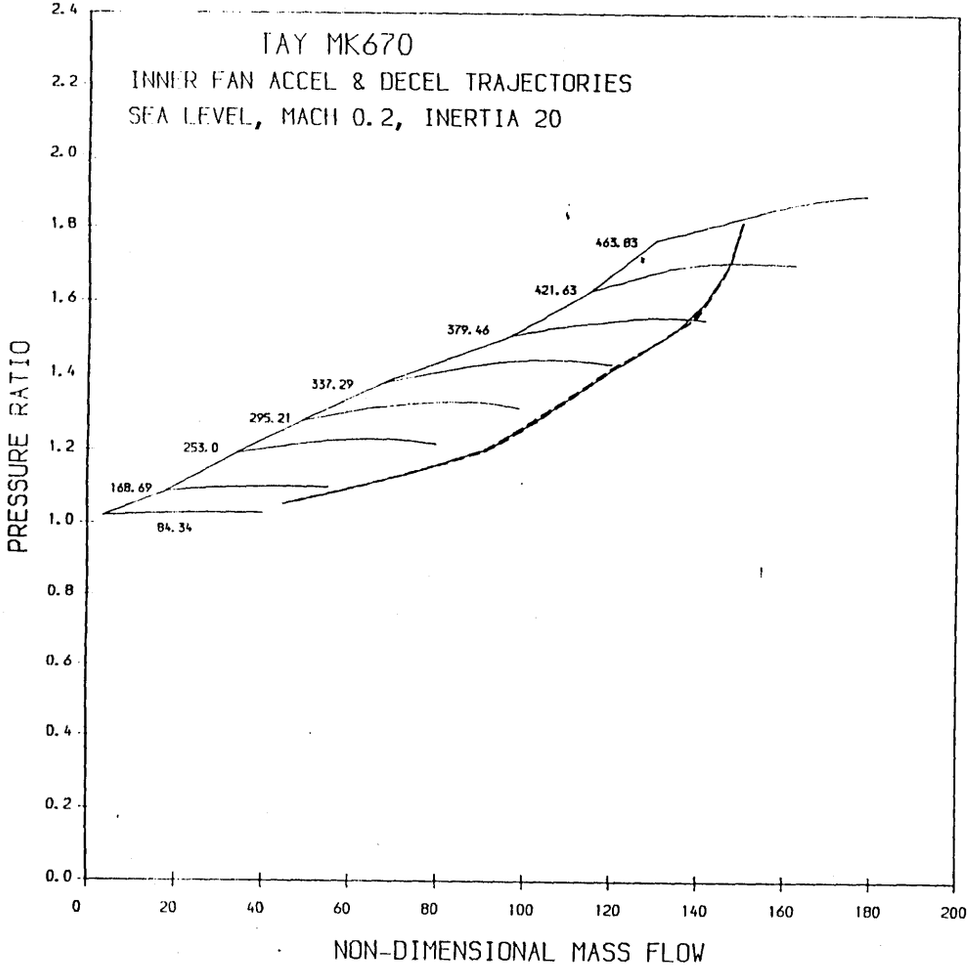

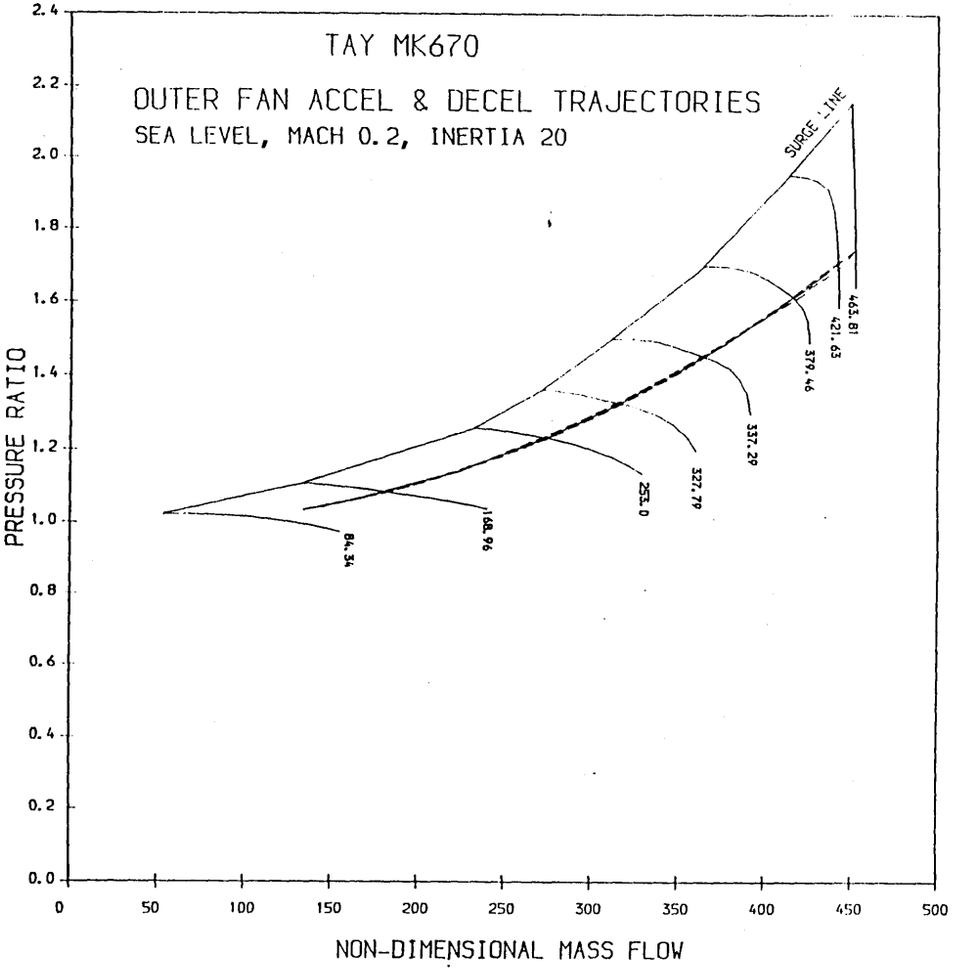

FIG 53 TAY MK670 ACCELERATION & DECELERATION TRANSIENTS OF THE I.P AND H.P COMPRESSORS AT SEA LEVEL, MACH 0.2.

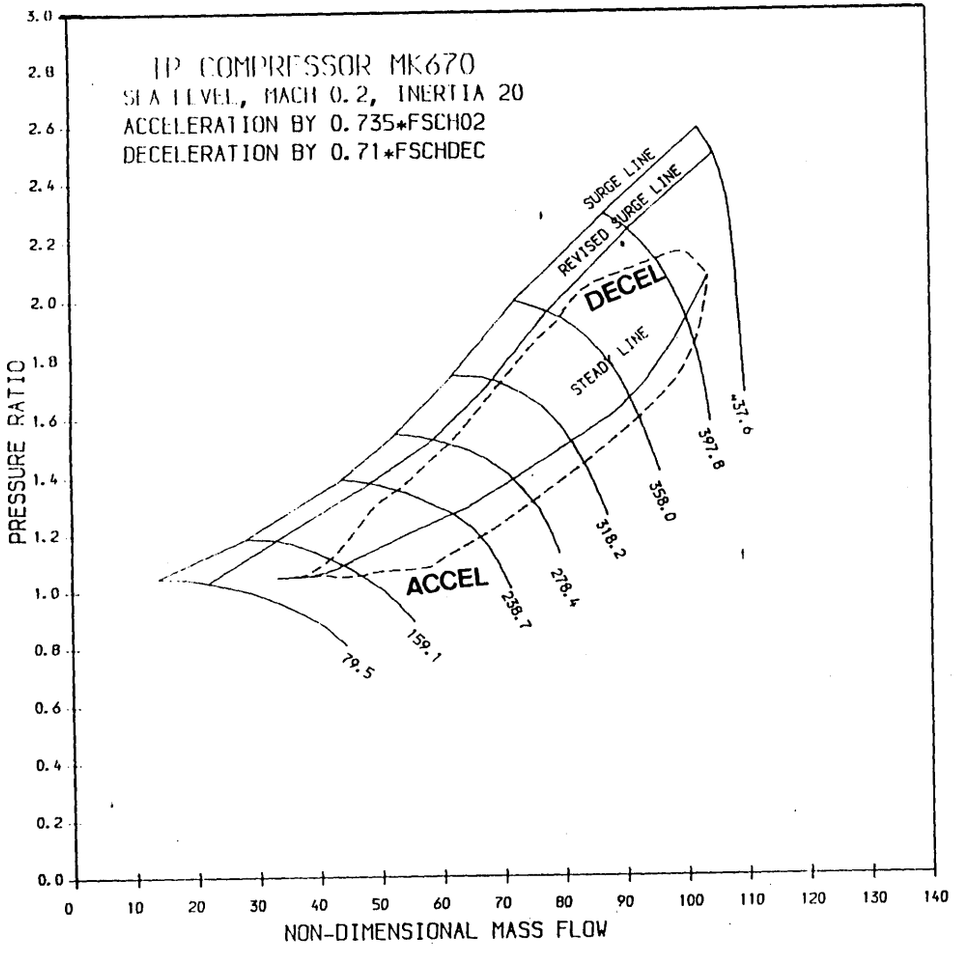

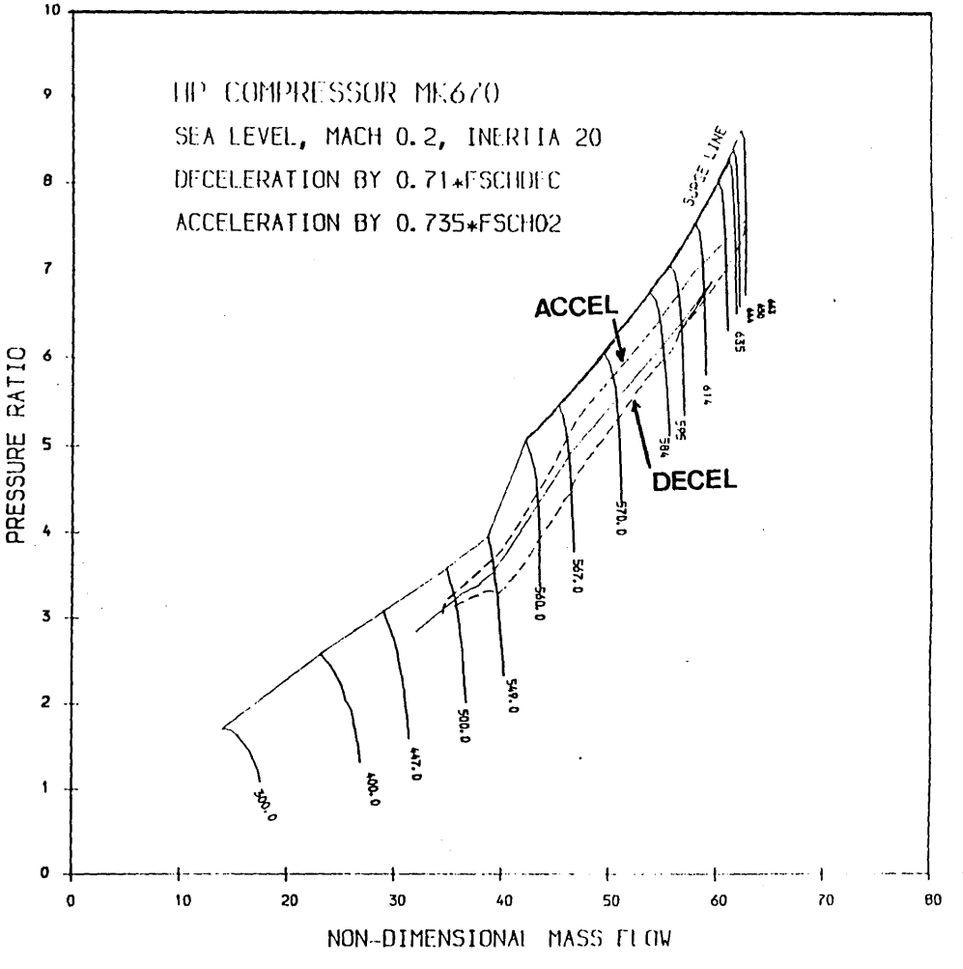

FIG 54 TAY MK670 PREDICTED LP & HP SHAFTSPEED RELATIONSHIPS

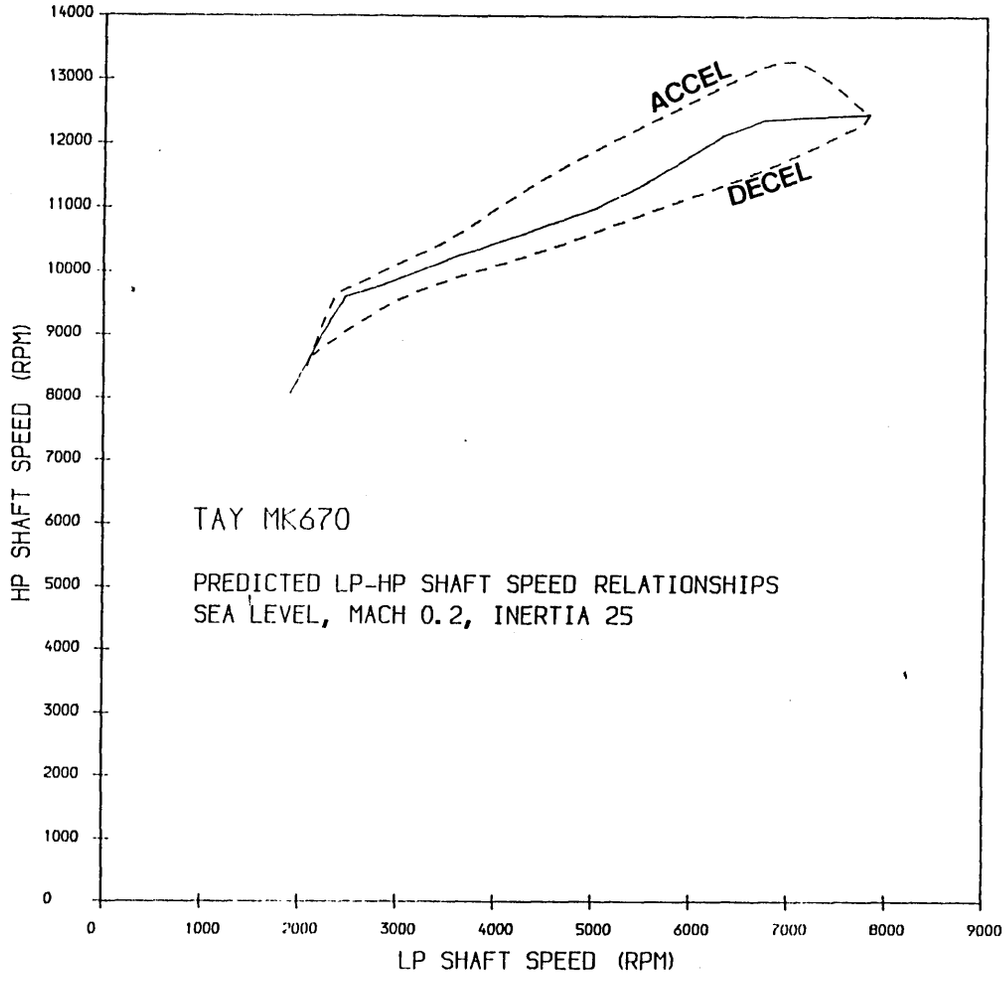

FIG 55 TAY MK670 PREDICTED ADIABATIC TRANSIENTS AT SEA LEVEL MACH 0.2

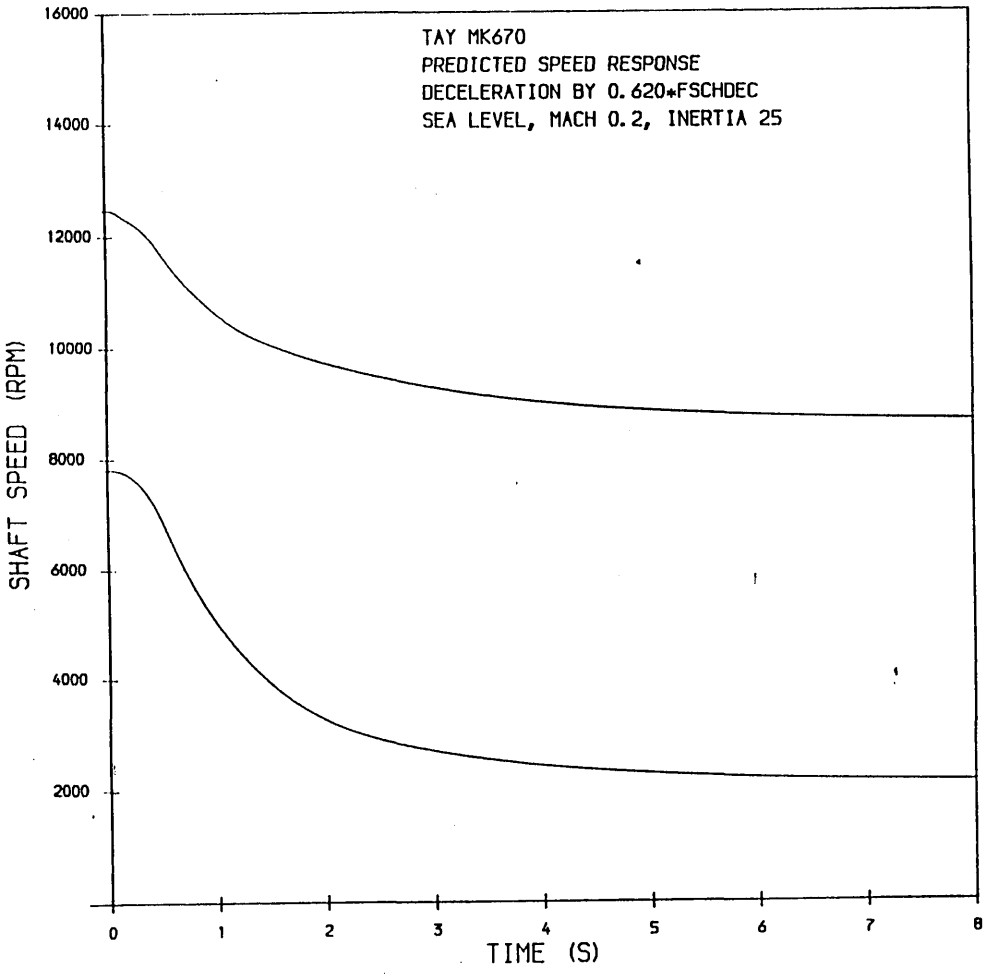

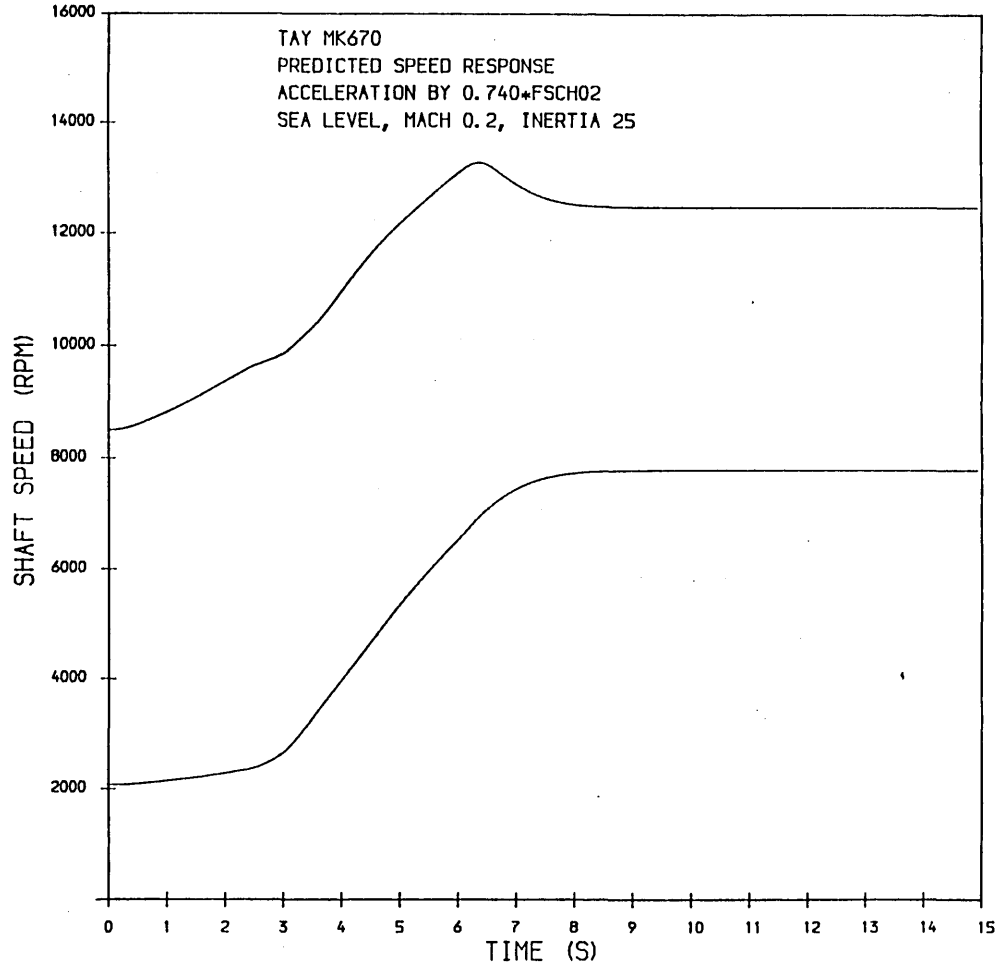

FIG 56 TAY MK670 PREDICTED ADIABATIC TRANSIENTS AT SEA LEVEL, MACH 0.2.

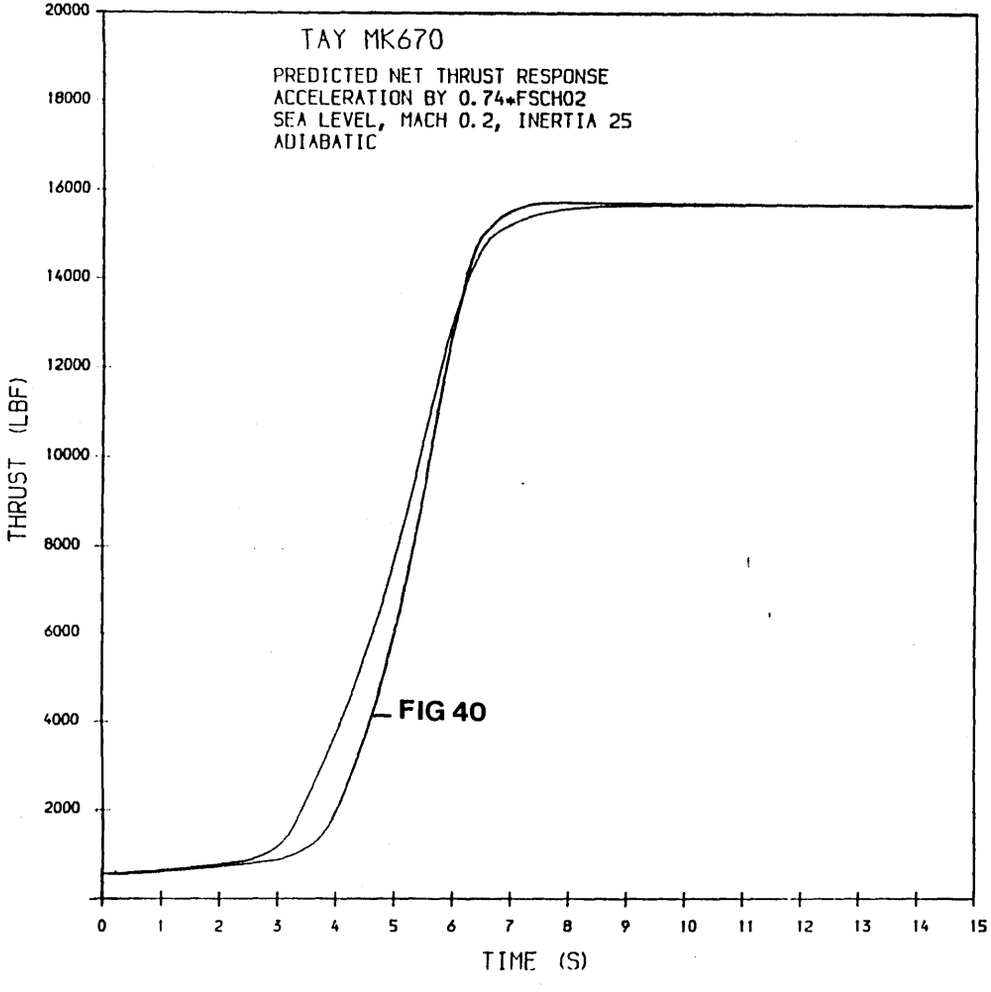

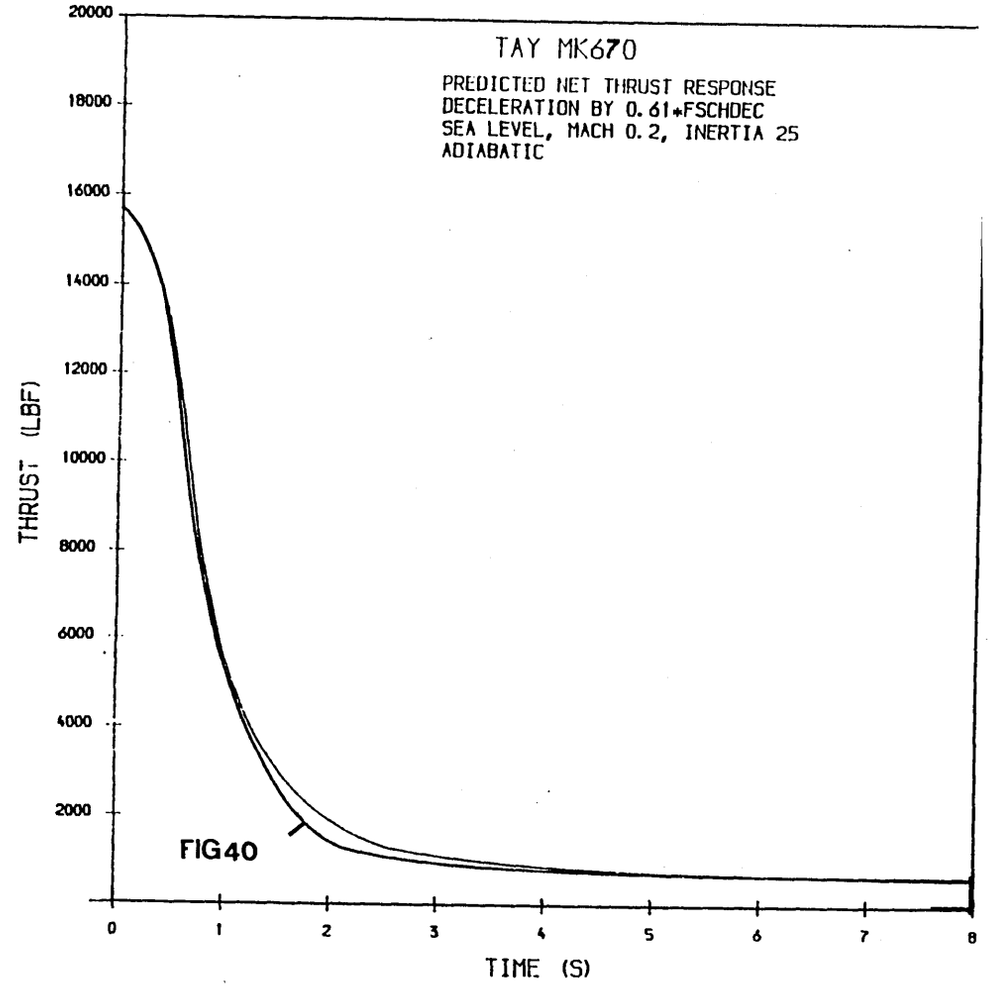

FIG 57 TAY MK670 PREDICTED PATHS OF FAN SECTION DURING TRANSIENT

ACCELERATION & DECELERATION AT SEA LEVEL MACH 0.2

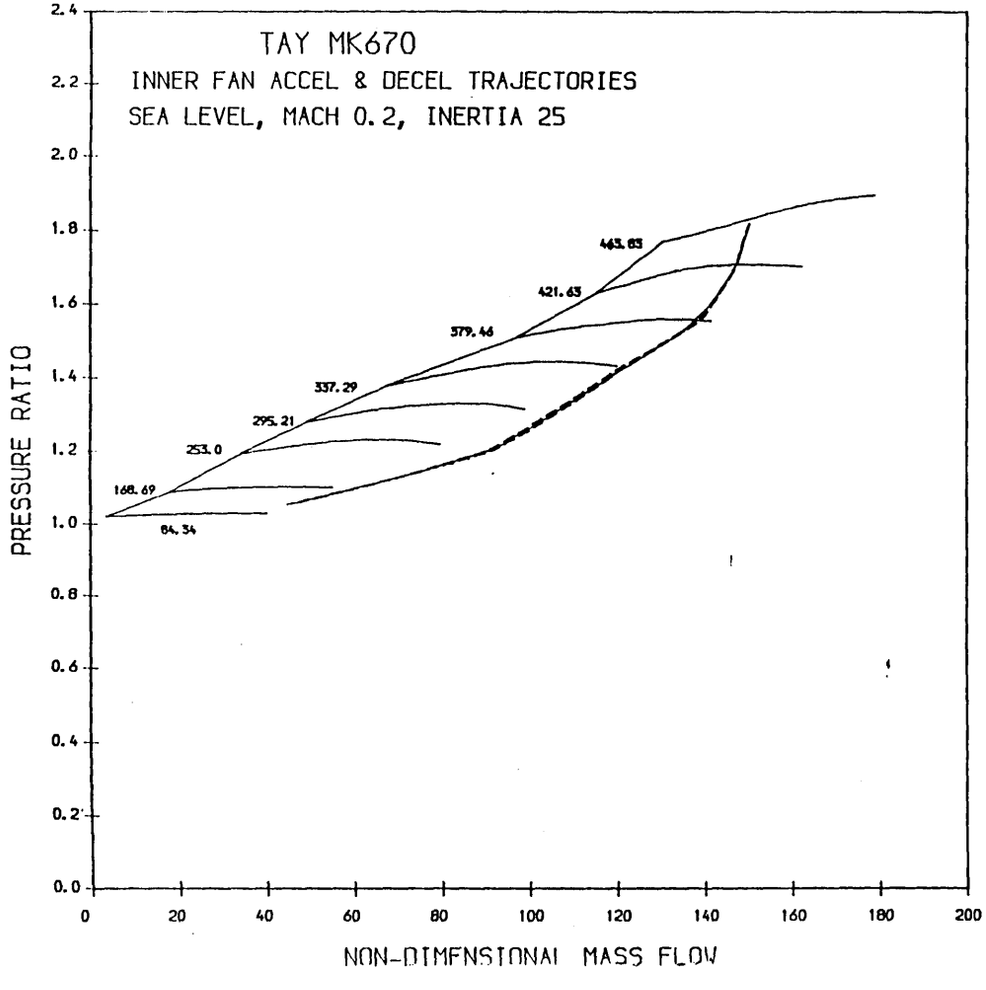

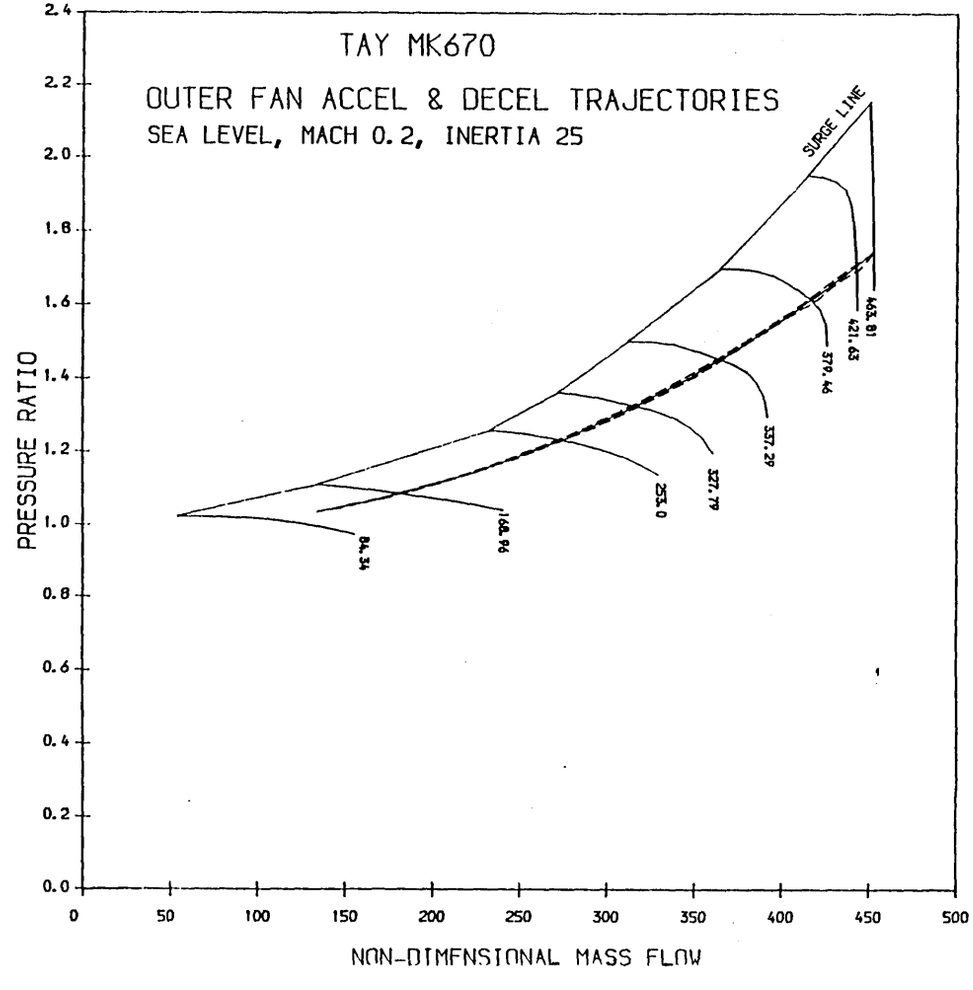

FIG 58 TAY MK670 ACCELERATION & DECELERATION TRANSIENTS OF THE I.P AND H.P COMPRESSORS AT SEA LEVEL, MACH 0.2.

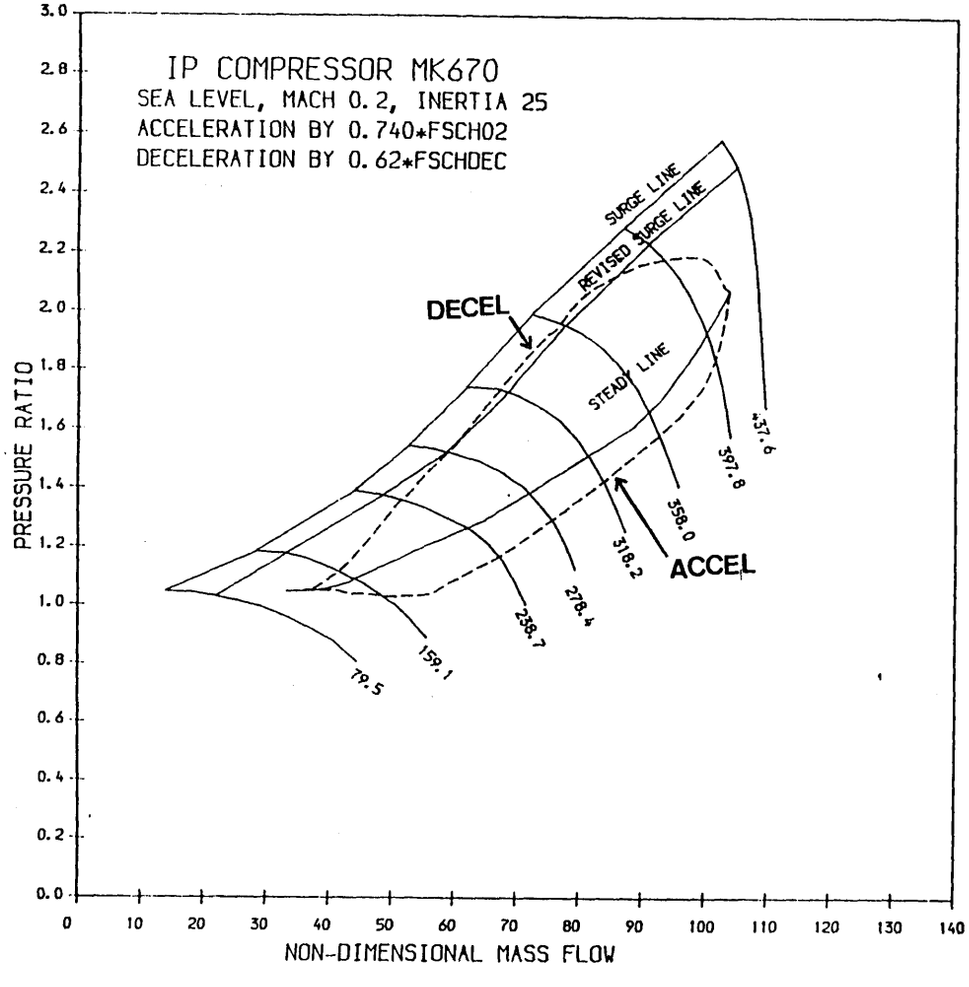

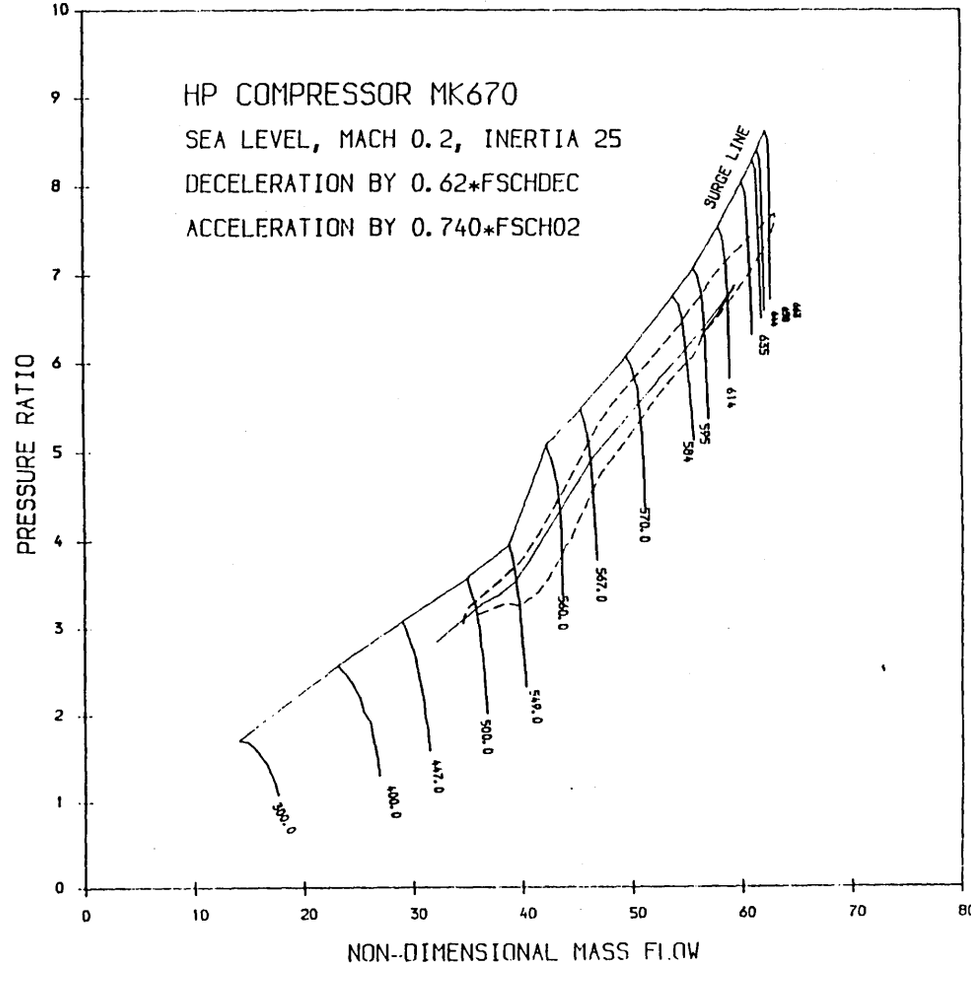

FIG 59 TAY MK670 PREDICTED LP & HP SHAFTSPEED RELATIONSHIPS

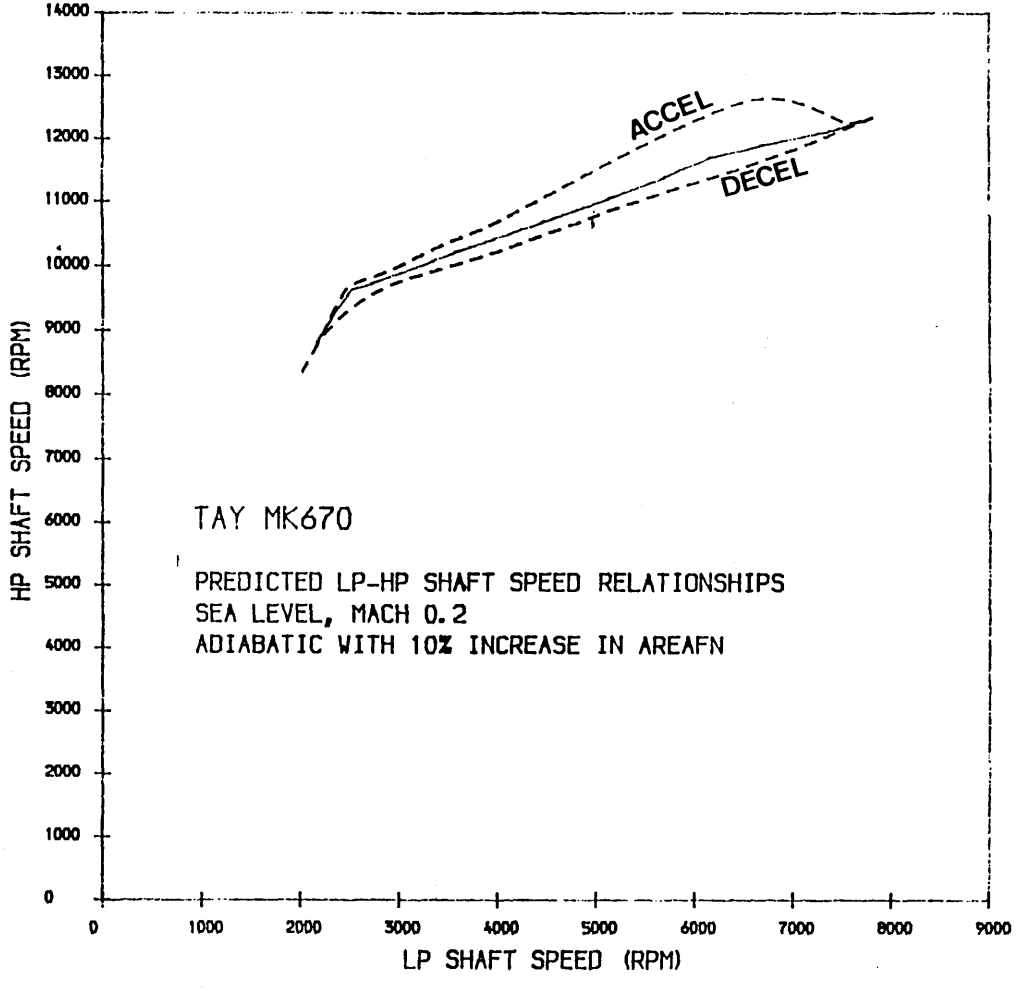

FIG 60 TAY MK670 PREDICTED ADIABATIC TRANSIENTS AT SEA LEVEL MACH 0.2

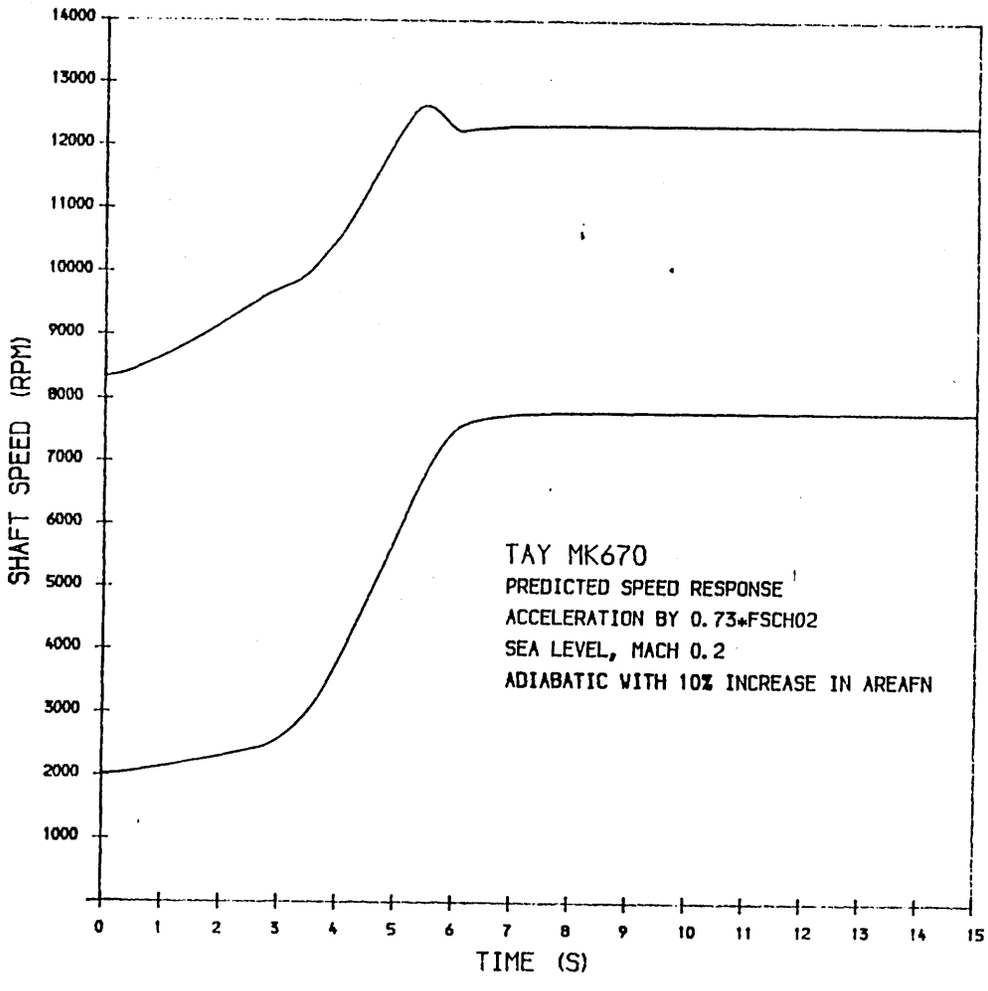

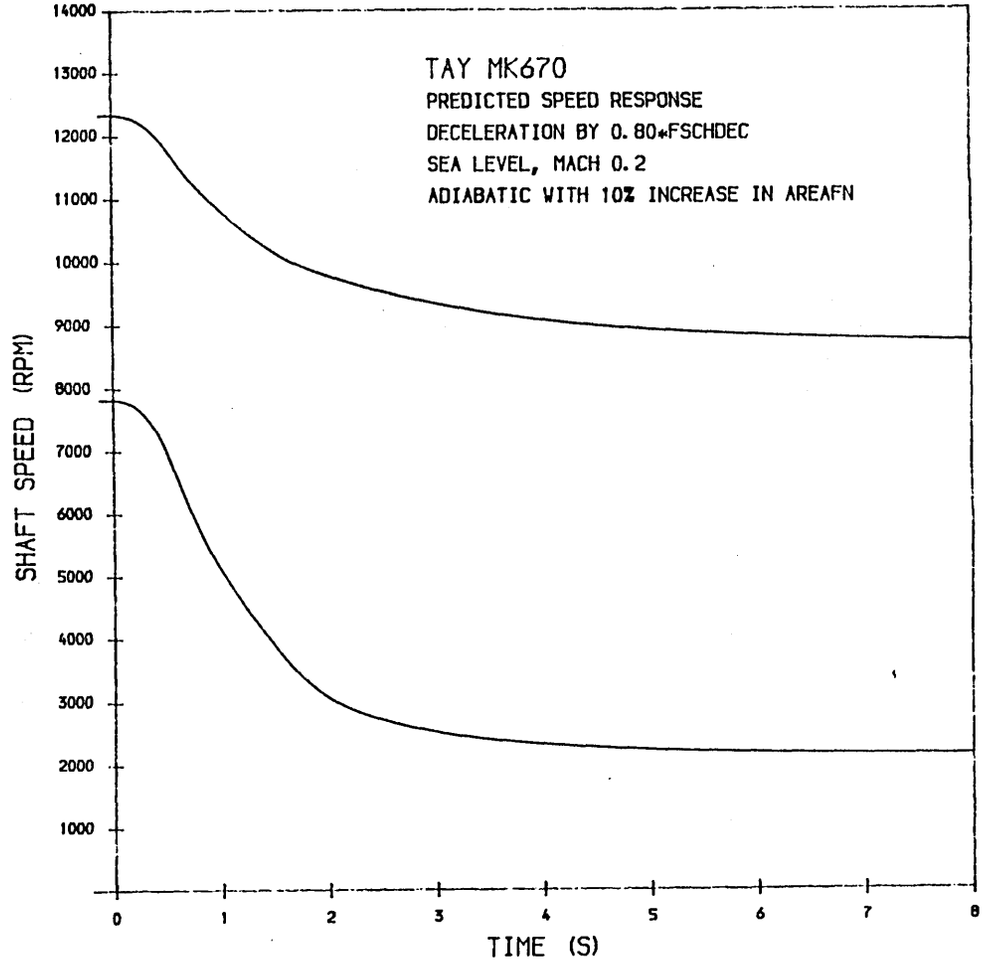

FIG 61 TAY MK670 PREDICTED ADIABATIC TRANSIENTS AT SEA LEVEL, MACH 0.2.

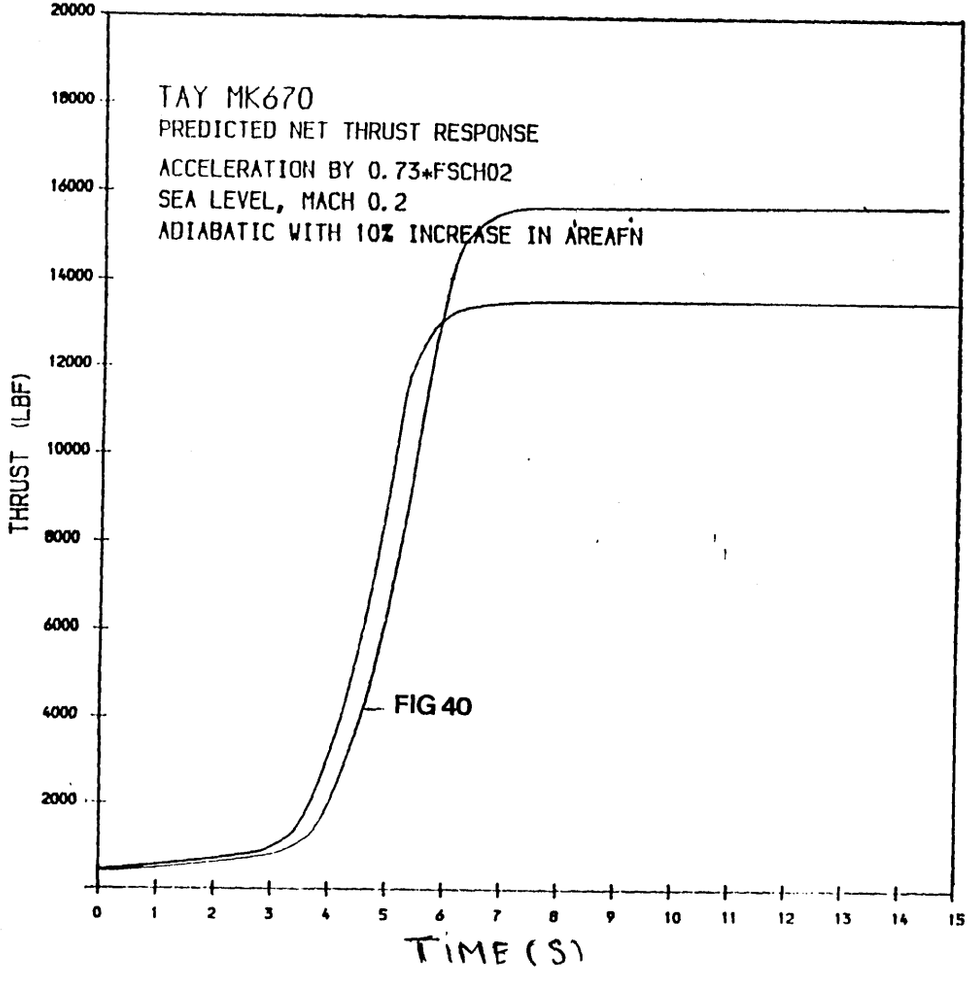

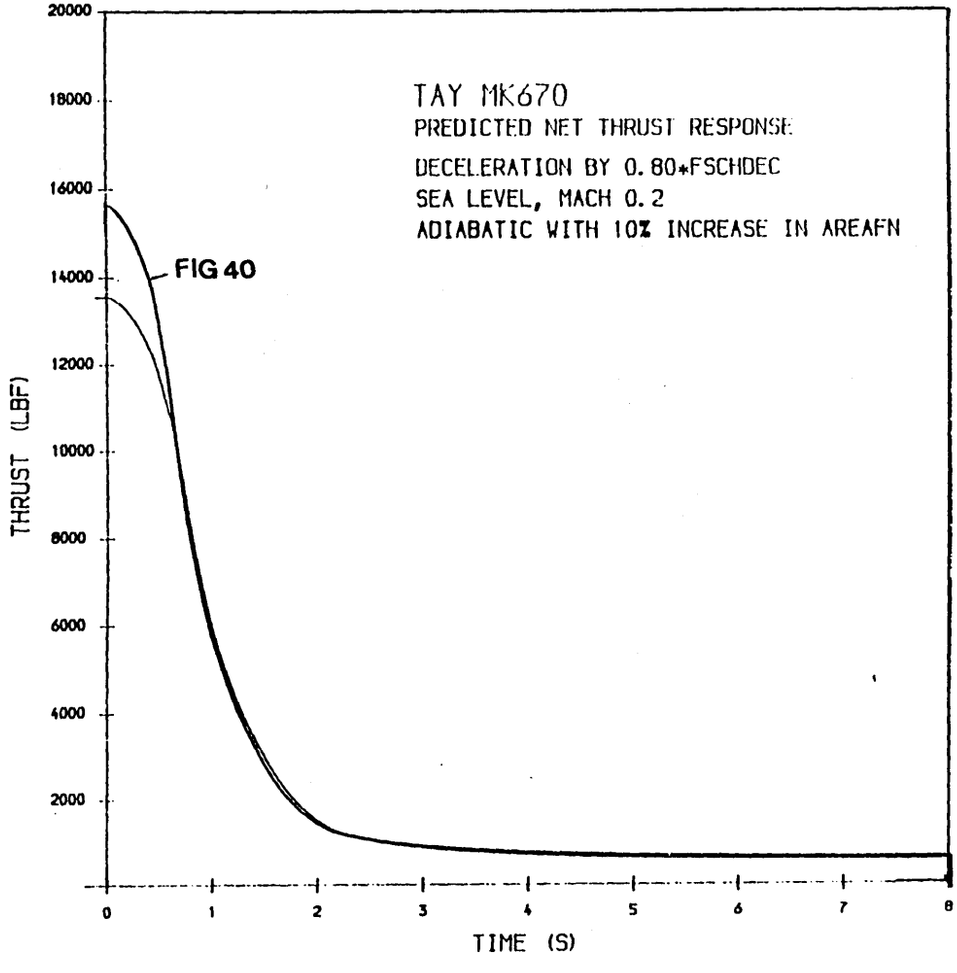

FIG 62 TAY MK670 PREDICTED PATHS OF FAN SECTION DURING TRANSIENT

ACCELERATION & DECELERATION AT SEA LEVEL MACH 0.2

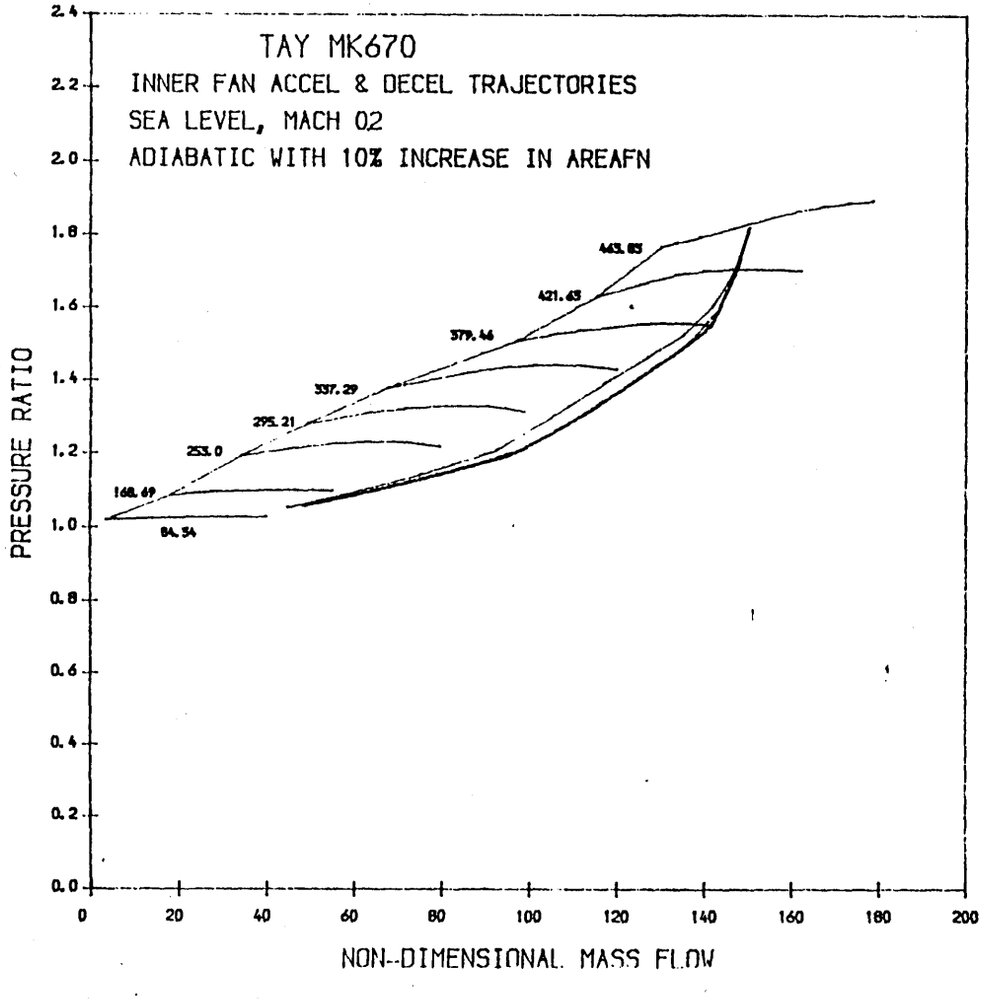

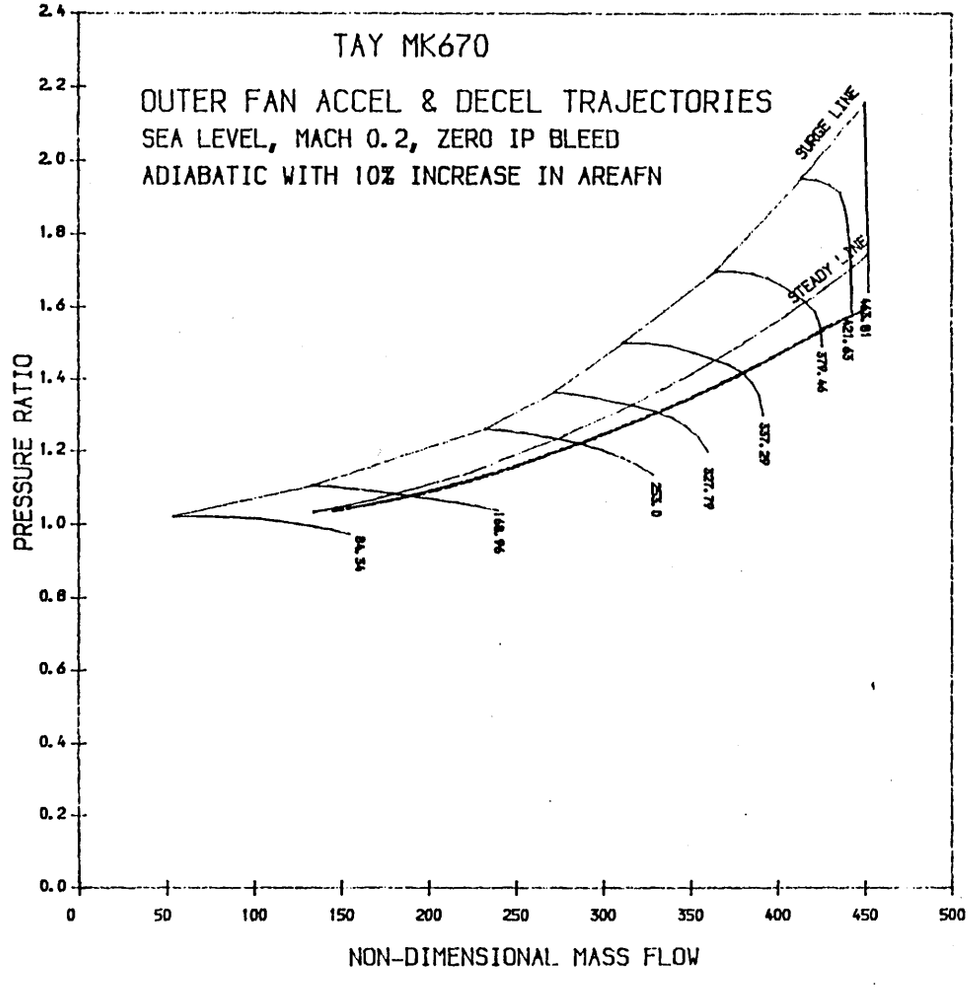

FIG 63 TAY MK670 ACCELERATION & DECELERATION TRANSIENTS OF THE I.P AND H.P COMPRESSORS AT SEA LEVEL, MACH 0.2.

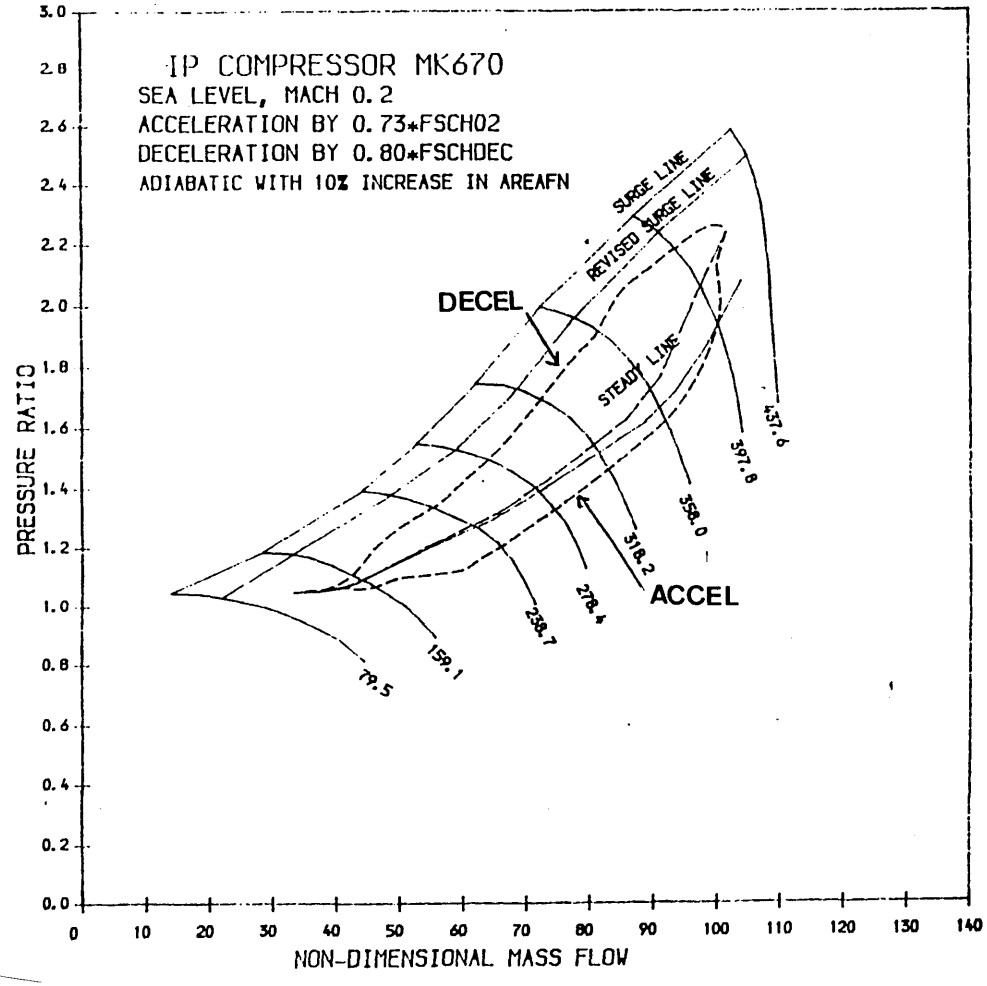

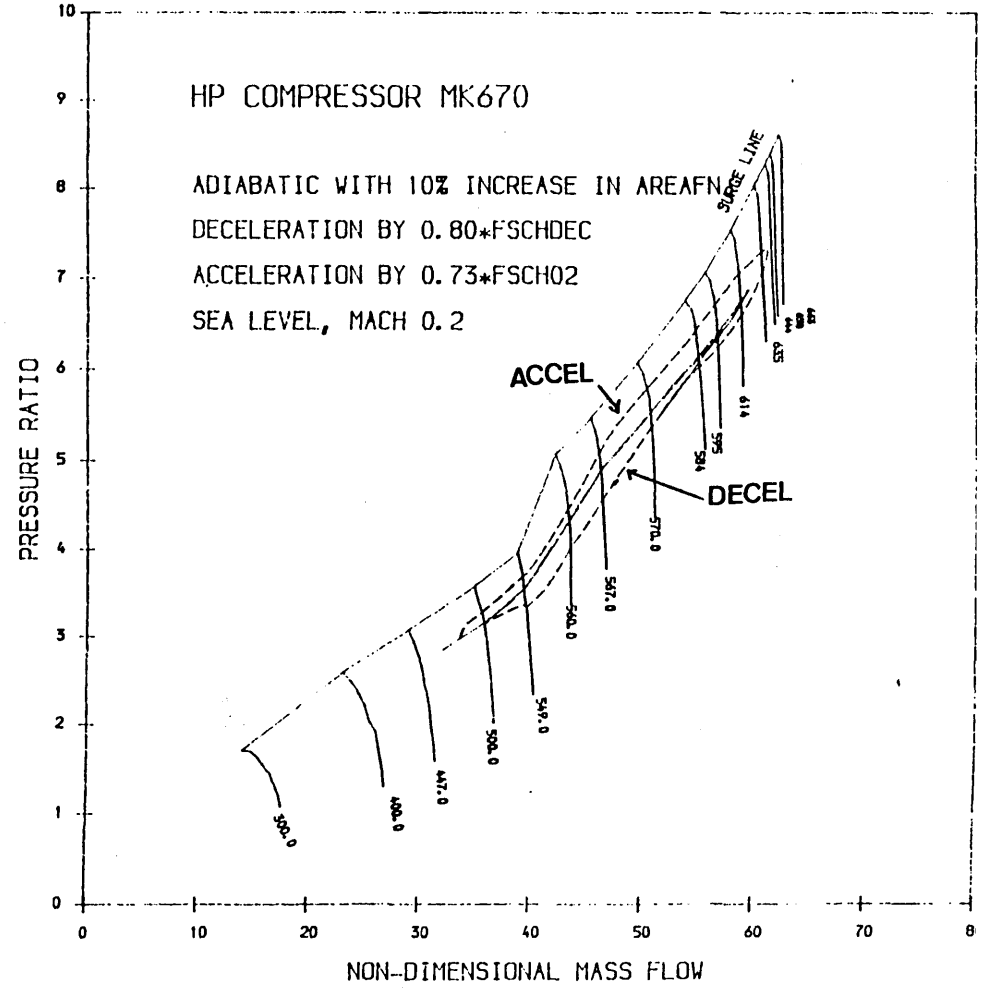

FIG 64 TAY MK670 PREDICTED LP & HP SHAFTSPEED RELATIONSHIPS

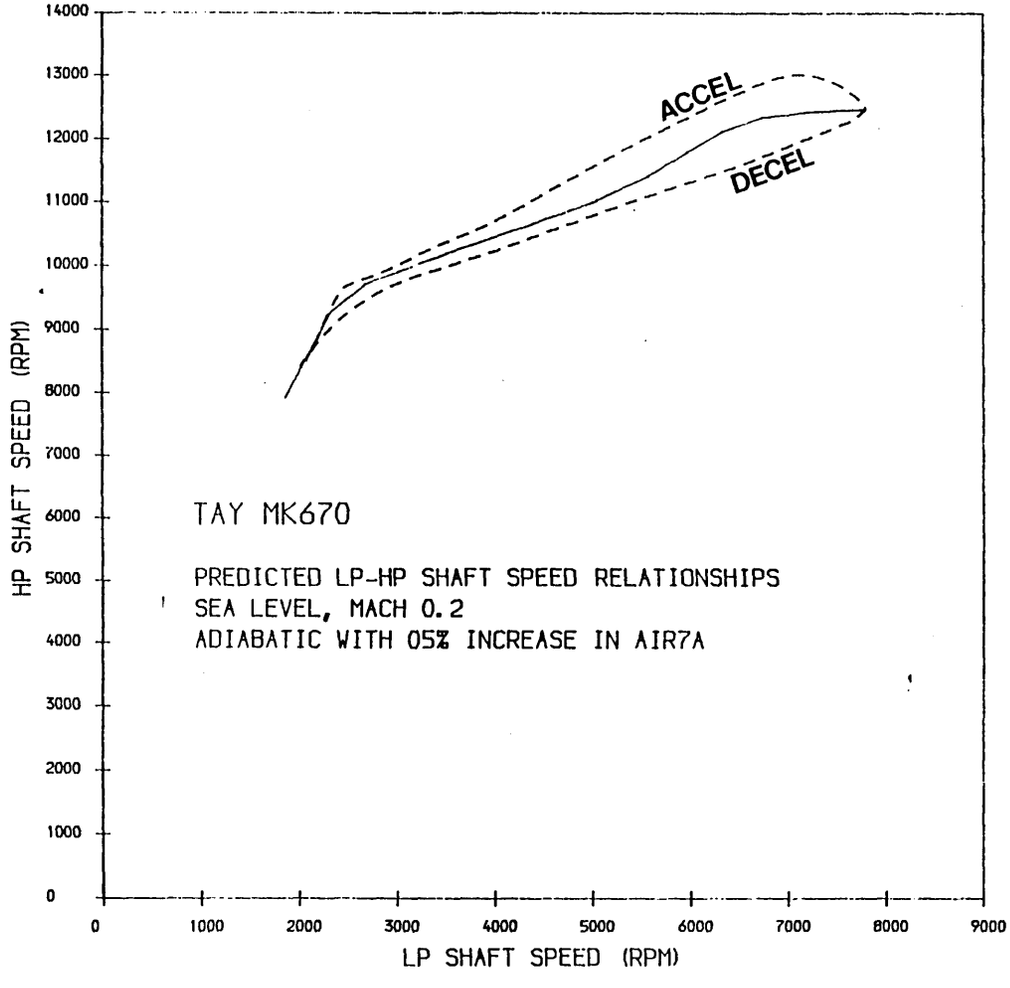

FIG 65 TAY MK670 PREDICTED ADIABATIC TRANSIENTS AT SEA LEVEL MACH 0.2

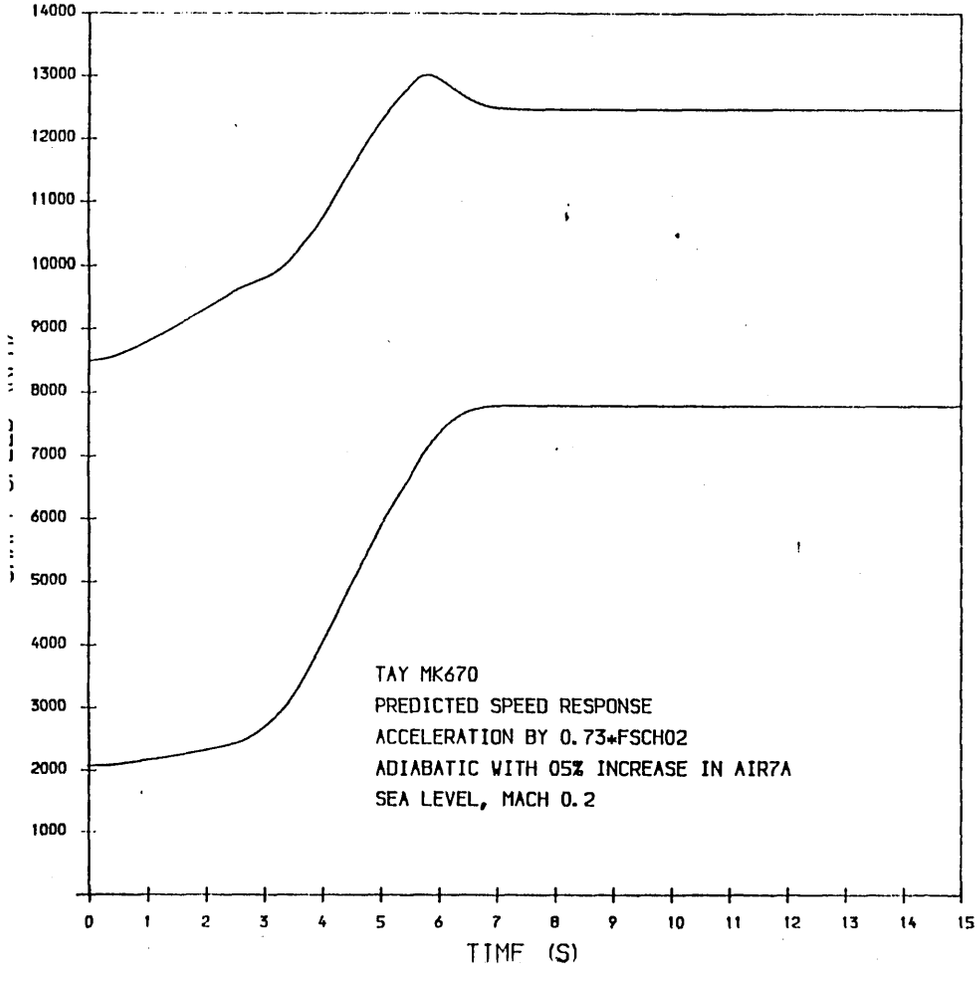

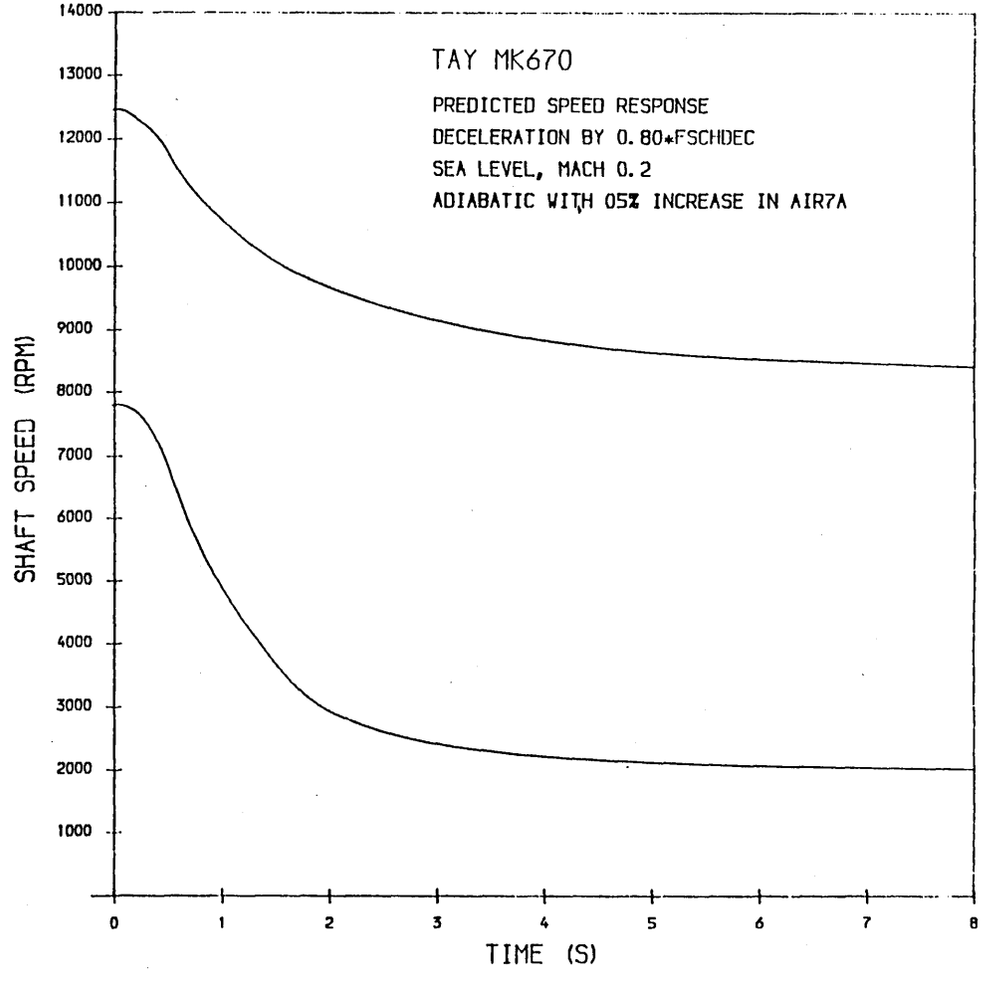

FIG 66 TAY MK670 PREDICTED ADIABATIC TRANSIENTS
AT SEA LEVEL, MACH 0.2.

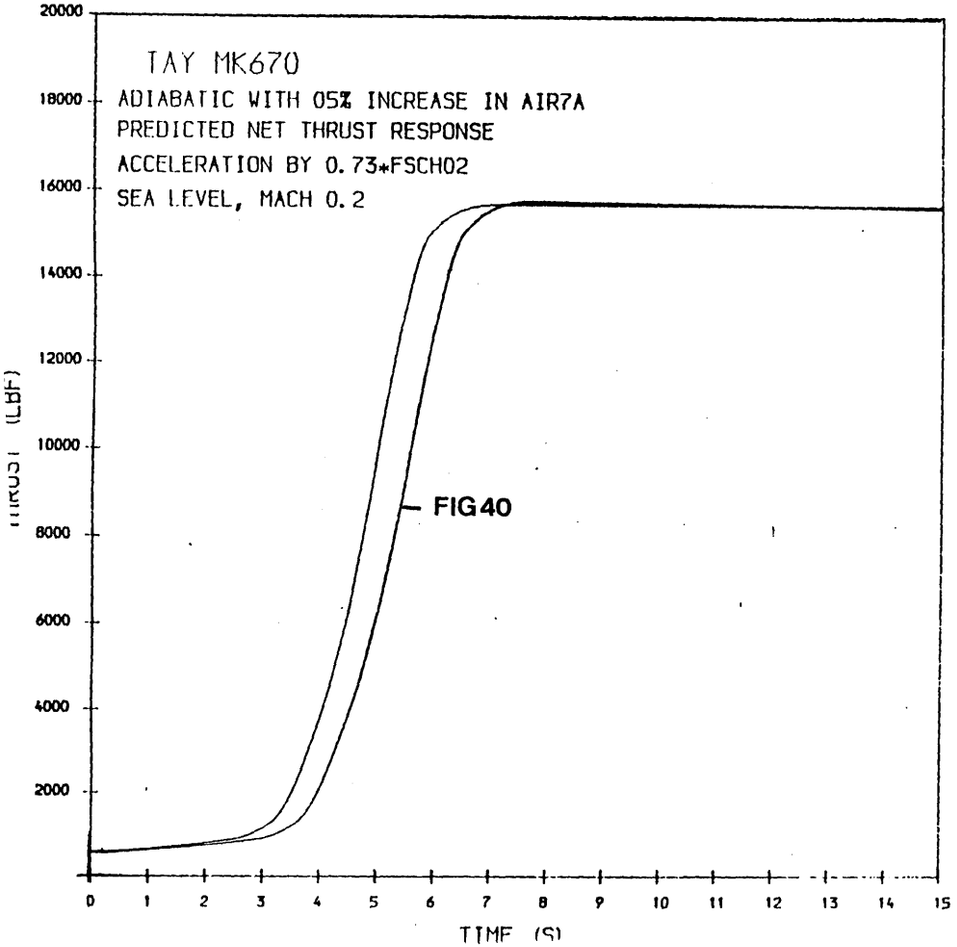

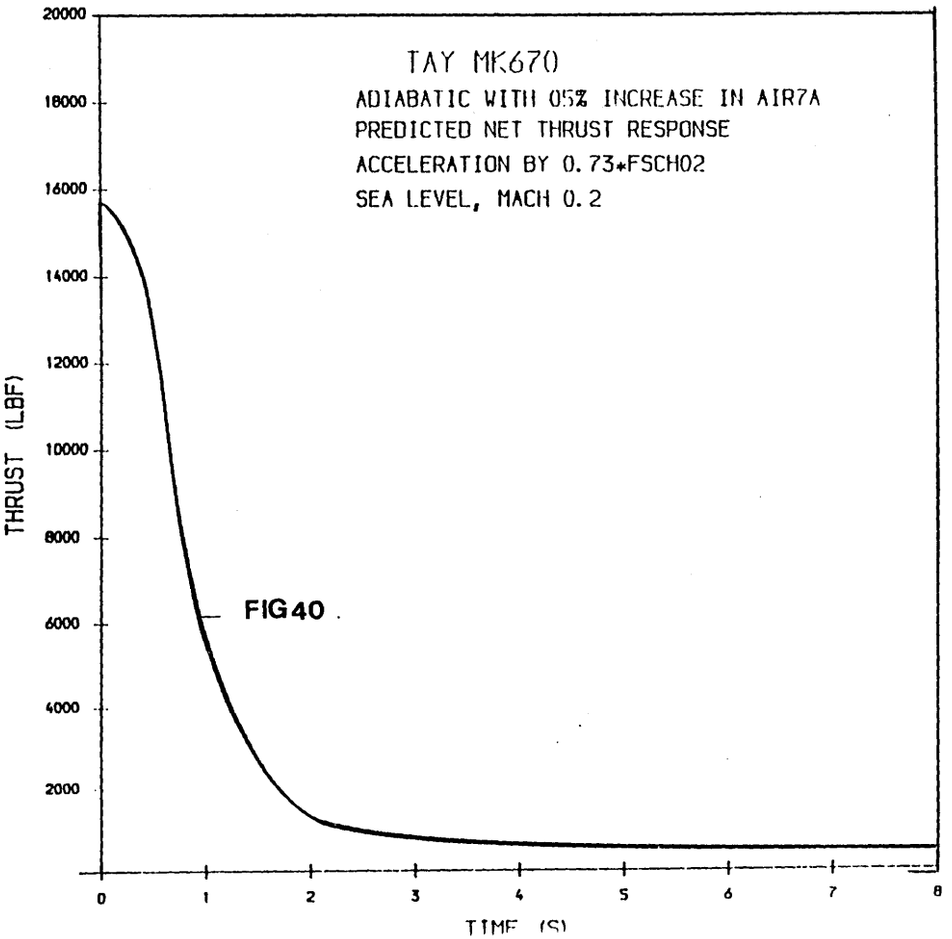

FIG 67 TAY MK670 PREDICTED PATHS OF FAN SECTION DURING TRANSIENT ACCELERATION & DECELERATION AT SEA LEVEL MACH 0.2

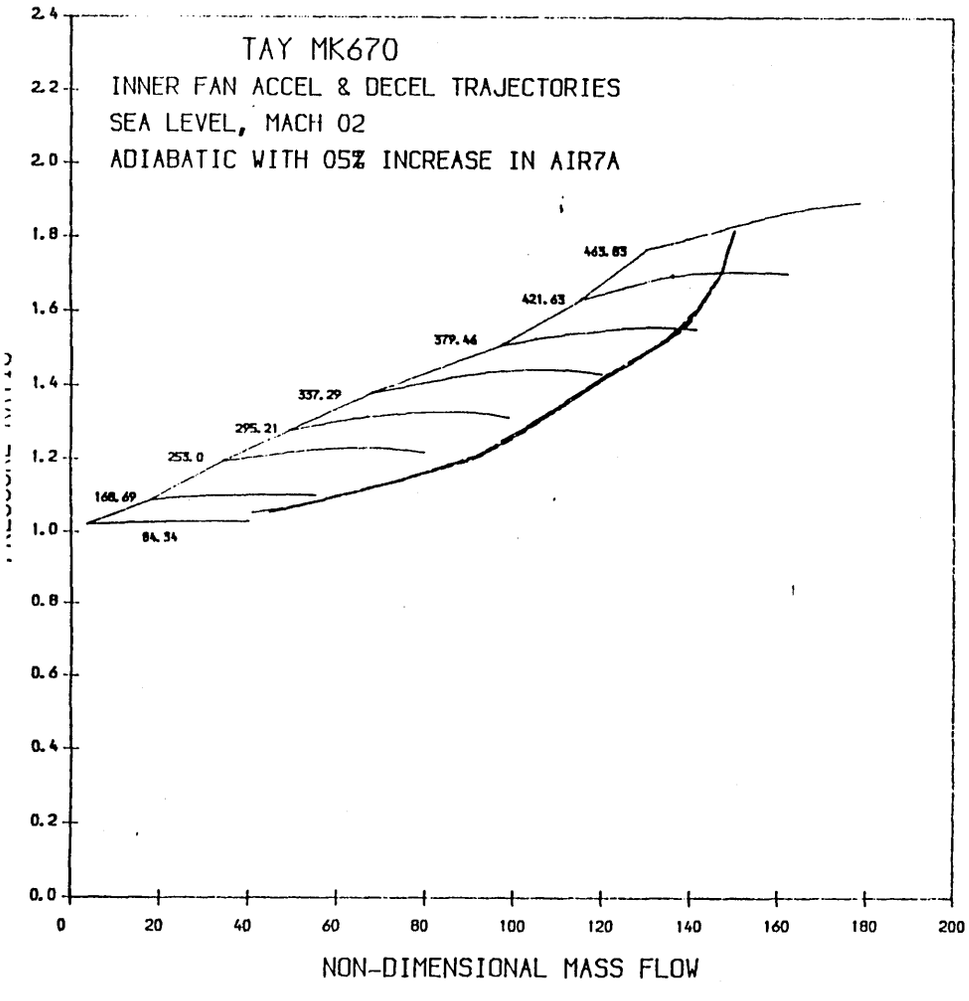

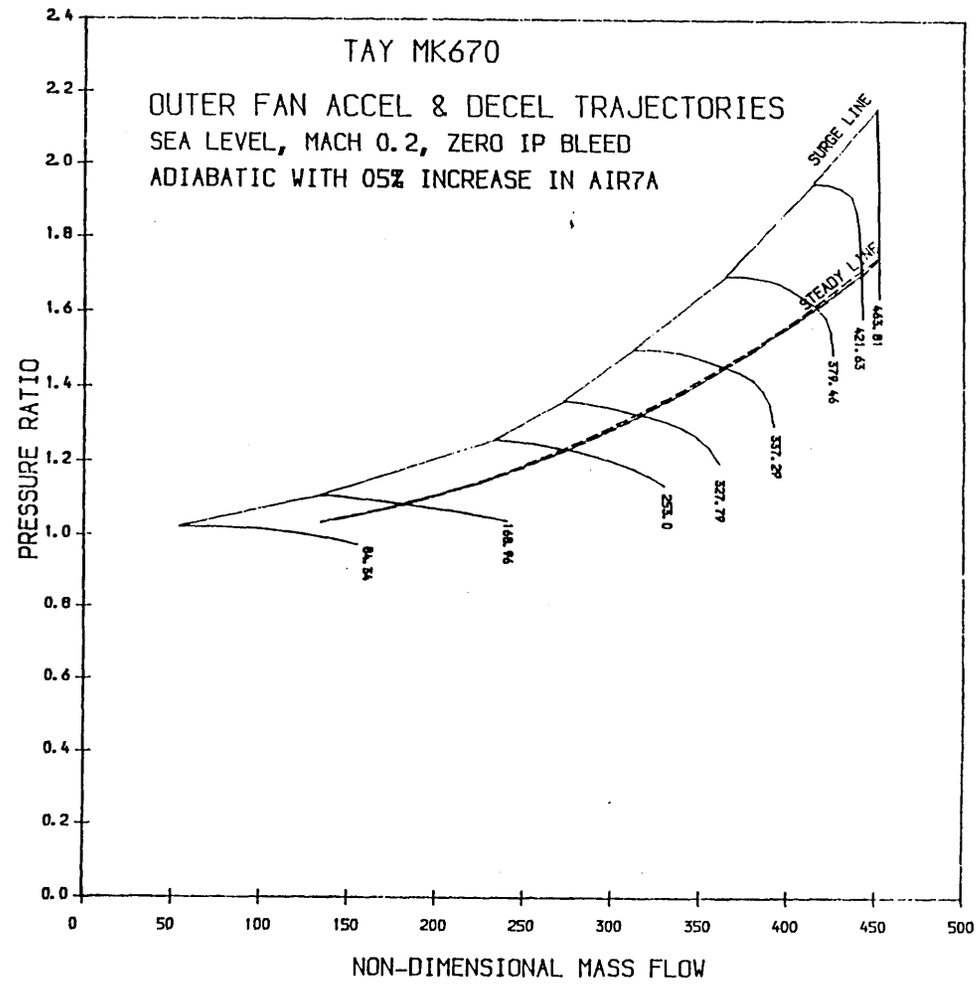

FIG 68 TAY MK670 ACCELERATION & DECELERATION TRANSIENTS OF THE I.P AND H.P COMPRESSORS AT SEA LEVEL, MACH 0.2.

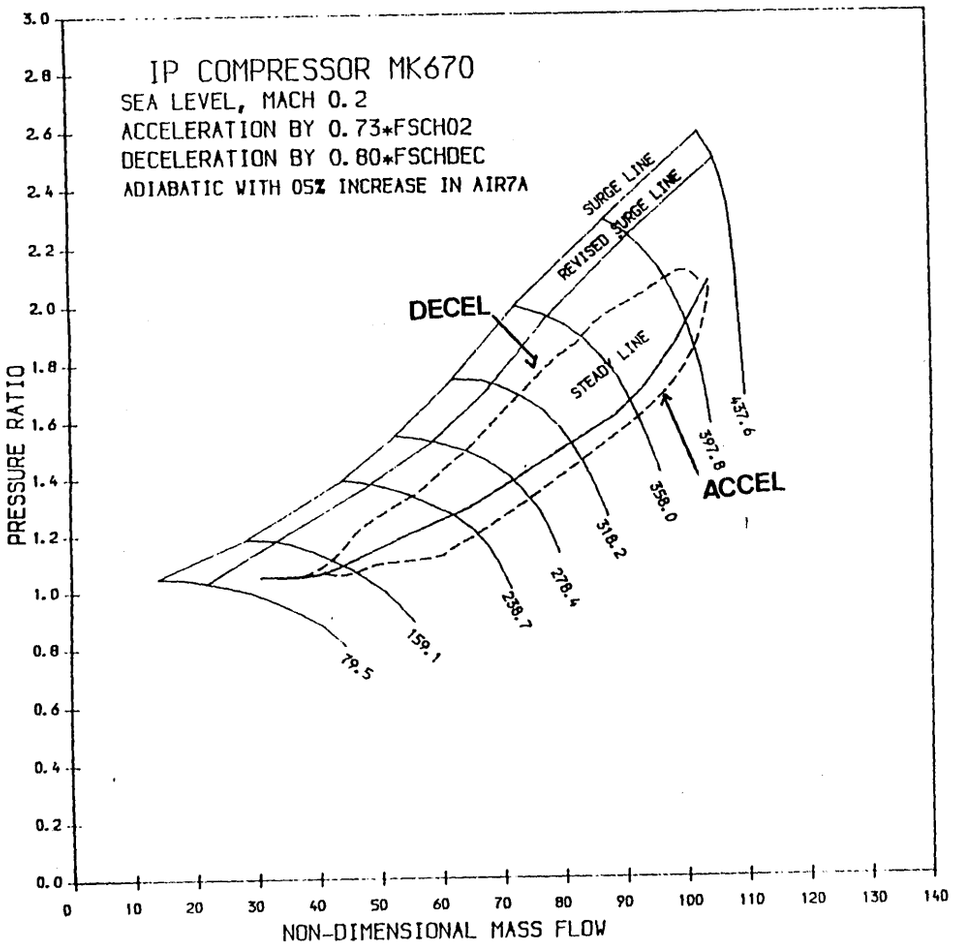

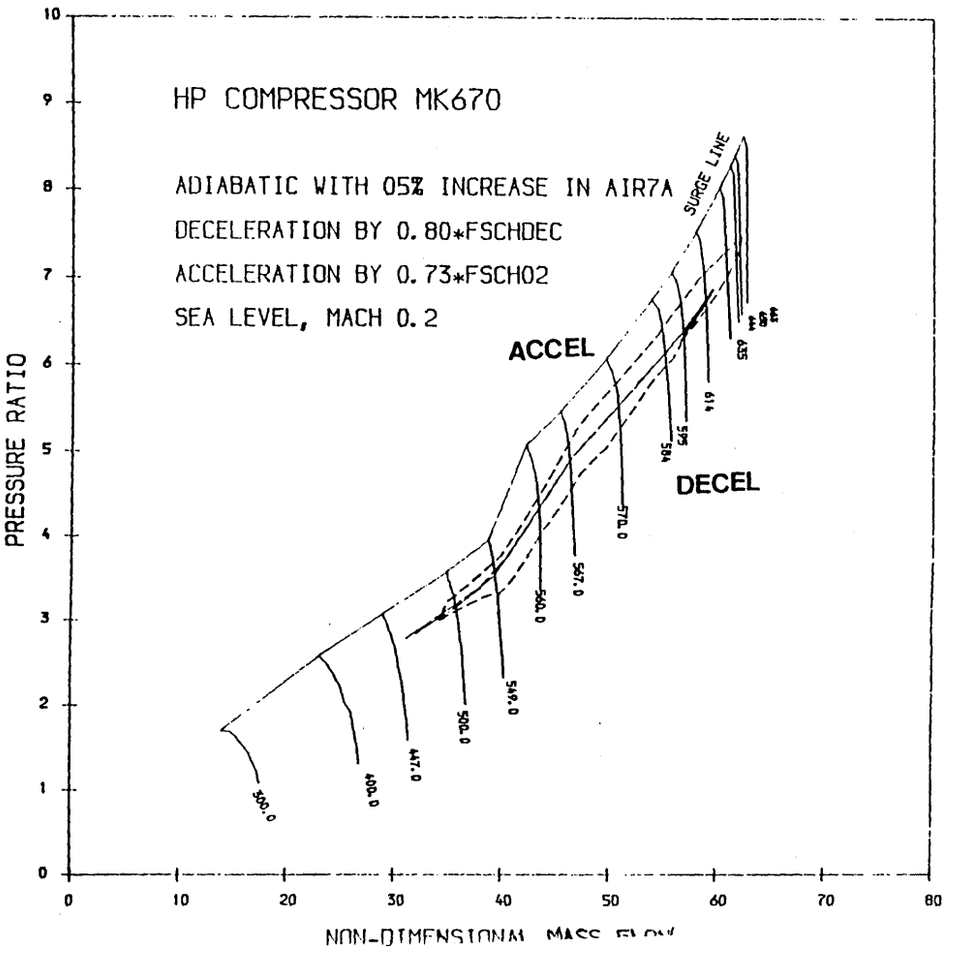

FIG 69 TAY MK670 PREDICTED LP & HP SHAFTSPEED RELATIONSHIPS

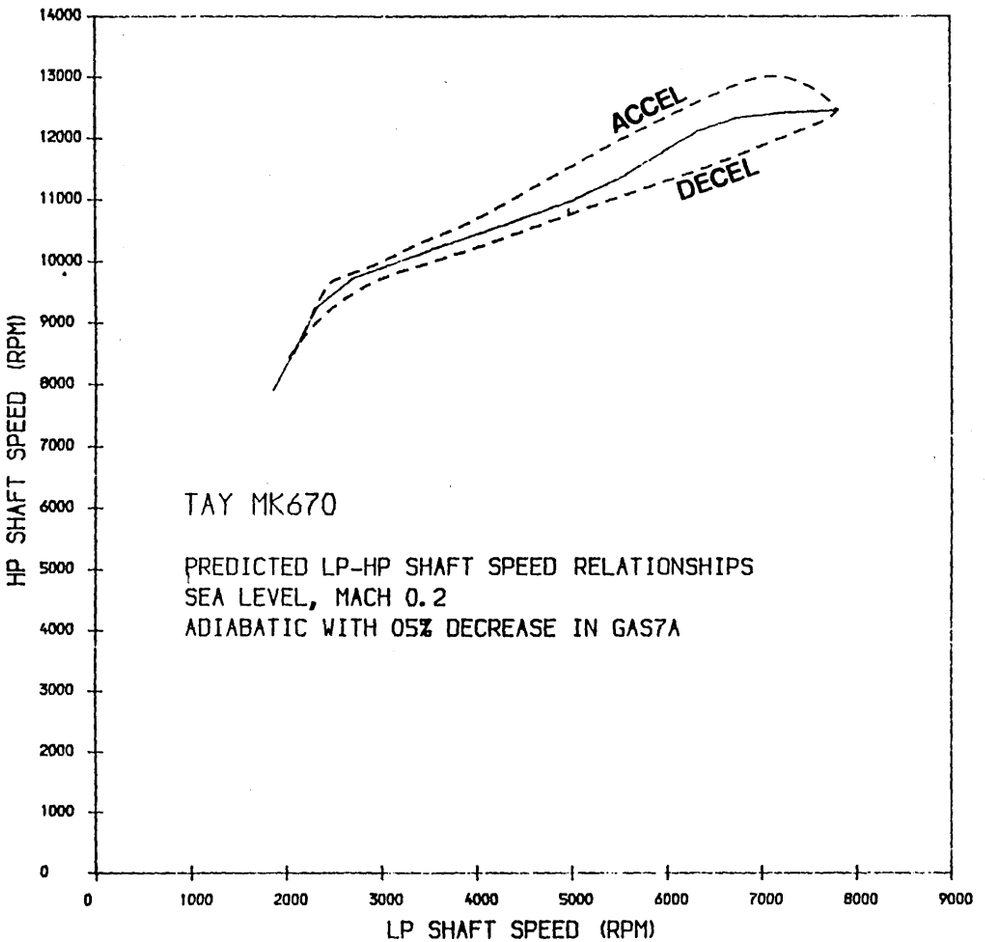

FIG 70 TAY MK670 PREDICTED ADIABATIC TRANSIENTS AT SEA LEVEL MACH 0.2

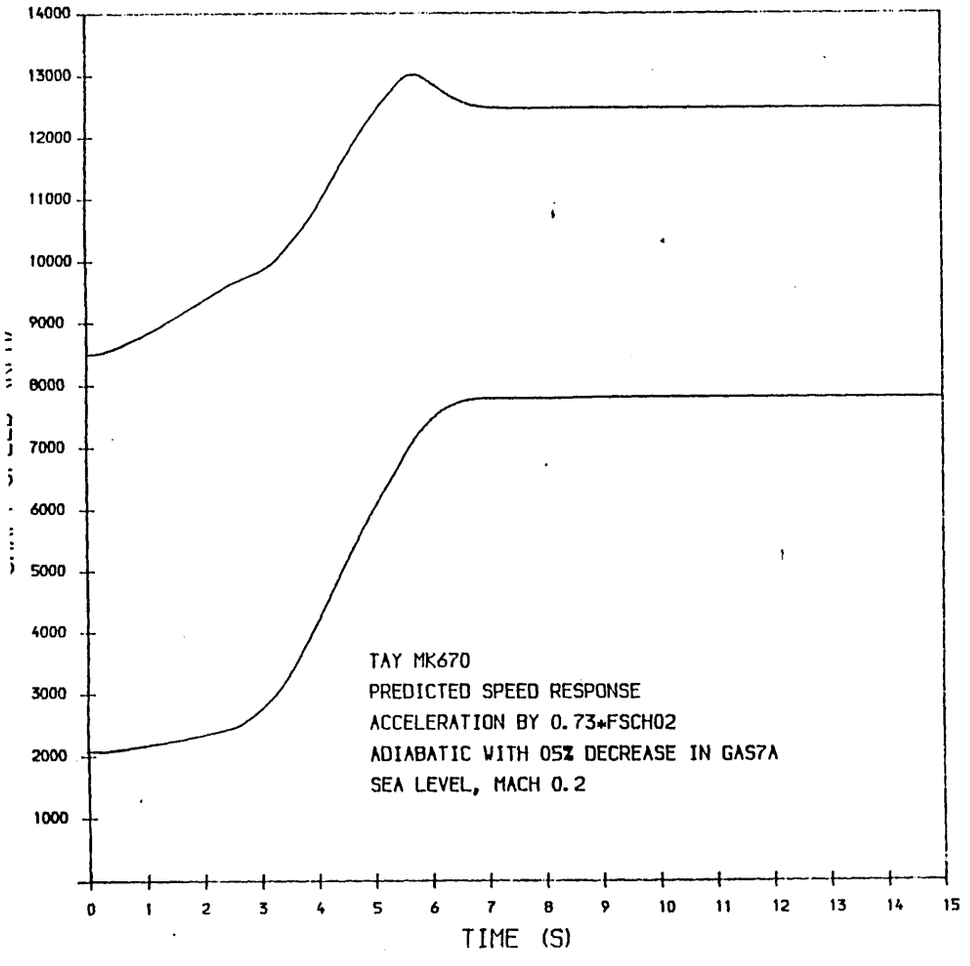

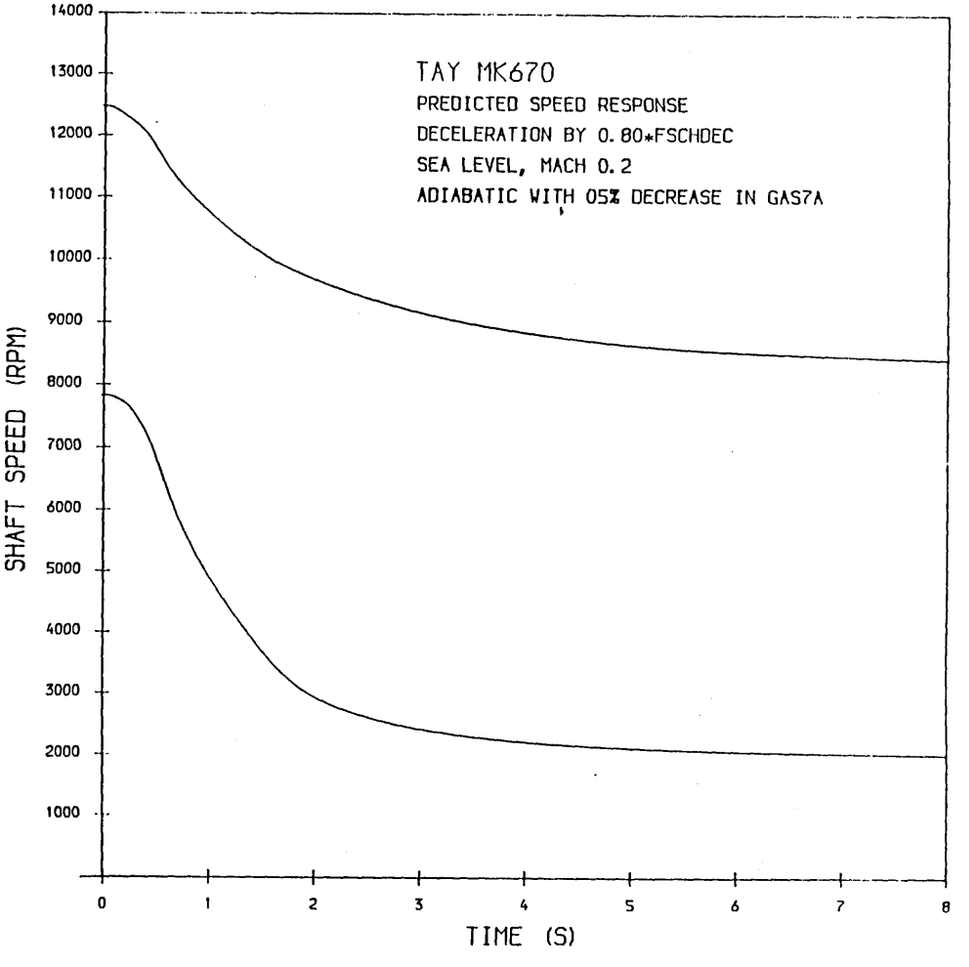

FIG 71 TAY MK670 ACCELERATION & DECELERATION TRANSIENTS OF THE I.P AND H.P COMPRESSORS AT SEA LEVEL, MACH 0.2.

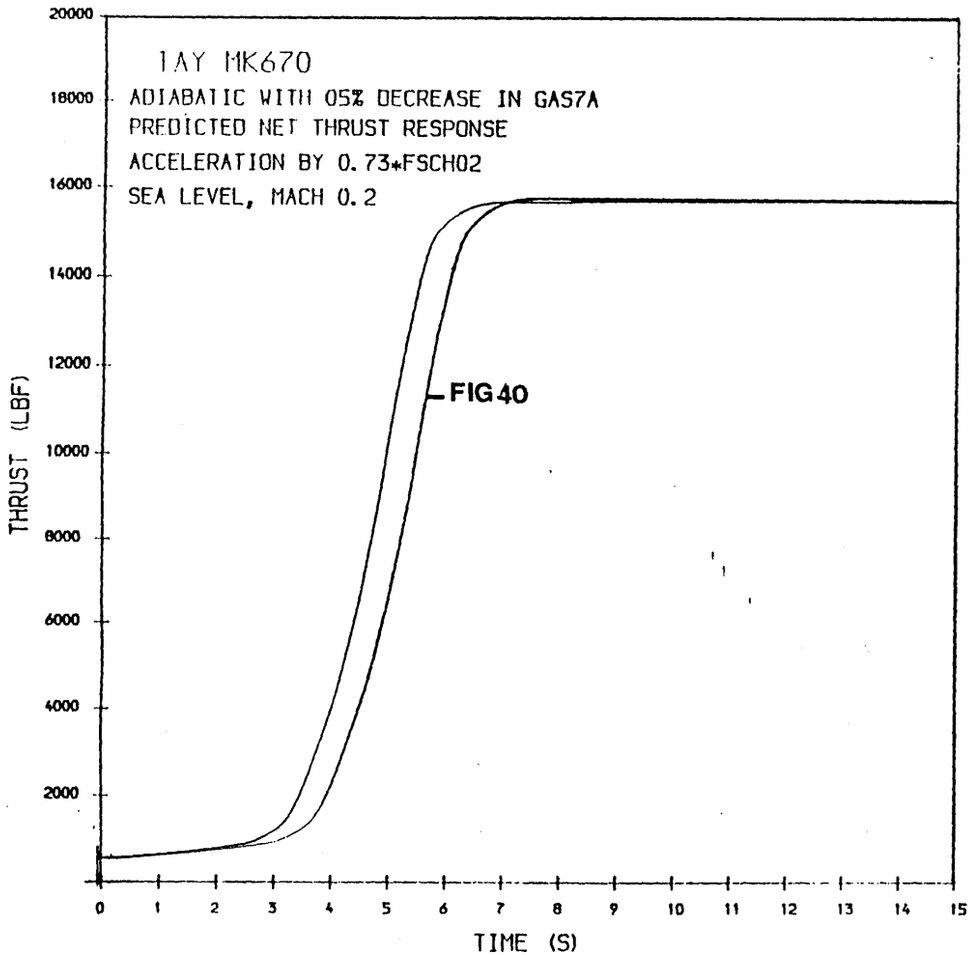

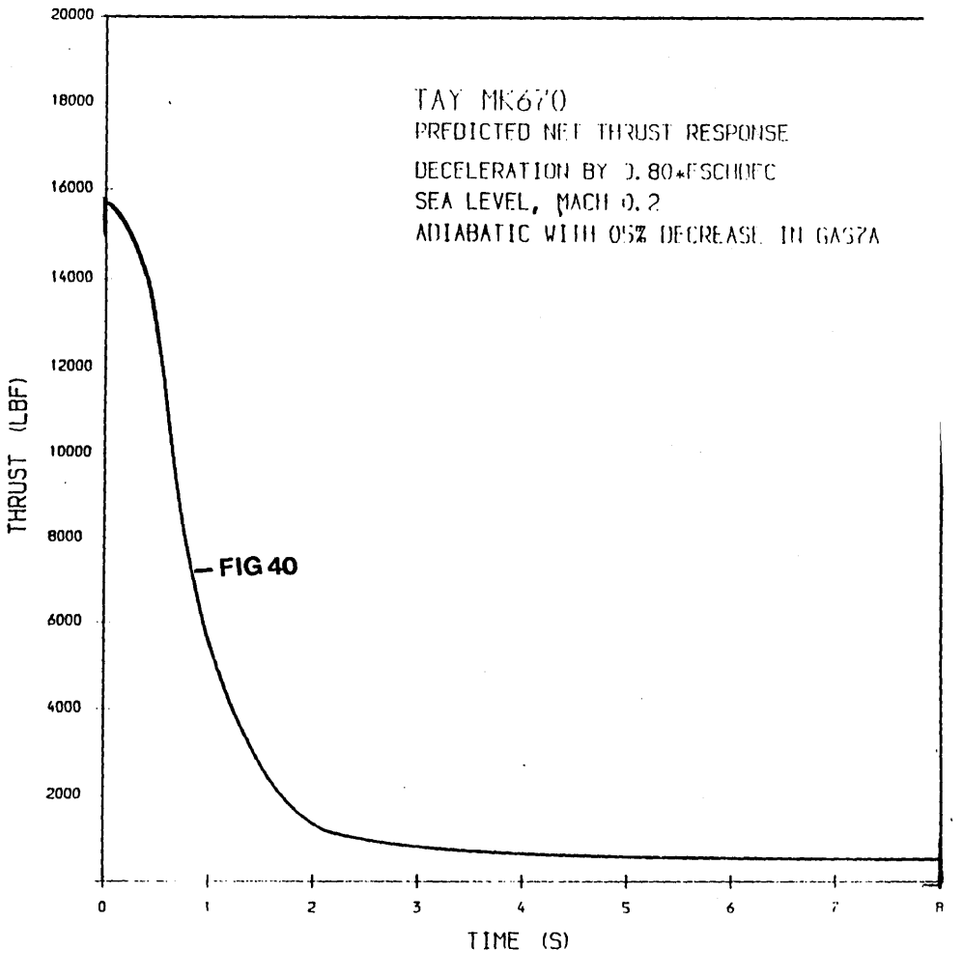

FIG 72 TAY MK670 PREDICTED PATHS OF FAN SECTION DURING TRANSIENT

ACCELERATION & DECELERATION AT SEA LEVEL MACH 0.2

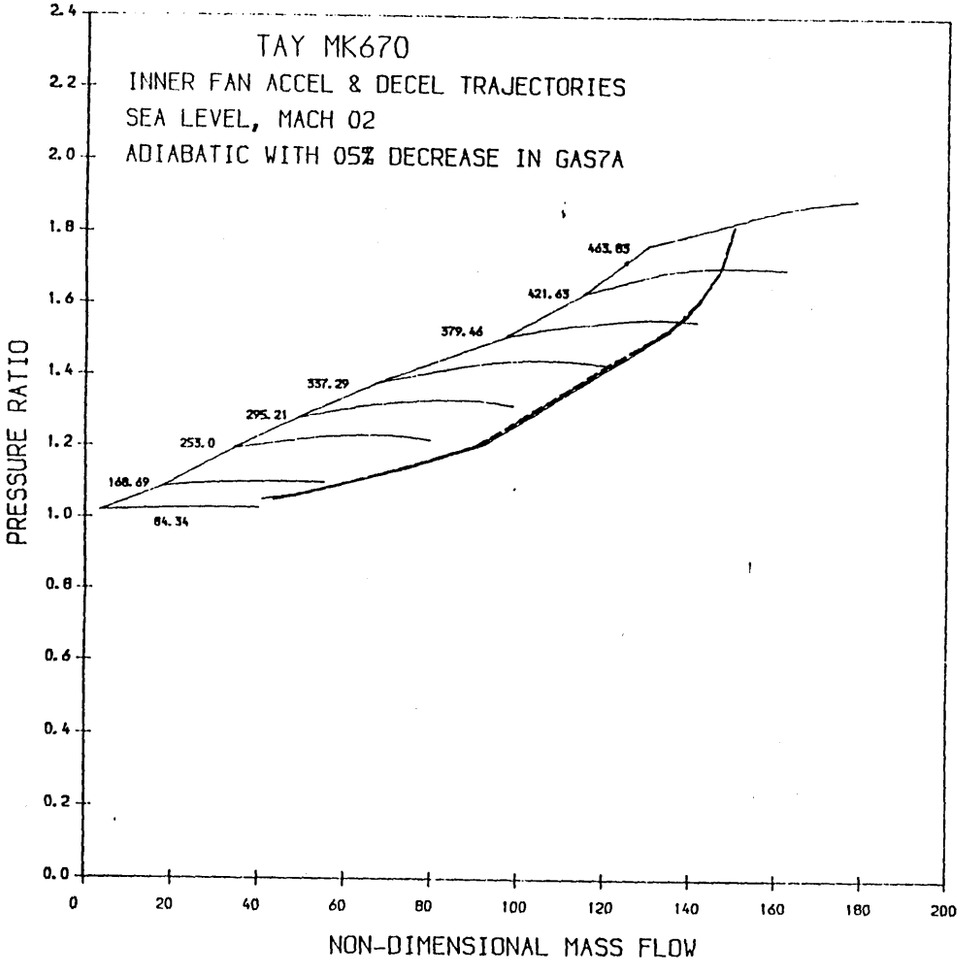

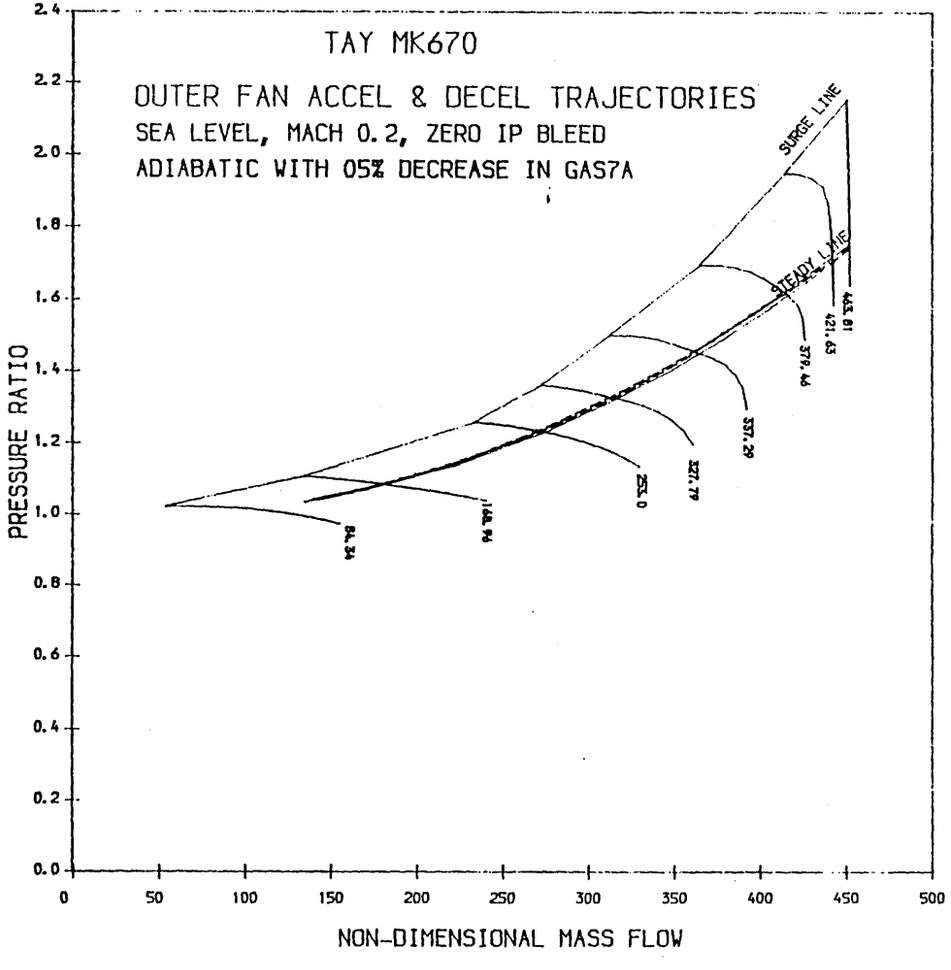

FIG 73 TAY MK670 ACCELERATION & DECELERATION TRANSIENTS OF THE I.P AND H.P COMPRESSORS AT SEA LEVEL, MACH 0.2.

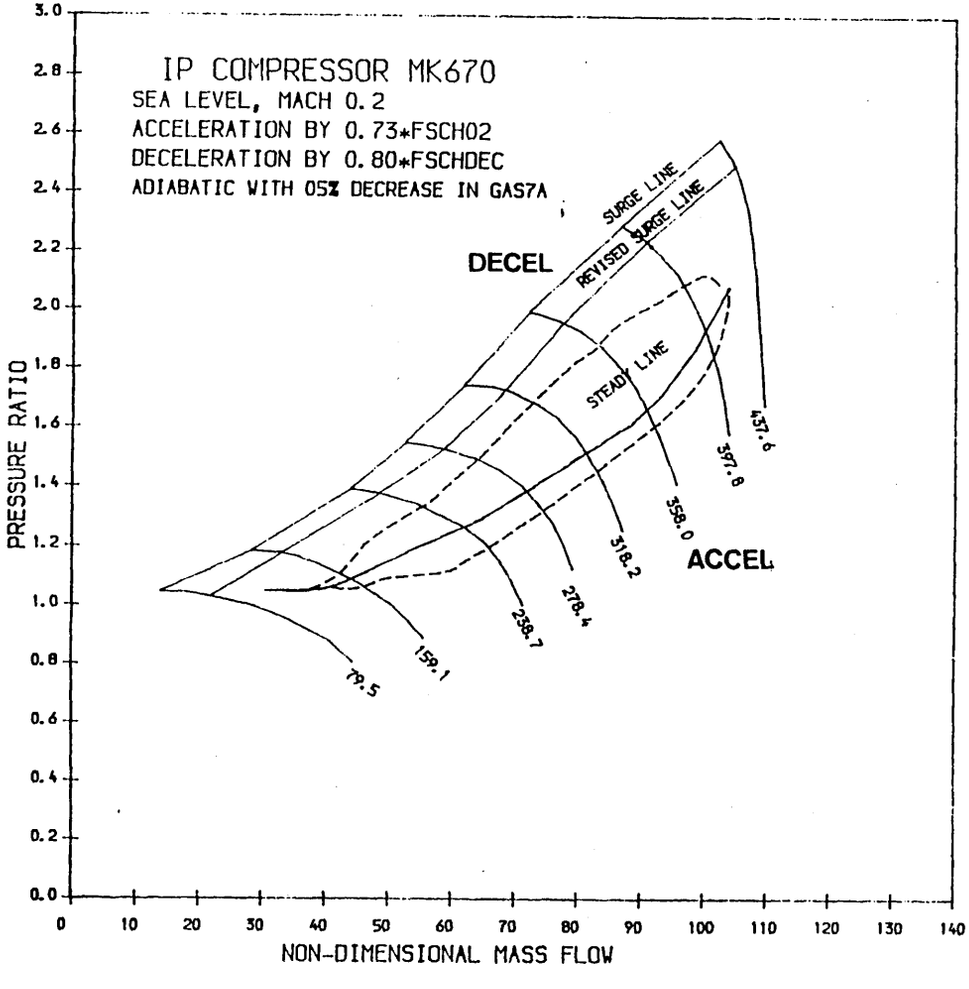

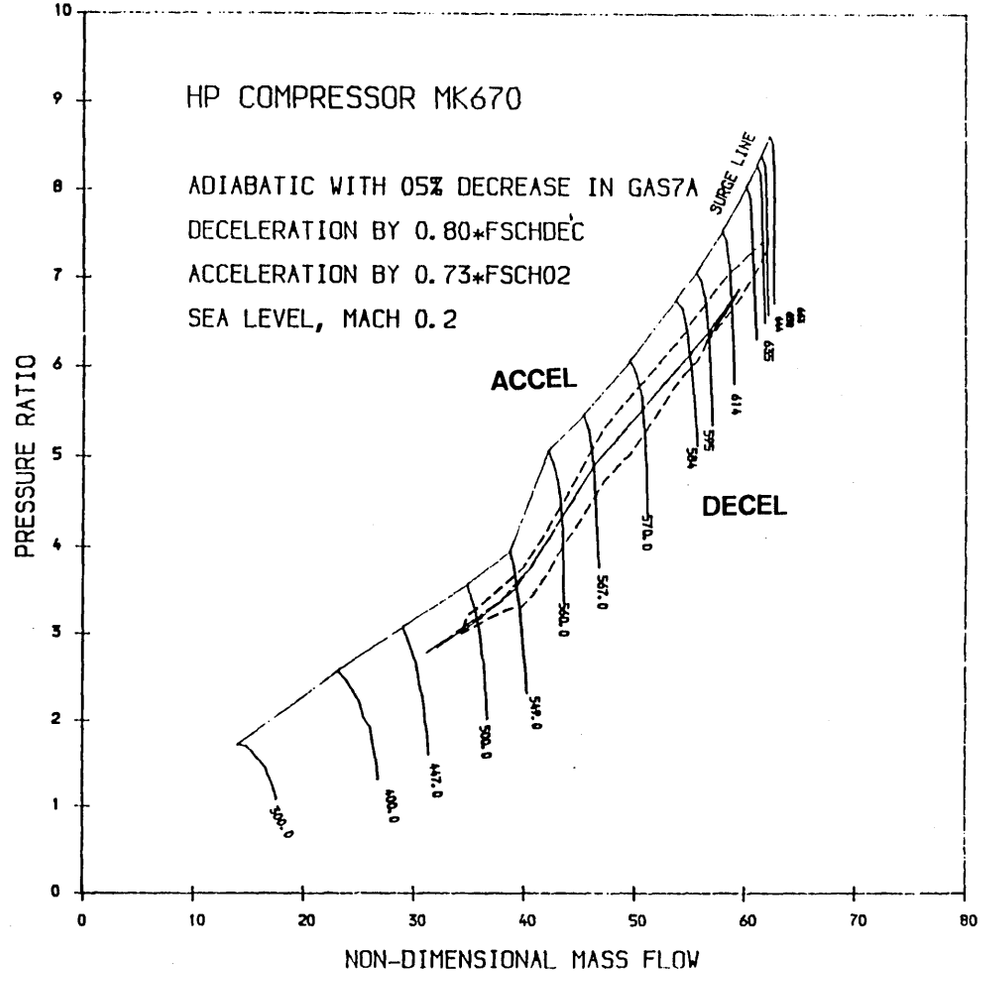

FIG 74 TAY MK670 PREDICTED LP & HP SHAFTSPEED RELATIONSHIPS

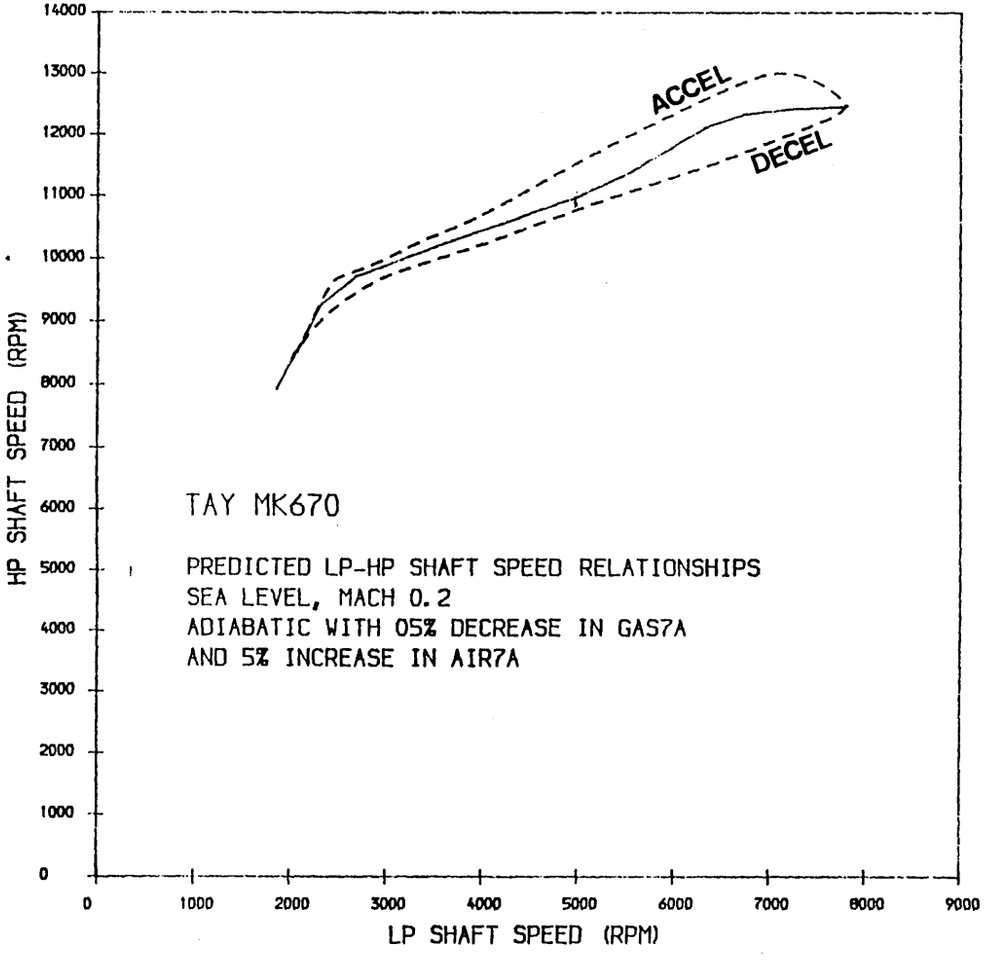

FIG 75 TAY MK670 PREDICTED ADIABATIC TRANSIENTS AT SEA LEVEL MACH 0.2

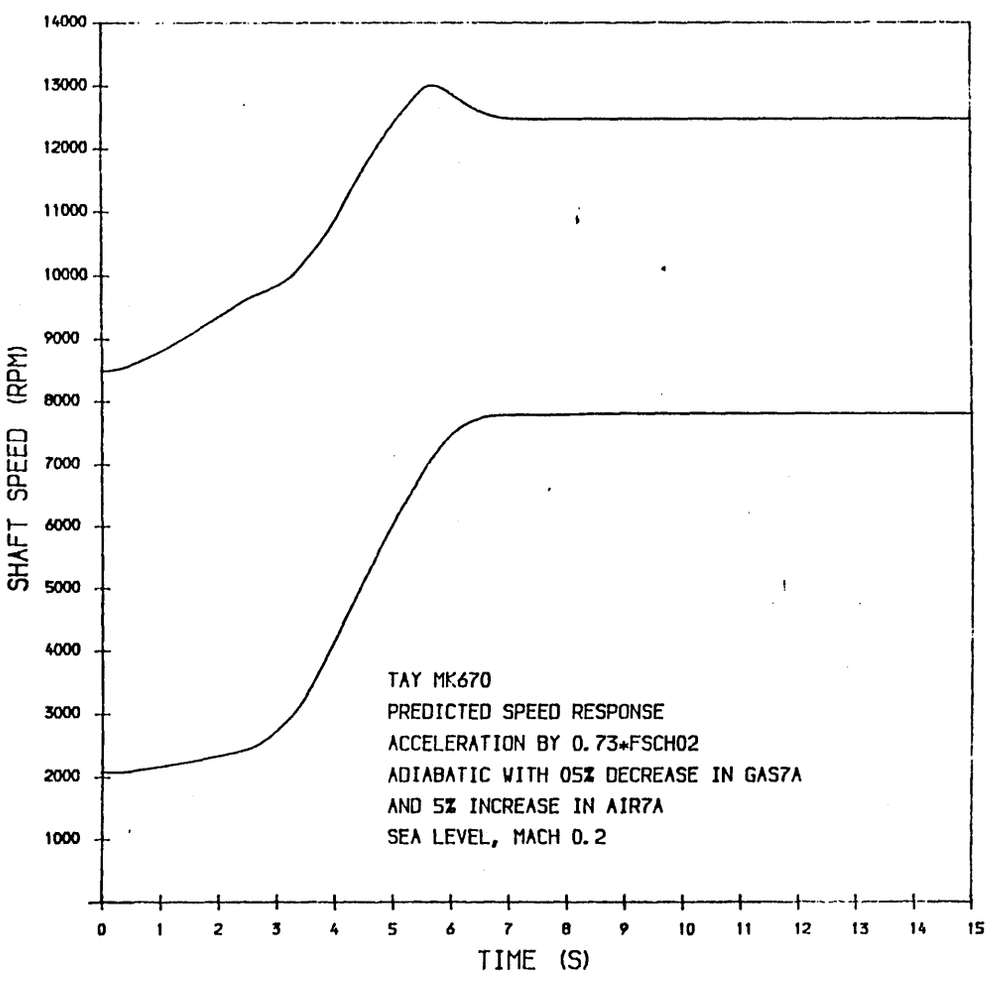

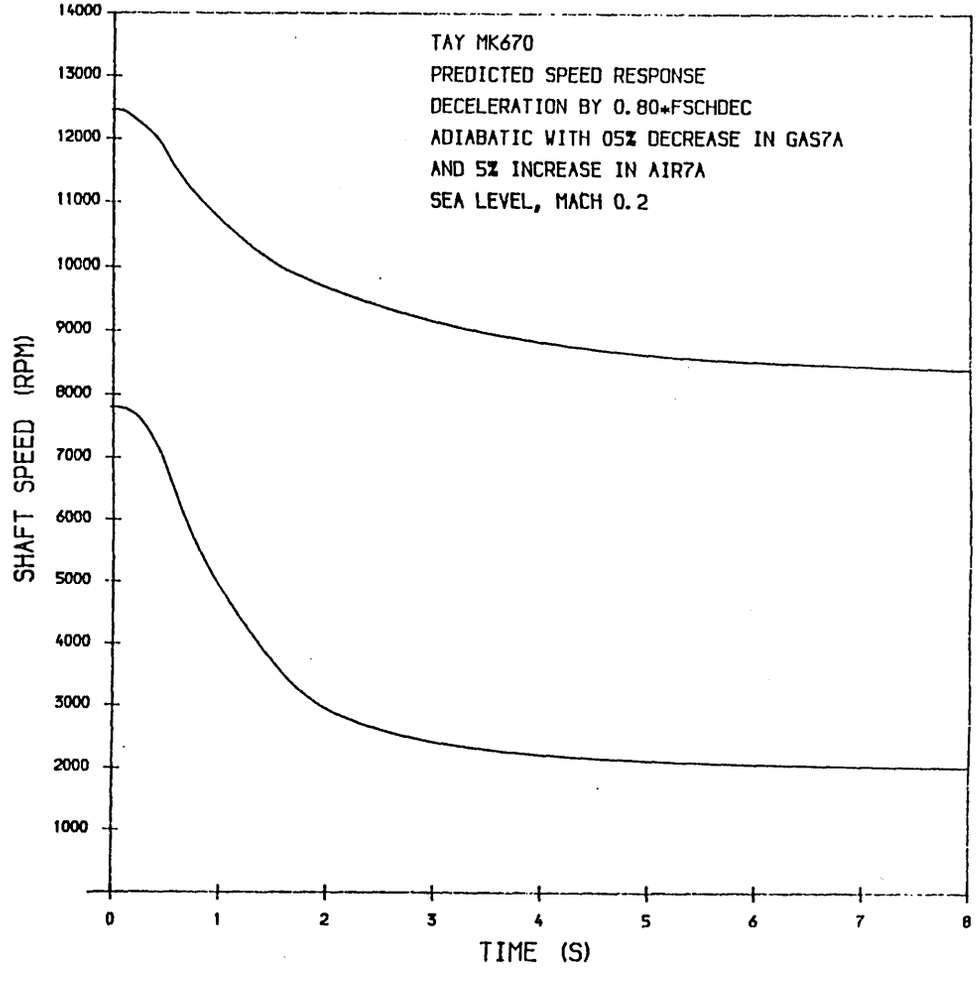

FIG 76 TAY MK670 PREDICTED ADIABATIC TRANSIENTS AT SEA LEVEL, MACH 0.2.

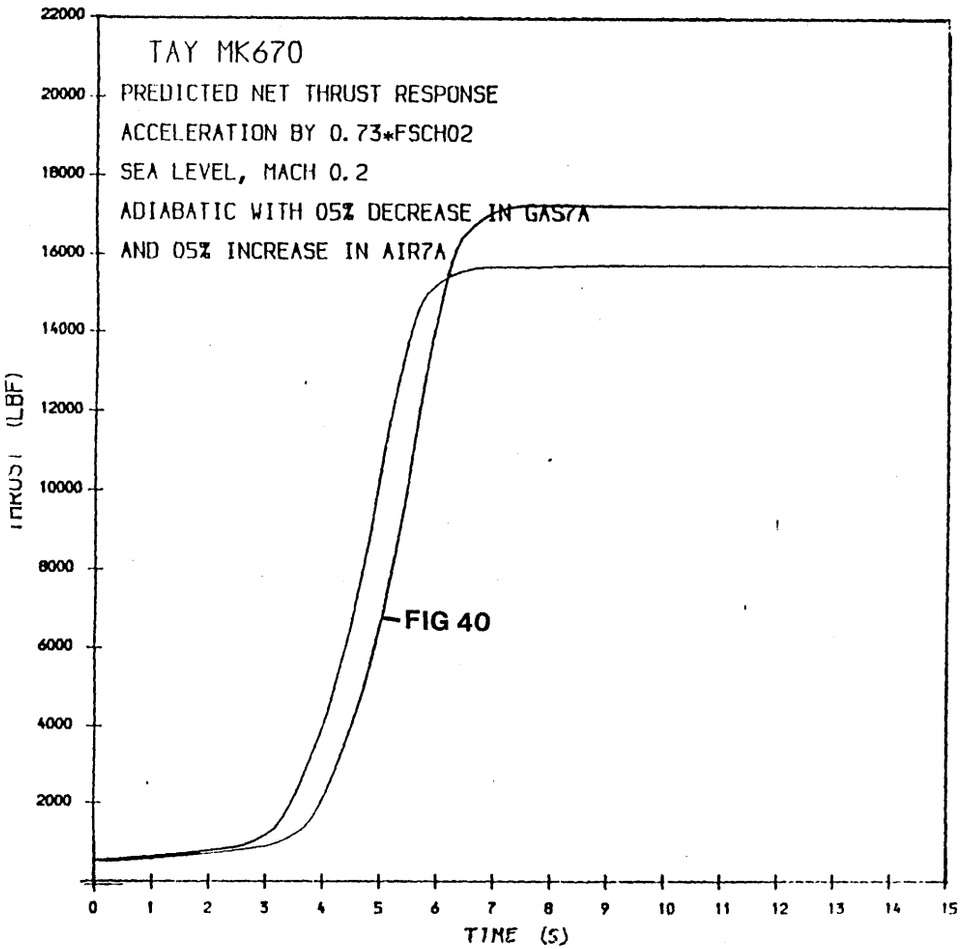

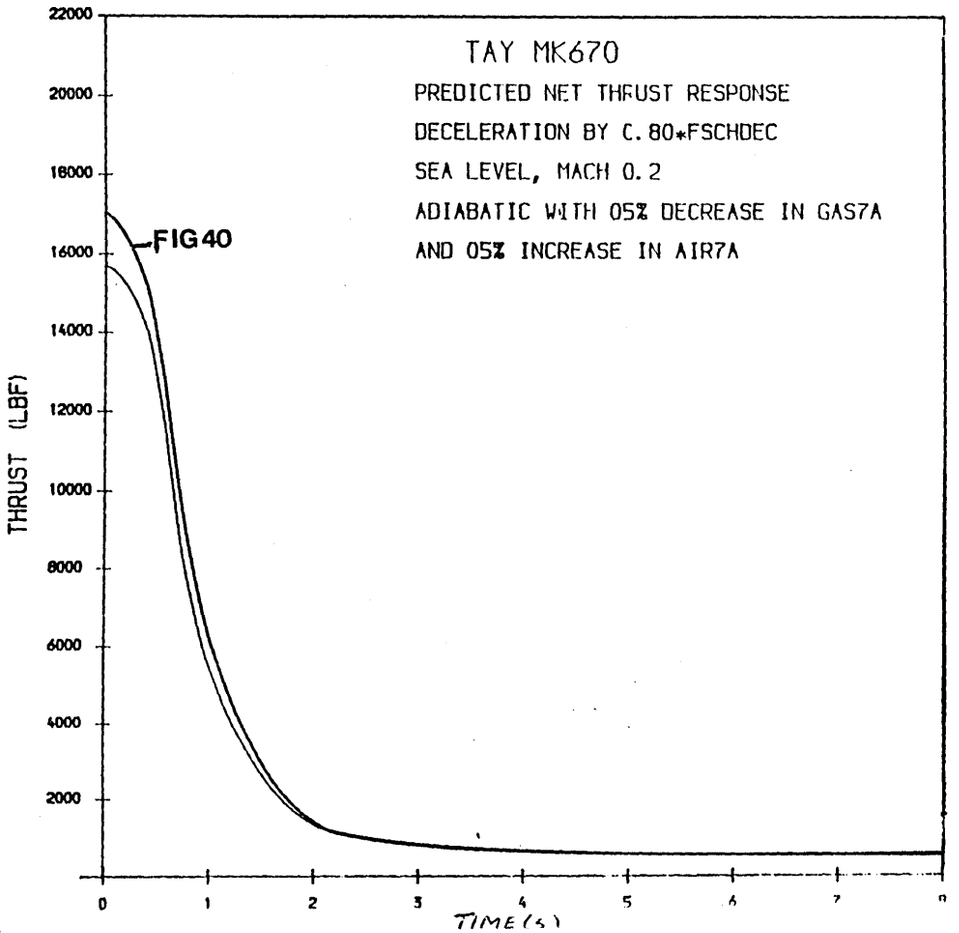

FIG 77 TAY MK670 PREDICTED PATHS OF FAN SECTIONS DURING TRANSIENT ACCELERATION AND DECELERATION AT SEA LEVEL, MACH 0.2.

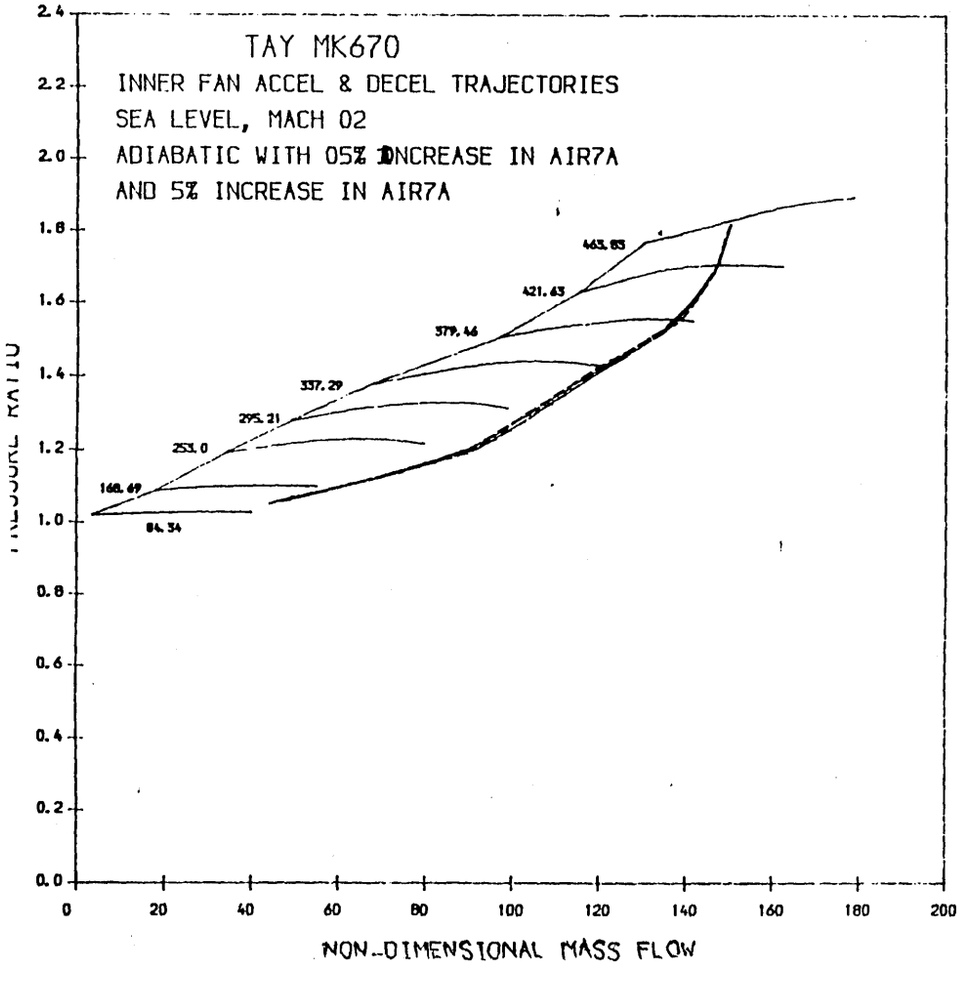

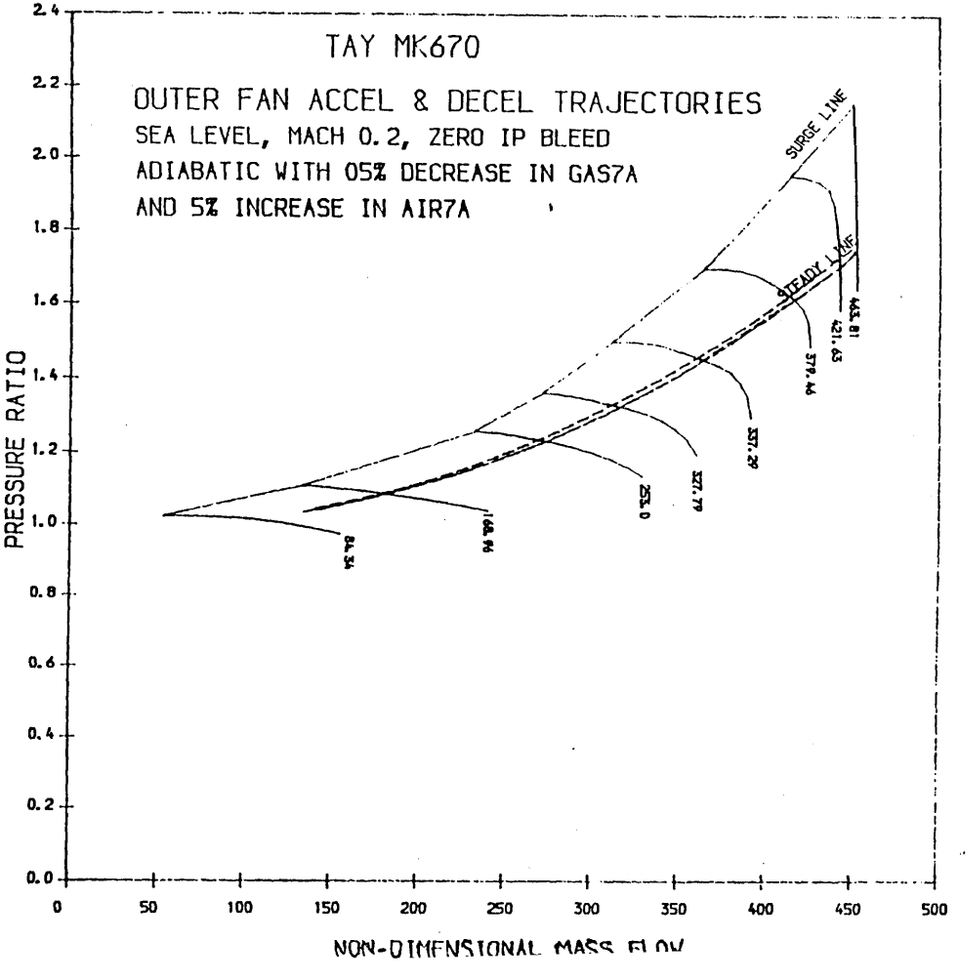

FIG 78 TAY MK670 ACCELERATION & DECELERATION TRANSIENTS OF THE I.P AND H.P COMPRESSORS AT SEA LEVEL, MACH 0.2.

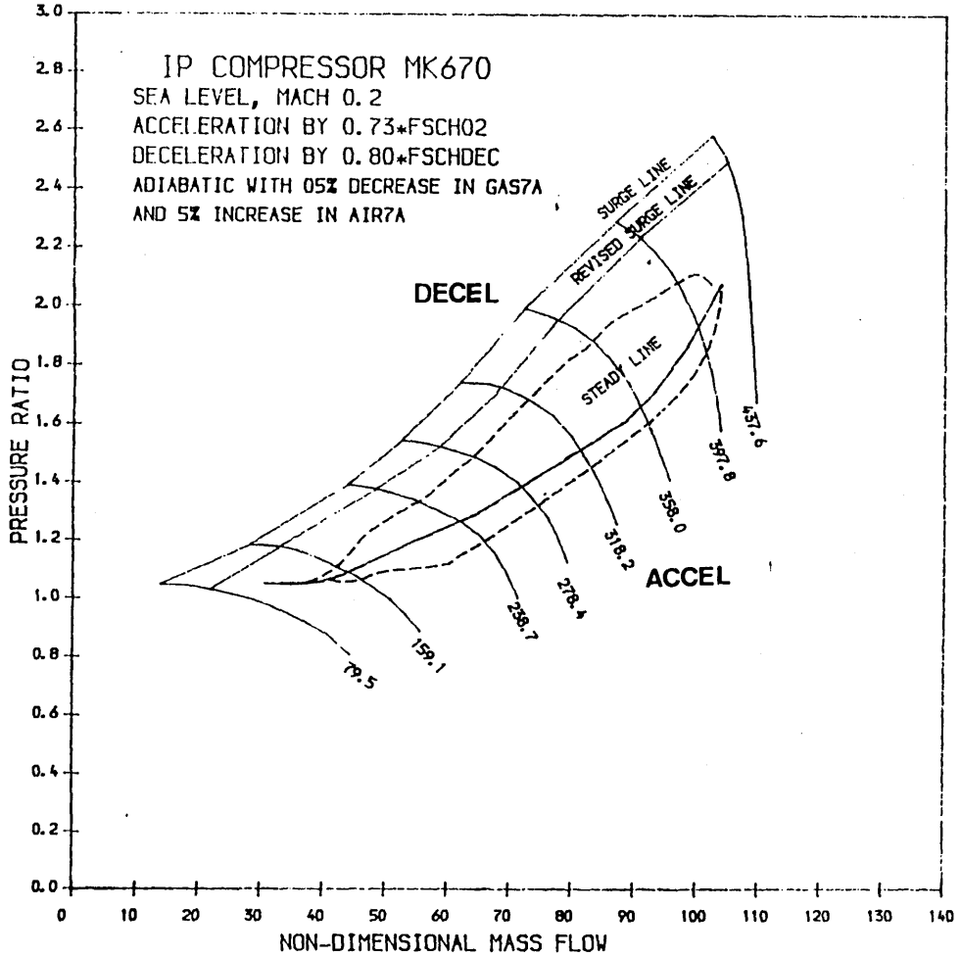

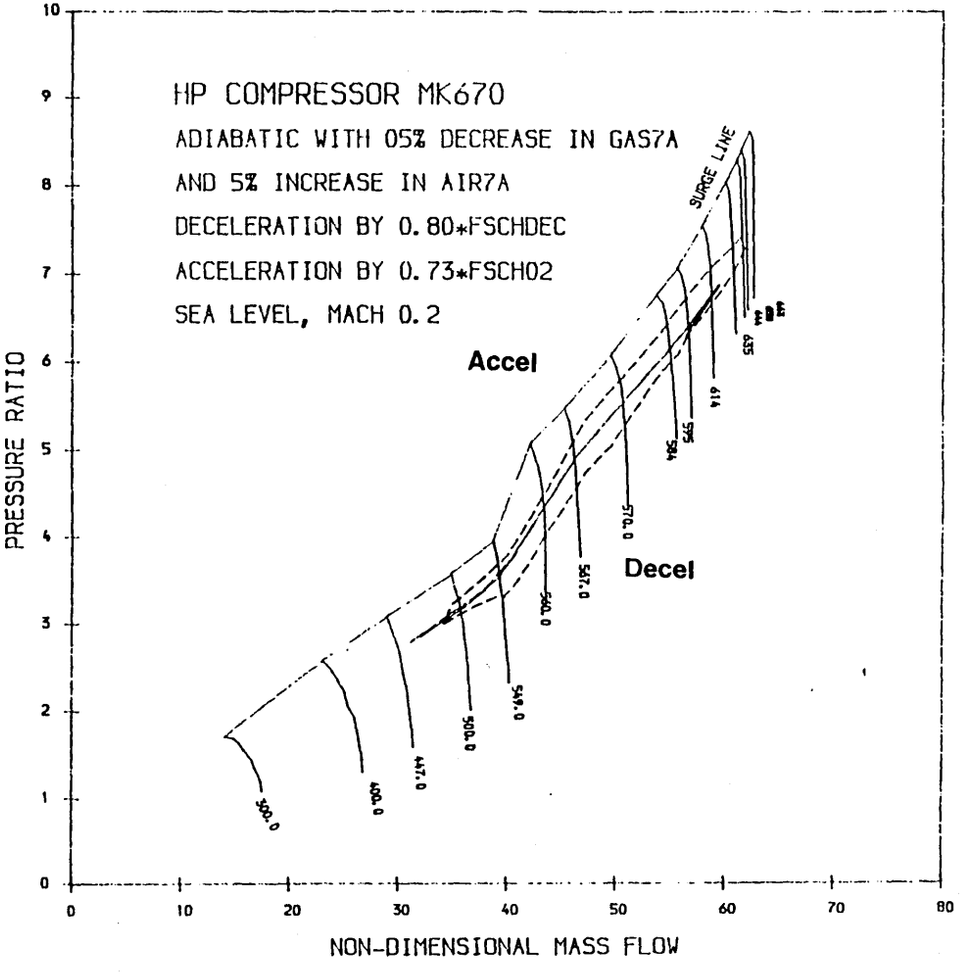

FIG 79 TAY MK670 ACCELERATION & DECELERATION TRANSIENTS OF THE I.P AND H.P COMPRESSORS AT SEA LEVEL, MACH 0.2.

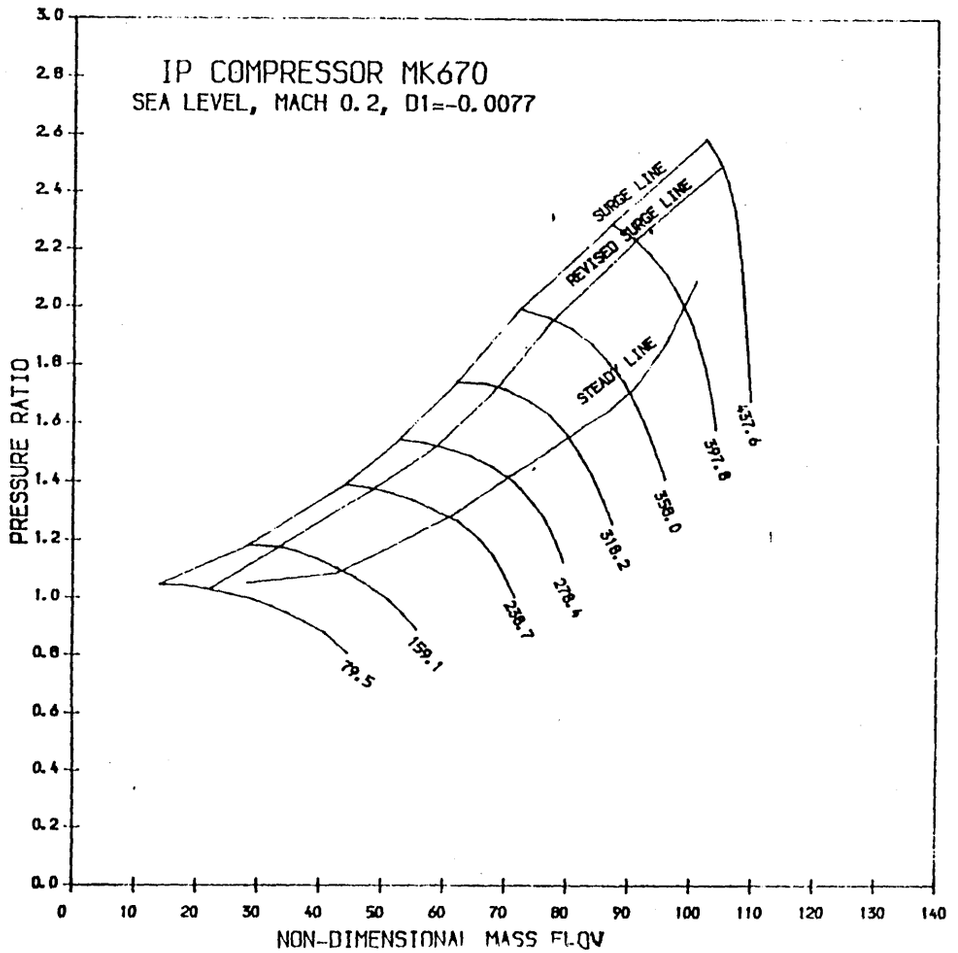

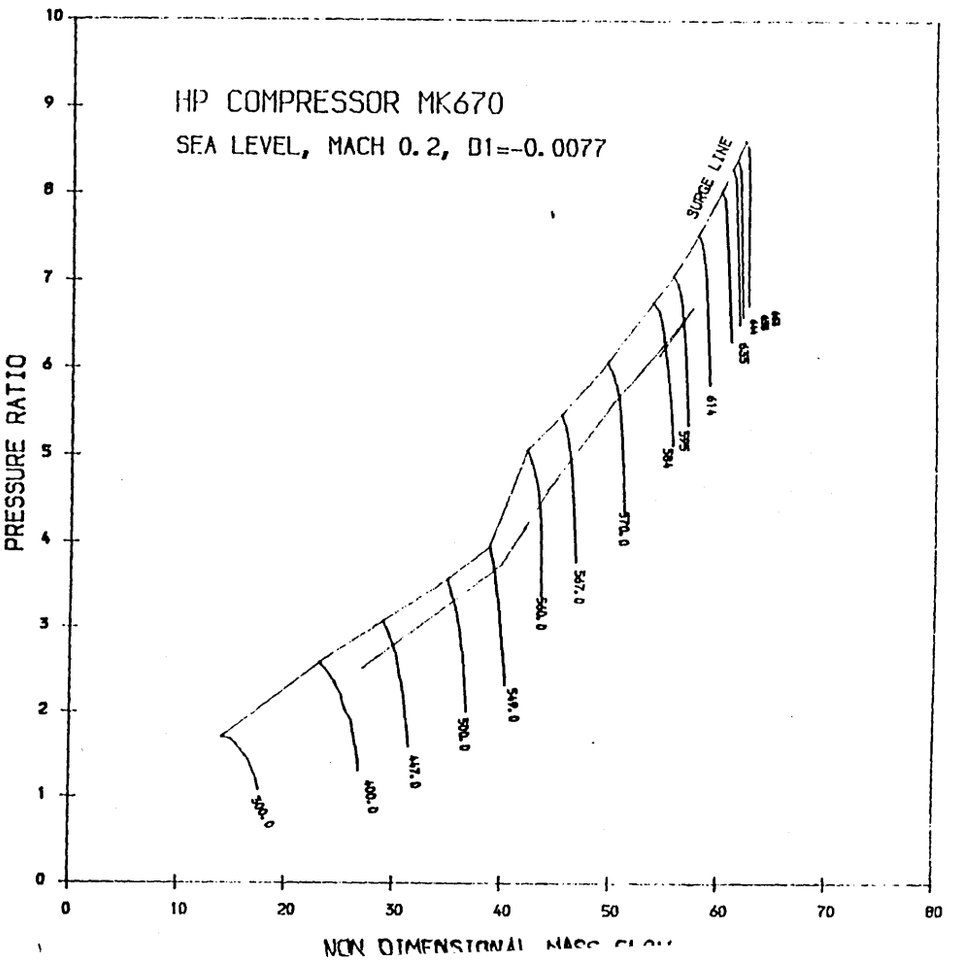

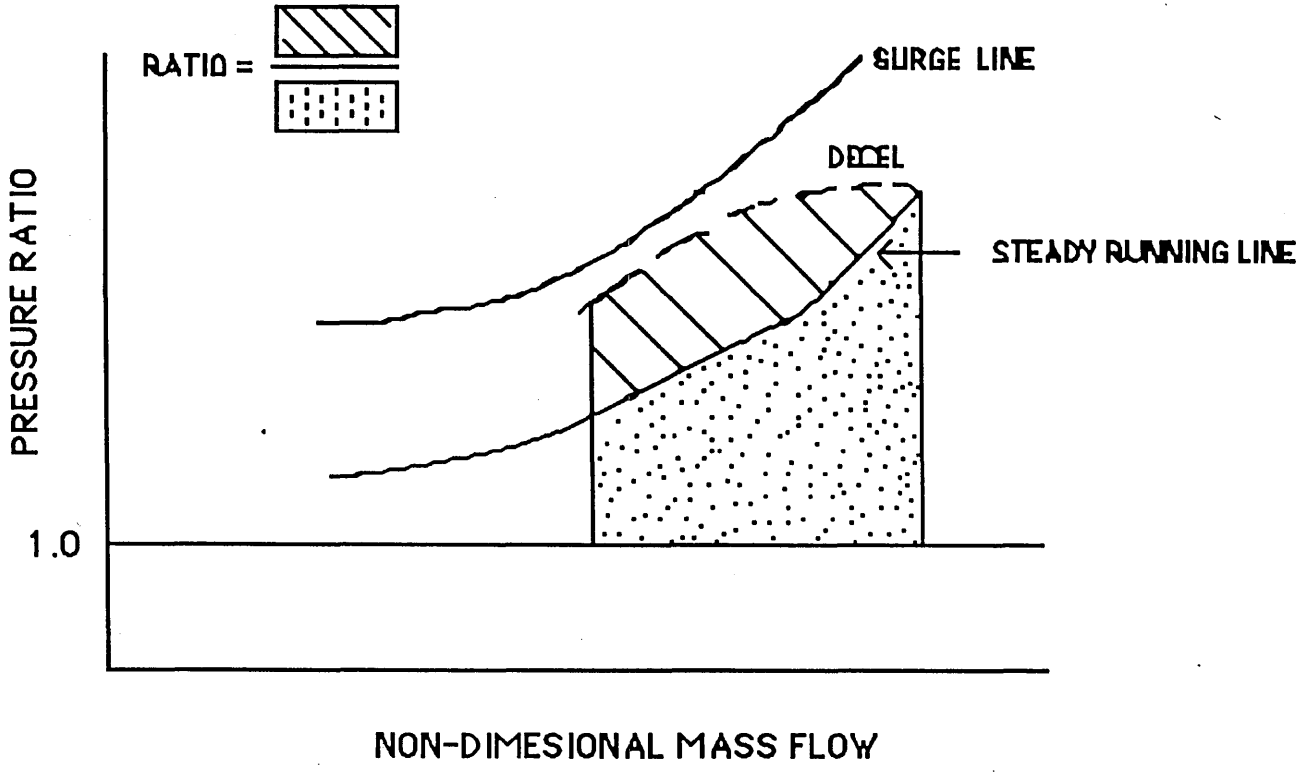

FIG 80 THE AREA RATIO FOR GIVING FRACTIONAL TRANSIENT TRAJECTORY DISPLACEMENT